Antenna diversity for Bluetooth

Breur, J.J.

Award date:
2004

TU/e technische universiteit eindhoven

Faculty of Electrical Engineering
Division Telecommunication Technology and Electromagnetics
Chair of Electromagnetics

Antenna Diversity for Bluetooth

by J.J. Breur

EM-5-04

August, 2004

Report of Master's project performed at
Philips Research and
Philips Semiconductors Nijmegen

Supervisor:
dr.ir. A.B. Smolders

Abstract

In this thesis antenna diversity to improve the quality of indoor Bluetooth radio communication is investigated. To investigate indoor radio wave propagation analytical and stochastic propagation models are introduced. A new propagation model, the hybrid model, is presented. The hybrid propagation model is a superposition of the free-space model and the cavity model. Furthermore, the behaviour of an antenna for incident waves arriving from all directions is investigated. The optimisation of the received signal is performed in a so-called diversity combiner. For some combining techniques, e.g., selection of the 'best' signal, the performance is analysed using a statistical analysis. For this project a Bluetooth antenna diversity demonstrator with embedded slot antenna was build, and the performance was measured on a special diversity test bench. The measured field strength distribution and bit error rate distribution are presented. The measured results can be explained using the propagation models. The quality of the radio link improves considerably if diversity is implemented in the Bluetooth transceiver.

Symbols and abbreviations

Symbols

a	(V)	amplitude of a signal
A	(m^2)	area
$\vec{A}$	(Amp)	magnetic vector potential, (complex vector)
BER	()	bit-error rate
c_0	(m/s)	speed of EM wave in vacuum
d	(m)	separation
e		envelope
$\vec{E}$	(V/m)	electric field strength, (complex vector)
$\langle\ \rangle$	()	expected value
f	(Hz)	frequency
h	(m)	height
I_0	(C/s)	current
I_0		zeroth order modified Bessel function of the first kind
J	(C/sm^2)	current density
J_0	()	zeroth order Bessel function of the first kind
$\vec{k}_0$	(1/m)	propagation constant in vacuum, (complex vector, we assume real)
k_0	(1/m)	propagation constant in vacuum
k_x	(1/m)	propagation constant in x-direction, (complex number)
m	()	integer number
n	()	integer number
p	()	power of a signal
P	(Watt)	power
Pr{ }	()	probability
r	(m)	distance defined as $\lvert\vec{r}\rvert$, coordinate in spherical co-ordinate system (r, θ, ϕ)
$\vec{r}$	(m)	location vector
R[]	()	auto correlation function, (complex number)
S_{21}	()	scattering parameter, transmission from port one to two, (complex number)
s_z	()	scattering parameter, reflection for z-direction
$\vec{S}$	($Watt/m^2$)	Pointing vector, (complex vector)
t	(s)	time
u	()	variable used to express real part of $w = u + iv$
$U()$	()	Heaviside step function
v	()	variable used to express imaginary part of $w = u + iv$
w	()	variable used to express complex number $w = u + iv$
x	(m)	coordinate of (x, y, z) right hand rectangular coordinate system
X	()	function of only x
y	(m)	coordinate of (x, y, z) right hand rectangular coordinate system
Y	()	function of only y
z	(m)	coordinate of (x, y, z) right hand rectangular coordinate system
Z	()	function of only z
Z_0	(Ohm)	characteristic impedance in vacuum $\approx 377\ \Omega$
γ	()	signal-to-noise ratio
Γ	()	reflection coefficient
ε	(F/m)	permittivity, (complex number, we assume real)
$\delta(x)$	(1/m)	Dirac distribution, when x has dimension m the distribution has dimension 1/m
θ	(rad)	angle with the z-axis, coordinate in spherical coordinate system (r, θ, ϕ)
λ	(m)	wavelength
μ	(H/m)	permeability, (complex number, we assume real)
ρ_{12}	()	complex correlation coefficient between signal one and two, (complex number)
ρ_{env}	()	correlation coefficient between the envelope of signal one and two

ϕ	(rad)	coordinate in spherical coordinate system (r, θ, ϕ)
Ω	(rad^2)	solid angle, $d\Omega = \sin\theta\, d\theta\, d\varphi$
$\Re\{\ \}$	()	real part
$\Im\{\ \}$	()	imaginary part
$\angle$	(rad)	angle between two vectors
#	()	cardinality of a set

Abbreviations

BER	bit-error-rate
Bt	Bluetooth
cdf	cumulative distribution function
dB	decibel
env.	envelope of the signal
GFSK	Gaussian frequency shift keying
ISM	Industrial, Scientific and Medical
LOS	line-of-sight
NLOS	non-line-of-sight
pdf	probability density function
r.m.s.	root mean square
RSSI	received signal strength indicator
s	second
SNR	signal-to-noise ratio
XPD	cross polar ratio

Contents

1 Introduction

1.1 Project description

The goal of this graduation project is to investigate antenna diversity techniques for Bluetooth communication. The project is organised as follows. First indoor radio wave propagation measurements are performed. Then a variety of radio wave propagation models are examined. After that diversity techniques are used in order to improve the measured performance. Finally a demonstrator with antenna switch is built and tested to validate the predicted performance improvements. The performance improvement is evaluated by virtue of the Bit Error Rate (BER). How the Bluetooth transceiver makes a connection is important for the BER and is discussed below.

1.2 Bluetooth

Bluetooth is a set of technology specifications for low-cost, robust and low power short-range wireless communication. The specifications answer the need for short-range wireless connectivity for ad hoc networking. Bluetooth uses frequency hopping spread spectrum to cope with interference and fading [Haartsen, 2002]. The radio uses the unlicensed ISM (Industrial Scientific Medical) band, which ranges from 2400 MHz to 2483.5 MHz. In this band 79 channels are defined to hop over. The transmitter and receiver of the information have to agree about the way they communicate, e.g., what frequency they use. This is why there is a Bluetooth radio protocol. A protocol is a set of rules for the communication between transceivers (transmitter and receiver). For Bluetooth the propagation changes every time the radio hops to a different frequency. In chapter 3 it is shown that the propagation is frequency dependent.

1.3 Propagation

The radio link for Bluetooth is intended for short-range indoor propagation [Haartsen, 2002]. This is accomplished through the use of omnidirectional antennas to make a Non-Line-of-Sight, (NLOS), radio link possible. With antennas that receive and transmit in all directions it is possible to make a radio link using reflective objects. In this case the electromagnetic waves follow an indirect path to arrive at the receiver. To investigate the performance of a radio connection, we need to know the properties of the electromagnetic (EM) field. Interfering of the radiated electromagnetic waves, shadowing and attenuation of the electromagnetic waves are the cause of indoors fading. Fading happens also with a FM car radio. The signal strength of radio signal changes fast from a strong to a very weak signal in the neighbourhood of buildings, bridges and tunnels, this is called fast fading. With a fade we mean a weak signal, i.e., the received signal strength is too low and the quality of the radio link is not acceptable. For simplified situations, e.g., when the propagation is considered to take place in free space, above a flat conducting plane or in a cavity with perfectly conducting walls, this EM field can be calculated analytically. For all other situations we have to resort to other methods to take the propagation and boundary conditions into account. These methods can be numerical, statistical or a combination of a numerical method and a statistical method. Most of the statistical models are based on outdoor long-distance environments. Bluetooth is typically employed in indoor, short-range environments. In the employment, a lot of reflections from the walls, floor and ceiling will be experienced. In practice the walls, floor and ceiling will not be perfectly electrically conducting. Therefore it is suggested that a model based on a combination of the rectangular cavity model and the (outdoor) long distance model will yield results close to reality.

A typical transmitter power for a Bluetooth radio is 1 mW. The receiver sensitivity is at minimum – 70 dBm. Then at the Bluetooth wavelength (12.5 cm), assuming isotropic transmit and receive antennas (0 dB gain), the radio equation [Smolders, 2000]

$$r = \sqrt{\frac{P_t G_t G_r \lambda^2}{P_r 16\pi^2}}, \tag{1.1}$$

gives a range r of 31.5 m. In this equation, P_t is the transmitted power, P_r is the received power, G_t and G_r are the gain of the transmit and receive antenna, respectively, and λ is the wavelength. However, for a proper radio link the signal level should be well above the noise level. The quality of the radio link for Bluetooth is expressed in the BER. In chapter 4 the relation for Bluetooth between BER and signal to noise ratio, (SNR), is given by

$$\mathrm{BER} = \frac{1}{2}\exp\left(-\frac{\mathrm{SNR}}{2}\right). \tag{1.2}$$

For Bluetooth the BER should be smaller than 0.1 % [www.bluetooth.com]. The SNR associated with a BER of 0.1 % is 11 dB. With the use of equation (1.1) this reduces the range where the BER is smaller than 0.1 % to about 9 m. The Bluetooth standard [www.Bluetooth.com] defines three power classes ranging from 0 dBm up to 20 dBm. Each power class has it own power range, e.g., class 1 ranges from 4 dBm to 20 dBm. For a transmitter power of 100 mW, using the radio equation (1.1), the range where the BER is smaller than 0.1 % increases 10 fold and becomes 90 m. The increased range could lead to a room-to-room radio link. In this report we concentrate on the propagation in a single room. In the remainder of this chapter we explain what is meant by diversity, antenna parameters and measurements and simulations. Finally the outline of the rest of the report is given.

1.4 Diversity

In mobile communication we mean with diversity the employment of adaptive receive or transmit techniques. For example, if we have two receive antennas it becomes possible to select the strongest signal. In this way diversity increases the quality of the radio link. In this report we concentrate on receiving diversity only. Diversity is used to combat signal fading or interference caused by, e.g., a household magnetron. In this report we consider only signal fading. Increasing the transmitted power or increasing the sensitivity of the receiver could also decrease the effect of fading. Increasing transmitter power from 4 dBm to 20 dBm would increases the SNR with 16 dB. However, a typical Bluetooth module is a low cost, battery powered and transmitter power limited device. For battery powered applications, e.g., a headset, increasing the power is not an option. If the receiver takes several samples of the received power at a different time, place, polarisation etc, the chance of a fade decreases. Statistical calculation in chapter 4 shows that the adaptive receiver will have a different distribution of power over the space indoors and less fades. We get the best performance when the received powers have a negative correlation. Then there is fade at one antenna and a peak in the received power at the other antenna. In practice it is sufficient to have independent received powers, i.e., the correlation is close to zero. Diversity techniques are listed in table 1.1.

table 1.1: *Overview of diversity techniques.*

Diversity technique	**Implementation**
Space diversity	separation in space between two or more antennas
Frequency diversity	separation in frequency
Polarisation diversity	different orientation of identical antennas (horizontal, vertical)
Field diversity	(electric) dipole antenna and a (magnetic) loop antenna
Angle/Pattern diversity	changing the antenna pattern by adding a reflector
Time diversity	separation in time to de-correlate two signals (try again)

The Bluetooth technology already uses frequency diversity (channel hopping) and time diversity. Furthermore, Bluetooth is a low cost technology so cheap solutions are preferred. Depending on the cause of the fading the best technique should be chosen. For example, we could use time diversity if blocking of the radio signal during a short time causes fading. Fading in space can be combatted with all the other techniques. Polarisation diversity would be useless if the fading over space distributes power mainly over the co-polarized direction. The co-polarized direction is, e.g., the vertical direction if the transmit antenna is a vertical monopole. In this case the cross-polarised antenna, e.g., a horizontal monopole, will hardly receive any power.
The simplest diversity technique to implement is space diversity. If we use two antennas separated at some distance we only need to switch between the two received powers. This is cheap and simple to implement in the already available Bluetooth module. Indoors a separation between the antennas of half a wavelength is mostly sufficient to get independent received powers [Leijten, 2001].

Another diversity technique is polarization diversity. If two antennas are used, one receive antenna is oriented in the co-polarisation direction and the other receive antenna is oriented in the cross-polarisation direction. The received powers in the different polarisation's are de-correlated, but the received power in the cross-polarisation direction is about 6 dB below the received power in the co-polarised direction [Kalliola et al, 2002]. This 6 dB difference in the received power is the reason that, after switching between the two antennas, the increase in received power will be lower compared to space diversity. However, if we switch between the received powers it will still be possible to reduce the possibility of a fade. A disadvantage can be the space we need to implement polarisation diversity. If the two antennas are integrated on a printed circuit board the size of the printed circuit board should be a least the length of the antennas squared.

Field component diversity can be used indoors. In an indoor environment there are a lot of standing waves. Standing waves have the property that when the time averaged electric field is small the magnetic field is large and vice versa. When the received power at a magnetic loop antenna is low we can expect that the received power at the electric dipole is high. Furthermore, the two antennas can be implemented on the same place and thus use less room than the solutions above. This solution is time consuming, it requires the design of two new antennas and that is why it is not implemented for this project.

Angle or pattern diversity can be implemented using a parasitic antenna that can be enabled using a switch. The parasitic antenna is in fact a reflector like the reflectors used in a TV antenna. Because the separation between the antennas is small, there is mutual coupling. The directivity of the radiation pattern increases. The direction of the radiation pattern changes depending on the position of the parasitic antenna. The antenna can have two states, e.g., depending on the load attached to an parasitic antenna. An advantage is that it does not take much room to implement it. When only two states are used the implementation is simple. A disadvantage can be the sensitivity to the surrounding conductors, which are also parasitic antennas. So every application has to be tuned to get independent antenna patterns.

1.5 Antenna parameters

The antenna parameters such as antenna gain are used when the antenna is in an open-or free-space. Then the EM waves propagate without being reflected. The radiated waves propagate in a radial direction away from the transmit antenna. If we were able to take snapshots of the wave front of a pulsed signal, we would see an expanding sphere. Far away from the transmit antenna the EM wave looks like a plane wave, the phase and polarisation of the waves are constant along the plane normal to the propagation direction. The transmit antenna is fed with a sinusoidal current and this causes the phase of the waves. Like light rays EM waves are polarised, when the polarisation of transmit antennas matches the polarisation of the receive antenna we receive the maximum power. When we assume that the transmit and receive antennas are in a free-space and have the same orientation, e.g., either horizontal or vertical, the radio equation (1.1) can be used to calculate the received power at the antenna input. When a plane wave arrives at the antenna we have to integrate the contribution of waves with the same phase and polarisation to calculate the received power.
If the transmitted EM waves are reflected they arrive at different angles at the receive antenna and the received power at the input of the antenna cannot be predicted easily. We have to integrate waves with different phases and polarisation to calculate the received power at the antenna input. We can describe the probability of the angle of arrival incident waves with a stochastic distribution. For example, in the horizontal plane the waves arrive with equal probability from all directions at the receive antenna and in the elevation direction the probability of arrival for a wave is Gaussian distributed with a maximum in the horizontal plane. Furthermore, the power of the incident waves is equally distributed over the horizontal and vertical polarisation. For this EM field the received power at the antenna terminals can be calculated. It is also possible to calculate the power received by an isotropic horizontal and vertical antenna. An isotropic antenna has a constant gain in all directions and is sensitive to only one polarisation. The ratio between the power received at the antenna terminals and the power received by the isotropic antennas is the Mean Effective Gain (MEG). The MEG is a measure of the ability of the antenna to receive power out of the incident EM field distribution. The Bluetooth antenna diversity demonstrator has an embedded slot antenna, an external antenna and a switch to select one of the antennas. The radiation pattern of the embedded slot antenna was simulated with Momentum, an EM simulator that uses the Method of Moments [Harrington, 1993]. The external antenna is a monopole antenna.

1.6 Measurements and simulations

For this project measurements were performed at Philips Research. A diversity test bench in an office room was used to perform propagation and BER measurements. The purpose of the propagation measurements was to investigate the EM field indoors. An office room where the EM waves are reflected against the walls and reflection objects like cabinets is a typical indoor environment. The measurements showed that the office room behaves like a cavity for EM waves and that an adaptive receiver will improve the quality of the radio link. After the propagation measurements BER measurements where done. BER measurements were performed with a Bluetooth module and a monopole antenna. Furthermore, the Bluetooth antenna diversity demonstrator with an embedded slot antenna and a monopole antenna was used to perform BER measurements.
The EM field inside a cavity with perfect conducting walls was calculated based on the results from [Dolmans, 1997]. Furthermore, the EM-field in free-space was calculated. Finally the measured and simulated EM-field distributions are compared.

The performance of an adaptive receiver is calculated and compared with the measured performance. A measure of the performance improvement is the diversity gain. For example, if we move through the room with the receiver and measure the received power we will find that 1 % of the received powers is below –60 dBm at a transmitter power of 0 dBm. When we perform the same measurement with an adaptive receiver we can lower the transmitter power to –6 dBm and still keep 1 % of the received powers below –60 dBm. In this case the diversity gain is 6 dB.

1.7 This report

This reports starts with an explanation of the Bluetooth protocol. In chapter 3 propagation models will be discussed. The so-called free-space model, two-ray model and the cavity model are deterministic models. The stochastic models are the so-called multi-ray model and the mode-stirred chamber model. For all these models the power distribution and frequency dependence of the propagation, coherence bandwidth, are calculated. At the end of chapter 3 we explore the behaviour of an antenna in a multi-path propagation environment. It appears that the calculation of the antenna performance is much more complex for multi-path as for single path propagation. Diversity techniques are investigated in chapter 4. Simple adaptive receiving systems that combine the received signals are discussed and a practical solution for Bluetooth is investigated. The simulated electrical performance of the antenna switch for the adaptive receiver is discussed in chapter 5. The slot antenna, one of the antennas designed for a practical diversity system, is analysed with Momentum. The EM field measurements, BER measurements and simulation data are displayed and discussed in chapter 6. We discuss what kind of stochastic model suits the measurements. The diversity gain is calculated for de-correlated signals. The project is summarised in chapter 7, resulting in conclusions and recommendations for further research. At the end of the report are the literature references, a paper written for the European Microwave week and the appendices.

Although reading of the total report is recommended some parts of the report maybe well-known to readers with a background in radio wave propagation. These readers might be interested in the following sections. A new propagation model is discussed in section 3.6. The sections of this report which are directly related to the Bluetooth module are 5.2.1 and 5.3.1 and 5.3.2. Finally, chapter 6 contains the measurements and simulations.

2 Bluetooth Protocol

2.1 History of Bluetooth

In 1994 Ericsson Mobile Communications AB initiated a study to investigate the feasibility of realizing a radio interface between mobile phones and their accessories. Key researcher emanating from this study and thought to be connected to the naming of the new radio interface protocol (Bluetooth) is the – by now well known - Dutchman J.C. Haartsen [www.ericson.com]. In February 1998 five companies, Ericsson, Nokia, IBM, Toshiba and Intel founded a special interest group in order to explore the possibilities of setting up a new global short range communication standard. This group consisted of two market leaders in mobile telephony, two market leaders in laptop computing and a market leader in digital signal processing.

The name Bluetooth originates from the Danish King Harald Blåtand. In Danish 'Blå' means dark complexion (Harald had dark hair) and 'tan' means great man. Bluetooth is then a rather strange translation in English. Perhaps it is more instructive to look at 'tand', being the Dutch word for tooth. Another popular explanation for the name 'Bluetooth' is that Harald loved Blueberries so that his teeth became stained with the color.

Harald Blåtand is known in history for bringing Christianity to Scandinavia and uniting and controlling Denmark and Norway in the 10th century. Ericsson erected a modern runic stone, see figure 2.1, to the memory of Harald Bluetooth who united Denmark and Norway like today the new Bluetooth technology unites wireless devices.

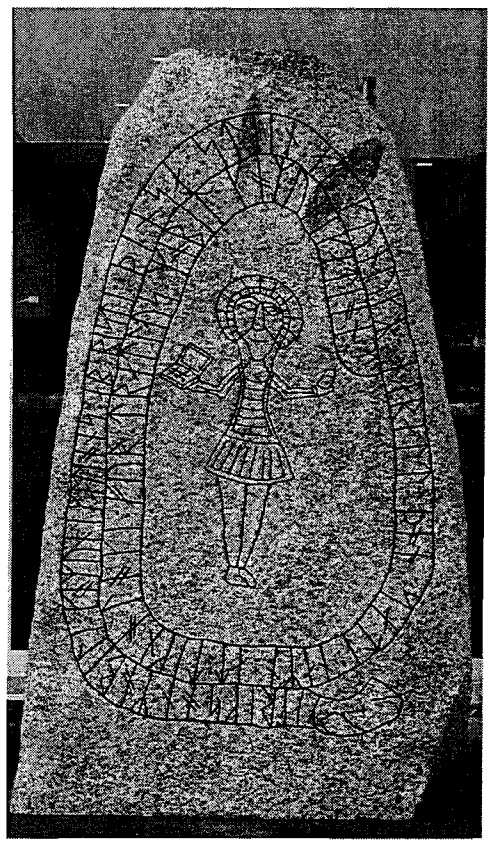

Figure 2.1: *Rune stone.*

2.2 Field of application

The Bluetooth standard and protocol are intended for small range (10 m) and low data rate (1 Mbit/s), communication. Bluetooth devices are intended to be small and cheap, being able to be plugged into computers, mobile phones, printers, etc. Most likely they will be employed in replacing cable connections, e.g., a computer-printer connection. The data rate and synchronous mode make it possible to transmit normal quality sound. By synchronous mode, we mean the mode wherein an almost continuous data stream is transmitted. An example of a commercially available Bluetooth device is a headset from Sony Ericsson, see figure 2.2, that uses a Philips module for connecting the headset and a mobile phone. Most applications nowadays are related to personal communication, computing and automotive.

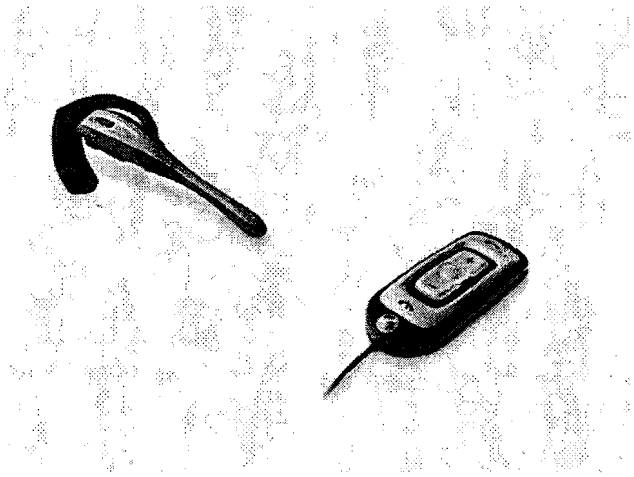

Figure 2.2: *Sony Ericsson headset, type HBH-30 with HBC-30 carkit.*

2.3 Other protocols

Besides the Bluetooth protocol, also the Wireless LAN (WLAN) or Wireless Fidelity (Wi-Fi) protocol (IEEE 802.11a and 802.11g) exists in the 2.4 GHz license-free ISM (Industry, Science and Medical applications) frequency band. The HomeRF standard also used to exist in the ISM band, but this standard is no longer being supported by vendors or working groups. The main difference between WLAN/WiFi, HomeRF and Bluetooth is the higher bandwidth, up to 11 Mbit/s for WLAN and 10 Mbit/s for HomeRF compared to only 1 Mbit/s for Bluetooth.

2.4 Relevant Bluetooth specifications

Bluetooth is a communication standard in the ISM band. It is still under development and the characteristics being referred to in this report are taken from the version 1.1 specification [www.bluetooth.com]. The most important radio specifications , i.e., the specifications related to the wireless part of the Bluetooth protocol, are listed in table 2.1. Abbreviations used in the table are explained underneath this table.

Table 2.1: *Most important Bluetooth radio specifications.*

Frequency	2.402 – 2.480 GHz (France: 2.454 - 2.476 GHz) $f = 2402 + k$ MHz $k = 0,1,2,\ldots,78$ 79 channels (France: 23 channels) hopping rate 1600 hops/s
Transmit Power	Class 1: 4 dBm to 20 dBm Class 2: 4 dBm Class 3: 0 dBm
Modulation	GFSK BT = 0.5 modulation index 0.28 - 0.35 deviation > 115 KHz symbol rate 1 Ms/s data rate 1 Mbit/s
Sensitivity	-70 dBm for a BER of 0.1 %
Interference	C/I ratio for a BER of 0.1 % co-channel: 11 dB adjacent 1 MHz: 0 dB adjacent 2 MHz: -30 dB Interfering signal for a BER of 0.1 % 2-3 GHz -27 dBm

The modulation is Gaussian Frequency Shift Keying, (GFSK), where BT is the normalized bandwidth B * T, B is the 3 dB bandwidth of the filter and T is the duration of a symbol period. To measure the quality of data transport the Bit Error Rate, (BER), is used. This is the ratio of bit errors and transmitted bits before error correction. For a BER of 0.1 % the ratio between Channel power and Interferer power, (C/I), is specified. The communication specifications are hardware implemented in the baseband part, see figure 2.3. The device that transmits data, e.g., a computer sending data to a printer, is called the Host.

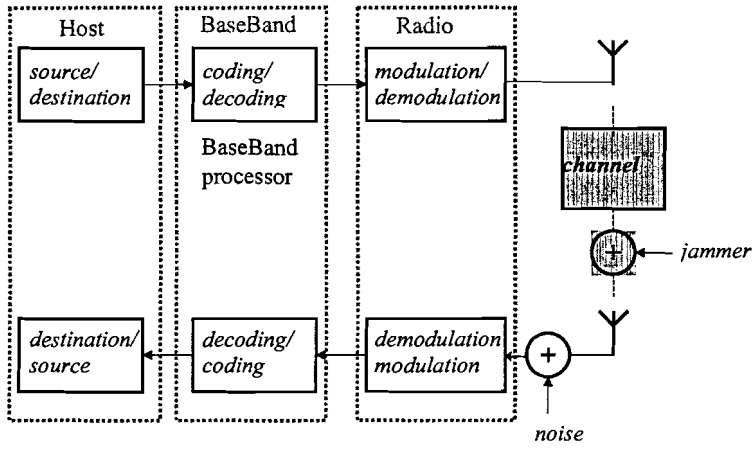

Figure 2.3: *Bluetooth communication system.*

Bluetooth uses frequency hopping to combat interference and fading. At baseband, time is divided into slots of 625 μs each and the baseband processor, see figure 2.3, controls the hopping sequence. The hopping sequence is the order in which the radio hops from one channel to the next channel. A channel is a frequency band centered at a Bluetooth frequency with a width of 1 MHz. The data is exchanged through packets, each package nominally covering a single slot, but - in the extreme – a packet may cover up to five slots. Each packet is transmitted on a different hop frequency as depicted in figure 2.4. The designations 'master' and 'slave' in this figure, refer to the controller of the piconet and a member of the piconet, respectively.

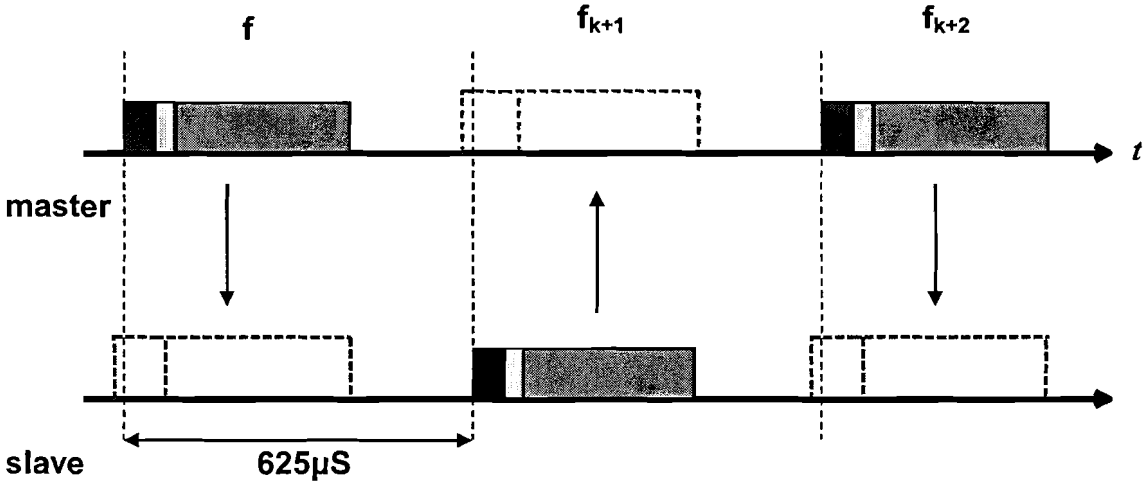

Figure 2.4: *Communication between master and slave in time.*

In the Bluetooth protocol five types of hopping sequences can be distinguished. These sequences with their specifics and use are listed in table 2.2.

Table 2.2: *Hopping sequences.*

Name	Specifics	Use
inquiry sequence	32 unique frequencies	look for devices
inquiry response sequence	32 frequencies of the inquiry sequence	return information about Bluetooth unit and its Bluetooth Host
page hopping sequence	32 unique equally distributed frequencies	initiate connection by continuously sending the access code of the receiver
page response hopping	32 frequencies in one to one correspondence to page sequence	return an acknowledgement
channels hopping sequence	equally distributed frequencies with very long period	data transmission

A connection between Bluetooth devices is set-up ad hoc and the master and slave or slaves that share the same hopping sequence form a so-called piconet. A piconet is a Bluetooth buzz-word for a miniature Local Area Network. In the piconet, a device is configured as Master. The Master can control up to seven Slaves. Connections can extend beyond the piconet level, i.e., between devices of individual piconets. A collection of this type of connections is called a scattered net, see figure 2.5. The network is now not longer limited to seven devices.

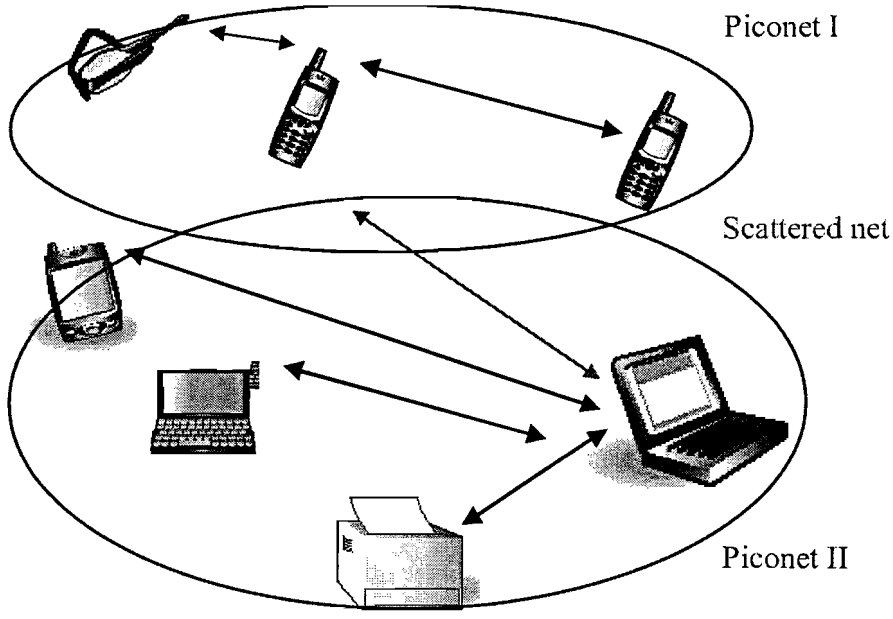

Figure 2.5: *A typical network topology.*

A unit can participate in different piconets using time division multiplexing. The unit acts then as Master in one piconet and Slave in another piconet. Time division multiplexing is the process wherein time is divided in slots that are used for different links.

A hopping sequence is generated in such a way that it is pseudo random, i.e., the auto-correlation is small over a short time. It is called pseudo random because it looks random although it is generated by an algorithm. So every sequence looks different, there is no common pattern. Statistically, auto-correlation is the expectation of the inner product of the sequence with the time-shifted sequence over a certain length. It is a measure of dependence, when the events A and B are independent the chance of that event A and B both occur is the chance of A times the chance of B. So the joint probability becomes a second-order chance. When we have 79 channels the chance that piconet A

is on channel 1 is 1/79. The chance that piconet A and B are both on channel 1 is then 1/79 * 1/79, i.e., second-order. If there is a jammer at one channel, e.g., a household magnetron, the independence in the hopping sequence minimises the chance that Bluetooth hops several times to the jammed channel in a short period. If data is lost in an asynchronous mode the data is retransmitted, in a synchronous mode the data is lost.
Bluetooth can support an asynchronous data channel, up to three simultaneous synchronous voice channels, or a channel that simultaneously supports asynchronous data and synchronous voice. For Bluetooth a physical channel is defined. It is a synchronized hopping sequence in a piconet. In an asynchronous physical channel the Master does not always transmit to the same Slave in a regular fashion. The data transfer can go from Master to Slave and vice versa or only from Master to Slave. A synchronous physical channel is connection oriented and the Master transmits regularly to the same Slave and vice versa.

For these different data channels, different data rates are being used:

- Synchronous 64 Kb/s per voice channel.
- Asynchronous 723.2 Kb/s asymmetric and 56.7 Kb/s return or 433.9 Kb/s symmetric.

The format of a packet is depicted in figure 2.6.

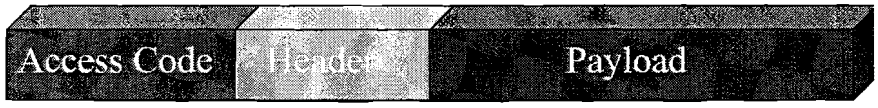

Figure 2.6: *Bluetooth packet structure.*

Every data packet consists of 72 bits access code followed by 54 bits header followed by the payload (the information containing part of the package) with a size between 0 and 2745 bits. For the receiving unit (radio) the first part of the signal is important because it is the access code. Furthermore, we assume that the receiver contains a Phase Locked Loop (PLL). The acces code is used for synchronization, DC offset compensation and identification. With synchronization we mean the phase locking of the PLL of the receiver. DC offset compensation is used with an open loop PLL demodulator to compensate for Voltage Controlled Oscillator (VCO) drift and RF frequency errors. The information in the access code is the access code of the source or destination. The access code consists of a preamble (bits without information) of 4 bits followed by a sync word of 64 bits and possible a trailer of 4 bits. The sync word is used to match the master and slave. It is constructed in such a way that it has excellent auto-correlation properties and low cross-correlation properties The decision to accept a packet is then quite reliable because it is based on the outcome of a correlator. Because the auto-correlation is excellent it is accepted at the right time. The outcome of the correlator has a strong peak at the right time and is very small at another time. Cross-correlation is the correlation between different sequences, e.g., access codes. The cross-correlation ensures that only the addressed Slave accepts the package.

2.5 Important specifications for this project

For the propagation we have to look at the whole Bluetooth frequency band which consists of 79 frequency channels. Frequency hopping is a frequency diversity technique employed for overcoming the negative aspects of frequency fading. With frequency fading we mean the dependence of the propagation on the frequency. Frequency fading at a position can be presented as a sequence of transmission coefficients. Each element of this sequence represents the propagation at a certain frequency channel. A robust radio channel is realized if hopping to a frequency is independent of the propagation at that frequency. The hopping sequence is pseudo random. The correlation between the constant sequence of transmission coefficients and the hopping sequence is almost zero. So hopping to a frequency and transmission at that frequency are independent. The

hopping technique then reduces the chance that the transmitter hops several times in the same fade over a short time interval.

In synchronous voice transmission, fading is observed by hearing 'clicks' in the output audio signal. From a consumer point of view, these 'clicks' are more serious than a slightly dropping bit rate that may occur in asynchronous data transfer. The occurrence of these clicks may be avoided by implementing a diversity scheme. Even when diversity gives no improvement on the average, it can dramatically decrease the chance of a fade and thereby minimize the occurrence of clicks.

When diversity is implemented the preamble signal has to be used for measuring the signal strength, making this preamble signal, the Receiver Signal Strength Indicator (RSSI) signal, see figure 2.6. In the Bluetooth specification the RSSI is optional. When employed, three detection ranges, are used:

1 6 dB above noise level (assumed at –70 dBm) or lower.
2 between 6 dB above noise level and –56 dBm.
3 -36 dBm ± 6 dB or higher.

A problem associated with measuring the preamble signal is the short time available (only 4 μs), wherein the signal has to be measured, analyzed and a diversity scheme has to be activated. Other methods are also possible. When a look up table is used the best antenna is selected for each channel.

2.6 Bluetooth and interference

The quality of service of Bluetooth depends not only on the propagation. As specified in table 2.1 the radio has to be able to reject other transmitters in the ISM band like Bluetooth, WLAN, HomeRF or even household microwave ovens. Interference can be the limiting factor of the radio link and not, as one would expect, propagation. The hopping technique reduces the chance that an interferer jams the hop channel continuously. Although diversity can be used to suppress an interferer, this aspect is not the goal of the project described in this report.

When another Bluetooth piconet is within range this can cause interference. The minimization of the auto-correlation ensures that collisions with other piconets, i.e., cross-correlations, are also minimized. A collision (cross-correlation) with another piconet occurs when both nets share the same channel. To get a feeling of the collision probability we will look at N piconets in the neighborhood of 1 piconet. If N transmitters are active at N un-correlated Bluetooth frequencies f_1 to f_N the collision probability for one piconet at frequency f with N piconets co-located is roughly given by [Haartsen, 2000]

$$\text{Probability}\{\text{no collision}\} = \Pr\{ f \neq f_1, \cdots, f \neq f_N \} = \left(\frac{78}{79}\right)^N . \qquad (2.1)$$

This means that for 2 piconets, which we will use to model a 0 dBm transmit-power Bluetooth radio with a range of 10 meter, the chance of a collision is 1- Pr{no collision} = 1.3 %. When we look in table 2.1 we see that when the received power from the interfering signal is 11 dB below the received power from the transmitter signal the receiving radio still works well. In equation (2.1) the distance between interferer and receiver and the distance between the transmitter and receiver are ignored. In practice the receiver will not de degraded by an interferer when the distance between transmitter and receiver is much smaller than the distance between interferer and receiver. This is why equation (2.1) is only a worst-case estimate. Each collision is considered catastrophic when power and distance are ignored. We can take into account the difference in received power between the wanted signal and an interferer. With the radio equation the received power is,

$$P_{received\,from\,transmitter} \propto 1/r^2_{transmitter}, \quad P_{received\,from\,interferer} \propto 1/r^2_{interferer}, \tag{2.2}$$

where $r_{transmitter}$ is the distance between transmitter and receiver and $r_{interferer}$ is the distance between interferer and receiver. The interference can be ignored when the received power from the interferer is 11 dB below the received power from the transmitter signal,

$$10\log\frac{r^2_{\text{interferer}}}{r^2_{\text{transmitter}}} = 11\text{dB}. \tag{2.3}$$

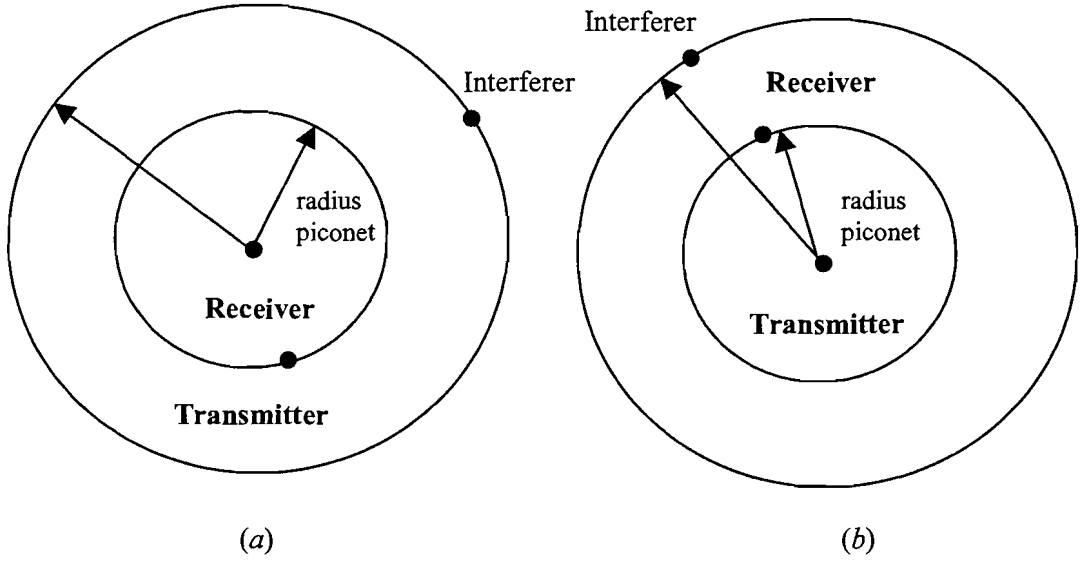

Figure 2.7: *Radio link with (a) receiver in the center and (b) receiver at the first circle.*

For instance, if we substitute 10 m in equation (2.3) for the interferer distance, the distance between transmitter and receiver should be at most 2.7 m or 3.5 times the radius of the piconet as depicted in figure 2.7a. For a radio link we also have to consider the opposite propagation direction depicted in figure 2.7b. In this case, with the interferer still at 10 m, the ratio between $r_{interferer}$ and $r_{transmitter}$ stays the same, 10/2.7. If we take the origin of the polar coordinates at the transmitter we get $(10-r)/r = 10/2.7$. And the distance between transmitter and receiver r should be at most 2.2 m. For this circular model we can conclude using equation (2.3) that the interference will not disturb the radio link if the distance to the interferer is at least 4.5 times the radius of the piconet.

3 Propagation models

In this chapter we discus EM wave propagation models and the receive antenna. We will start with the free-space model. This is the simplest model to investigate indoor propagation and can be used for a Line-Of-Sight, (LOS), radio link. In section 3.3 we will look at the next step, line of sight propagation in combination with one reflected ray. This will then be extended to multiple reflected rays propagating in a plane. This model is capable of describing a LOS radio link with reflections or a Non-Line-Of-Sight, (NLOS), radio link. In the remaining sections of this chapter a deterministic example of a reflective room, a cavity with perfect conducting walls, is analysed. Next we discuss a mode stirred chamber, a cavity with stochastic properties. The last model, the hybrid model, a combination of the free-space model and the cavity model, is presented in section 3.6. Finally, an antenna placed in a multi-path environment is discussed.

3.1 Introduction

The radio link is very comprehensive and consists of the indoor environment and the antenna properties. To keep the analysis simple we will only consider the electric dipole and the isotropic antenna with polarisation in the θ-direction in order to separate the environment from the antenna. In this way we can concentrate on the propagation only. The effects of antenna parameters like radiation pattern and polarisation sensitivity are discussed in section 3.7. All the media are considered being linear, isotropic and homogeneous. We will assume for all cases a homogeneous medium with permittivity ε_0 and permeability μ_0.

In the multi-path environment we have a direct wave and reflected waves. When the time delay difference between the direct wave and reflected wave is larger than the symbol time (1 μs for Bluetooth), inter-symbol interference occurs. The associated path difference (time delay difference times speed of light) in free-space for Bluetooth is 300 m. Due to this rather long path difference, this kind of fading may be neglected, provided that multiple reflections decay fast enough.

In a typical Bluetooth environment, transmitter and receiver do not remain static, but change position in time. Therefore a receiving ray undergoes a Doppler shift

$$\Delta f = \frac{v}{\lambda}\cos\vartheta_i, \tag{3.1}$$

where v is the relative speed between transmitter and receiver, λ is the used wavelength and ϑ_i is the angle of the incoming once reflected ray (see figure 3.8). Average walking speed, being 140 cm/s, at a wavelength of 12.5 cm results in a frequency shift of 11.2 Hz. This frequency shift value is well below the Bluetooth drift specification [Bray, 2001]. Therefore, also Doppler shifts may be neglected in the analysis of a Bluetooth radio link.

In indoor environments, also diffraction will occur, but this effect will be neglected as well, the field strengths being far below those experienced in the direct line of sight situation. The diffraction is treated as a reflection in the stochastic model. Now, having understood primary and secondary effects in the propagation link, we move on to the calculation of the received power.

3.2 Free-space model

We will start the analysis with a space without any reflections. This 'free-space model' serves as a first-order approximation of a practical indoor situation. In addition, the free-space model can be

easily extended to a more complicated multi-path model. The configuration of the free-space model is shown in figure 3.1.

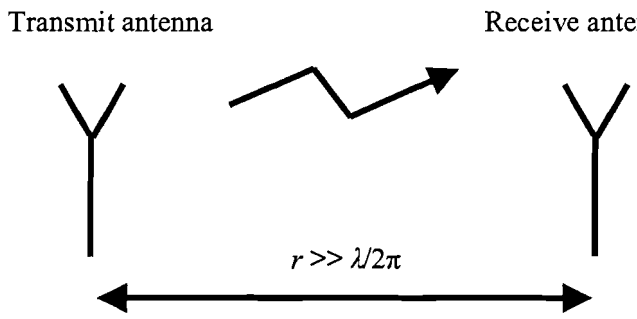

Figure 3.1: *Free-space model configuration.*

3.2.1 Field/Power calculation

Propagation can be analysed with the power density of the EM field. The receive antenna integrates the incident field. When the incident field is a plane wave, power density times the effective aperture of the receive antenna gives the received power. We start with the radiated field of a Hertzian dipole. This is a dipole with a length l very short compared to the wavelength. A practical antenna can be represented as a superposition of Hertzian dipoles. When the transmit antenna is in the vertical z-direction the electric field in spherical coordinates is given by [Smolders, 2000]

$$\vec{E} = E_\theta \vec{e}_\theta = j\frac{I_0 l}{4\pi} Z_0 \sin\theta \frac{k_0}{r} e^{-jk_0 r}\, \vec{e}_\theta \quad \text{for} \quad r >> \lambda/2\pi \quad \text{with} \quad E_\varphi = 0, \tag{3.2}$$

where k_0 is the propagation constant with $k_0 = 2\pi/\lambda$, Z_0 is the characteristic impedance ($Z_0 = 120\pi$ Ω in air), r is the radius (with respect to the antenna coordinate system) and where an $\exp(j\omega t)$ time dependence of the field is assumed and suppressed. Equation (3.2) is only valid in the far field, this is why the inequality for the radius r and the wavelength λ is needed. Further, E_θ is the θ-component of the electric field, I_0 is the amplitude of the current and l the length of the dipole.

For this thesis the standard spherical coordinate system as depicted in figure 3.2 is used.

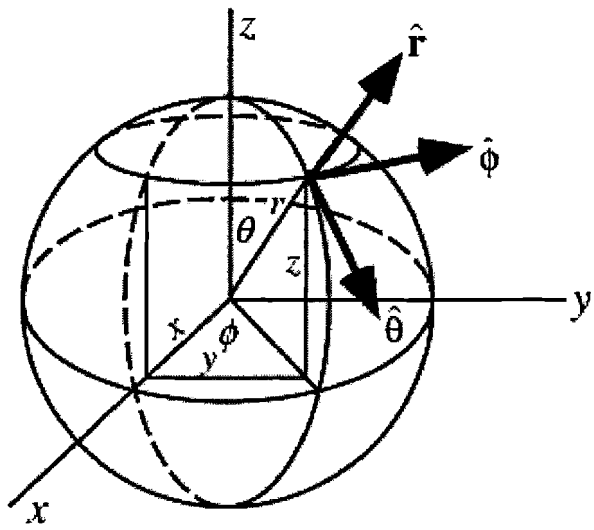

Figure 3.2: *Spherical coordinate system.*

For the Hertzian dipole the vertical current density can be written as:

$$\vec{J} = I_0\,\delta(\vec{r}-\vec{r}_s)\,\vec{e}_z\,, \tag{3.3}$$

where δ is the Dirac distribution and $\vec{r}_s$ is the position of the source. Note that every current distribution can be written as a summation using Eq. (3.3), so every antenna is equivalent to a summation of Hertzian dipoles. We can normalise the total radiated power to 1 Watt using the dipole moment $I_0 l$ [Smolders, 2000]

$$I_0 l = \sqrt{\frac{12\pi\, P_{transmitted}}{Z_0\, k_0^2}} \approx \sqrt{\frac{1}{10\, k_0^2}}\,. \tag{3.4}$$

It is now possible to calculate the electric field strength in the z-direction,

$$E_z = E_\theta \sin\theta = j\frac{30}{\sqrt{10}\,r}\,e^{-jk_0 r}\sin^2\theta\,. \tag{3.5}$$

For Bluetooth the wavelength $\lambda = c/f = 12.5\,\text{cm}$. The far-field criterion is $r > 2D^2/\lambda$, where D is the diameter of the antenna. For a $\lambda/2$ dipole the far field starts at $\lambda/2$ or 6.25 cm. The time average power density or Pointing vector modulus S [Watt/m^2] at $\theta = 90°$ is

$$S(r,\theta=90^o) = \frac{|E_z|^2}{2Z_0} = \frac{3}{8\pi r^2}\,. \tag{3.6}$$

The isotropic antenna radiates equally in all directions and we get

$$S(r) = \frac{|E_\theta|^2}{2Z_0} = \frac{1}{4\pi r^2}\,. \tag{3.7}$$

The power density in the far field region between 1 meter and 3 meter for an isotropic radiator is depicted in figure 3.3.

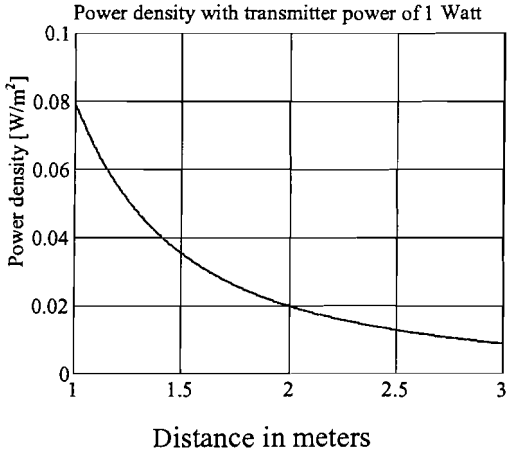

Figure 3.3: *Power density as function of the radius caused by a radiating isotropic antenna.*

3.2.2 Power distribution

A convenient way of analysing the performance of a radio link in a multi-path environment is to look at the statistics of the power density. We will introduce two statistical parameters to describe the distribution of the power, i.e., the cdf (cumulative distribution function) and the pdf (probability density function) [Dehling, 1995]. For a random variable X, the probability that $X \leq x$ is expressed as

$$\text{cdf} = F(x) = \Pr\{X \leq x\}, \tag{3.8}$$

where Pr is the probability. The derivative of the cdf $F(x)$; is called the pdf of the random variable X:

$$\text{pdf} = f(x) = \frac{dF(x)}{dx}, \tag{3.9}$$

or

$$F(x) = \int_{-\infty}^{x} f(u)\,du \quad \text{with} \quad \int_{-\infty}^{\infty} f(u)\,du = 1, \tag{3.10}$$

note that the pdf, $f(x)$ can be larger then one. The probability that X is in an infinitsimal interval is:

$$\Pr\{x < X \leq x + dx\} = F(x + dx) - F(x) = f(x)\,dx. \tag{3.11}$$

In our situation X is the power density. For simplicity we will restrict our analysis to the power density in a region with minimum radius $r_{\min}$ and maximum radius $r_{\max}$ in the plane $\theta = 90°$, as depicted in figure 3.4.

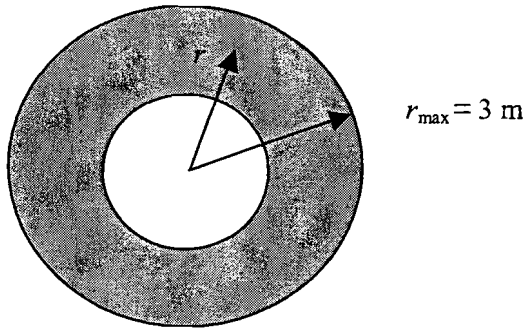

Figure 3.4: *The annulus where the power density distribution is calculated.*

The probability that the power density S is in the interval $\{ s < S \leq s + \mathrm{d}s\}$ is derived from probability that the associated radius R is in the interval $\{ r < R \leq r + \mathrm{d}r\}$. Furthermore, we assume that each position within the region has the same probability. The probability that the position has a radius R is

$$\begin{aligned} \Pr\{r < R \leq r + dr\} = f_r(r)\,dr &= \frac{\text{area with radius } r}{\text{total area}}, \\ &= \frac{2\pi r\,dr}{\pi r_{\max}^2 - \pi r_{\min}^2} = \frac{2r}{r_{\max}^2 - r_{\min}^2}\,dr, \end{aligned} \tag{3.12}$$

where f_r is the pdf of r. We can express r in S and for a Hertzian dipole we get with Eq. (3.6),

$$S(r) = \frac{3}{8\pi r^2} = \frac{s_1}{r^2} \quad \text{and} \quad r(s) = \sqrt{\frac{s_1}{S}}, \tag{3.13}$$

where s_1 is the power density at 1 meter. We can express the pdf of the power density f_S in the pdf of the radius f_r and we get [Dehling, 1995],

$$f_s(s) = f_r(r(s)) \left| \frac{d}{ds} r(s) \right| = \frac{s_1}{r_{\max}^2 - r_{\min}^2} \frac{1}{s^2}, \tag{3.14}$$

and the cdf is

$$F(s) = \int_{s_{\min}}^{s} \left\{ \frac{s_1}{r_{\max}^2 - r_{\min}^2} \frac{1}{s^2} \right\} ds = \frac{s_1}{r_{\max}^2 - r_{\min}^2} \left(\frac{1}{s_{\min}} - \frac{1}{s} \right). \tag{3.15}$$

The pdf of the power density distribution for a transmitted power of 1 Watt at the plane $\theta = 90°$ in an annulus with a radius between 1 m and 3 m is depicted in figure 3.5.

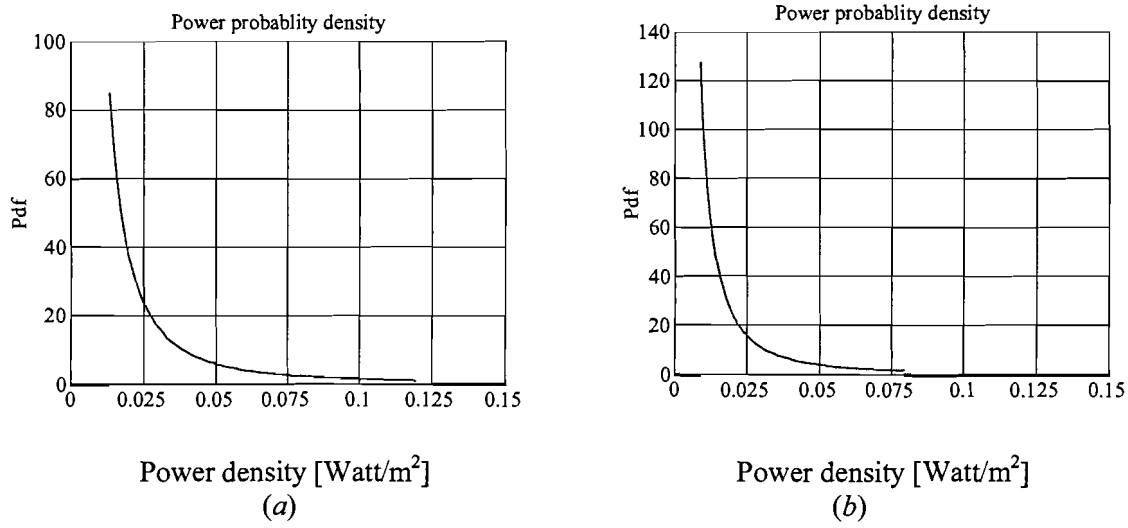

Figure 3.5: *The pdf of the power density for (a) the Hertzian dipole and (b) the isotropic antenna for an annulus with a radius between 1 m and 3 m.*

In figure 3.5 we can observe that the probability density of a power density of 0.1 Watt/m^2 , at a distance of about 1 meter from the transmitter, is low compared to the probability density of a low power density of 0.025 Watt/m^2 at about 3 meter from the transmitter.
The cdf of the power density for a transmitted power of 1 Watt at the plane $\theta = 90°$ in an annulus with a radius between 1 m and 3 m is presented in figure 3.6.

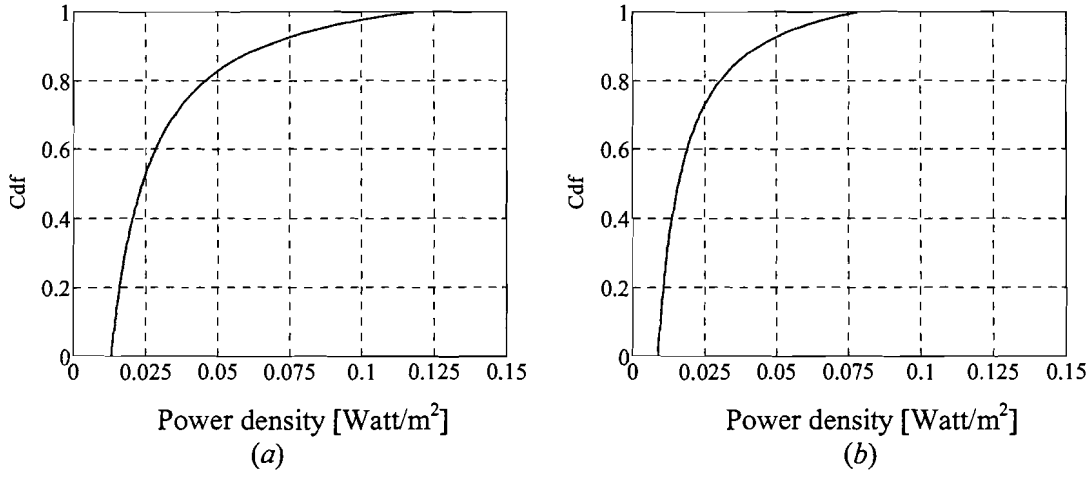

Figure 3.6: *The cdf of the power density for (a) the Hertzian dipole and (b) the isotropic antenna for an annulus with a radius between 1 m and 3 m.*

Since in the free-space model we do not have reflections the delay spread is zero and the corresponding coherence bandwidth is zero.

3.3 Multi-path model

The multi-path model assumes the electromagnetic, (EM), field to propagate in free-space (within the enclosures of a finite size room) and further assumes the existence of a limited number of reflected waves, as depicted in figure 3.7.

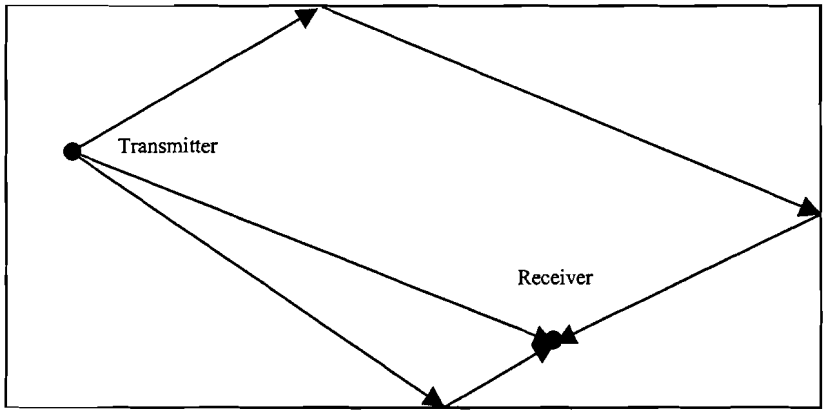

Figure 3.7: *Ray propagation in closed room.*

The figure shows the position of a transmitter and a receiver (by black dots), the direct ray between them and some of the propagation paths for rays that undergo reflections at the walls. The receiver is assumed to be in the far field of the transmitter. Furthermore, the antennas are not too close to the walls (at least a wavelength for a $\lambda/2$ dipole). Due to the linearity of the field equations, the total electric field at the position of the receiver may be obtained as a superposition of the fields arriving from the different discrete directions. In a Cartesian coordinate system, the x-component of the electric field, for example, is obtained than as

$$E_x(x,y,z,t) = \sum_{n=1}^{N} E_x^n(x,y,z)\exp(j\omega(t+\tau_n)), \tag{3.16}$$

where τ_n is the time delay introduced by ray n. In a similar way the y- and z-component of the electric field can be obtained.

3.3.1 Two-ray model

We start by considering the situation where we have a transmitter and a receiver above a reflecting ground. We consider the existence of a direct ray and a reflected ray, as shown in figure 3.8. In this case we use isotropic antennas, the use of Hertzian dipoles would make the multi-path analysis more complicated.

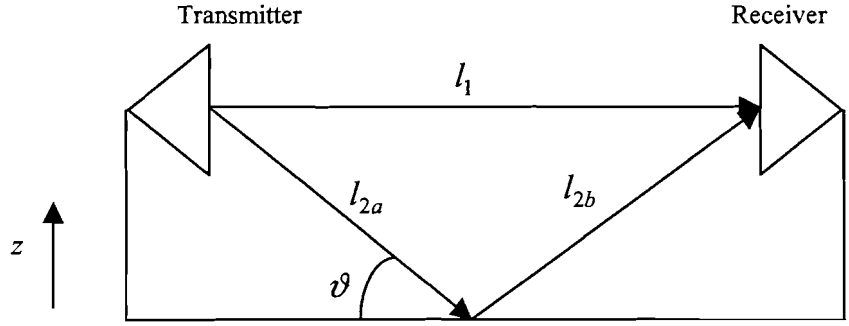

Figure 3.8: *Two-ray model, path length difference* $\Delta l = l_{2a} + l_{2b} - l_1$.

The received electric field consists of the field received via the direct link, $\vec{E}_{direct}$, with path length l_1, and the received field via the reflection link, $\vec{E}_{reflected}$, with path length $l_2 = l_{2a} + l_{2b}$.

3.3.1.1 Field calculation

At the receive antenna the time average field power density S for z-polarised waves in the far-field is [Herben, 2000]

$$S = \frac{|E_z|^2}{2Z_0} = \frac{\left|\vec{E}_{direct} + \vec{E}_{reflected}\right|^2}{2Z_0}. \tag{3.17}$$

Due to the difference in path length between the direct wave and reflected wave, $\Delta l = l_{2a} + l_{2b} - l_1$, we get a phase difference. The reflection coefficient adds another phase difference and a magnitude factor. This phase change, 0° or 180°, depends on the polarisation and the angle of incidence. For the environment of figure 3.8 the waves propagate through air with dielectric constant ε_0 and the reflected medium has a relative dielectric constant ε_r. The reflection coefficient s_v is [Herben, 2000]

$$s_v = \frac{\varepsilon_r \sin\vartheta - \sqrt{\varepsilon_r - \cos^2\vartheta}}{\varepsilon_r \sin\vartheta + \sqrt{\varepsilon_r - \cos^2\vartheta}}, \tag{3.18}$$

for vertically or perpendicularly polarised waves with respect to the plane of incidence. When the floor is perfectly conducting,

$\varepsilon_r \rightarrow -j\infty$, the reflection coefficient is 1. If the antennas are on the same height we get $l_1 = l_2 \cos\upsilon$. When the separation between the antennas is large compared to the height the angle of incidence is small and $l_1 \approx l_2$. Furthermore, if $l_1 \approx l_2$, there is mainly a vertical component of the electric field and the power density is,

$$S = \frac{\left|E_z/l_1 + s_v\, e^{jk_0(l_2-l_1)}\, E_z/l_2\right|^2}{2Z_0} \xrightarrow{l_1 \approx l_2} \frac{|E_z|^2}{2\,Z_0\, l_1^2}\left|1 + s_v\, e^{jk_0(l_2-l_1)}\right|^2. \tag{3.19}$$

At grazing angle, $\upsilon = 0$, the reflection coefficient is -1 and l_2-l_1 is small so the received power has a minimum and can be written as:

$$S_{received} \approx S_{direct}\,(k_0 \Delta l)^2. \tag{3.20}$$

At this angle there is also another propagating phenomena: the surface wave. This wave propagates, if we do not have a perfect conducting ground, along a dielectric interface. For microwave frequencies, surface wave propagation can be ignored [Vaughan et al, 2003].

3.3.1.2 Power distribution

The power density depends on free-space attenuation and interference. Using Eq. (3.19), the power density can be written as

$$S \approx \frac{|\vec{E}_z|^2}{2\,Z_0\, l_1^2}\left|1 + s_v\, e^{jk_0(l_2-l_1)}\right|^2 = S_{direct}\left|1 + s_v\, e^{jk_0(l_2-l_1)}\right|^2 = S_{direct}\,|H(l)|^2. \tag{3.21}$$

When we move 1 m above the ground and assume that the direct wave and reflected wave have the same magnitude we get at 2.4 GHz a pattern as shown in figure 3.9.

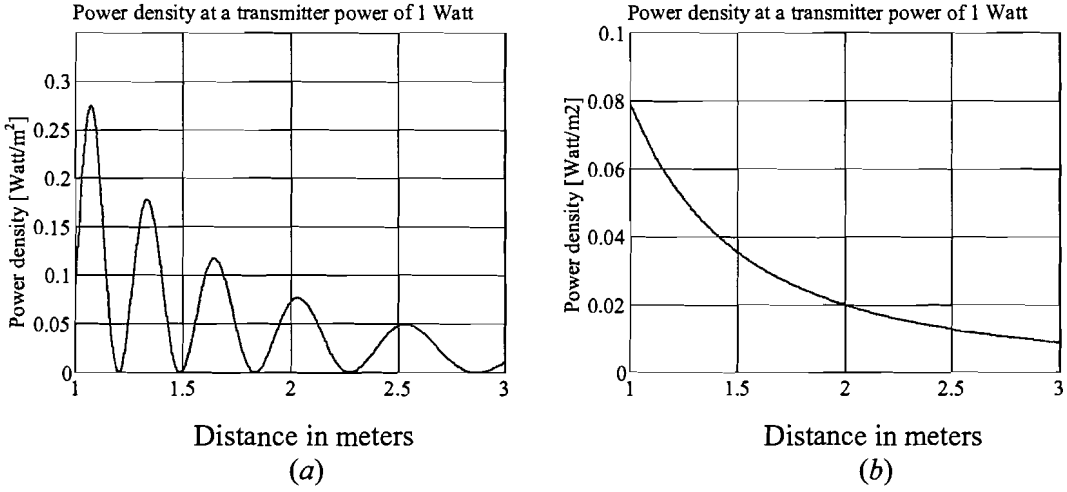

Figure 3.9: *Power transfer of the (a) two-ray model and (b) one-ray model, isotropic antennas are assumed.*

From this figure we can observe that the mean power density is twice the mean power density for the free-space model. This can be explained if we assume that the radiated field is generated by an antenna above the conducting ground, and a mirrored antenna below the conducting ground. When the waves are in phase the amplitude of the electric field strength and the magnetic field strength doubles and the power density increases by a factor of 4. The second factor in equation (3.21) is the transfer function and has the form,

$$\left|H(l)\right|^2 = \left|1 + s_v\, e^{jk_0\,(l_2 - l_1)}\right|^2 = 1 + s_v^2 + 2s_v \cos k_0 \Delta l, \quad \Delta l = l_2 - l_1, \tag{3.22a}$$

and substituting $k_0 = \omega / c_0$ in Eq. (3.22a) gives in the frequency domain,

$$\left|H(\omega)\right|^2 = 1 + s_v^2 + 2s_v \cos \omega \Delta \tau, \tag{3.22b}$$

where $\Delta\tau = \Delta l / c$ is the propagating time difference. The pdf of the power transfer function can be derived using Eq. (3.22a) or (3.22b). When we use Eq. (3.22a) the receiving antenna moves uniform in the horizontal l-direction and every position has an equal probability. And equivalent when we use Eq. (3.22b) the frequency distribution is uniform in such a way that the phase changes uniformly between 0° and 180°. In a similar way as Eq. (3.9) we get

$$f_{|H|^2}(|H|^2) = f_{\Delta l}(\Delta l) \left| \frac{\partial \Delta l}{\partial |H|^2} \right| \tag{3.23}$$

with $0 \le \Delta l \le \dfrac{\lambda}{2}$, $f_{\Delta l}(\Delta l) = \dfrac{2}{\lambda}$, $\left(\int_0^{\lambda/2} f_{\Delta l}(\Delta l)\, d\Delta l = 1 \right)$ and

$$\Delta l = \frac{\lambda}{2\pi} \arccos\left(\frac{|H|^2 - (1 + s_v^2)}{2s_v} \right), \tag{3.24}$$

and finally

$$f_{|H|^2}(|H|^2) = \frac{1}{\pi \sqrt{(2s_v)^2 - (|H|^2 - (1 + s_v^2))^2}}\,. \tag{3.25}$$

When the reflection coefficient s_v has modulus one, this simplifies to

$$f_{|H|^2}(|H|^2) = \frac{1}{\pi \sqrt{|H|^2 (4 - |H|^2)}}\,. \tag{3.26}$$

This distribution has a bath-tub shape as shown in figure 3.10. From this distribution we observe that probability density of a fade, $|H| = 0$, and a peak, $|H| = 4$ in the power transfer is small. Furthermore, using Eq. 3.22 we observe that the expected power transfer is 2. This was expected, the transmitted power is distributed over the half space.

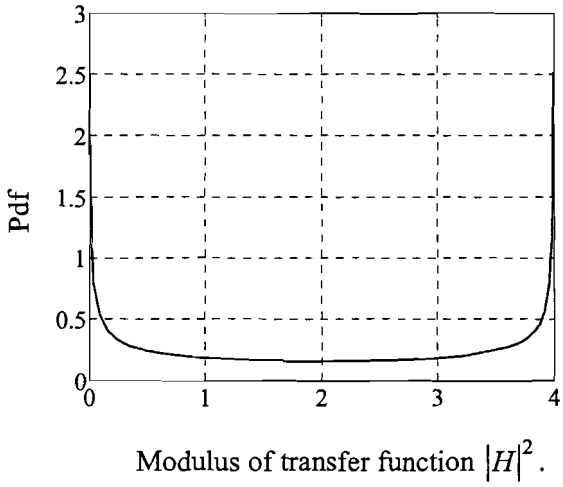

Figure 3.10: *The pdf of the power density transfer function* $|H|^2$ *for a perfect conducting ground.*

3.3.1.3 Delay spread and coherence bandwidth

Now that we know how the power density is distributed we can look at the power distribution in time and frequency domain. The delay spread is measured using the power distribution in time, the so-called power profile. To get the received power we need to multiply the power density with the effective antenna aperture. The field distributions in time and frequency are related by the Fourier transform. This is why we can start with the more intuitive response in the time domain and will arrive later in the frequency domain. In the time domain we have two rays propagating with the same speed but arriving at a different time due to the difference in path length. We will start the time-domain analysis by defining the impulse response of the radio channel as shown in figure 3.8. The transmitter cannot transmits a carrier modulated with a Dirac shaped pulse. However, the time response $h(t)$ of the two-ray model can be written as [Vaughan et al, 2003],

$$h(t) = \delta(t - t_1) + s_v \exp(j\alpha_2)\, \delta(t - t_2), \tag{3.27}$$

where the direct wave has a delay time t_1 and the reflected wave has a time delay t_2. The factor $s_v \exp(j\alpha_2)$ represents the reflection coefficient and a phase factor to account for path length difference. We can simplify Eq. (3.27) by shifting in time with the delay t_1, which results in

$$h(t) = \delta(t) + s_v \exp(j\alpha_2)\, \delta(t - \tau). \tag{3.28}$$

where $\tau = t_2 - t_1$. The received power P is then

$$P(t) = \frac{d}{dt} \int_{-\infty}^{t} \left\langle |h(u)|^2 \right\rangle du. \tag{3.29a}$$

The integral of equation (3.29) is not trivial. However, the power and magnitude of the signal have the same time dependence. The power profile can be written as [Vaughan et al, 2003]

$$P(t) = \delta(t) + s_v^2 \delta(t - \tau) \tag{3.29b}$$

The time response of the power, the power profile, is an important measure of the multi-path behaviour of the radio link. For the two-ray model the width of the power profile is small when the direct wave is strong compared to the reflected wave or when there is little time difference. The

standard deviation of this profile is the delay spread. The standard deviation is related to the first two moments of the power profile and is given by [Dehling et al, 1995]

$$\tau = \sqrt{\langle t^2 \rangle - \langle t \rangle^2}\,, \tag{3.30}$$

where the operator $\langle\ \rangle$ represents the expectation and t is time. The moments originate from statistics. Most probability distributions have a moment generating function [Dehling et al, 1995]. The derivatives of this function form a series containing the expectations of the powers of the stochastic variable. The first moment and second moment are [Vaughan et al, 2003]

$$\langle t \rangle = \frac{\int_0^\infty tP(t)\,dt}{\int_0^\infty P(t)\,dt} \quad \text{and} \quad \langle t^2 \rangle = \frac{\int_0^\infty t^2 P(t)\,dt}{\int_0^\infty P(t)\,dt}, \tag{3.31}$$

where $P(t)$ is the received power. For the two-ray model we get using Eq. (3.29) and (3.30) a delay spread:

$$\tau = \sqrt{\frac{s_v^2 t_1^2}{1+s_v^2} - \left(\frac{s_v^2 t_1}{1+s_v^2}\right)^2} = \frac{s_v t_1}{1+s_v^2}\,. \tag{3.32}$$

For periodic signals, the delay spread causes interference like inter symbol interference and fading. From an electrical engineering point of view the radio link or channel behaves like a combiner with different delays. The combiner behaves like a filter for periodic signals. For an ideal filter the frequency response is flat and the time response would be a Dirac pulse. A wider delay spread tells us that the radio link behaves like a narrow bandpass filter.

The next step is to investigate the channel response in the frequency domain. In the frequency domain the delay spread transforms to the coherence bandwidth. The coherence bandwidth B_c is a statistical measure over frequency over which the channel can be considered 'flat', that is all spectral components have approximately equal gain and linear phase [Leyten, 2001]. The coherence is defined using the auto-correlation in frequency [Vaughan et al, 2003],

$$C(\Omega) = \left|\frac{R(\Omega)}{R(0)}\right|, \tag{3.33}$$

where the frequency offset is Ω. The coherence function C is the modulus of the normalised auto-correlation R. If we evaluated the coherence over a finite bandwidth we get [Vaughan et al, 2003],

$$C(\Omega) = \frac{\int_{\omega 1}^{\omega 2} H(\omega)H^*(\omega+\Omega)\,d\omega}{\int_{\omega 1}^{\omega 2} H(\omega)H^*(\omega)\,d\omega} \quad \xleftarrow{\text{estimate}} \quad \frac{P(t)}{\int_{t1}^{t2} P(t)dt} = \frac{\left\langle |h(t)|^2 \right\rangle}{\int_{t1}^{t2} \left\langle |h(t)|^2 \right\rangle dt}. \tag{3.34}$$

This expression is exact for a transform over the frequency and time domain that contains all the energy. The auto-correlation has a maximum for $\Omega = 0$, in the time domain this is the power peak at $t = 0$, so without the propagation delay. For example when we have an ideal bandpass filter, a rectangle, the coherence or auto-correlation function is a triangle. Strictly the time average and

sample average should be equal, i.e., the signals are ergodic. To simplify the calculation and to remove the propagation delay we shift the power profile $-\tau/2$ in time and normalise the power,

$$P(\tau)=\frac{\delta(t-\tau/2)+s_v^2\delta(t+\tau/2)}{1+s_v^2}. \tag{3.35}$$

We then get for the coherence function

$$C(\Omega)=\frac{\exp(j\Omega\tau/2)+s_v^2\exp(-j\Omega\tau/2)}{1+s_v^2}. \tag{3.36}$$

The coherence bandwidth, $\Omega_C=2\pi B_C$ [rad/sec], is the bandwidth defined by the decrease in the coherence function compared to the maximum value. The decrease factor taken by various authors is between 1/e to 0.9. To calculate the bandwidth we first have to calculate the magnitude of the coherence function. When the modulus of the reflection s_v is one Eq. (3.36) becomes

$$\left|C(\Omega)\right|=\left|\cos(\Omega\tau/2)\right|. \tag{3.37}$$

At 1/e, 3 dB and 0.9 decrease the coherence bandwidth in Hertz B_C is respectively,

$$B_{C1/e}=\frac{1}{\pi\tau}\arccos(0.37)=\frac{1}{2.6\tau},\quad B_{C3dB}=\frac{1}{3\tau}\quad\text{and}\quad B_{C0.9}\approx\frac{1}{2\pi\tau}. \tag{3.38}$$

We can use the coherence in frequency to predict coherence in space. This is important for spatial diversity where we need an optimum separation between the antennas. Changing the phase using the frequency at a fixed distance is equivalent to changing a distance at a fixed frequency. The two equations (3.22a) and (3.22b) show this equivalence. The change in distance is here the change in path length difference Δl between the direct wave and the reflected wave. The relation between them is

$$\Delta l=\sqrt{height_{antenna}^2+l^2}-l=q\lambda=q\frac{c_0}{f},\quad \Delta l\left(1\pm\Delta\Delta l/\Delta l\right)=q\frac{c_0}{f\left(1\mp\Delta f/f\right)}, \tag{3.39}$$

where q is a function of l, the separation between the antennas. In figure 3.8 and 3.11 the difference in path length, Δl, at 3 m separation is 60 cm. This gives a delay difference of about 2 ns. Using equation (3.39) we see that the associated coherence bandwidth for a minimum coherence is about $1/2\tau = 250$ MHz. Assuming a centre frequency of 2400 MHz, the 10 % change in frequency gives a change of about 10 % in path difference or 6 cm. This is as expected $\lambda/2$, the path length difference between to waves with the same phase and waves with an opposite phase. When the path difference is 6 cm, the distance between transmit antenna and receive antenna changes about 40 cm. This is in good agreement with the separation between peak and fade at 3 m depicted in figure 3.9a. For the two-ray model we can achieve a negative power correlation with an antenna separation between 10 cm and 40 cm in the 1 to 3 meter range, as can be observed from figure 3.9a.

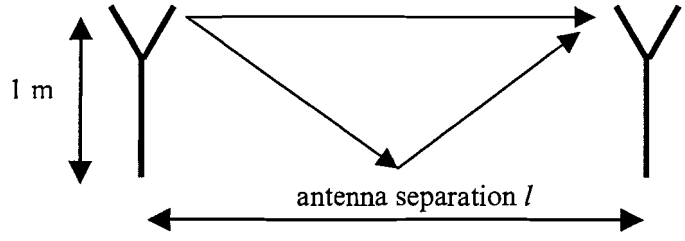

Figure 3.11: *Configuration of two-ray model.*

3.3.2 Multi-ray model using stochastic techniques

Multiply reflected waves can be treated in a similar way as the two-ray model. A more effective approach is to use a stochastic model that uses some properties of the reflected waves. It can be proven that for equal ray powers the power distribution of the multi-ray model converges to the stochastic model when the number of rays increases [Vaughan, et al 2003]. The stochastic approach seems plausible when we consider received power distribution in the neighbourhood of an antenna. Then the amplitude of the arriving rays stays almost the same but the phase changes fast.

3.3.2.1 Field/power distribution

In Appendix A the details of statistical fading distributions for an indoor environment are presented. The most important amplitude distribution is the well-known Rayleigh-Rice distribution, of which the pdf is given by [Vaughan et al, 2003]:

$$f_a(a) = \frac{a}{\sigma^2} \exp\left(-\frac{a^2 + m^2}{2\sigma^2} \right) I_0\left(\frac{ma}{\sigma^2} \right) U(a), \tag{3.40}$$

where a is the amplitude of the received signal, σ^2 is the power of the reflected signals, m is the amplitude of the line of sight signal, I_0 is the modified Bessel function of the firts kind order zero and U is the unit step function. The amount of line of sight and non-line-of-sight of the radio link is expressed using a ratio K,

$$K(\vec{r}) = \frac{\text{power direct waves}}{\text{power scattered waves}} = \frac{\sum_{i=1}^{N} m_i^2/2}{\sum_{i=1}^{N} \sigma_i^2}, \tag{3.41}$$

where N is the number of degrees of freedom. For the Rayleigh–Rice distribution $N = 2$ and

$$K_{Rice} = \frac{m^2}{2\sigma^2}. \tag{3.42}$$

The power in the direct waves is the sum of the means squared and the power in the reflected waves is the sum of the variances in the variates $n\sigma^2$ or the variance in the envelope σ^2. This makes it possible to write the distribution using K as a parameter and Eq. (3.40) becomes

$$f_a(a) = \frac{a}{\sigma^2} \exp\left(-\frac{a^2}{2\sigma^2} - K \right) I_0\left(\frac{a}{\sigma}\sqrt{2K} \right) U(a). \tag{3.43}$$

The distribution of the received power p and the distribution of the amplitude a are related by

$$a = \sqrt{2p}, \quad f_p(p) = f_a(a) \left| \frac{d\sqrt{2p}}{dp} \right| = \frac{f_a(a)}{a}. \tag{3.44}$$

The result is the following expression for the power distribution [Vaughan et al, 2003],

$$f_p(p) = \frac{1}{\sigma^2} \exp\left(-\frac{p}{\sigma^2} - K \right) I_0\left(\frac{2\sqrt{pK}}{\sigma} \right) U(p). \tag{3.45}$$

If $K = 0$ we have non-line-of-sight, this distribution is called the Rayleigh distribution. When $K >> 1$ the direct wave is dominant and for $K \rightarrow \infty$ we have the free-space model. For a small area the power ratio between direct waves and indirect waves stays the same and K is constant. For the complete domain, e.g., an office room, we can make connected subdomains with the same K to approximate the propagation. The amplitude distribution with parameter K is depicted in figure 3.12a. Furthermore, the phase distribution is presented in figure 3.12b.

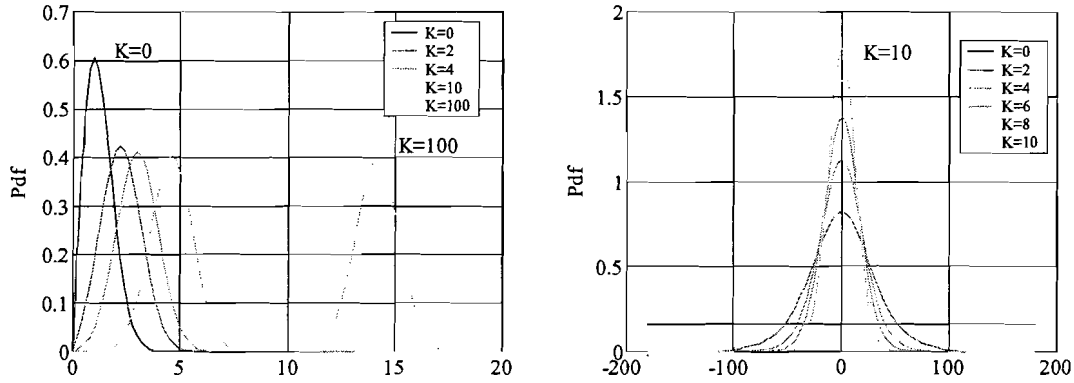

(*a*) (*b*)

Figure 3.12: *Pdf of (a) the envelope and (b) the phase for various values of K.*

A high K means line-of-sight with a limited number of scatterers, so a good radio link. In the situation where K is small, antenna diversity will be most effective. With increasing K, the de-correlation distance increases (see Appendix B), which makes antenna diversity less effective.

3.3.2.2 Coherence bandwidth

In the time domain the impulse response is the sum of the direct wave and the scattered waves. The waves that travel along the longest path have the largest time delay. Taking into account that the power in a radio channel decreases quadratically with the distance and that the field is attenuated by reflections, we can derive the following expression for the expected power profile [Vaughan et al, 2003]

$$P(\tau) = \frac{r^2}{2}\delta(t - t_1) + \frac{\sigma^2}{\Delta\tau}\exp\left(-(t - t_1)/\tau\right). \tag{3.46}$$

The first term in Eq. (3.46) is the direct wave with a time delay t_1 and the second term represents the reflected waves where τ is the rms delay spread. It is convenient to remove the delay t_1. For Rayleigh fading the first term is zero and Eq.(3.46) becomes

$$P(\tau) = \frac{\sigma^2}{\Delta\tau}\exp(-t/\tau). \tag{3.47}$$

The corresponding coherence bandwidth at 3 dB is given by [Vaughan et al, 2003]

$$B_C = \frac{1}{\Delta\tau} \tag{3.48}$$

3.4 Cavity model

In this section an analytical model is described to calculate the electromagnetic field in an indoor environment. The indoor environment is modelled as a rectangular cavity with perfect electrically conducting walls. Within this cavity the Maxwell equations apply, subject to the boundary conditions imposed by the walls of the cavity. As a first step the electromagnetic field generated by a point source, the so-called Green's function, will be calculated. Once the Green's function is known, the radiated electromagnetic field generated by an arbitrary antenna may be obtained as a superposition of point sources distributed over this antenna.

3.4.1 Model description

We will consider the configuration as depicted in figure 3.13. The room is enclosed by the boundary S which consists of perfect conducting walls ($\sigma \rightarrow \infty$). The electric field $\vec{E}(\vec{r})$ and the magnetic field $\vec{H}(\vec{r})$ in a homogenous region satisfy Maxwell's equations [Smolders, 2000],

$$\nabla \times \vec{E}(\vec{r}) = -j\omega\mu \vec{H}(\vec{r}), \tag{3.49a}$$

$$\nabla \times \vec{H}(\vec{r}) = j\omega\varepsilon \vec{E}(\vec{r}) + \vec{J}(\vec{r}), \tag{3.49b}$$

$$\nabla \cdot \vec{H}(\vec{r}) = 0, \tag{3.49c}$$

$$\nabla \cdot \vec{E}(\vec{r}) = \frac{\rho_e(\vec{r})}{\varepsilon}, \tag{3.49d}$$

where μ is the permeability of the medium in the cavity, ε is the permittivity of the medium and ρ_e and $\vec{J}$ represent the electric charge density and the electric current density on the transmitting antenna. Time harmonic fields are assumed, meaning that an $\exp(j\omega t)$ time dependence is assumed and suppressed. The medium in the cavity is assumed to be isotropic, homogeneous and linearly reacting with:

$$\varepsilon = \varepsilon' - j\varepsilon'', \tag{3.50a}$$

$$\mu = \mu' - j\mu''. \tag{3.50b}$$

We will assume that $\varepsilon = \varepsilon_0$ and $\mu = \mu_0$ in the rest of this section. Since the walls are perfectly conducting we have the following boundary conditions on the surface S:

$$\vec{n} \times \vec{E}(\vec{r}) = \vec{0}, \quad \vec{r} \in S, \tag{3.51}$$

where $\vec{n}$ is the inward directed normal on the cavity surface as depicted in figure 3.13,

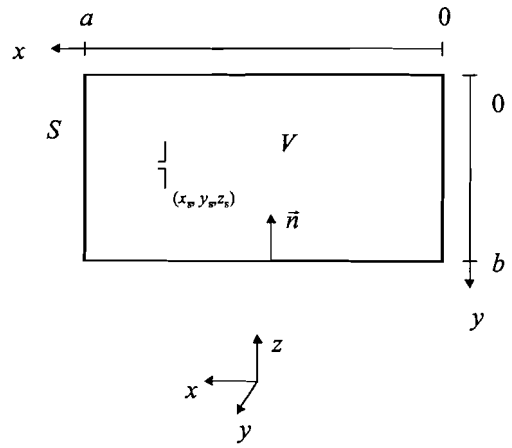

Figure 3.13: *Two-dimensional projection of the cavity with volume V, surface S and $\vec{n}$ normal to S.*

where a is the length in the x-direction, b is the length in the y-direction, c is the length in the z-direction and (x_s, y_s, z_s) are the coordinates of the antenna.

3.4.1.1 Green's function

The calculation of Green's function of the magnetic vector potential and Green's function of the electric field x-component is done in detail in Appendix C. In the following part we follow the core of the derivation. When we know the field equations, excitation function and boundary conditions the problem is well posed, i.e., the solution exists, is unique and stable [Strauss, 1992]. The magnetic field is divergence free, $\nabla \cdot \vec{H} = 0$. The magnetic field $\vec{H}$ can be presented as the curl of a magnetic vector potential $\vec{A}$,

$$\vec{H}(\vec{r}) = \frac{1}{\mu} \nabla \times \vec{A}(\vec{r}), \tag{3.52}$$

where $\vec{A} = A_x \vec{e}_x + A_y \vec{e}_y + A_z \vec{e}_z$. In the cavity the vector potential satisfies the Helmholtz equation [Smolders, 2000],

$$\nabla^2 \vec{A}(\vec{r}) + k_0^2 \vec{A}(\vec{r}) = -\mu J(\vec{r}). \tag{3.53}$$

In the above equation $k_0^2 = \omega^2 \varepsilon \mu$, where k_0 is the wave number. The electric field can be expressed in terms of the vector potential by substituting Eq. (3.52) into Eq. (3.50b) and using the Lorentz gauge [Smolders, 2000],

$$\vec{E}(\vec{r}) = -j\omega \left[\vec{A}(\vec{r}) + \frac{1}{k_0^2} \nabla \nabla \cdot \vec{A}(\vec{r}) \right]. \tag{3.54}$$

The expressions for the magnetic and electric field are:

$$\vec{H}(\vec{r}) = \frac{1}{\mu} \begin{bmatrix} \partial_y A_z - \partial_z A_y \\ \partial_z A_x - \partial_x A_z \\ \partial_x A_y - \partial_y A_x \end{bmatrix}, \tag{3.55}$$

$$\vec{E}(\vec{r}) = -\frac{j\omega}{k_0^2}\begin{bmatrix}(k_0^2+\partial_x^2)A_x+\partial_x\partial_y A_y+\partial_x\partial_z A_z\\(k_0^2+\partial_y^2)A_y+\partial_x\partial_y A_x+\partial_y\partial_z A_z\\(k_0^2+\partial_z^2)A_z+\partial_x\partial_z A_x+\partial_y\partial_z A_y\end{bmatrix}. \tag{3.56}$$

The Green's function is now defined as the magnetic vector potential created by a unit electric current source. The magnetic vector potential resulting from a current distribution $\vec{J}(\vec{r})$ is then found by writing this current distribution as a summation of an infinite number of elementary unit sources and integrating the contributions of these elementary sources. The point source with the direction $\vec{J} = J_x\vec{e}_x + J_y\vec{e}_y + J_z\vec{e}_z$ at $\vec{r}_s$ the source is represented by:

$$\vec{J}(\vec{r}) = I_o\delta(\vec{r}-\vec{r}_s)\frac{\vec{J}}{|\vec{J}|} \quad [\mathrm{Am}^{-2}], \tag{3.57}$$

and the magnetic vector potential becomes

$$\vec{A}(\vec{r}) = \iiint_{V_0}\overline{\overline{G}}_A(\vec{r},\vec{r}_0)\cdot\vec{J}(\vec{r}_0)\,dV_0\,, \tag{3.58}$$

where V_0 is a volume that encloses the source currents. The dyadic Green's function can be presented in matrix form by:

$$\overline{\overline{G}}_A = \begin{bmatrix}G_{Axx} & G_{Axy} & G_{Axz}\\G_{Ayx} & G_{Ayy} & G_{Ayz}\\G_{Azx} & G_{Azy} & G_{Azz}\end{bmatrix}. \tag{3.59}$$

When only a x-directed point source is present Eq. (3.53) reduces to a scalar parabolic partial differential equation

$$\nabla^2 G_{Axx} + k_0^2 G_{Axx} = -\mu_0\delta(\vec{r}-\vec{r}_o)\,. \tag{3.60}$$

To solve Eq. (3.60) we need to translate the boundary conditions of the electric and magnetic fields into the boundary conditions for the magnetic vector potential. We can substitute Eq. (3.56) in Eq. (3.51), which results in the boundary conditions for G_{Axx} at the cavity surface S:

$$G_{Axx}(x,0,z) = 0\,, \qquad G_{Axx}(x,b,z) = 0\,, \tag{3.61a}$$

$$G_{Axx}(x,y,0) = 0\,, \qquad G_{Axx}(x,y,c) = 0, \tag{3.61b}$$

$$\frac{\partial}{\partial x}G_{Axx}(x,y,z)\Big|_{x=0} = 0\,, \qquad \frac{\partial}{\partial x}G_{Axx}(x,y,z)\Big|_{x=a} = 0\,. \tag{3.61c}$$

The cavity is a box so we can describe the field using a Fourier triple series. It is possible to write G_{Axx} as a double series due to the boundary conditions in the y and z boundaries. Using the expansion in Fourier series we can express G_{Axx} as:

$$G_{Axx} = \sum_{m=1}^{\infty}\sum_{n=1}^{\infty}\sin(k_{ym}y)\sin(k_{zn}z)F_{mn}(x) \text{ with } k_{ym} = \frac{m\pi}{b} \text{ and } k_{zn} = \frac{n\pi}{c}\,. \tag{3.62}$$

An important next step is to write the source current as a Fourier series by making use of the orthogonality relation of the sine function [Dolmans, 1996],

$$\delta(\vec{r}-\vec{r}_s)=\frac{4}{bc}\sum_{m=1}^{\infty}\sum_{n=1}^{\infty}\sin(k_{ym}y)\sin(k_{ym}y_s)\sin(k_{zn}z)\sin(k_{zn}z_s)\,\delta(x-x_s). \tag{3.63}$$

Substitution of Eq. (3.62) and Eq. (3.63) in Eq.(3.60) results in a of one-dimensional differential equation:

$$\begin{aligned}&\frac{d^2}{dx^2}F_{mn}(x)+k_x^2F_{mn}(x)=-\frac{4\mu_0}{bc}\sin(k_{ym}y_s)\sin(k_{zn}z_s)\,\delta(x-x_s),\\&k_x=\sqrt{k_0^2-k_{ym}^2-k_{zn}^2},\end{aligned} \tag{3.64}$$

where $F_{mn}(x)$ is a linear combination of a homogenous part and a particular part. The solution is divided in two parts:

$$F_{mn}(x)=\begin{cases}F_{mn}^1(x) & 0<x\le x_s,\\ F_{mn}^2(x) & x_s<x<a.\end{cases} \tag{3.65}$$

The function $F_{mn}(x)$ can be expanded in a Fourier series:

$$\begin{aligned}F_{mn}^1(x)&=A_{mn}^1\cos(k_xx)+B_{mn}^1\sin(k_xx),\\F_{mn}^2(x)&=A_{mn}^2\cos(k_x(x-a))+B_{mn}^2\sin(k_x(x-a)).\end{aligned} \tag{3.66}$$

If $F_{mn}(x)$ is a solution of Eq. (3.64), $F_{mn}(x)$ has to be continuous at $x=x_s$,

$$F_{mn}^1(x_s)=F_{mn}^2(x_s). \tag{3.67}$$

The first derivative $\frac{d}{dx}F_{mn}(x)$ has a discontinuity at $x = x_s$. When we substitute Eq. (3.66) in Eq. (3.64) we arrive at

$$-\frac{d}{dx}F_{mn}^2(x_s+\varepsilon)+\frac{d}{dx}F_{mn}^1(x_s-\varepsilon)=-\frac{4\mu}{bc}\sin(k_{ym}y_s)\sin(k_{zn}z_s). \tag{3.68}$$

At this point six boundary conditions are available for solving the four unknowns in Eq. (3.66). First the boundary condition Eq. (3.61c) and Eq.(3.66) are used. The result is $B_{mn}^1=0$ and $B_{mn}^2=0$. To obtain the relationship between A_{mn}^1 and A_{mn}^2, we need the boundary condition at $x = x_s$ (see Appendix C). The final result for the vector potential G_{Axx} is:

Interval 1: $0\le x\le x_s$

$$G_{Axx}=-\frac{4\mu_0}{bc}\sum_{m=1}^{\infty}\sum_{n=1}^{\infty}\sin(k_{ym}y)\sin(k_{ym}y_s)\sin(k_{zn}z)\sin(k_{zn}z_s)\frac{\cos k_x(x_s-a)\cos(k_xx)}{k_x\sin(k_xa)} \tag{C.69}$$

Note that the Green's function and the delta function are expanded in the orthogonal eigenfunctions

$$\sin(k_{ym}y)\sin(k_{zn}z), \tag{3.70}$$

of the differential operator $\nabla^2 + k_0^2$, and Eq. (3.60) is equivalent to a matrix equation. Substituting the Green's function of the magnetic vector potential into Eq. (3.54) we can derive the Green's function of the electric field. Finally we get the expression for xx-component of the Green's function of the electric field:

Interval 1: $0 \le x \le x_s$

$$G_{Exx} = \frac{4\mu_0}{bck_0^2} \sum_{m=1}^{\infty} \sum_{n=1}^{\infty} (k_0^2 - k_x^2) \sin(k_{ym} y) \sin(k_{yn} y_s) \sin(k_{zn} z) \sin(k_{zn} z_s) \frac{\cos k_x (x_s - a) \cos(k_x x)}{k_x \sin(k_x a)} \tag{3.71}$$

$$G_{Exx} : (x, y, z, f, m_{\max}, n_{\max}) \rightarrow R$$

where k_x is the propagation constant in the x-direction. We see that the fields are reciprocal, by the symmetry of the Green's function $\overline{\overline{G}}(\vec{r}, \vec{r}_s) = \overline{\overline{G}}(\vec{r}_s, \vec{r})$. Further we notice that modes of the Green function can be zero. The modes with infinite amplitude, $k_x a = n\pi$ in Eq. 3.71, represent the resonant modes of the cavity.

3.4.1.2 Electromagnetic fields

With the Green's function of the electric field we finally can calculate the electric field components. In general we would need the dyad with all the Green's functions. For an antenna the current in the volume containing the antenna has to be integrated to get the total electric field

$$\vec{E}(\vec{r}) = -j\omega \int_{V_0} \overline{\overline{G}}_E(\vec{r}, \vec{r}_0) \vec{J}(\vec{r}_0) dV_0 . \tag{3.72}$$

For simplicity we only consider x-components and Eq. (3.72) reduces to

$$\vec{E}_x(\vec{r}) = -j\omega \int_{V_0} \overline{\overline{G}}_{Exx}(\vec{r}, \vec{r}_0) I_x f(\vec{r}_0) \vec{e}_x dV_0, \tag{3.73}$$

where

$$\vec{J}_x = I_x f(\vec{r}_0) \vec{e}_x, \tag{3.74}$$

is the current on the antenna surface where the amplitude of the current, $I_x f(\vec{r}_0)$, depends on the position along the antenna.

3.4.1.3 Numerical field solution

By using expression (3.71) the electromagnetic fields inside a cavity can be determined. This expression can only be evaluated by means of a numerical computation. This implies that the infinite double series needs to be truncated, which results in an approximation of the exact result. In this section we will investigate the truncation error. We can distinguish two domains in our numerical calculation. Domain D_1 represents the propagating waves with:

$$\left(\frac{m\pi}{b}\right)^2 + \left(\frac{n\pi}{c}\right)^2 - k_0^2 \le 0. \tag{3.75}$$

Domain D_2 is the region with evanescent waves and is determined by:

$$\left(\frac{m\pi}{b}\right)^2+\left(\frac{n\pi}{c}\right)^2-k_0^2>0. \tag{3.76}$$

Both domains are illustrated in figure 3.14. In domain 2 we can estimate the modulus of the truncation error by:

$$\left|G_{Exx}\right|_{\beta>k_0}\le\frac{4\mu_0}{bck_0^2}\sum_{m\in D_2}\sum_{n\in D_2}(k_0^2+\alpha_2^2)\frac{(e^{\alpha_2(x_s-a)}+e^{\alpha_2(x_s-a)})(e^{\alpha_2 x}+e^{\alpha_2 x})}{2\,\alpha_2(e^{-\alpha_2 a}-e^{\alpha_2 a})}, \tag{3.77}$$

where $\beta=\sqrt{(m\pi/b)^2+(n\pi/c)^2}$, $\alpha_2=|k_x|=\sqrt{(m\pi/b)^2+(n\pi/c)^2-k_0^2}$ and G_{Exx} represents the Green's function in domain 2. This can be rewritten as

$$\left|G_{Exx}\right|_{\beta>\beta_{\min}}\le\frac{2\mu_0}{bck_0^2}\sum_{m\in D_2}\sum_{n\in D_2}(k_0^2+\alpha_2^2)e^{\alpha_2(x-x_s)}g_1(\alpha_2), \tag{3.78}$$

with

$$g_1(\alpha_2)=\frac{(1+e^{-2\alpha_2(a-x_s)})(1+e^{-2\alpha_2 x})}{1+e^{-2\alpha_2 a}}. \tag{3.79}$$

Because $\frac{\partial g_1(\alpha_2)}{\partial\alpha_2}<0$ we get $g_1(\alpha_2)\le g_1(\alpha_{2\min})$ for $\alpha_2\ge\alpha_{2\min}$.

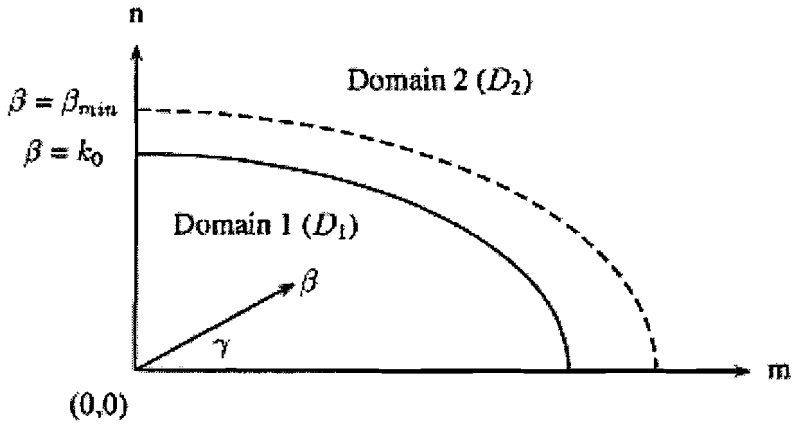

Figure 3.14: *Propagating domain D_1 and D_2 is the region with evanescent waves.*

In [Dolmans, 1997] the final expression for the absolute error is given for $0\le x<x_s$:

$$\left|G_{Exx}\right|_{\beta>\beta_{\min}}\le\frac{\mu g_1(\beta_{\min})}{\pi k^2}\left[-\frac{\beta_{\min}^2 e^{\varsigma}}{(x-x_s)}+2\frac{\sqrt{\beta_{\min}^2-k_0^2}\,e^{\varsigma}}{(x-x_s)^2}-2\frac{e^{\varsigma}}{(x-x_s)^3}\right] \tag{3.80}$$

where $\varsigma=\sqrt{\beta_{\min}^2-k_0^2}\,(x-x_s)$. In the neighbourhood of the source x_s, there is a problem with convergence. Figure 3.15 shows an example of the truncation error that is made for a realistic example, a room with dimensions of 5.2 x 3.65 m^2 at 2.4 GHz.

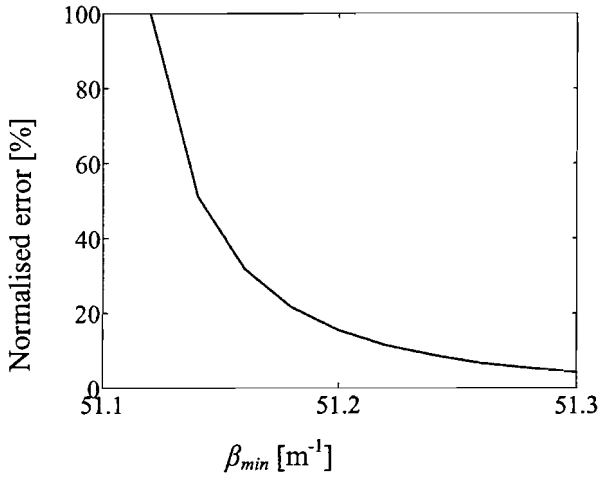

Figure 3.15: *Truncation error versus β_{min} (k_0 is about 50.27).*

The magnitude of the modes near the edge of the two domains D_1 and D_2 can become very large, on the edge the magnitude is infinite. The magnitude of the modes m, n for which k_x becomes very small behaves as k_x^{-2} as depicted in figure 3.16a and 3.16b.

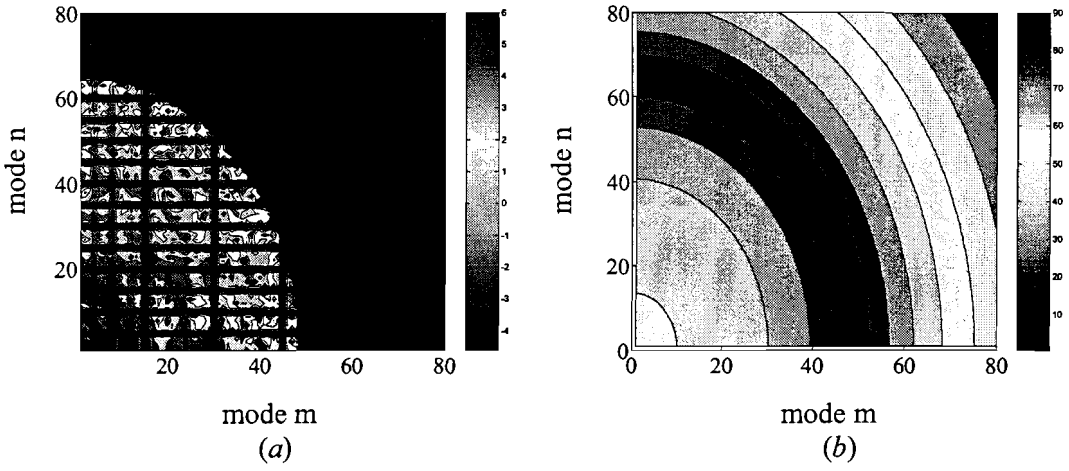

Figure 3.16: *Magnitude of the modes of G_{Exx} in log scale (a) and (b) magnitude of propagation factor k_x with 80 modes in y and 80 modes in z and the source at x = .752.*

It is now possible to estimate the minimum number of modes that are needed for an accurate result. The number of modes must be large enough, i.e., $(m\pi/b)^2 + (n\pi/c)^2 > \beta_{\min} > k_0^2 = (2\pi/\lambda)^2$. For a room with a size of 5.2 m by 3.65 m by 2.1 m, (a x b x c), and a wavelength of 12.5 cm we get

$$\left(\frac{m\pi}{3.65}\right)^2 = \left(\frac{2\pi}{.125}\right)^2 \text{ and } \left(\frac{n\pi}{2.1}\right)^2 = \left(\frac{2\pi}{.125}\right)^2, \tag{3.81}$$

which results in $m_{\min} = 59$ and $n_{\min} = 34$. For this room with dimension 5.2 x 3.65 m all the propagating modes and a part of the evanescent modes are calculated if we use 80 x 80 modes. A computer program was developed in Matlab using for loops to calculate the electromagnetic field in a cavity. Calculation of the field with a Pentium *II* 667 MHz with m_{min}=70, n_{min}= 70, 2601 points in the plane and 81 frequencies takes about 8 hours!. The result is a matrix of: (81 frequencies) x (number points x-direction) x (number of points y-direction) x (number of points in the z-direction). Numerical problems can occur when the magnitude of a mode is extremely high (near resonance). This is why the magnitude of the modes is displayed to check whether the combination of position

and frequency is too close to resonance. This resonant behaviour is due to a singularity in the denominator of the Green's function. The calculated electric field is very sensitivity to changes in the dimension of the room and in chances in the propagation constant.

3.4.1.4 Coherence bandwidth

The cavity with perfect conducting walls is an extremely resonant structure with an infinite Q. If the Q is infinite, the coherence bandwidth is zero and the coherence function is a delta function. Furthermore, Eq. 3.34 shows that the coherence function and the time response are a Fourier pair, so a delta function in the coherence transforms to a uniform distribution in the time domain. The power profile is infinite because the impulse response does not decay. The cavity model with perfect conducting walls does not give a realistic coherence bandwidth. A more realistic cavity has lossy walls or dielectric walls [Dolmans, 1997]. A lossy cavity has an exponential power profile [Collin, 1991]. An exponential power profile is typical for indoors [Vaughan et al, 2003]. The average power profile can be expressed as

$$P(\tau) = P_o \exp(-\tau/\Delta\tau) \text{ , with } \Delta\tau = \frac{Q}{\omega}, \tag{3.82}$$

where $\Delta\tau$ is the delay spread and Q is the quality factor. For the frequency coherence function we need the auto-correlation which is the Laplace transform of (3.83). We obtain,

$$P(\tau) = \frac{P_o}{\Delta\tau}\exp(-\tau/\Delta\tau) \leftrightarrow R(\Delta\omega) = P_o \frac{1}{1 + j\Delta\omega\Delta\tau}. \tag{3.83}$$

The correlation is given by

$$\rho = \left|\frac{R(\Delta\omega)}{R(0)}\right|^2 = \left|\frac{C(\Delta\omega)}{C(0)}\right|^2, \tag{3.84}$$

and for a zero mean amplitude the 3 dB bandwidth is

$$\frac{1}{2} = \left|\frac{1}{1 + j\Delta\omega\Delta\tau}\right|^2 \Rightarrow \Delta\omega = \frac{1}{\Delta\tau} = \frac{\omega}{Q}. \tag{3.85}$$

The same result can be derived by calculating the field energy [Jackson, 1963]. When the resonant frequencies are close to each other (the mode density is high), and the cavity is lossy, the frequency response of a resonant mode is not so sharp and there is some overlap between the frequency response of resonance modes. This will lead to a smoother frequency response of the cavity.

3.5 Mode stirred chamber

We can use the mode stirred chamber model to investigate the behaviour of an antenna in a 3-dimensional space where the incident waves arrive uniform over all the spatial angles. In practice the incident waves distribution will be somewhere between a uniform 2-dimensional and a uniform 3-dimensional model.
Perturbation of the lossless cavity is important because it gives a more realistic EM-field. For example, an office room is rectangular but all kinds of objects in the room perturb the EM-field. The perturbed field can be calculated by inserting a small lossy object in the cavity. Using the first variation of the field we end up with a complex propagating constant [Collin, 1991]. An extreme perturbation is present in the mode stirred chamber. This is a Faraday's cage with an antenna and a fan to stir the EM-field. This is interesting because it is a rectangular cavity but it is also realistic because takes into account all kinds of perturbations. The resulting field distribution is almost uniform and ergodic, i.e., the statistics over time and space yield to a similar result. The theory to model the statistical behaviour of the fields was first published by [Hill, 2002]. The assumption for this theory is that on average the field is uniform over all the angles of arrival. In short, at each point in the cavity the incident waves are independent in direction, polarisation and phase. This leads to the so-called entropy condition, the ensemble average power is equally distributed over the x, y and z-component of the field. For indoor propagation this represents the theoretical limit of six degrees of freedom of the incident waves. The mode stirred chamber is a lossy cavity, and when cw power is turned off the response is an exponentially decaying power.

The moments of the field are [Dijk, 2001]:

$$\left\langle \vec{E}(\vec{r}) \right\rangle = 0, \tag{3.86}$$

$$\left\langle \left| \vec{E}(\vec{r}) \right|^2 \right\rangle = E_0^2, \tag{3.87}$$

where E_0 is constant independent of position. We have a uniform distribution and for the rectangular components we get,

$$\left\langle |E_x|^2 \right\rangle = \left\langle |E_y|^2 \right\rangle = \left\langle |E_z|^2 \right\rangle = \frac{E_0^2}{3}. \tag{3.88}$$

This is called the entropy property like in statistical mechanics. The energy in the cavity is now simply the average EM energy density W times the volume V [Pozar, 1998]. Furthermore, there is an energy exchange between the electric field energy and the magnetic field energy in a cavity. The time average of both energies is equal and the energy is,

$$U = \langle W \rangle V = (\varepsilon E_0^2/2 + \mu H_0^2/2)\, V = \varepsilon E_0^2 V = \varepsilon E_0^2 abc. \tag{3.89}$$

where a, b and c are the length, width and the height of the cavity, respectively. The power is χ^2 distributed with two degrees of freedom (in phase and quadrature current),

$$f(p) = \frac{1}{2\sigma^2} \exp\left(-\frac{p}{2\sigma^2} \right). \tag{3.90}$$

The envelope of the electric field is χ distributed with six degrees of freedom (see Appendix A),

$$f(|E|) = \frac{|E|^5}{8\sigma^6} \exp\left(-\frac{|E|^2}{2\sigma^2} \right). \tag{3.91}$$

3.6 Hybrid model

The cavity model as presented in the previous section differs from practice, since in practice a room will have six dielectric walls. Extension of our cavity model to include the dielectric walls is not practical, because it would result in a complex model with extensive computing time. We propose here a more pragmatic solution that combines the cavity model with the free-space model. Furthermore, the measurements in the office room presented in chapter 6 show that for a NLOS radio link the cavity model is dominant, and for a LOS radio link the free-space propagation is dominant. The power loss of the not-perfect conducting cavity walls is equivalent with a power flow out of the cavity. The Pointing vector of both losses has the same direction and magnitude.

3.6.1 Model development

From the measurement results in chapter 6 it will become clear that there is a difference between the lossless cavity model and the measured data. But overall the cavity model appears to be the dominant model. The proposed hybrid model is a superposition of the two models. The hybrid model is a modified Rayleigh-Rice model. The Rayleigh-Rice model is characterised by the parameter $K(\vec{r}) = \dfrac{\text{power direct waves}}{\text{power scattered waves}}$, where the in phase and 180° out of phase components of scattered waves have Gaussian distribution. For the hybrid model we get

$$K(\vec{r}) = \frac{\text{power direct waves}}{\text{power perfect conducting cavity waves}}. \tag{3.92}$$

The electric field can be calculated using the two Green's functions of the models:

$$\begin{aligned} \vec{E}(\vec{r}) &= -j\omega \int_{V_0} \overline{\overline{G}}_E(\vec{r},\vec{r}_0)\cdot \vec{J}(\vec{r}_0)dV_0 \\ &= -j\omega \int_{V_0} [\overline{\overline{G}}_{Ecavity}(\vec{r},\vec{r}_0) + a_1\, \overline{\overline{G}}_{Efree}(\vec{r},\vec{r}_0)]\cdot \vec{J}(\vec{r}_0)dV_0 \end{aligned} \tag{3.93}$$

where $\overline{\overline{G}}_{Ecavity}(\vec{r},\vec{r}_0)$ is the Green's function of the cavity, $\overline{\overline{G}}_{Efree}(\vec{r},\vec{r}_0)$ the Green's function of the free-space propagation and a_1 is a constant related to the K-factor.

3.6.2 Field/Power calculation

The ratio between the cavity model and the free-space model a_1 can be fitted to the measurement data. One way to estimate the ratio a_1 between the field strength of the EM-field in cavity model and the free space model is to look at the temporal phase spread as depicted in figure 3.17a. In figure 3.17a measured data was used see also chapter 6.

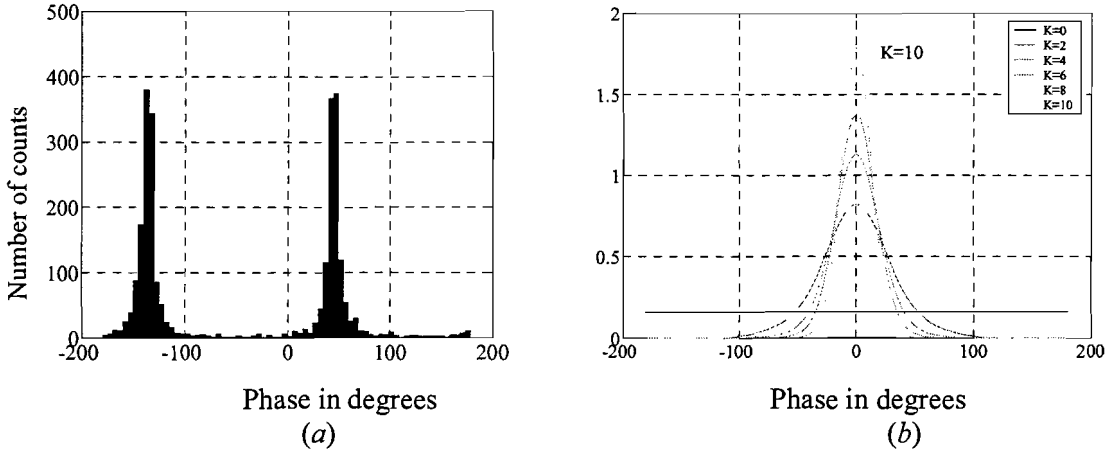

Figure 3.17: *Histogram of (a) measured propagation phase on the xy-table and (b) pdf of the phase for Rayleigh-rice fading at a fixed position of the xy-table.*

The cavity model predicts two phases for the field strength, -90° and 90° out of phase with the current, while the free-space model predicts a uniform phase distribution. In figure 3.17a we see that the cavity model is dominant. If we assume that the cavity component is larger than the free-field component we can estimate the composition,

$$E_z = E_{z\,cavity} + E_{z\,freespace}, \quad \vec{E}_z = |\vec{E}_{z\,cavity}| \angle \{-90,90\} + |\vec{E}_{z\,freespace}| \angle [0,2\pi], \tag{3.94}$$

where the electric field vector calculated with the cavity model has a discrete phase distribution at -90° and 90° and the electric field vector calculated with the free space model has a uniform phase distribution. The superposition of the two vectors is depicted in figure 3.18. The phasor of the electric field from the cavity model stays at a fixed position and the phasor of the electric field from the free-space model rotates. The phase-spread angle in figure 3.17a is:

$$\tan(\angle\text{spread}) \approx \frac{|\vec{E}_{z\,freespace}|}{|\vec{E}_{z\,cavity}|} \quad \angle\text{spread} \approx 30° \Leftrightarrow \tan(\angle\text{spread}) = 0.58 \tag{3.95}$$

The pdf of the phase of a dominant signal with a fixed phase and a smaller signal with a uniform phase distribution was already derived for the Rayleigh-Rice distribution, and is shown in figure 3.17b.

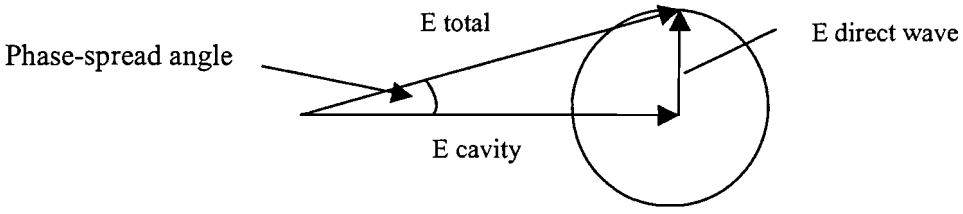

Figure 3.18: *The circle represents the locus of the total electric field vectors.*

From figure 3.17 we can observe that this measurement in not exactly a perfectly conducting room, behaves for 75 % like a cavity and for 25 % like a free-space model without reflections. The energy ratio is

$$\frac{Energy_{free-space}}{Energy_{cavity}} = \frac{|E_z|^2}{|E_z|^2} = \frac{0.58^2}{1^2} \approx 33\,\%. \tag{3.96}$$

When this energy ratio of 33 % (a_1 = 0.05) is used to calculate the EM-field using Eq. (3.93) we obtain the phase distribution depicted in figure 3.19a.

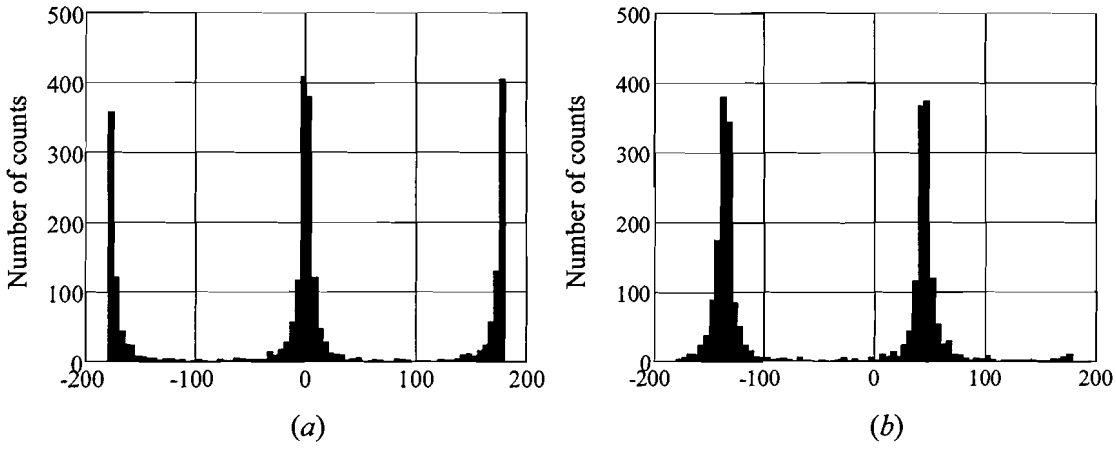

Figure 3.19: *Simulated phase distribution (a) and measured phase distribution (b).*

This figure shows that the measured data and the simulation with the hybrid model are in good agreement when we compare the phase distributions.

It is also possible to use the time response of the cavity to calculate the energy ratio. The rms delay spread of the measured data is about 40 nS. When the cavity model is used we find that the rms delay spread is infinite, the reflected waves do not decay. The simulation of the time response with the hybrid model with an energy ratio of 33 % results in a rms delay spread of 140 ns.

The EM field calculated with the hybrid model will be smoother, i.e., there will be less deep fades when the free-space propagation has more effect.

3.7 Antenna in a multi-path environment

In this paragraph we discuss the open-circuit voltage at the antenna terminals when the antenna is placed in a multi-path environment as depicted in figure 3.20. The receive antenna is in the far field of the transmit antenna. Furthermore, the radiation pattern of the receive antenna is the same as the radiation pattern for free-space propagation. In practice the antenna should be not to close to an object, then the radiation pattern of the antenna is not influenced by surrounding objects.

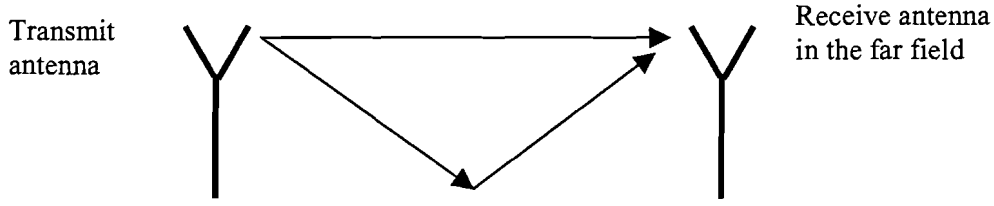

Figure 3.20: *Antenna configuration.*

When the incident field is a plane wave propagating in the horizontal plane we get for the a linear wire antenna with length L as shown in figure 3.21a,

$$V_{oc} = \left|\vec{E}_i\right| L \sqrt{\eta_{pol}}, \tag{3.97}$$

where V_{oc} is the open circuit voltage at the antenna terminals and η_{pol} is the polarisation efficiency. The polarisation efficiency is [Vaughan et al, 2003],

$$\eta_{pol} = \left|\vec{e}_i \cdot \vec{e}_r\right|^2, \tag{3.98}$$

where $\vec{e}_t \cdot \vec{e}_r$ is the inner product of the incident and the receive polarisation unit vectors.

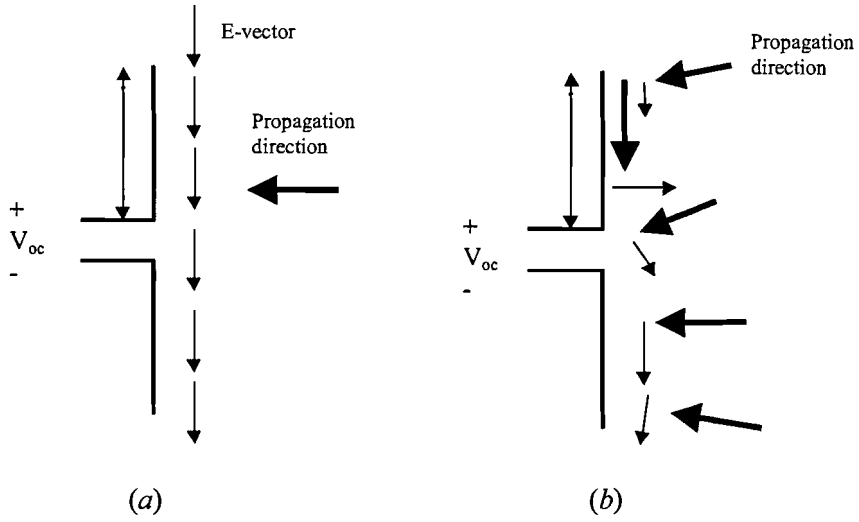

Figure 3.21: *Dipole receiving (a) a plane wave and (b) incident electric field in a multi-path environment.*

For a linear antenna, e.g., a dipole, the receive polarisation vector has the same direction as the antenna wire. The summation of the incident waves with different polarisations and phases can be expressed with an integral [Vaughan et al, 2003]

$$V_{oc} = \iint_{\Omega} \vec{E}_i(\theta,\varphi) \cdot \vec{h}(\theta,\varphi) \sin\theta \, d\theta \, d\varphi, \tag{3.99}$$

where $\vec{h}(\theta,\varphi) = h_\theta(\theta,\varphi)\vec{e}_\theta + h_\varphi(\theta,\varphi)\vec{e}_\varphi$, $\vec{E}_i(\theta,\varphi) = E_\theta(\theta,\varphi)\vec{e}_\theta + E_\varphi(\theta,\varphi)\vec{e}_\varphi$, h is the effective height and E_i is the incident electric field strength. The spherical angles in Eq. (3.99) are with respect to the antenna coordinate system. In Eq. (3.99) there is no r-component of the electric field. If the propagating wave has an r-component, the Poynting vector of the wave is not directed to the antenna and the wave does not arrive at the antenna if the antenna is small. The inner product takes care of the proper addition of different phases and polarisation. This is more complex than the free-space equation and important for diversity calculations. The antenna gain G is related to the complex height [Vaughan et al, 2003],

$$G(\theta,\varphi) \propto \left|\vec{h}(\theta,\varphi)\right|^2. \tag{3.100}$$

When we use an antenna sensitive to all spatial angles and two polarisations in an incident field the voltage at the antenna terminal, V_{oc} in Eq. (3.99), becomes a distribution with 4 degrees of freedom. Using Eq. (3.99) we see that an antenna that is electrically large and sensitive to different polarisations is already a diversity combiner using space and polarisation diversity.

3.7.1 The mean effective antenna gain

If the antenna is moving through a room the incident field and received power will be different at every position. This statistical behaviour of the received power can be described with the radiation pattern of the antenna and the distribution of the incident field. When we look at the effective antenna gain in a multi-path environment we can use the so-called Mean Effective Gain, (MEG). It is defined as [Taga, 1990]

$$\mathrm{MEG} = G_e = \frac{\langle p_{rec} \rangle}{\langle p_\theta \rangle + \langle p_\varphi \rangle} = \frac{P_{rec}}{P_V + P_H} \quad [\mathrm{dBi}], \tag{3.101}$$

where p_{rec} is the power received by the antenna, p_φ and p_θ are the powers for incident φ and θ-polarised waves, respectively. In Eq. (3.101) P_{rec} is the average received power, P_V and P_H are the average powers received of the incident for vertically and horizontally polarised waves, respectively, along a random route of the receiver. It is a measure of the ability of the antenna to absorb power out of the incident field. We may add the incident powers in the horizontal and vertical direction because we assume they are de-correlated. The cross-polarisation discrimination ratio (*XPD*) for the incident field is

$$XPD = P_V / P_H \,. \tag{3.102}$$

The received power is [Taga, 1990]

$$P_{rec} = \int_0^{2\pi} \int_0^{\pi} \left[P_1 G_\theta(\theta,\varphi) P_{\theta n}(\theta,\varphi) + P_2 G_\varphi(\theta,\varphi) P_{\varphi n}(\theta,\varphi) \right] \sin\theta \, d\theta \, d\varphi \,, \tag{3.103}$$

where P_1 and P_2 are the power received by the isotropic φ and θ-polarised antennas, receptively, G_θ and G_φ are the antenna power gain for θ and φ-polarised waves, respectively. $P_{\theta n}$ and $P_{\varphi n}$ are the normalised power densities for incident θ and φ-polarised waves, respectively. The antenna power gain G of a transmitting antenna in the far field is given by [Smolders, 2000],

$$G(\theta,\varphi) = \frac{P(\theta,\varphi)}{P_{in}/4\pi}, \tag{3.104}$$

where P_{in} is the input power at the antenna terminals. If the antenna efficiency is one Eq. (3.104) becomes

$$G(\theta,\varphi) = \frac{P(\theta,\varphi)}{P_t/4\pi}, \tag{3.105}$$

where P_t is the transmitted power. The antenna power gains for a receiving antenna G_θ and G_φ are then given by,

$$G_\theta(\theta,\varphi) = \frac{P_\theta(\theta,\varphi)}{P_t/4\pi}, \quad G_\varphi(\theta,\varphi) = \frac{P_\varphi(\theta,\varphi)}{P_t/4\pi}, \tag{3.106}$$

where P_{out} is the output power at the antenna terminals. The antenna power gains for a receiving antenna G_θ and G_φ have to satisfy the following condition:

$$\int_0^{2\pi}\int_0^{\pi}\{G_\theta(\theta,\varphi)+G_\varphi(\theta,\varphi)\}\,\sin\theta\,d\theta\,d\varphi=4\pi\,. \tag{3.107}$$

The normalised power densities $P_{\theta n}$ and $P_{\varphi n}$, with dimension [m^{-2}], have to satisfy the following condition:

$$\int_0^{2\pi}\int_0^{\pi}P_{\theta n}\sin\theta\,d\theta\,d\varphi=\int_0^{2\pi}\int_0^{\pi}P_{\varphi n}\sin\theta\,d\theta\,d\varphi=1\,. \tag{3.108}$$

The MEG becomes

$$G_e=\frac{1}{P_V+P_H}\int_0^{2\pi}\int_0^{\pi}\left[P_V G_\theta(\theta,\varphi)P_{\theta n}(\theta,\varphi)+P_H G_\varphi(\theta,\varphi)P_{\varphi n}(\theta,\varphi)\right]\sin\theta\,d\theta\,d\varphi\,. \tag{3.109}$$

For a vertical $\lambda/2$ dipole inclined at angle α as shown in figure 3.22 we obtain (see Appendix D),

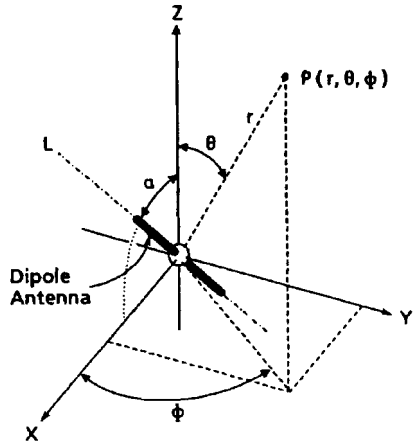

Figure 3.22: *Coordinate system with a $\lambda/2$ dipole inclined at an angle α [Taga,1990].*

$$G_\theta(\theta,\varphi)=1.641(\cos\theta\cos\varphi\sin\alpha-\sin\theta\cos\alpha)^2\,\frac{\cos^2((\pi/2)\xi)}{(1-\xi^2)^2}, \tag{3.110}$$

$$G_\varphi(\theta,\varphi)=1.641\sin^2\varphi\sin^2\alpha\,\frac{\cos^2((\pi/2)\xi)}{(1-\xi^2)^2}, \tag{3.111}$$

where $\xi=\sin\theta\cos\varphi\sin\alpha+\cos\theta\cos\alpha$. The antenna gains G_θ and G_φ are depicted in figure 3.23. For Rayleigh fading the incident field is uniform distributed both in phase and in arriving angle in the horizontal plane. To give an example, we calculate the MEG for a horizontal $\lambda/2$ dipole ($\alpha = 90°$), when the incident field is in the horizontal direction (xy-plane). In this case the incident field is

$$P_{\theta n},P_{n\varphi}=\frac{1}{2\pi}\delta(\theta-\pi/2)\ \text{and}\ XPD=1. \tag{3.112}$$

The power received by the isotropic antennas is

$$P_{1,2} = \int_0^{2\pi}\int_0^{\pi} \frac{1}{2\pi}\delta(\theta-\pi/2)\sin\theta\, d\theta\, d\varphi = 1. \tag{3.113}$$

The power received by the horizontal dipole is,

$$\begin{aligned} P_{rec} &= \int_0^{2\pi}\int_0^{\pi}\left[P_1 G_\theta(\theta,\varphi)P_\theta(\theta,\varphi) + P_2 G_\varphi(\theta,\varphi)P_\varphi(\theta,\varphi)\right]\sin\theta\, d\theta\, d\varphi, \\ &= \int_0^{2\pi}\int_0^{\pi}\left[0 + P_2 1.641\sin^2\varphi \frac{\cos^2((\pi/2)\sin\theta\cos\varphi)}{(1-\sin^2\theta\cos^2\varphi)^2}\frac{\delta(\theta-\pi/2)}{2\pi}\right]\sin\theta\, d\theta\, d\varphi, \\ &= \int_0^{2\pi}\frac{1}{2\pi}1.641\frac{\cos^2((\pi/2)\cos\varphi)}{\sin^2\varphi}d\varphi = 0.73, \end{aligned} \tag{3.114}$$

where $\int_0^{2\pi}\frac{\cos^2((\pi/2)\cos\varphi)}{\sin^2\varphi}d\varphi = 2.795$. And the MEG is $\frac{P_{rec}}{P_V + P_H} = 0.37 = -4.4$ dBi. When the $\lambda/2$ dipole is in the vertical position ($\alpha = 0°$), the MEG is – 0.85 dBi (-3 dBi + 2.15 dBi). So if we want to measure the incident power for this EM field in one polarisation with a dipole we clearly get a huge error.

A more realistic model for the incident field is a Gaussian distribution of the incident normalised power distribution in the elevation and in the azimuth direction [Taga, 1990],

$$P_{\theta n}(\theta,\varphi) = \frac{A_\theta}{2\pi}\exp\left(-\frac{(\theta-\theta_0)^2}{2\sigma_\theta^2}\right), \tag{3.115}$$

$$P_{\varphi n}(\theta,\varphi) = \frac{A_\varphi}{2\pi}\exp\left(-\frac{(\theta-\varphi_0)^2}{2\sigma_\varphi^2}\right). \tag{3.116}$$

where A_θ and A_φ are constants determined by Eq. (3.108), θ_0 and φ_0 are, respectively, the average elevation angle of each vertical and horizontal polarised wave distribution, and σ_θ and σ_φ are, respectively, the standard deviation of each vertical and horizontal polarised wave distribution. A good start for a 3-dimensional multi-path model is $\sigma_\theta = \sigma_\varphi = 40°$ and $\theta_0 = \varphi_0 = 90°$ [Green et al, 2000]. Then the arriving waves are scattered waves without a dominant direct wave and propagate mainly around the horizontal plane. For Rayleigh–Rice fading we have LOS propagation and we can write the arriving waves in a scatter component and a direct component. The incident field can be described with Rice-*K* factors for the vertical and horizontal polarisation [Glazunov, 2002]. With the two Rice-*K* factors an expression for the MEG in Rician channels can be derived [Glazunov, 2002].

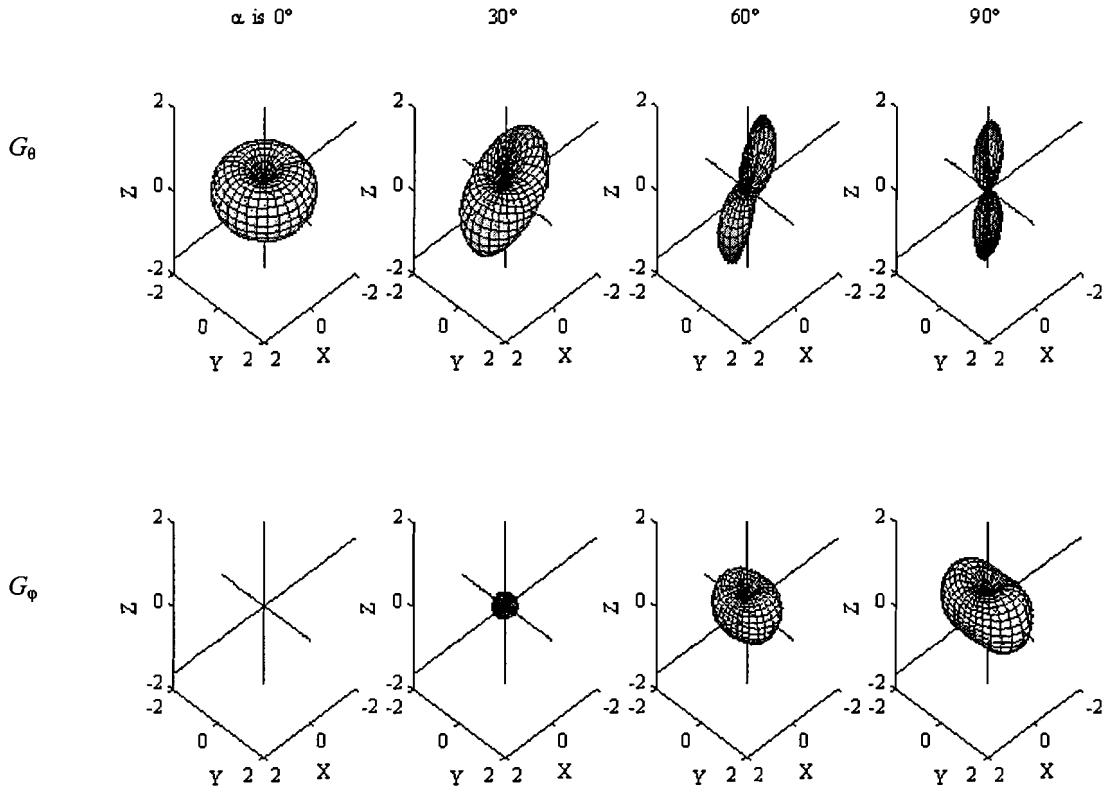

Figure 3.23: *Antenna gain patterns of a λ/2 dipole with different angles α (α=0° is vertical and α=90° is horizontal), the antenna gain in the direction (x, y, z) is represented by the magnitude of the vector with direction (x, y, z), starting in the origin and ending in the depicted surface.*

3.7.2 Received power of a λ/2 dipole

The EM-field generated by a Dirac source was calculated in section 3.4. When a very short antenna is used the received power will chance very rapidly when the receiving antenna is moved in a cavity. A realistic transmit antenna source is a superposition of sources and this superposition gives a statistically smoother EM-field. The same phenomena occurs at the receive side, if we receive the incident EM-field at a length of a half wavelength this smoothes the received power. The radiated EM field is calculated using the current distribution along the dipole axis [Hill, 1999].

$$I(t) \approx I_0 \frac{\sin k_0 (H - |z|)}{\sin k_0 H} \quad , z \in [0, H], \quad k_0 H < \pi, \tag{3.117}$$

where I_0 is the current at the antenna terminal, $2H$ is the total length of the dipole and z is the coordinate along the dipole axis. We use the Green's function and the midpoint integration method to calculate the field radiated by a $\lambda/2$ dipole with total length $2H$,

$$\begin{aligned} \vec{E}_x(\vec{r}) &= -j\omega \iiint_{V_0} \overline{\overline{G}}_{Exx}(\vec{r}, \vec{r}_s)\, \vec{J}_x \, dV_0 \\ &\approx \frac{-j\omega I_0}{\sin k_0 H} \sum_{i=-2}^{2} \overline{\overline{G}}_{Exx}(\vec{r}, x_s + iH/5, y_s, z_s) \sin k_0 (H - |iH/5|) \vec{e}_x \, 2H/5 \end{aligned} \tag{3.118}$$

The calculation of the received power is done using the induced-EMF method [Hill, 1999] and [Dolmans, 1997],

$$V_{oc} = -\frac{1}{I_0}\int_{-H}^{H} E_x^i(x_r)\, I(x_r)\, dx_r \approx -\frac{1}{I_0 \sin k_0 H}\sum_{n=-2}^{n=2} E_x^i(x_r)\sin k_0\left(H - \left|iH/5\right|\right) 2H/5, \quad . \quad (3.119)$$

$$\text{with} \quad I_{load} = \frac{V_{oc}}{Z_d + Z_l} \quad \text{if} \quad Z_l = Z_d^* \quad P_r = \frac{\left|V_{oc}\right|^2}{4\Re\{Z_d\}},$$

where Z_d is the impedance of the antenna and Z_l is the impedance of the load. Now we can export simulate E_x or V_{oc} due to a current J_x.

4 Diversity techniques

4.1 Introduction

When a radio link is made between portable devices, the quality of the radio link is continuously changing. The radio link changes in time, e.g., when a door opens in a room or when the devices move around. The radio-channel characteristics discussed in chapter 3 (fading, delay spread and coherence bandwidth) are the cause of the changing quality of the radio link. Within a diversity system one or more interfaces to the radio channel, diversity branches, are connected to a receiver. The diversity system should be adaptive to adjust to the changing radio channel. When the system is well designed the interfaces to the radio channel should fade independently, which means that the probability that all signals fade is reduced considerably. The Bluetooth protocol already uses frequency and time diversity to combat fading [Bray et al, 2001]. In the rest of this chapter we only consider antenna diversity. In chapter 6 we will use a mixture of space and polarisation diversity in a Bluetooth module with an embedded slot antenna.

4.2 Diversity

Diversity of the Bluetooth receiver can be implemented in several ways as mentioned in chapter 1.4. The most widely used diversity techniques are space and polarisation diversity. Other possibilities are the combination of using an electrical antenna with a magnetic antenna [Leyten, 2001] or radiation pattern diversity [Matthijssen, 2004]. The principle of diversity is based on the stochastic nature of the received power in an indoor environment. The principle is simple: assume we have a 10 % chance that the signal to noise ratio (SNR) of the received signal at one antenna is smaller than a certain threshold, we get a 1 % chance that the SNR of both antennas is smaller than the threshold. This is only true if the two signals are independent and have the same probability density function, (pdf). When there is still positive correlation the chance will be somewhere between 1 % to 10 %. In this case the pdf of the received power can be derived using the joint pdf or with the eigenvalues of the correlation matrix [Vaughan et al, 2003]. The indoor environment usually gives excellent spatial and polarisation de-correlation of the received powers. The correlation ρ of the received powers is a combination of space and polarisation correlation [Saunders, 1999],

$$\rho \approx \rho(d)\,\rho(\alpha)\,, \tag{4.1}$$

where d is the distance between the antennas and α is the angle between, e.g., dipole antennas. Using polarisation and space diversity the separation between the antennas can decrease. When only space diversity is used we normally get de-correlated received powers at an antenna separation of $\lambda/2$. Using Eq. (4.1) we see that to achieve the same de-correlation of the received powers space diversity in combination with polarisation diversity will decrease the distance between the antennas. It can be expected that it is possible to expand Eq. (4.1) when there is also radiation pattern diversity. Then the correlations should be independent, e.g., the radiation pattern of each antenna is different but sensitive for the same polarisation. Under this condition we get (see Appendix E),

$$\rho \approx \rho(d)\,\rho(\alpha)\,\rho(\textit{radiation pattern difference})\,. \tag{4.2}$$

4.2.1 Space diversity

The most fundamental way of obtaining diversity is to use two antennas, sufficiently separated in space so that the relative phases of the multi-path contributions are significantly different at the two antennas. Figure 4.1a shows two receive antennas, which are separated by a distance *d*.

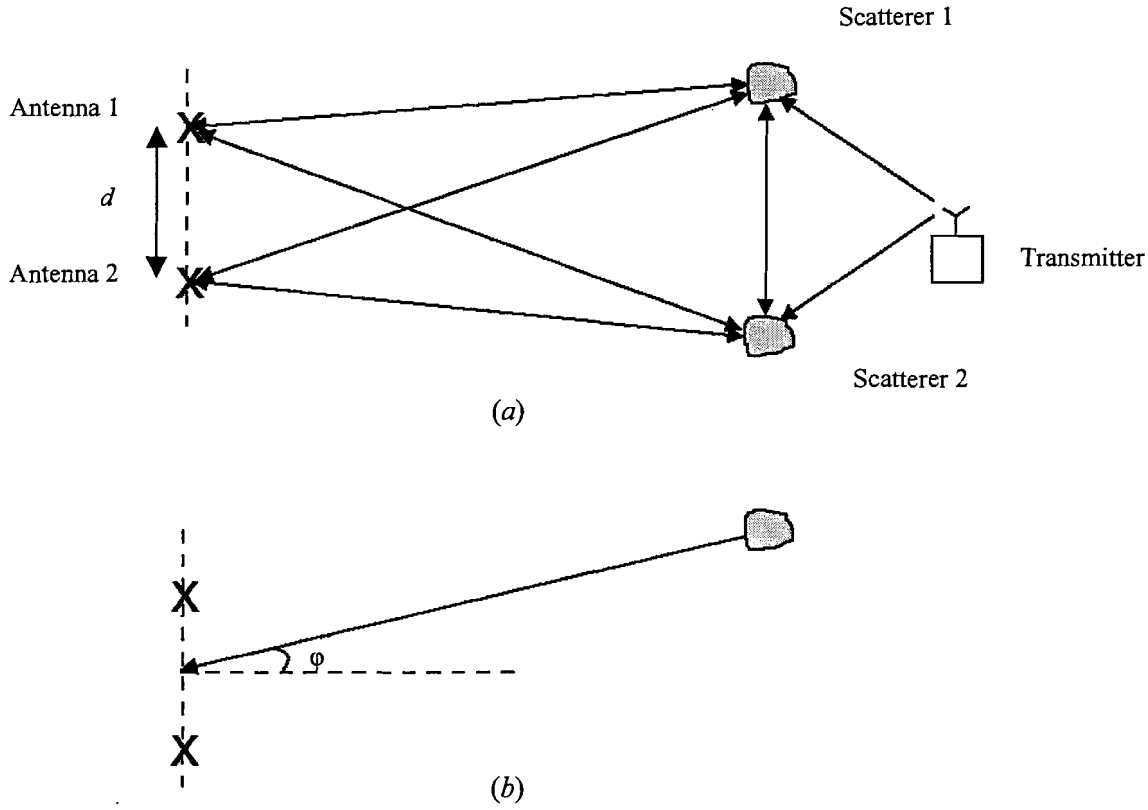

Figure 4.1: *Two-dimensional scatter model (a) and (b) geometry for calculation.*

The waves transmitted by the transmitter have to travel along a different path to arrive at the two antennas. Furthermore the reflection coefficients of the scatterers can be different. The result is that the amplitude and phase of the received signals at the two receive antennas will be different. The space correlation of the amplitude and power, as function of the separation between the two antennas, can be estimated with a simple two-dimensional model. For Rayleigh-fading the reflection coefficients of the scatterers have a Gaussian distribution with zero mean and the phase has a uniform distribution [Vaughan et al, 2003]. Furthermore, we assume that the incident waves arrive in a plane, e.g., normal to the orientation of a linear antenna, with equal angle of arrival probability. In Appendix B the correlation for the envelope and the power is derived:

$$\rho_{env}(d) \approx \rho_{power}(d) = \left[J_0\left(\frac{2\pi d}{\lambda}\right)\right]^2, \tag{4.3}$$

where d is the distance between the antennas and J_0 is theBessel function of the first kind order zero. In figure 4.2 the power correlation is depicted, for Rayleigh fading the incident waves arrive from all directions and the arrival angle distribution is uniform.

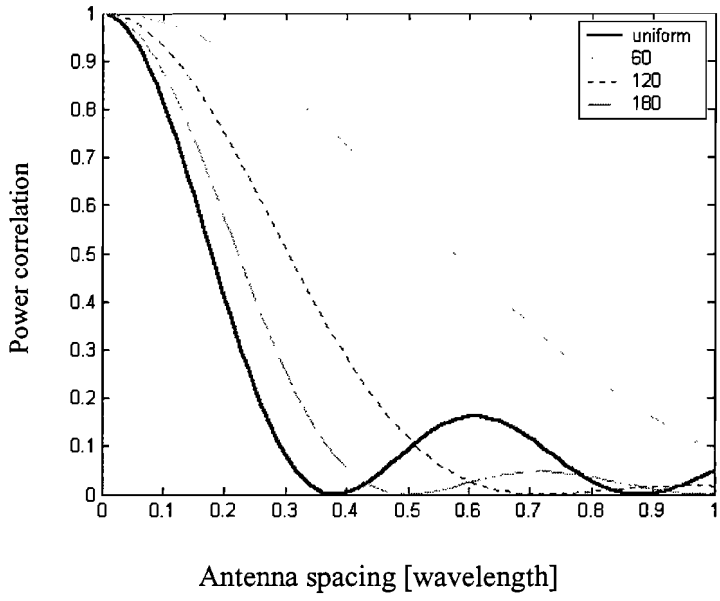

Figure 4.2: *Power correlation as function of the antenna spacing and angle of arrival spread.*

The mutual coupling of the antennas has to be taken into account when the antennas are close, i.e., less than a wavelength. When the antennas have the same radiation pattern this coupling can lead to an even smaller distance, as less as one tenth of a wavelength or 1.25 cm [Saunders, 1999]. When the antennas are close to each other the radiation pattern of each antenna is changing and has to be calculated numerically. With this antenna coupling we also get radiation pattern diversity [Matthijssen, 2000].

4.2.2 Polarisation diversity

The polarisation of the electromagnetic field is the direction of the electric field vector which is different at different positions in a room. A linear antenna is sensitive to the polarisation along its axis. When the orientation of the electromagnetic field and the antenna do not match, the received power is reduced. The received power is reduced by a factor, the so-called polarisation efficiency. Every polarisation vector can be de-composed in its orthogonal base vectors. When for example three orthogonal linear antennas are used the chance of a fade due to polarisation mismatch is reduced. Such an antenna array is no longer sensitive to the polarisation of the incoming waves. Polarisation diversity with a x and z–directed antenna is depicted in figure 4.3.

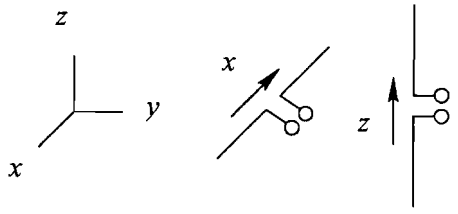

Figure 4.3: *Polarisation diversity.*

The indoor environment leads to a considerable amount of cross-polarisation. Measurements show [Kalliola et al, 2002] that the power in the cross-polarisation direction is about 6 dB below the power in the co-polarisation direction. A way to express this is the cross-polar discrimination ratio,

$$XPD = \frac{\left\langle |\vec{E}_{cross}|^2 \right\rangle}{\left\langle |\vec{E}_{co}|^2 \right\rangle} \approx \frac{1}{4}, \tag{4.4}$$

where $\vec{E}_{\text{cross}}$ and $\vec{E}_{\text{co}}$ refer to the cross-polarised electric field and the co-polarised electric field, respectively. The distribution of power in co- and cross-polarisation can be understood by considering the example of a vertical dipole that emits a θ-polarised electrical field. In Cartesian coordinates three components are transmitted. The boundary, i.e., walls, can have an arbitrary shape. The reflection coefficient is depending on the angle of arrival and polarisation. It is plausible that there will be a distribution over both polarisations, vertical and horizontal, depending on the shape of the boundary and radiation pattern of the transmit antenna. The received power for orthogonaly oriented antennas, e.g., horizontal and vertical, is de-correlated. When the transmit antenna is a vertical dipole, the co-polarisation is the z-direction and the cross-polarisation components are the x- and y-direction. Indoors the mean power in the x and y-polarisation is about 6 dB below the power in the co-polarised direction [Kalliola et al, 2002]. When the co-polarisation antenna is in a fade and the receiver switches to the cross-polarisation antenna the expected increases in received power is 6 dB lower. However, in a deep fade of 30 dB or more at the co-polarised antenna polarisation diversity can still give a significant increase in received power at a cross-polarized antenna.

4.3 Combining methods

Before the signals arrive at the receiver they have to be processed with a combiner. Combining of the received signals can be done in several ways. The goal of combining is to optimise the SNR at the receiver output depicted in figure 4.4. The optimum method uses complex weight factors. The signals are shifted to the same phase and scaled so that the signal with the largest SNR is dominant (we ignore interference). This involves phase shifters and a signal-processing unit to optimise the phase shifting and scaling. A more simple combining technique is a switch. With the switch the signal with the largest SNR can be selected to optimise the SNR at the receiver. It is also possible to use a passive power combiner that adds the signals.

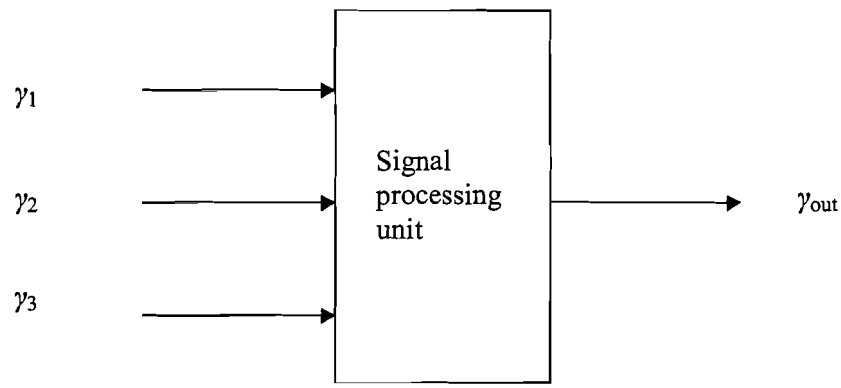

Figure 4.4: *Combiner with three input signals with SNR γ_1, γ_2 and γ_3 and output SNR γ_{out}.*

The array gain in this context is the expected mean improvement of the SNR using a combiner and multiple antennas,

$$G_{array} = \text{array gain} = \frac{\langle SNR_n \rangle}{\langle SNR_1 \rangle} = \frac{\langle S_n/N_n \rangle}{\langle S_1/N_1 \rangle}, \tag{4.5}$$

where S_1 is the received power of one antenna, N_1 is the noise power of one antenna and S_n and N_n are the received power and noise power when n antennas are used. The array gain for Rayleigh fading depends on the combining technique [Leyten, 2001]. The noise powers are de-correlated and can be added but the signals are correlated in time. The expected signal to noise ratio for a single antenna is γ_0 and for N antennas the array gain is:

$$G_{array} = \frac{\int_0^\infty f_n(\gamma)\,\gamma\,d\gamma}{\int_0^\infty f_1(\gamma)\,\gamma\,d\gamma} = \frac{\int_0^\infty f_n(\gamma)\,\gamma\,d\gamma}{\gamma_0}, \tag{4.6}$$

where f_n is the pdf of the SNR for N antennas with selection, f_1 is the pdf of the SNR for one antenna and γ is the SNR. For Rayleigh fading and selection combining f_n is given by Eq. (4.7),

$$f_n = \frac{N}{\gamma_0}\exp(-\gamma/\gamma_0)[1-\exp(-\gamma/\gamma_0)]^{N-1}, \tag{4.7}$$

and the array gain becomes

$$G_{array}^{selection} = \frac{\int_0^\infty f_n(\gamma)\,\gamma\,d\gamma}{\gamma_0} = \frac{\int_0^\infty \frac{N}{\gamma_0}\exp(-\gamma/\gamma_0)[1-\exp(-\gamma/\gamma_0)]^{N-1}\,\gamma\,d\gamma}{\gamma_0}, \tag{4.8}$$

$$= \frac{1}{\gamma_0}\sum_{n=0}^{N-1} N(-1)^n \binom{N-1}{n} \int_0^\infty \frac{\gamma}{\gamma_0}\exp\left(-\frac{\gamma}{\gamma_0}(n+1)\right)d\gamma,$$

$$= \frac{N}{\gamma_0}\sum_{n=0}^{N-1}(-1)^n \binom{N-1}{n}\frac{\gamma_0}{(n+1)^2} = N\sum_{n=0}^{N-1}(-1)^n \binom{N-1}{n}\frac{1}{(n+1)^2},$$

$$= \sum_{n=0}^{N-1}(-1)^n \frac{N(N-1)!}{(n+1)n!(N-1-n)!}\frac{1}{n+1} = \sum_{k=1}^{N}(-1)^{k+1}\binom{N}{k}\frac{1}{k} = \sum_{n=1}^{N} 1/n,$$

where $\sum_{k=1}^{N}\frac{(-1)^{k+1}}{k}\binom{N}{k} = \sum_{n=1}^{N} 1/n$ is a finite sum in [Gradshteyn, 1994].

When the N signals are phase shifted to the same phase and added we get equal gain combining and the array gain for Rayleigh fading is

$$G_{array}^{equal} = \frac{\left\langle \frac{1}{2}\left(\sum_1^N r_n\right)^2 \right\rangle \Big/ NP_{noise}}{\gamma_0} = \frac{N\langle r^2\rangle + (N-1)N\langle r\rangle^2}{2\gamma_0 NP_{noise}} = \frac{2\sigma^2 + (N-1)\pi/2\ \sigma^2}{2\gamma_0 P_{noise}}, \tag{4.9}$$

$$= \frac{2\gamma_0 + (N-1)\pi/4\ 2\gamma_0}{2\gamma_0} = 1 + (N-1)\pi/4, \quad \text{with} \quad \gamma_0 = \frac{\sigma^2}{P_{noise}}.$$

For maximum ratio combining, the amplitude is also weighted, the SNR = $\sum_1^N \gamma_n$ and the array gain for equal branches and Rayleigh fading is

$$G_{array}^{max\,ratio} = \frac{\left\langle \sum_{1}^{N} \gamma_n \right\rangle}{\gamma_0} = \frac{N\langle\gamma\rangle}{\gamma_0} = \frac{N\,\gamma_0}{\gamma_0} = N\,. \tag{4.10}$$

The array gain as function of the combining technique and number of branches is given in table 4.1.

Table 4.1: *Array gain in dB for different combining methods and number of branches.*

Branches (N)	1	2	3	4	10
Selection	0	1.76	2.63	3.19	4.67
Equal gain	0	2.52	4.10	5.26	9.07
Maximum ratio	0	3.01	4.77	6.02	10

From table 4.1 we observe that selection combining has the lowest array gain. Furthermore, for selection combining the array gain is hardly increasing if we use more antennas. If we want to improve the overall performance of a receiver, i.e., not only in a fade, maximum ratio or equal gain combining are better combining techniques. However, these techniques are more complex to implement in a receiver. In the next section we discuss the ability of the combiner to reduce the chance of a fade.

4.3.1 Diversity gain

We can compare the diversity system and the system without diversity at a certain level of service of the radio link. A common level of service is that 1 % of the received power is too low for a good radio link. The percentage of the space where the SNR is below a certain threshold is also called the outage. Complementary to this is the coverage, so outage + coverage = 1. The expected difference in transmitter power to get the same level of service is called the diversity gain. The radiated powers needed for a diversity system and for a single antenna system are:

- Diversity system, radiated power needed for an outage of 1 % is $P_{diversity}$
- Single antenna system, radiated power needed for an outage of 1 % P_{single}

The diversity gain at an outage of 1 % is defined by:

$$\text{diversity gain (outage} = 1\,\%) = \frac{P_{single}(\text{outage} = 1\,\%)}{P_{diversity}(\text{outage} = 1\,\%)}. \tag{4.11}$$

For Bluetooth a good criterion for the level of service is an outage for a BER of 0.1 %. This is still an acceptable bit error rate according to the Bluetooth specification. The definition of the diversity gain can be modified to express the diversity gain based on the BER,

$$\text{diversity gain } (\Pr\{\text{BER} > 0.1\%\} = 1\,\%) = \frac{P_{single}(\Pr\{\text{BER} > 0.1\%\} = 1\,\%)}{P_{diversity}(\Pr\{\text{BER} > 0.1\%\} = 1\,\%)}. \tag{4.12}$$

4.3.2 Switching and selection

The signal-processing unit determines whether the combiner depicted in figure 4.4 acts as a switching combiner or a selection combiner. With switching combining we mean, switching to the largest SNR if the signal is under a certain threshold, above this threshold the switch is not activated. Switching is simple but has the lowest diversity gain. It can still be sufficient when we are mainly interested in avoiding fades, e.g., clicks in an audio link. Selection has a different combining scheme, the branch with the highest SNR is selected. This results in a higher diversity gain but a similar performance if one of two branches is in a fade.

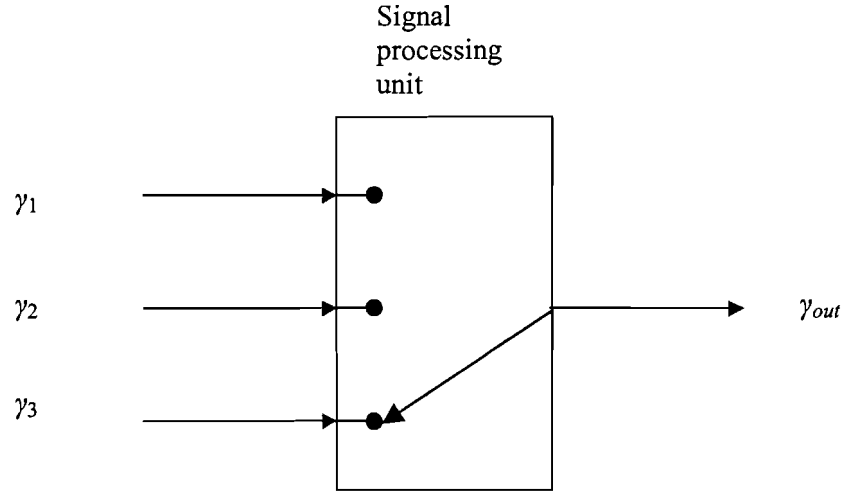

Figure 4.5: *Switching or selection combiner with three input signals with SNR γ_1, γ_2 and γ_3 and output SNR γ_{out}.*

Now that we know how the received signals are processed in the combiner we can start to calculate the improvement in the received signal-to-noise ratio if we use for example two receive antennas and a selection combiner. It is possible to calculate the chance that the SNR, γ, is smaller than a reference. The probability, Pr, that both signals are smaller than the reference is the integration of the joint pdf $f_{\gamma_1\gamma_2}$,

$$\Pr\{\gamma_1 < \gamma_{ref} \text{ and } \gamma_2 < \gamma_{ref}\} = \int_0^{\gamma_{ref}} \int_0^{\gamma_{ref}} f_{\gamma_1\gamma_2}(\gamma_1,\gamma_2)\, d\gamma_1 d\gamma_2 . \tag{4.13}$$

If the two signals are de-correlated (independent) this becomes,

$$\Pr\{\gamma_1 < \gamma_{ref} \text{ and } \gamma_2 < \gamma_{ref}\} = \int_0^{\gamma_{ref}} f_{\gamma_1}(\gamma)\, d\gamma_1 \int_0^{\gamma_{ref}} f_{\gamma_2}(\gamma)\, d\gamma_2 = F_{\gamma_1}(\gamma_{ref}) F_{\gamma_2}(\gamma_{ref}), \tag{4.14}$$

where F_{γ_1} is the cumulative distribution function. The probability that the SNR is smaller than a certain threshold is also called the outage. The expression $F_{\gamma_1}(\gamma_{ref})$ for Rayleigh fading is derived in Appendix A

$$\Pr\{\gamma_1 < \gamma_{ref}\} = 1 - \exp(-\gamma_{ref}/\gamma_0), \tag{4.15}$$

where γ_0 is the mean SNR. The mean SNR is the mean of the SNR values when the receive antenna moves through the entire space of interest and is proportional to the transmitted power,

$$\gamma_0 \propto P_{\text{radiated}} \cdot \tag{4.16}$$

For N de-correlated branches we get using Eq. (4.14) and (4.15)

$$\Pr\{\gamma_1 < \gamma_{ref} \text{ and,} \cdots \text{and } \gamma_n < \gamma_{ref}\} = \left(1 - \exp(-\gamma_{ref}/\gamma_0)\right)^N . \tag{4.17}$$

The pdf of the signal-to-noise ratio for N branches with selection is

$$f(\gamma) = \frac{d}{d\gamma} F_\gamma(\gamma) = \frac{d}{d\gamma}(1 - \exp(-\gamma/\gamma_0))^N = \frac{N}{\gamma_0} \exp(-\gamma/\gamma_0)[1 - \exp(-\gamma/\gamma_0)]^{N-1} \tag{4.18}$$

The most interesting situation is a deep fade with a small SNR, $\gamma_{ref} << \gamma_0$. For that case Eq. (4.17) can be rewritten and we obtain

$$\Pr\{\gamma_1, \gamma_2, \cdots \gamma_n < \gamma_{ref}\} = \left(1 - \exp(-\gamma_{ref}/\gamma_0)\right)^N \approx (\gamma_{ref}/\gamma_0)^N \qquad \gamma_{ref} << \gamma_0 . \tag{4.19}$$

If we calculate the required increase in transmitter power to reduce the outage by a factor of 10, we get for a single antenna and for N antennas at an outage of 1 %,

$$(\gamma_{ref}/\gamma_{\text{single}}) = (-\gamma_{ref}/\gamma_{\text{div}})^N = 0.01 \quad \gamma_{ref} << \gamma_{\text{single}}, \tag{4.20}$$

where γ_{single} is the expected SNR with one antenna and γ_{div} is the expected SNR if N antennas are used. Hence, the mean power increase to decrease the outage with a factor of 10 is 10 dB for the receiver with one antenna and $10/N$ dB for a receiver with N antennas. With two antennas there is already a transmitter power gain of 5 dB for small outage levels. Furthermore, it is clear that the maximum gain is 10 dB. If we want to decrease the outage with a factor of 10 it is sufficient to use only a few antennas. The gain difference between three and four antennas is already only 0.8 dB, so a maximum number of four antennas is sufficient.

Next, we will compare a receiver with a single antenna and a receiver with multiple antennas at the same outage level. At an outage level of 1 % the cumulative probability is 1 %. The diversity gain is the difference in transmitted power with the same outage x,

$$1 - \exp\left(-\frac{\gamma_{ref}}{\gamma_{\text{single}}}\right) = \left(1 - \exp\left(-\frac{\gamma_{ref}}{\gamma_{\text{div}}}\right)\right)^N = x . \tag{4.21}$$

We can decouple the signal-to-noise ratios in Eq. (4.21) and we get:

$$\begin{cases} 1 - \exp(-\gamma_{ref}/\gamma_{\text{single}}) = x, \\ (1 - \exp(-\gamma_{ref}/\gamma_{\text{div}}))^N = x, \end{cases} \tag{4.22}$$

which can be rewritten as,

$$\begin{cases} \gamma_{\text{single}} = -\gamma_{ref}/\ln(1-x), \\ \gamma_{\text{div}} = -\gamma_{ref}/\ln(1-x^{1/N}). \end{cases} \tag{4.23}$$

The diversity gain is the ratio of the average SNR ratios at an outage x,

$$G_{div} = \frac{\gamma_{\text{single}}}{\gamma_{\text{div}}} = \frac{\ln(1-x^{1/N})}{\ln(1-x)}, \qquad 0 \le x < 1 . \tag{4.24}$$

where G_{div} is the diversity gain. Note that the average SNR is related to the radiated power. The asymptotic expression for the diversity gain at a small outage, $0 < x << 1$, is:

$$G_{div} = \frac{\ln(1-x^{1/N})}{\ln(1-x)} \approx \frac{x^{1/N}}{x}. \tag{4.25}$$

For an outage of 1 %, $x = 0.01$, this becomes

$$G_{div} = \gamma_{\text{single}}[dB] - \gamma_{\text{div}}[dB] = 20 - \frac{20}{N}[dB]. \tag{4.26}$$

If $N = 2$ we need 10 dB less power to get the same outage of 1 %. So the diversity gain is 10 dB for a Rayleigh channel with two de-correlated antennas at an outage of 1 % as is shown by the arrow in figure 4.6. In general, for small-normalised SNR, $\gamma_{ref} << \gamma_0$, at an outage x we get

$$G_{div} \approx -10\log x + \frac{10\log x}{N}[dB]. \tag{4.27}$$

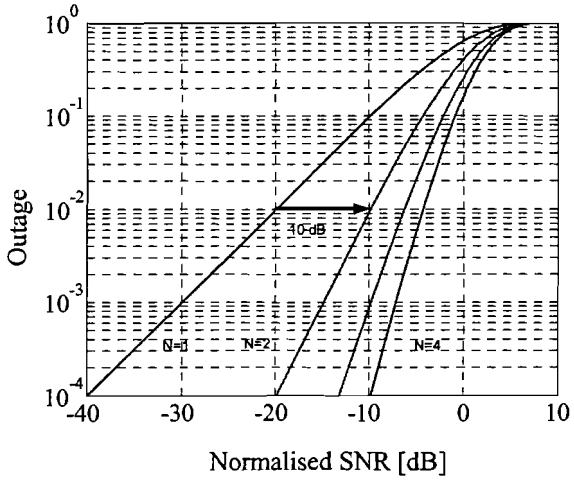

Figure 4.6: *Outage with the number of branches N as parameter. The arrow is the diversity gain of 10 dB at an outage of 1 % and N =2.*

For large values of the SNR we have to use Eq.(4.24). When we investigate the diversity gain for infinite branches, $(N \to \infty)$, we get at an outage x,

$$G_{div} = \frac{\ln(1-x^{1/N})}{\ln(1-x)} \xrightarrow{N\to\infty} \frac{\ln(0^+)}{\ln(1-x)} = \frac{-\infty}{\ln(1-x)} = \infty \quad \text{for} \quad N \to \infty, \quad 0 \le x < 1. \tag{4.28}$$

The Rayleigh distribution is a statistical and not a physical model and allows amplitudes and powers from zero to infinity. For example, if the transmitted power is 1 Watt, there is a very small area in a room where received power is larger then 1 Watt! When we have a large number of small receive antennas, e.g., Hertzian dipoles, and a very low radiated power the chance is still large that one of the antennas will still receive a signal that is larger than the threshold. So, the radiated power needed for an outage x becomes infinitesimally small for an infinite number of receive antennas. In practice, the transmitted power should be at least the received power needed for the signal-to-noise threshold. So, in reality there is an upper limit for the diversity gain if we increase the number of receive antennas.

4.3.3 Equal gain combining

When received signals are combined using an equal gain combiner the phase of the signals is shifted to the same phase and the amplitudes are added. From calculations with the cavity model as presented in chapter 3.4 it is clear that for the electric field in a cavity only two phases are present, in phase (0°) and 180° out of phase with the current in the transmitting antenna. When two antennas in a cavity receive the signals s_1 and s_2, the phase of the signals will be the same or the signals will be 180° out of phase. Selection between the signals, $s_1 + s_2$ or $s_1 - s_2$ as shown in figure 4.7, will result in a new signal s_{out}. The amplitude of s_{out} is the sum of the amplitudes of s_1 and s_2. When received signals in a cavity are combined, using the combiner depicted in figure 4.6, s_1 and s_2 are shifted to the same phase and the amplitudes are added. For signals in a cavity the simple combiner of figure 4.6 behaves as an equal-gain combiner.

$$(s_1, s_2) \xrightarrow{\text{equal gain}} |s_1| + |s_2| . \tag{4.29}$$

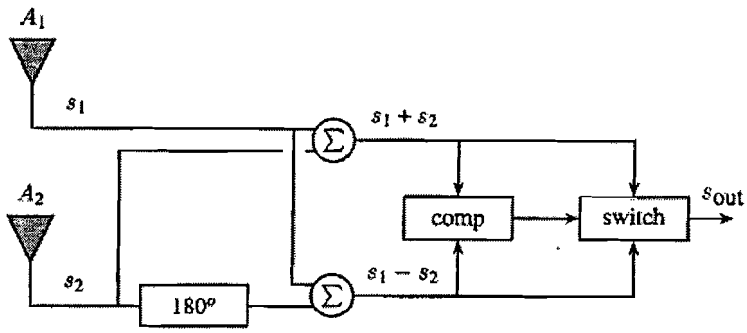

Figure 4.7: *Simple adaptive combiner.*

The probability that the amplitude at the output of an equal-gain combiner is below a reference becomes,

$$\Pr\{|s_1| + |s_2| < s_{ref}\} = F_{|s_1|+|s_2|}(s_{ref}) = \int_0^{ref} f_s(s) F_s(s_{ref} - s)\, ds . \tag{4.30}$$

An equal-gain combiner ads not only the amplitudes of the signals but also the noise associated with the signals. The input signals at the two-branch equal-gain combiner is [Bektas, 2003]:

$$\begin{aligned} a_1 &= s_1 e^{j\theta_1} + n_1 \\ a_2 &= s_2 e^{j\theta_2} + n_2 \end{aligned} \tag{4.31}$$

where the signal amplitude of the first branch is s_1 and the noise amplitude of the first branch is n_1. At the output of the equal-gain combiner the signal becomes:

$$\begin{aligned} a &= (s_1 e^{j\theta_1} + n_1)\, e^{-j\theta_1} + (s_2 e^{j\theta_2} + n_2)\, e^{-j\theta_2}, \\ &= s_1 + s_2 + n_1\, e^{-j\theta_1} + n_2\, e^{-j\theta_2}, \end{aligned} \tag{4.32}$$

where we assume that the equal gain is able to measure the phase of the signal. The SNR at the output of a 2-branch equal gain combiner for equal de-correlated branch noise is [Bektas, 2003]

$$\gamma = \frac{(s_1+s_2)^2/2}{\left\langle |n_1+n_2|^2 \right\rangle/2} = \frac{s_1^2+2s_1s_2+s_2^2}{n_1^2+n_2^2} = \frac{s_1^2+s_2^2+2s_1s_2}{4N},$$
$$= \frac{s_1^2+s_2^2}{4N} + \frac{s_1}{n}\frac{s_2}{n} = \frac{\gamma_1+\gamma_2+2\sqrt{\gamma_1\gamma_2}}{2} \quad (4.33)$$

where γ_1 and γ_2 represent the SNR of each branch and N is the noise power. When the two branches have an equal SNR the gain, γ / γ_1, is 3 dB. The maximum gain is $\gamma_{\max}[dB] - \gamma_{\min}[dB] + 3$ dB. This can be derived using

$$\gamma_{\max} = a_2\gamma_{\min}, \quad (4.34)$$

where $\gamma_{\max}$ is the SNR of the branch with highest SNR, $\gamma_{\min}$ is the SNR of the branch with lowest SNR and a is the ratio $\gamma_{\max}/\gamma_{\min}$ with $a_2 \geq 1$. The gain can be expressed with the ratio $\gamma/\gamma_{\min}$

$$\frac{\gamma}{\gamma_{\min}} = \frac{\gamma_1+a_2\gamma_1+2\sqrt{\gamma_1 a_2\gamma_1}}{2\gamma} = \frac{1}{2}+\sqrt{a_2}+\frac{a_2}{2} \quad (4.35)$$

When we compare the gain for equal gain, $\gamma/\gamma_{\min}$, with the gain for selection, $\gamma_{\max}/\gamma_{\min}$, we obtain

$$\frac{\gamma_{equal\,gain}}{\gamma_{selection}} = \frac{\gamma}{\gamma_{\min}a_2} = \frac{1}{2a_2}+\frac{1}{\sqrt{a_2}}+\frac{1}{2}, \quad (4.36)$$

with a maximum of ratio 2 when $a = 1$ and a minimum ratio of ½ for $a \to \infty$. We get a maximum ratio in Eq. (4.34) when the two signals have the same SNR. For $a \geq 1$, the derivative of Eq. (4.36) is monotonically decreasing

$$\frac{d}{da}\left[\frac{1}{2a}+\frac{1}{\sqrt{a}}+\frac{1}{2}\right] = -\frac{1}{2a^2}-\frac{1}{2a^{3/2}} < 0, \quad (4.37)$$

and from this it follows that the maximum ratio of 2 for $\gamma_{equal}/\gamma_{sel}$ is a global maximum. At a 10 dB gain with selection, a =10, we get 9.4 dB gain for equal gain combining. Equal gain combining has a 3 dB larger gain for signals with equal power. Equal gain combining gives a lower gain for signals with a difference larger than 5.3 dB. The expected gain, the array gain, is for equal gain combining for Rayleigh fading and two antennas 0.76 dB larger than the array gain of selection. The outage of the equal-gain combining technique is depicted in figure 4.8.

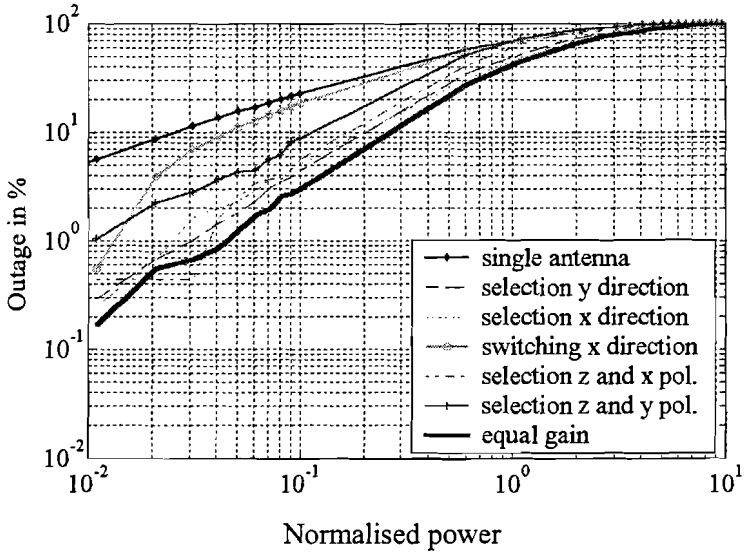

Figure 4.8: *Outage of the measured data after selection and equal gain combining.*

From figure 4.8 we observe that there is an average additional gain compared to switching of 1 dB at an outage of 1 %. In a fade when $|s_1| << |s_2|$ or vice versa, switching and selection will give a better gain than equal gain. When in a fade $|s_1| \approx |s_2|$, the gain is 3 dB compared to selection. So the expected additional gain will be between 0 dB and 3 dB for equal signals. The overall improvement compared to selection is according to table 4.1 is 0.76 dB. Only when the phase shift and adder loss of the combiner is smaller than 0.7 dB this technique is overall better than selection.

4.3.4 Maximum ratio combining

The combining technique with the highest gain is maximum ratio combining. In this technique not only is the phase of the signals optimised, but the amplitude is weighted as well. The optimum weight factor is a factor proportional to the received envelope [Sampei, 1997]. Equal gain combining gives a lower gain than maximum ratio combining, only for equal branch powers the gain is the same. The expression for maximum ratio combining with equal mean powers for Rayleigh fading is [Vaughan et al, 2003]

$$\Pr\{\gamma < \gamma_{ref}\} = 1 - \exp(\gamma_{ref}/\gamma_0) \sum_{n=1}^{N} \frac{(\gamma_{ref}/\gamma_0)^{n-1}}{(n-1)!}, \tag{4.38}$$

where N is the number of branches. Equal gain combining gives about 1 dB less gain but is much simpler. The ratio in diversity gain between selection and maximum ratio combining can be expressed with the elegant expression. At the same outage and for small signals, $\gamma_{ref} << \gamma_0$, we get [Vaughan et al, 2003]

$$\left(\frac{\gamma_{ref}}{\gamma_S}\right)^N = \frac{1}{N!}\left(\frac{\gamma_{ref}}{\gamma_{MR}}\right)^N, \tag{4.39}$$

where γ_S is the mean SNR with selection, γ_{MR} is the mean SNR with maximum ratio combining. And finally we arrive at

$$\frac{\gamma_S}{\gamma_{MR}} \approx \sqrt[N]{N!} \tag{4.40}$$

So the difference in diversity gain between maximum ratio combining and selection combining is,

$$10\log\frac{\gamma_S}{\gamma_{MR}} = 10\log\sqrt[N]{N!} = \frac{10}{N}\log N! \quad [dB]. \tag{4.41}$$

For small signals, $\gamma_{ref} << \gamma_0$, and two branches, the diversity gain of maximum ratio combining is 1.5 dB larger than the diversity gain of selection combining.

4.4 Our choice for Bluetooth

Bluetooth is a low-cost consumer product so only a simple combining technique is appropriate. The combiner has to optimise the SNR each time a frequency hop occurs. A practical problem is the fact that the preamble is very short, only 4 bits or 4 μs. This requires an adaptive and fast combining technique. Therefore we decided to use switching diversity or selection diversity. The relation between the BER and the SNR appears to be simple for Bluetooth [Sampei, 1997],

$$\text{BER} = \frac{1}{2}\exp\left(-\frac{\gamma}{2}\right). \tag{4.42}$$

For Rayleigh fading and selection combining the expected BER will be the BER as function of the SNR times the probability of the SNR using selection combining Eq. (4.17), integrated over all the signal to noise ratios

$$\langle BER\rangle = \int_0^\infty BER(\gamma) f(\gamma)\, d\gamma, \tag{4.43}$$

where $f(\gamma)$ is the pdf of the SNR for Rayleigh fading with selection, Eq (4.17). The integral now becomes

$$\langle BER\rangle_N = \int_0^\infty \frac{1}{2}\exp\left(-\frac{\gamma}{2}\right)\frac{N}{\gamma_0}\exp\left(-\frac{\gamma}{\gamma_0}\right)\left[1-\exp\left(-\frac{\gamma}{\gamma_0}\right)\right]^{N-1} d\gamma, \tag{4.44}$$

where N is the number of antennas. With the binomial theorem [Dehling et al, 1995] this can be rewritten as:

$$\begin{aligned}\langle BER\rangle_N &= \sum_{n=0}^{N-1}\frac{1}{2}N(-1)^n\binom{N-1}{n}\frac{1}{n+1}\int_0^\infty \exp\left(-\frac{\gamma}{2}\right)\frac{n+1}{\gamma_0}\exp\left(-\frac{\gamma}{\gamma_0}(n+1)\right)d\gamma, \\ &= \frac{1}{2}N\sum_{n=0}^{N-1}(-1)^n\binom{N-1}{n}\frac{1}{n+1+\gamma_0/2}.\end{aligned} \tag{4.45}$$

For one antenna and for two antennas we get, respectively,

$$\langle BER\rangle_1 = \frac{1}{2+\gamma_0}, \quad \langle BER\rangle_2 = \frac{1}{2+3\gamma_0/2+\gamma_0^2/4}. \tag{4.46}$$

The improvement in the mean BER, when two antennas are used with de-correlated powers instead of one antenna, can be expressed in a ratio of the expected bit error rates,

$$\frac{\langle BER \rangle_1}{\langle BER \rangle_2} = \frac{2+3\gamma_0/2+\gamma_0^2/4}{2+\gamma_0} = 1+\frac{\gamma_0}{4} = 1+a_3 P_{transmitted}, \tag{4.47}$$

where a_3 is a constant.

4.5 Correlated signals

For two branches, with correlated Gaussian signals ,i.e., Rayleigh fading, we can get asymptotic equations for the equivalent two-branch signal-to-noise ratio. The asymptotic equation (4.46) is only valid when the correlation is not to close to unity [Vaughan et al, 2003]. For two equal power and correlated branch powers, the equivalent de-correlated SNR is

$$\gamma_{de-correlated} \approx \gamma_{correlated}\sqrt{1-|\rho|^2}, \tag{4.48}$$

where ρ is the complex correlation. The geometric mean of two equal power correlated branches γ_1 and γ_2 satisfies

$$\frac{\gamma_2}{\gamma_{mean}} = \frac{\gamma_{mean}}{\gamma_1}, \tag{4.49}$$

and we get

$$\gamma_{de-correlated} \approx \sqrt{\gamma_1\gamma_2}. \tag{4.50}$$

Substituting Eq. (4.50) in Eq. (4.48) results in

$$\frac{\gamma_2}{\gamma_1} \approx 1-|\rho|^2 \approx 1-\rho_{envelope}, \tag{4.51}$$

where $\rho_{envelope}$ is the envelope correlation. This expression gives a relation between diversity gain with unequal de-correlated branch powers and correlated branches with equal power. For example, the diversity gain for equal branch powers with a power correlation of 0.75 is similar to the diversity gain of de-correlated branches with a power difference of 6 dB. When polarisation diversity is used with a branch power difference of 6 dB we get the same performance as space diversity with a power correlation of 0.75. When the separation between the branches is small compared to the de-correlation distance the received signals are correlated and the antenna array behaves like a single antenna. This effect occurs mainly outdoors where signals can be correlated over several wavelengths.

We can conclude that a simple combining technique like selection is sufficient if our goal is to decrease the probability of a fade.

5 Bluetooth module with embedded diversity

To test antenna diversity for Bluetooth a demonstrator has been built. This demonstrator is a modified version of an existing Bluetooth radio module with a diversity switch and an embedded slot antenna. To keep the switch simple, antenna diversity is used in receive mode only. The function blocks of the Bluetooth module are discussed in section 5.1. In section 5.2 we will discuss the design of the diversity switch and in section 5.3 we will investigate the design of the embedded slot antenna.

5.1 Block diagram

A demonstrator Bluetooth radio module (System-in-Package) was developed to show the improvement that can be obtained with a complete Bluetooth system by using antenna diversity. Figure 5.1 shows the schematic of this radio.

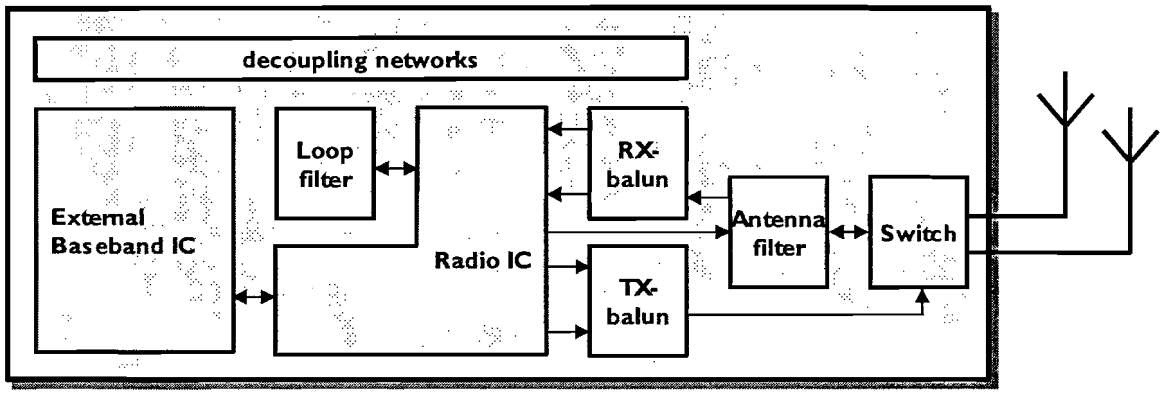

Figure 5.1: *Schematic of the Bluetooth radio module with antenna diversity.*

It consists of a low-IF BiCMOS transceiver, TX and RX baluns, a diversity switch and an antenna filter for out of band blocking. The module also contains a very small-size slot antenna that is optimised over the Bluetooth frequency band. The other antenna that is used in the diversity scheme is external and will typically be an inverted-F or monopole antenna. The total size of the module is approximate 140 mm^2. The radio is built on a thick-film ceramic substrate in which several RF functions are integrated. In receive mode both the internal as well as the external antenna can be selected by means of the two control signals that are generated via the baseband processor. In transmit mode only the external antenna is used. The selection of the 'best' antenna is done by the baseband processor and based on RSSI (Received Signal Strength Indicator) information. Diversity switching from the baseband can be done using two methods: 1) using the received RSSI information at the beginning of each slot (preamble), or 2) the selection of an optimal antenna can be put into a look-up table, where for each frequency an optimal antenna is allocated. The first scenario is difficult to use in practice, since the pre-amble consists of 4 bits only. This is due to the fact that the Bluetooth V1.1 protocol was not written to support diversity. The second method can be used successfully if the look-up table is continuously updated with new information.

The module has to be soldered on a PCB as shown in figure 5.2. In figure 5.2 a module without slot antenna is shown. Normally the slot antenna is integrated on the module and on the PCB. The substrate is made of LTCC, low temperature coefficient ceramic, having an ε_r of 9.5 and a tan δ of 0.0016 at 2.4 GHz. The total thickness from top layer (layer 1) to bottom layer (layer 6) is 550 μm. The thickness of the substrate is 150 μm from the bottom (layer 6) to the fifth layer and between the other layers the thickness is 100 μm.

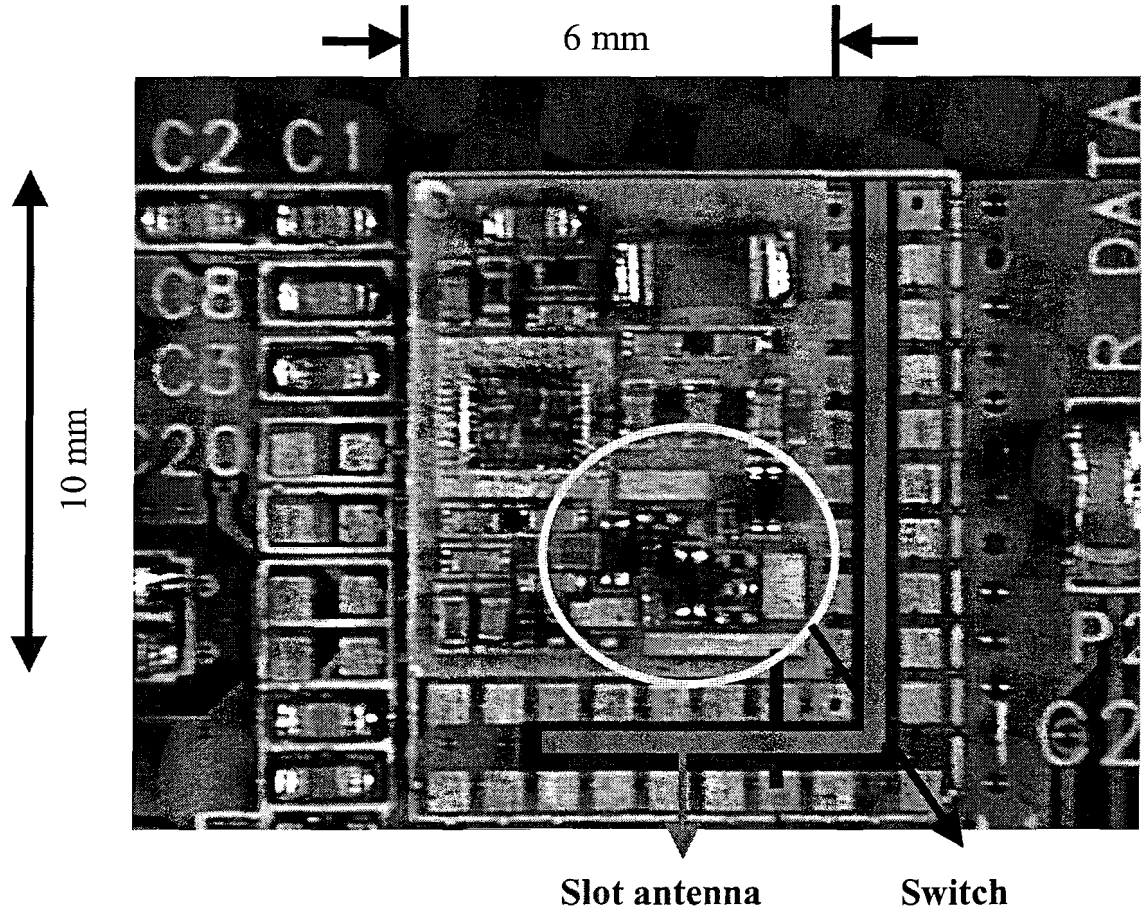

Figure 5.2: *Bluetooth antenna diversity demonstrator mounted on a motherboard.*

5.2 Design of the diversity switch

The diversity switch is shown in figure 5.3 and is built up with three low-cost PIN diodes, giving excellent isolation and low insertion loss.

5.2.1 Principle of the diversity switch

The schematic of the switch is depicted in figure 5.3. The state of the diversity switch is determined by the control lines V_1 and V_2. The PIN diodes D_1, D_2 and D_3 can be activated by applying a voltage of 3 V. The current through the diodes is determined by the value of the resistors R_1 and R_2. When only the control signal V_1 is enabled a current of about 3 mA flows through the PIN diodes. The Radio Frequency, (RF), impedance of the PIN diodes D_3 and D_2 is very low at 3 mA, about 2 + 12j Ω at 2.4 GHz. Diode 2 is a path to ground and the $\lambda/4$ line is a quarter-wave transformer. It transforms the load impedance of D_2 parallel to 50 Ω,

$$Z_{in} = Z_0^2 / Z_{load}\,, \tag{5.1}$$

where Z_{in} is the input impedance at the input of the transformer, Z_0 is the characteristic impedance of the transmission line and Z_{load} is load impedance at the end of the transformer.

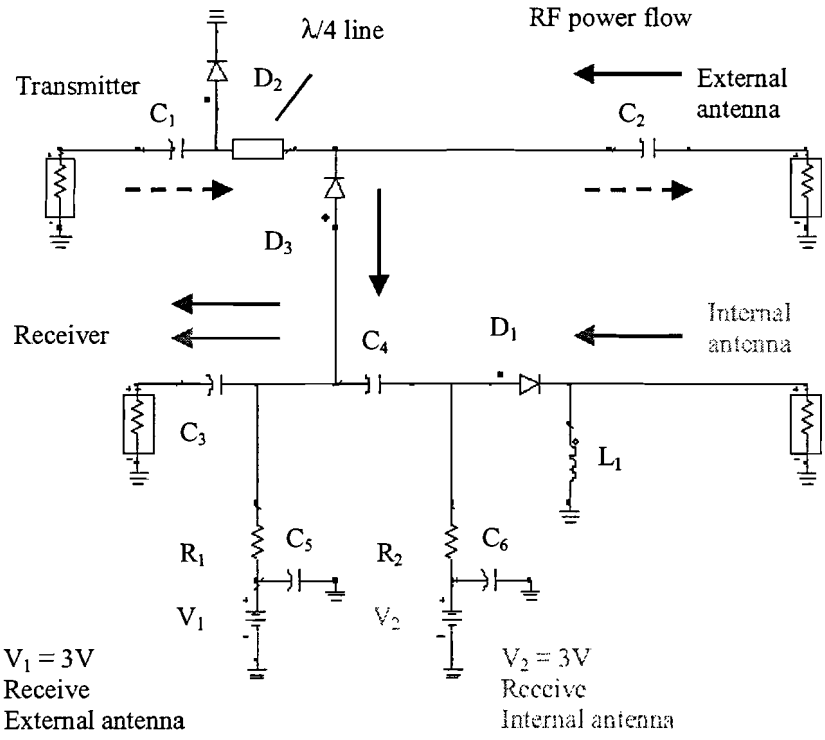

$R_{1,2}$	=	1 KΩ
L_1	=	10 nH
C_1	=	1.8 pF
$C_{2,3,4}$	=	10 pF
$C_{5,6}$	=	4.6 pF

V_1 [v]	V_2 [v]	State	Antenna
3	0	receive	external
0	3	receive	internal
0	0	transmit	external

Figure 5.3: *Schematic of diversity switch with PIN diodes, all terminals are 50 Ω.*

The result is a low-loss path from the external antenna to the receiver at 2.4 GHz. The capacitors are chosen with enough capacitance so that the RF path from external antenna to the receiver has a low series lumped impedance. The 50 Ω source at the external antenna 'sees' a 50 Ω load at the receiver.
When the control signal V_2 is enabled the DC current flows through D_1 and coil L_1 to the ground and the path from the internal antenna to the receiver is enabled. If both sources are disabled the PIN diodes have a high impedance for RF and the RF path from transmitter to external antenna is enabled.

One advantage of this switch is that the low-power RF signal flows through the diodes and the high power flows through the linear components. Distortion only occurs when the signals are large and the received signals are of the order –40 dBm, so the distortion is negligible. The design can be analysed with a network approach and an electromagnetic approach. The quarter-wave transformer is analysed with electromagnetic theory and for the components we use a network approach. For the network analysis we used the circuit simulator of ADS. In the simulation we neglected the effect of solderpads and interconnects between the discrete components. Only the electrical length of the $\lambda/4$ transformer is critical. Therefore, we used an accurate model for this.

5.2.2 Simulated performance

The performance of the switch is evaluated using a *S*-parameter simulator (ADS). The performance of the switch depends on the loss in the signal path and the isolation to the other ports. The Bluetooth protocol does not allow full duplex so the isolation between transmitter and receiver is not critical. Strictly we can only use *S*-parameters if we assume that the network is linear or locally

linear. The PIN diodes are non-linear devices, but since we are dealing with small signals we will use the linear model as depicted in figure 5.4 [Philips semiconductors].

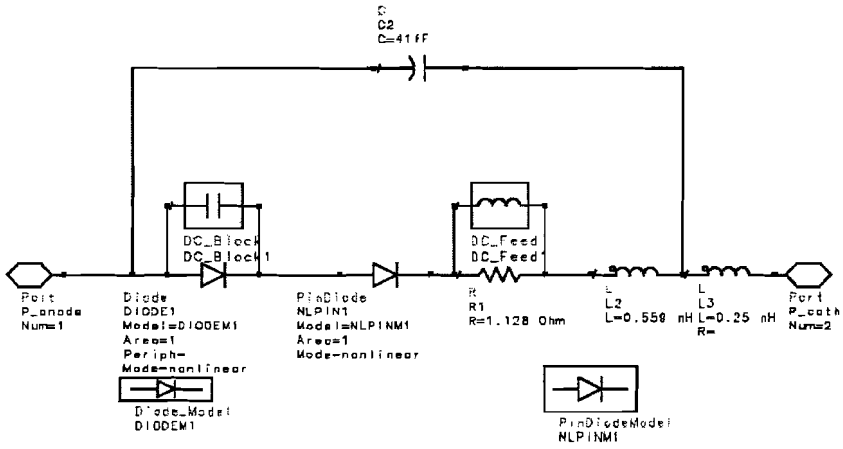

Figure 5.4: *Model of the PIN diode in on-state and off-state.*

The silicon PIN diode of the Philips semiconductors BAP51-01 is designed to operate as a low-loss high-isolation switching element, and is capable of operating with low intermodulation distortion. The model consists of two diodes, in order to achieve a fit on both DC and RF behaviour. Diode1 is used to model the DC voltage-current characteristics, Diode 2 is the PIN diode built in model of ADS and is used to model the RF resistance versus DC current behaviour of the PIN diode-model. Both diodes are connected in series to ensure the same current flow. For RF the PIN junction Diode1 is shorted by an ideal capacitor (DC block), while the portion of the RF resistance, which reflects the residual amount of series resistance, is modelled with R_1=1.128 Ω. To avoid affecting the DC performance this resistor is shunted with the ideal Inductor (DC feed). Capacitance C_2 and inductors L_2 and L_3 reflect the package parasitics. The here described model is a linear model that emulates the DC and RF properties of the PIN diode from 6 MHz up to 6 GHz.

The quarter-wave transformer consists of a quarter-wave transmission line loaded with a PIN diode connected to ground and the output impedance of the transmitter. The impedance of the transmission line for the $\lambda/4$ transformer is simulated using the Linecalc model that is available within ADS as depicted in figure 5.6.

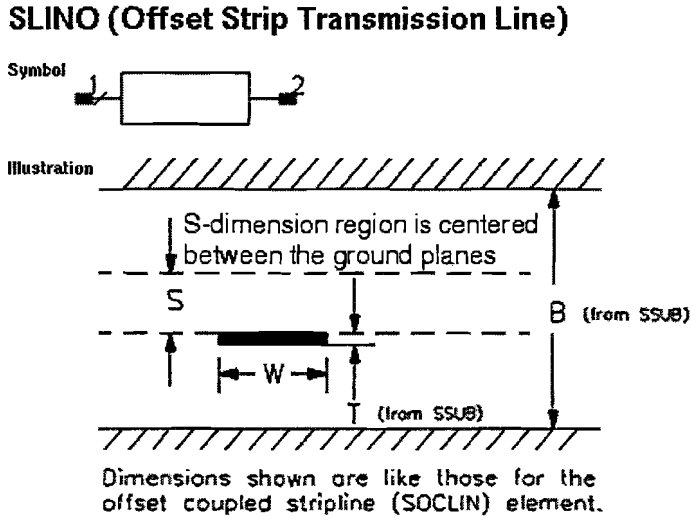

Figure 5.5: *Lay out of the transmission line used for the $\lambda/4$ transformer.*

The simulated structure is a stripline as shown in figure 5.5. It has three conductors with a homogeneous dielectric and can support a TEM wave [Pozar, 1998]. The strip in layer 5 is 150 μm above the bottom layer and 100 μm below layer 4. For a TEM wave in a homogenous dielectric we can use the capacitance to calculate the impedance [Pozar, 1998],

$$Z_0 = \sqrt{\frac{L}{C}} = \frac{\sqrt{LC}}{C} = \frac{\sqrt{\varepsilon_r}}{c_0 C}, \tag{5.2}$$

where L is the inductance per meter, C is the capacitance per meter and c_0 is the speed of light in vacuum. The simulated impedance of the transmission line is about 33 Ω, 86° with Linecalc as depicted in figure 5.6.

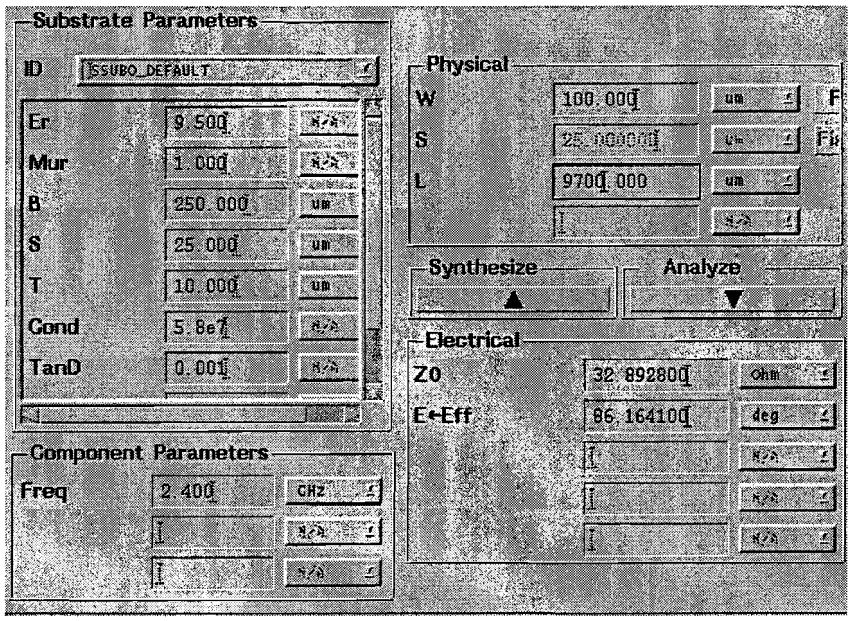

Figure 5.6: *Simulation results with Linecalc of the non-symmetrical stripline.*

The impedance of the stripline is too low and using Eq. (5.2) we see that we have to decrease the capacitance per meter. The capacitance decreases if we decrease the line width. However, we have to follow the design rules of the substrate manufacturer and we cannot decrease the line width. The reflection coefficient from 50 Ω to the 33 Ω transmission line is -0.2. The reflection coefficient of the $\lambda/4$ transformer without loss and loaded with 50 Ω parallel with 2 + 12j Ω can be expressed using a series expansion [Pozar, 1998], and the result is,

$$\Gamma = \frac{\Gamma_1 - \Gamma_3}{1 - \Gamma_1 \Gamma_3}. \tag{5.3}$$

where Γ is the reflection coefficient at the input of the transformer, Γ_1 is the partial reflection at the input of the transmission line and Γ_3 is the partial reflection coefficient at the load. The voltage reflection coefficient S_{11} of the transformer for this load, 4.4 + 10.5j Ω, is about 0.43 -0.58j Ω and the impedance of the transformer is $50*(1+S_{11})/(1-S_{11})$ = 36.5 -88.3j Ω. The impedance of 36.5 - 88.3j Ω is parallel to the impedance of about 50 Ω. The total impedance from diode D_3 is 35.8-14.4j Ω. The modulus of the transmission coefficient from the external antenna, 50 Ω to the diode D_3, 52 + 12j Ω is 0.87 or -1.2 dB. Furthermore, power is lost due to the pin diode D_3 in the path to the receiver. The Pin diode decreases the current through the receiver and the loss is $50^2/(50^2 + 12^2)$ or 0.25 dB. The total loss is about 1.35 dB and the simulated loss with the ADS circuit simulator is 1.2 dB as depicted in figure 5.8a.

The loss from the internal antenna to the receiver is caused by reflections at the network/antenna interface, losses in the network and power leakage to other ports. When the source and load are 50 Ω the power transfer magnitude is $|S_{21}|^2$. The switch performs well from internal antenna to receiver with a loss of 0.66 dB, the isolation between the internal antenna and the transmitter and external antenna is at least 21.5 dB as depicted in figure 5.7b.

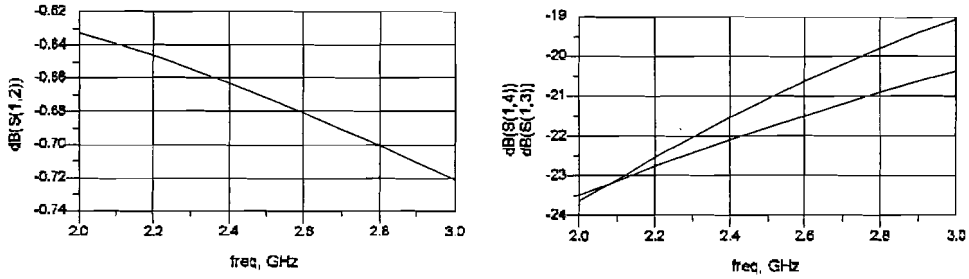

(a) *(b)*

Figure 5.7: *Simulated power loss from (a) the internal antenna to the receiver, (b) isolation between internal antenna and transmitter and isolation between internal antenna and external antenna.*

The power loss and isolation of the RF path from the external antenna to the receiver is depicted in figure 5.8. From external antenna to the receiver the loss is 1.1 dB and the isolation is 13 dB.

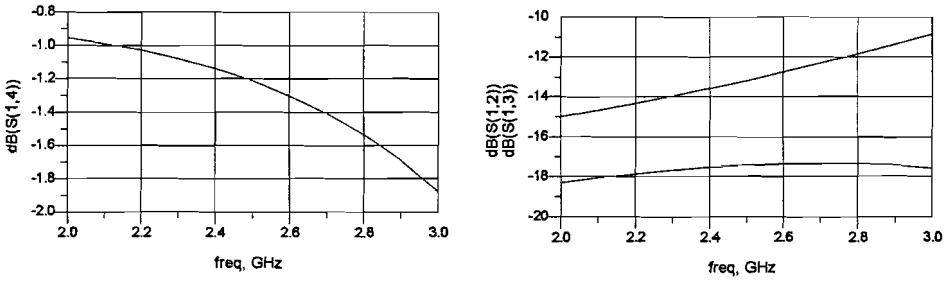

(a) *(b)*

Figure 5.8: *Simulated power loss from (a) the external antenna to the receiver, (b) isolation between external antenna and transmitter and isolation between external antenna and internal antenna.*

The performance of the RF path from the transmitter to the external antenna is depicted in figure 5.9. From external antenna to the transmitter the loss is 0.47 dB and the isolation to the other ports is 12 dB.

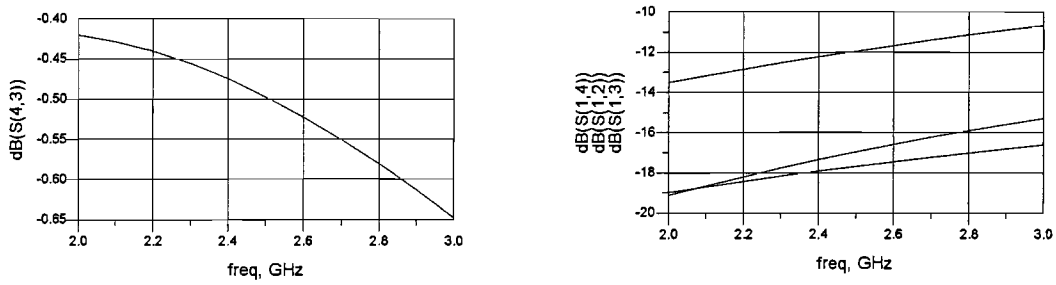

(a) *(b)*

Figure 5.9: *Simulated power loss from (a) the transmitter to the external antenna, (b) isolation between internal antenna and transmitter and isolation between external antenna and internal antenna.*

The simulated loss should be far below the expected gain from the adaptive receiver. In a fade the gain is about 30 dB and the array gain for Rayleigh-fading is 1.76 dB. So, for the receiver we improve the performance in a fade and we improve the overall performance with this diversity switch. The switch decreases the output power with 0.5 dB. Which means that we are still able to reach the specified 0 dBm output power.

5.3 Slot antenna analysis

The quality of the radio link depends on the antenna properties such as the radiation pattern. In a multi-path environment the product of the incident power distribution and antenna gain pattern results in the received power at the antenna terminals. Furthermore, the polarisation of incident waves and antenna gain has to be taken into account. The antenna pattern can be calculated for free -space propagation. We assume that the antenna pattern indoors is the same as the antenna pattern for free-space propagation. The slot antenna is not sensitive for surrounding objects [Grauw, 2001]. The incident field indoors is complex because all the objects in the room influence the EM-field. In general the incident EM-field has to be modelled. The internal antenna, embedded in the Bluetooth module, used for the diversity measurement is a slot antenna. The external antenna is a monopole antenna. The layout of the slot antenna is depicted in figure 5.10. The Black area is copper, with a thickness is larger than the skin depth at 2.4 GHz.

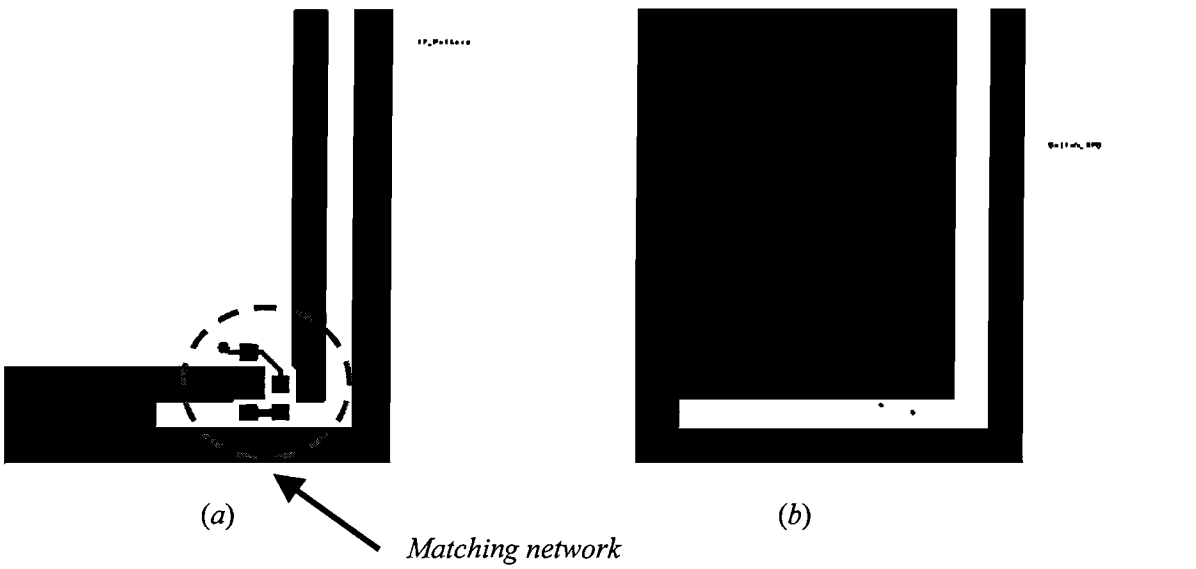

Figure 5.10: *Top (a) and bottom metalisation (b) of the antenna.*

The top layer and bottom layer are connected by via's and are connected to the ground. The antenna has an unbalanced feed with a matching network to transform the impedance to 50 Ω. The wavelength depends on the propagation constant in the substrate, so the physical slot length is smaller on the ceramic ($\varepsilon_r = 9.6$) than on the motherboard ($\varepsilon_r = 4.6$).

5.3.1 Operating modes of the slot antenna

The antenna operates in three modes depending on the frequency at the feed terminals [Grauw, 2001]

- mode 1: LC-resonator

Apart from a rigorous Method-of-Moments analysis we can also model the slot antenna using a much simpler transmission-line model. This model can be used when the distance between the slot and the edge of the ground plane is much smaller than a quarter wavelength. We then get a quarter wavelength transformer that is open on the $\lambda/4$ side and shortened on the feed side. The electric equivalent is a parallel LC-resonator, and there is hardly any radiated power.

- mode 2: RLC-resonator

When the distance between the slot and the edge of the ground plane is about $\lambda/4$ the antenna becomes resonant. The ground-plane behaves as a (asymmetric) dipole. The electric equivalent is a parallel RLC-resonator. So the real part of the input impedance increases and the antenna starts to radiate. The resonance frequency and bandwidth are now sensitive to changes in the ground plane.

- mode 3: Magnetic current in the slot

The ground-plane is no longer a resonant structure is when the distance between the slot and the edge of the ground plane is larger than $\lambda/4$. Now we can use the equivalence between an electric dipole, with an electric current flowing in a conductor, and a magnetic dipole with a magnetic current flowing through a slot. This equivalence is Babinet's principle [Jackson, 1963]. The slot is fully complementary to a conductor with the size of the slot. Furthermore, the ground plane is complementary to free-space, so the ground plane should be infinite. Like an electric monopole is mirrored by a perfect conducting ground plane, the magnetic monopole is mirrored by an electric wall, and looks like a dipole. When E and H are interchanged, the polarisation of E is also interchanged. The resonance frequency and bandwidth are now defined by the slot size.

5.3.2 Simulation with Momentum of the slot antenna

The layout with port definition for the simulation is depicted in figure 5.11.

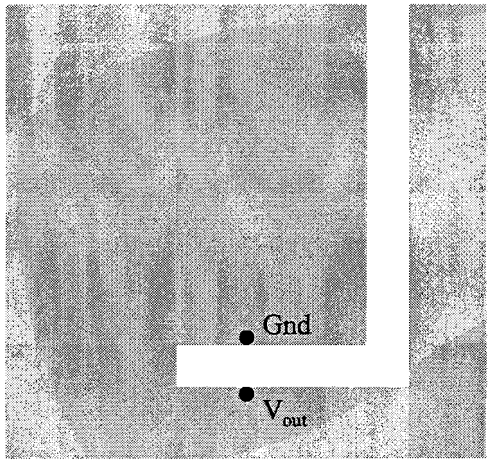

Figure 5.11: *Configuration used for simulation with feed at the dots.*

In the simulation we use an effective ε_r to take into account the difference between top and bottom layer. The tan δ, size of the substrate and the thickness and conductivity of the conducting layer must be defined. For the simulation we use free space around the pcb. The current distribution on the layout is calculated with the Method-of-Moments [Harrington, 1993]. The layout is divided in subdomains using a mesh. The mesh size is related to the size of the subdomain basis function in the numerical calculation. When the current changes rapidly we need a small mesh size. A rule of thumb is a mesh size of about $\lambda/10$.

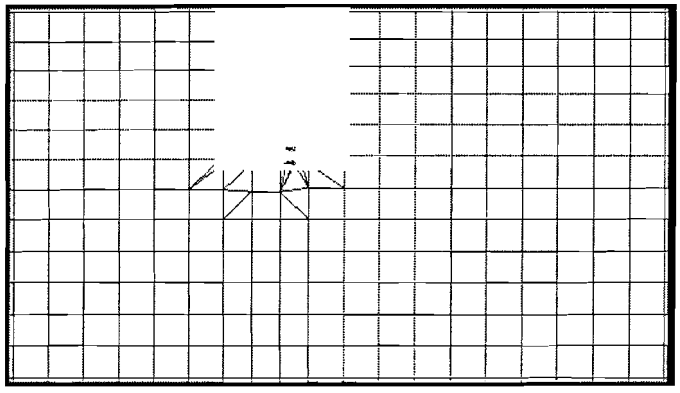

Figure 5.12: *Meshing of the groundplane.*

A commercial tool, Momentum, was used to perform the electromagnetic simulation. To approximate the currents on the layout Momentum uses roof-top basis functions, triangles, in the subdomain for the currents in the x- and y-direction. To take into account the rapid increase of tangential current on the edges, [Smolders, 1994], there is a small mesh on the edges. For a proper simulation we have to use a full-wave simulation that takes into account the complete set of Maxwell equations. We have to define the frequency range in which the simulator can use an adaptive sweep to minimise the number of frequencies. When the simulation starts the Green's functions are calculated and the matrix is solved. This results in a solution for the current distribution. We end up with an approximation of the current over the complete domain. The current at the feed port is known and the S-parameters at the feed port can be displayed to examine the matching. With post processing the radiation pattern is calculated from the currents. An example of the current distribution is depicted in figure 5.13.

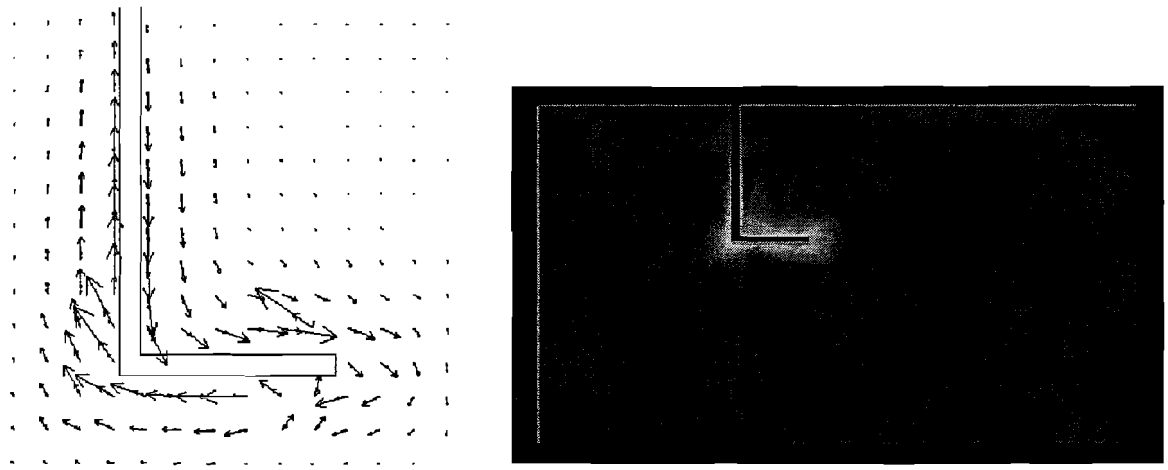

(*a*) (*b*)

Figure 5.13: *Example of the current density of the slot antenna near resonance along the slot (a) and (b) on the PCB.*

The current flows mainly along the edges of the slot. It is possible to show one period of the current and then it becomes clear that the current changes periodic in time over the complete layout. The currents along both sides of the slot are 180° out of phase, corresponding to an odd mode.

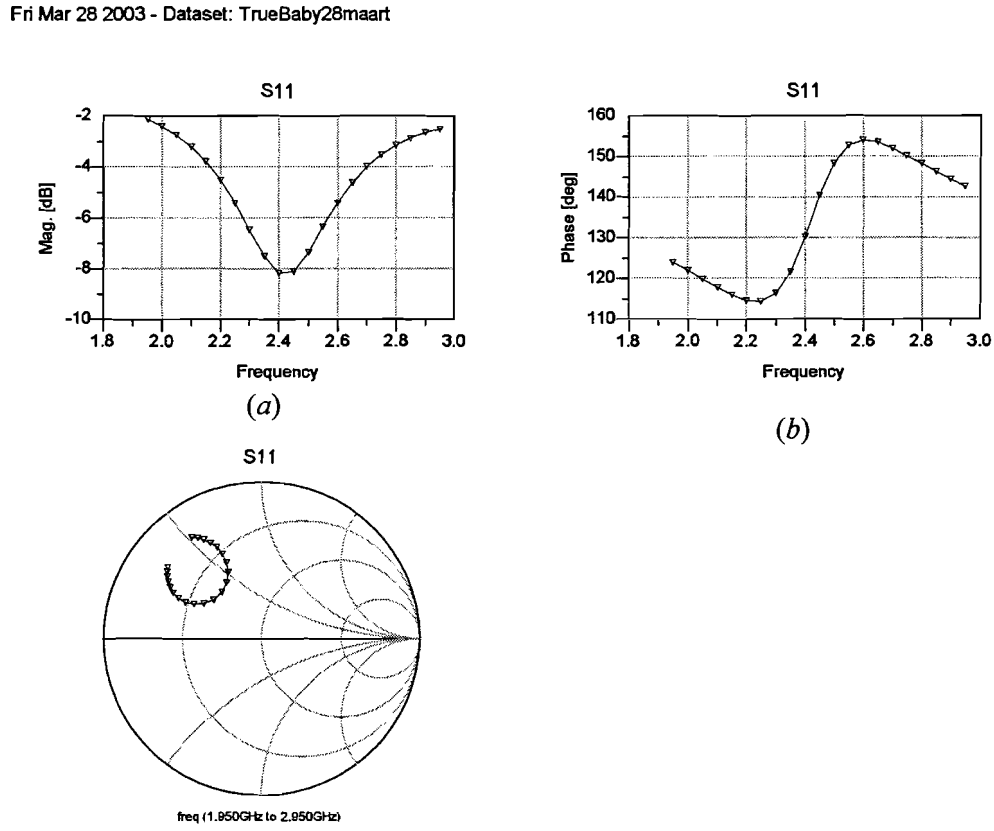

(*a*) (*b*) (*c*)

Figure 5.14: *Magnitude of S_{11} (a) at and (b) phase of S_{11} and (c) Smith chart of S_{11} at the feed port.*

The resonance frequency is indeed in the neighbourhood of 2.4 GHz, but the matching needs to be improved. There are several possible matching networks, a few simple networks are: a parallel coil with series capacitance, a parallel capacitor with a series coil and a series resistor with a series capacitance. The calculated radiation patterns are depicted in figure 5.15 and 5.16.

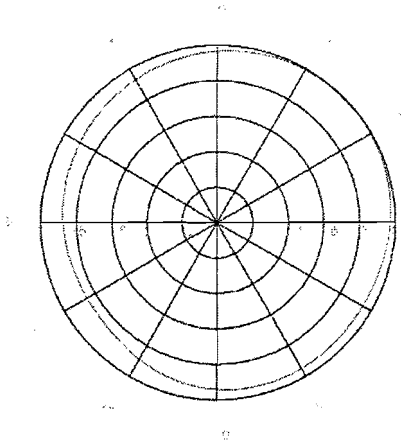

φ in degrees

(*a*)

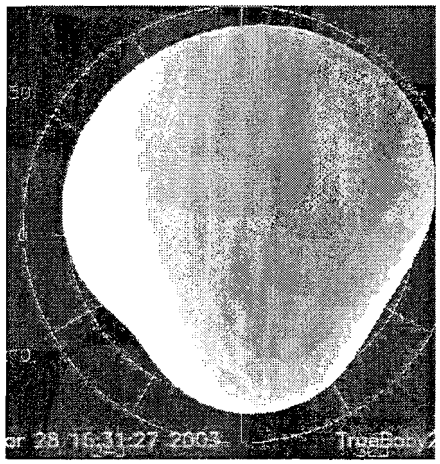

(*b*)

Figure 5.15: *Two-dimensional radiation pattern with log scale (a) and a three-dimensional radiation pattern with linear scale (b) at $\theta = 45°$ (top view) at 2.44 GHz.*

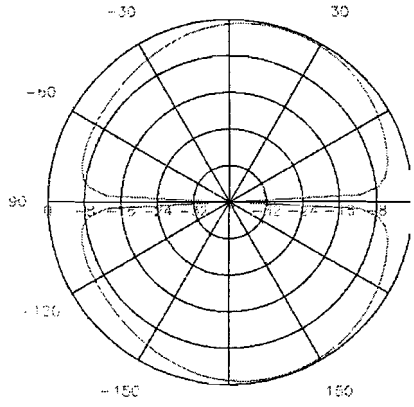

φ in degrees

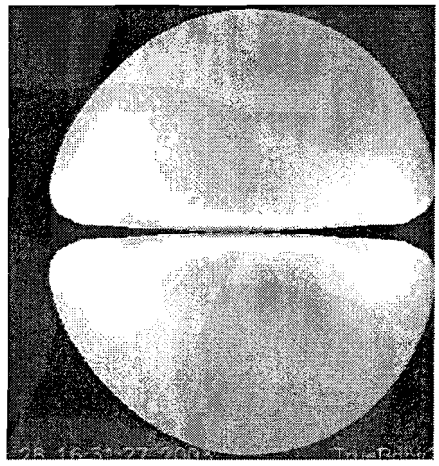

(*a*)

(*b*)

Figure 5.16: *Radiation pattern at $\varphi = 0°$ and 2.44 GHz, with log scale (a) and three-dimensional colour graded side view where low radiation intensity is yellow and high intensity is red.*

For antenna diversity it is also important to consider the polarisation properties of the antenna. The simulation decomposes the radiated electric field in two orthogonal components, the co-polar field and the cross-polar field.

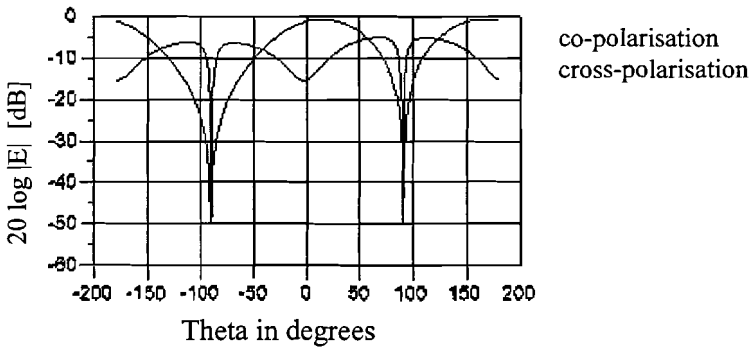

Figure 5.17: *Radiation pattern at $\varphi = 0°$, $\theta = 0$ is perpendicular to the surface of the slot antenna.*

From figure 5.17 we observe that, although the cross-polar component is smaller than the co-planar component, this component cannot be ignored. The power efficiency is also calculated and is almost 80 %.

5.3.3 Electromagnetic model

More insight is obtained when the slot antenna is analysed using a magnetic current in the slot. For this analysis we need the dimensions of the slot antenna as depicted in figure 5.18.

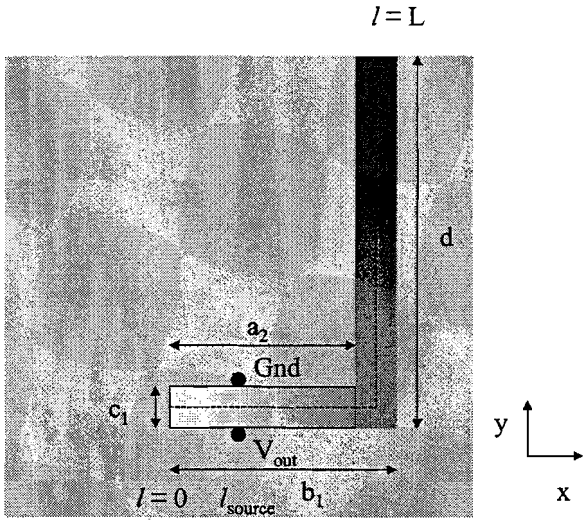

Figure 5.18: *Dimensions of the slot antenna.*

where c_1 is the width of the slot, a_2 is the length of the horizontal part and L is the length of the slot. A wire antenna and a slot antenna are complementary with E and H interchanged [Kraus, 1992]. An analogy with the electric current on a wire is the introduction of a magnetic current in the slot. This maps all the electric current sources on the metalisation layers to a magnetic current in the slot area. The relation between the magnetic current and the electric field is [Smolders, 2000]:

$$\vec{M} = \vec{E}(\vec{r}_0) \times \vec{e}_n, \tag{5.4}$$

where $\vec{e}_n$ is normal to the slot surface. We can use a Fourier series to approximate the E-field in the slot. The field in the slot surface can be described using the parameter l along the slot. With boundary condition $\vec{E}(t) = \vec{0}$ at the start of the slot inside the PCB and $\vec{r}_0(l)$ we obtain:

$$\vec{E}(t)=\sum_{n=0}^{m}C_n\sin\left(\frac{n\,l\pi}{2L}\right)\left[-\vec{e}_x U(l-a_2)+\vec{e}_y\{U(l)-U(l-b_1)\}\right]\quad l\in[0,L],$$
$$V=\int_{y=0}^{y=c_1}E\,dy=c_1\sum_{n=0}^{m}C_n\sin\left(\frac{n\,l_{source}\,\pi}{2L}\right), \tag{5.5}$$

where V is the voltage at the feed terminals and C_n is the magnitude of mode n. The slot is divided in three domains to take into account the direction of the magnetic current. From figure 5.18 we can observe that the first domain is $0 < l \le a_2$, the second domain is $a_2 < l \le b_1$ and the third domain is $b_1 < l \le c_1$. Substituting Eq. (5.5) into Eq. (5.4) gives the magnetic current,

$$\vec{M}=\vec{E}(t)\times\vec{e}_z=\sum_{n=0}^{m}C_n\sin\left(\frac{n\,l\pi}{2L}\right)\left[\vec{e}_x\{U(l)-U(l-b_1)\}+\vec{e}_y U(l-a_2)\right]. \tag{5.6}$$

The Lorentz-Larmor theorem [Smolders, 2000], states that for the field outside a volume, all sources in a volume can be replaced by sources on the surface of the volume. The electric field can be written as function of an equivalent electric and magnetic current with as kernel of the integration the Green's function of free-space. However, the surface boundary conditions allow surface currents on the whole surface and not only at the edge of the aperture.
When we consider the surface just above and below the printed circuit board (pcb), we get $\vec{E}(\vec{r})\times\vec{e}_n=\vec{0}$ above the metalisation layer and $\vec{E}(\vec{r})\times\vec{e}_n\neq\vec{0}$ in the slot. This might be untrue at the edges of the pcb but it can be considered a good approximation. The H-field is a generated by the slot edge currents. Due to odd modes, opposite symmetrical currents along the slot edge, the H-field is almost zero outside the slot area. Furthermore, the H-field has a different direction due to the odd modes, $\vec{e}_n\times\vec{H}_{left}=-\vec{e}_n\times\vec{H}_{right}$, and in the slot surface $\vec{H}(\vec{r}_0)=H\,\vec{e}_n$. With these approximations, the Lorentz-Larmor theorem applied on the surface S results in integration over the slot surface only:

$$\begin{aligned}\vec{E}(\vec{r})&=\nabla_r\times\int_S[\,\vec{e}_n\times\vec{E}(\vec{r}_0)]\,\varphi\,dS+\frac{1}{j\omega\varepsilon_0}\nabla_r\times\nabla_r\times\int_S[\vec{e}_n\times\vec{H}(\vec{r}_0)]\,\varphi\,dS,\\&\approx\nabla_r\times\int_{Slot}\vec{M}\,\varphi\,dS=-jk_0\vec{e}_r\times\int_{Slot}\vec{M}\,\varphi\,dS,\end{aligned} \tag{5.7}$$

where $\nabla_r\times$, the curl operator operating on $\vec{r}$, can be replaced by $-jk_0\vec{e}_r\times$, $\vec{r}_0$ is in the slot surface and φ is the Green's function of free-space,

$$\varphi(\vec{r},\vec{r}_0)=\frac{1}{4\pi}\frac{\exp\left(-jk_0|\vec{r}-\vec{r}_0|\right)}{|\vec{r}-\vec{r}_0|}\approx\frac{\exp(-jk_0r)}{4\pi r}\exp(jk_0(x_0u+y_0v)), \tag{5.8}$$

where $u=\sin\theta\cos\varphi$ and $v=\sin\theta\sin\varphi$. The radiation pattern and the field distribution in the slot in equation (5.7) are a pair with a transform similar to the Fourier transform. So a slot with a small width and a constant current along the slot transforms to a uniform radiation pattern in the φ-direction and a sinc radiation pattern in the θ-direction. We can calculate the electric field per mode,

$$
\begin{aligned}
\vec{E}_n(\vec{r}) &\approx -jk_0 \int_{Slot} \vec{e}_r \times \vec{M}\, \varphi\, dS, \\
&= \int_{Slot} C_n \sin\left(\frac{nl\pi}{2L}\right) \varphi \left[\vec{e}_r \times \vec{e}_x \{U(l) - U(l-b_1)\} - \vec{e}_r \times \vec{e}_y U(l-a_2)\right] dt, \\
&\approx \frac{-jk_0 \exp(-jk_0 r)}{4\pi r} \int_0^{b_1}\int_0^{c_1} C_n \sin\left(\frac{nl\pi}{2L}\right) \vec{e}_r \times \vec{e}_x \exp(jk_0(lu + y_o v))\, dy_0\, dt \\
&+ \frac{-jk_0 \exp(-jk_0 r)}{4\pi r} \int_{a_2}^{L}\int_{a_2}^{b_1} C_n \sin\left(\frac{nl\pi}{2L}\right) \vec{e}_r \times \vec{e}_y \exp(jk_0(x_0 u + lv))\, dx_0\, dt.
\end{aligned}
\tag{5.9}
$$

We can rewrite Eq. (5.9) using

$$
\begin{aligned}
&\vec{e}_r \times \vec{e}_x = \vec{e}_\varphi \cos\theta \cos\varphi + \vec{e}_\theta \sin\varphi, \\
&\vec{e}_r \times \vec{e}_y = \vec{e}_\varphi \cos\theta \sin\varphi - \vec{e}_\theta \cos\varphi\ , \\
&k_0 c = k_0(b_1 - a_2) << 1.
\end{aligned}
\tag{5.10}
$$

The radiated electric field generated by the n^{th} mode of the magnetic current is,

$$
\begin{aligned}
\vec{E}_n(\vec{r}) \approx{}& \frac{-jk_0 \exp(-jk_0 r)}{r} c_1 \int_0^{b_1} C_n \sin\left(\frac{nl\pi}{2L}\right) \exp(jk_0 lu)\, dl\, [\vec{e}_\varphi \cos\theta \cos\varphi + \vec{e}_\theta \sin\varphi] \\
&+ \frac{-jk_0 \exp(-jk_0 r)}{r} c_1 \int_{a_2}^{L} C_n \sin\left(\frac{nl\pi}{2L}\right) \exp(jk_0 lv)\, dl\, [\vec{e}_\varphi \cos\theta \sin\varphi - \vec{e}_\theta \cos\varphi].
\end{aligned}
\tag{5.11}
$$

For the mode $n = 0$ the radiated electric field is:

$$
\begin{aligned}
\vec{E}_0(\vec{r}) \approx{}& E_0 \frac{-jk_0 \exp(-jk_0 r)}{r} \frac{\sin(k_0 b_1 u/2)}{k_0 b_1 u/2} [\vec{e}_\varphi \cos\theta \cos\varphi + \vec{e}_\theta \sin\varphi] \\
&+ E_0 \frac{-jk_0 \exp(-jk_0 r)}{r} \frac{\sin(k_0(L-a_2)v/2)}{k_0(L-a_2)v/2} [\vec{e}_\varphi \cos\theta \sin\varphi - \vec{e}_\theta \cos\varphi].
\end{aligned}
\tag{5.12}
$$

In analogy with an electric dipole we can assume that the mode $n = 1$ is dominant. Furthermore, the magnetic current is mirrored at the open end ($l = L$). The open end is a magnetic wall for 'magnetic currents', and the short is an electric wall for electric currents. Numerical calculations are done for several modes as shown in figure 5.19, 5.20 and 5.21. From figure 5.19 we can observe that the second mode is probably a dominant mode. This radiation pattern looks omni directional like the Momentum simulation. The second mode is the mode we expect in a dipole. The antenna is a superposition of a horizontal and vertical magnetic monopole.

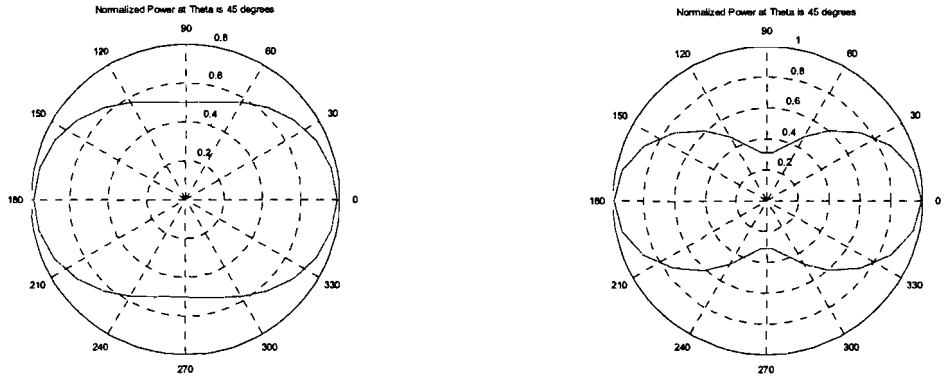

(*a*) (*b*)

Figure 5.19: *Radiation pattern as function of the angle φ, (a) mode n=1 and mode n=2 (b) of magnetic current at θ = 45°.*

The radiation pattern in *θ*-direction is depicted in figure 5.20. Like the simulation with Momentum there is no radiation in the horizontal plane.

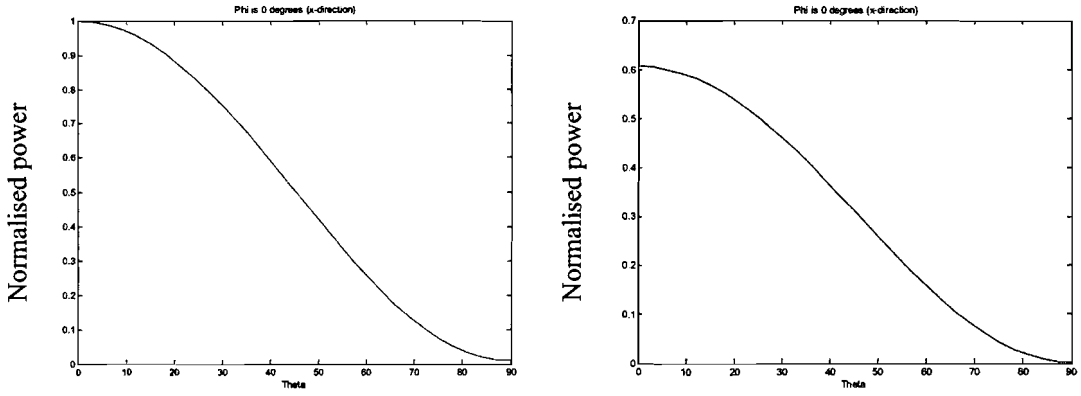

(*a*) (*b*)

Figure 5.20: *Radiation pattern (a) second mode and (b) third mode of magnetic current at φ= 0°.*

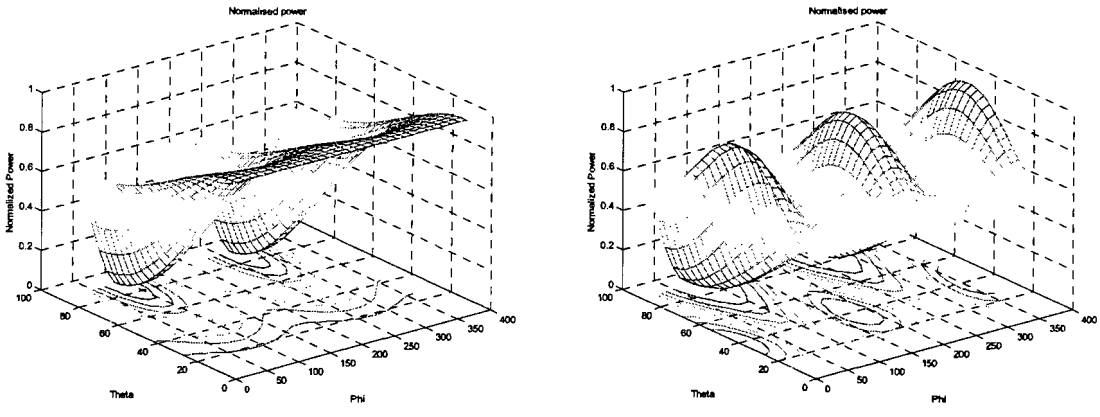

(*a*) (*b*)

Figure 5.21: *Radiation pattern (a) second mode and (b) third mode of the magnetic current.*

The radiation pattern as function of the spatial angles is depicted in figure 5.21.

When the incident waves arrive from all angles and are Gaussian distributed in phase and polarisation we have four degrees of freedom. There is a co-polarisation component with a phase (two degrees) and a cross-polarisation component with a phase. In case of the slot antenna with an almost uniform radiation pattern we get almost identical distributions for every variate we can expect that the received power is χ^2 distributed with $n = 4$ for NLOS. For LOS we can expect that the received power is non-central χ^2 distributed.

6 Measurements and simulations

In chapter 3 propagation models were discussed. The indoor EM field was calculated using Hertzian dipoles for the cavity model and the hybrid model. In this chapter, the results of the simulations and measurements with monopole antennas are presented and compared. In addition, diversity tests were done with a Bluetooth module with diversity and an embedded slot antenna.
The measurements were performed using a special diversity test bench in a normal office room at Philips Research. The purpose of the measurement is to get an idea of the propagation properties of an indoor environment at the Bluetooth frequencies. The indoor propagation is analysed using transmit and receive antennas. The ratio between transmitted and received power, expressed in *S*-parameters, is a measure of the propagation. In the last section of this chapter the Bluetooth antenna diversity demonstrator from chapter 5 is used to switch between two receiving antennas. The receive antennas, a slot antenna and a monopole, have a different position, polarisation and radiation pattern. In this case the ratio between the bit errors, without error correction, and the total number of transmitted bits is used to measure the indoor propagation properties.

6.1 Field strength measurement set-up

The measurement set-up is depicted in figure 6.1. The set-up consists of a network analyser for the propagation measurement and a *xy*-table with step engines. The set-up is controlled by a personal computer. The transmit antenna, a $\lambda/4$ monopole, moves from point to point where the distance between the points is for example $\lambda/10$. The antenna follows a trace as depicted in figure 6.2.

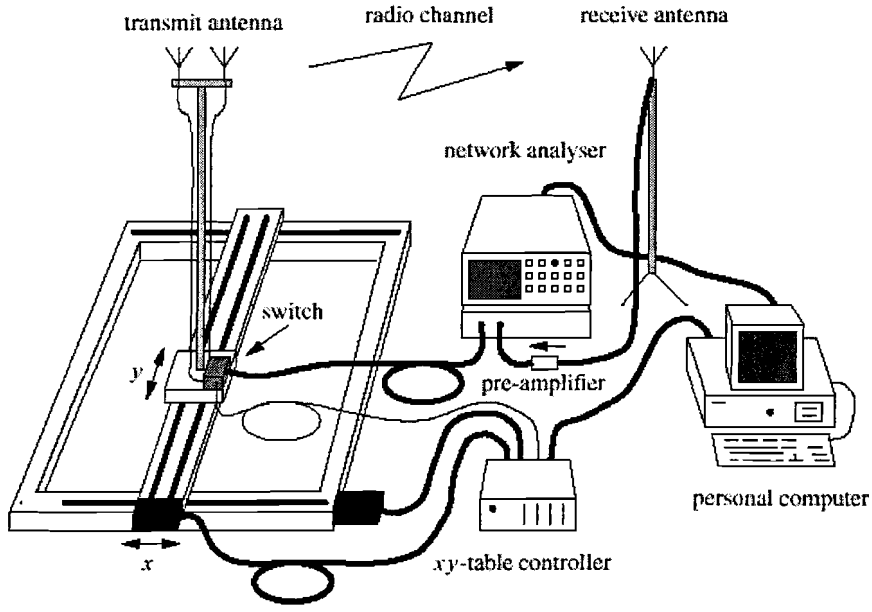

Figure 6.1: *Measurement set-up for the propagation measurements.*

At each position the *S*-parameters are measured and the result is put in a matrix where the rows represent the *x*-position and the columns the *y*-position.

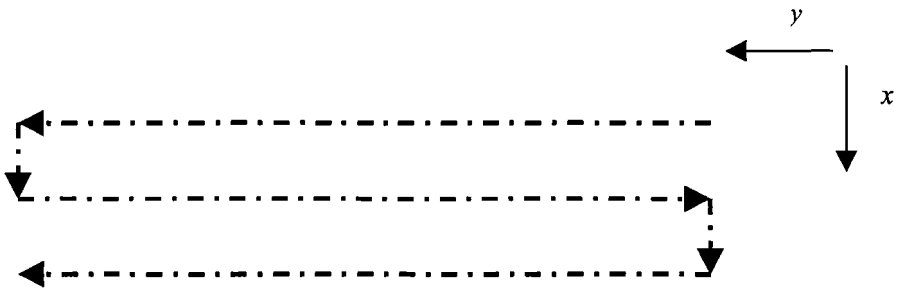

Figure 6.2: *Movement of the antenna mounted on the xy-table.*

The dimensions of the measurement room and the position of the antennas in the room are shown in figure 6.3. In the room are also chairs, tables etc. These objects reflect and absorb the radiated EM waves. For this measurement they provide a realistic indoor propagation environment.

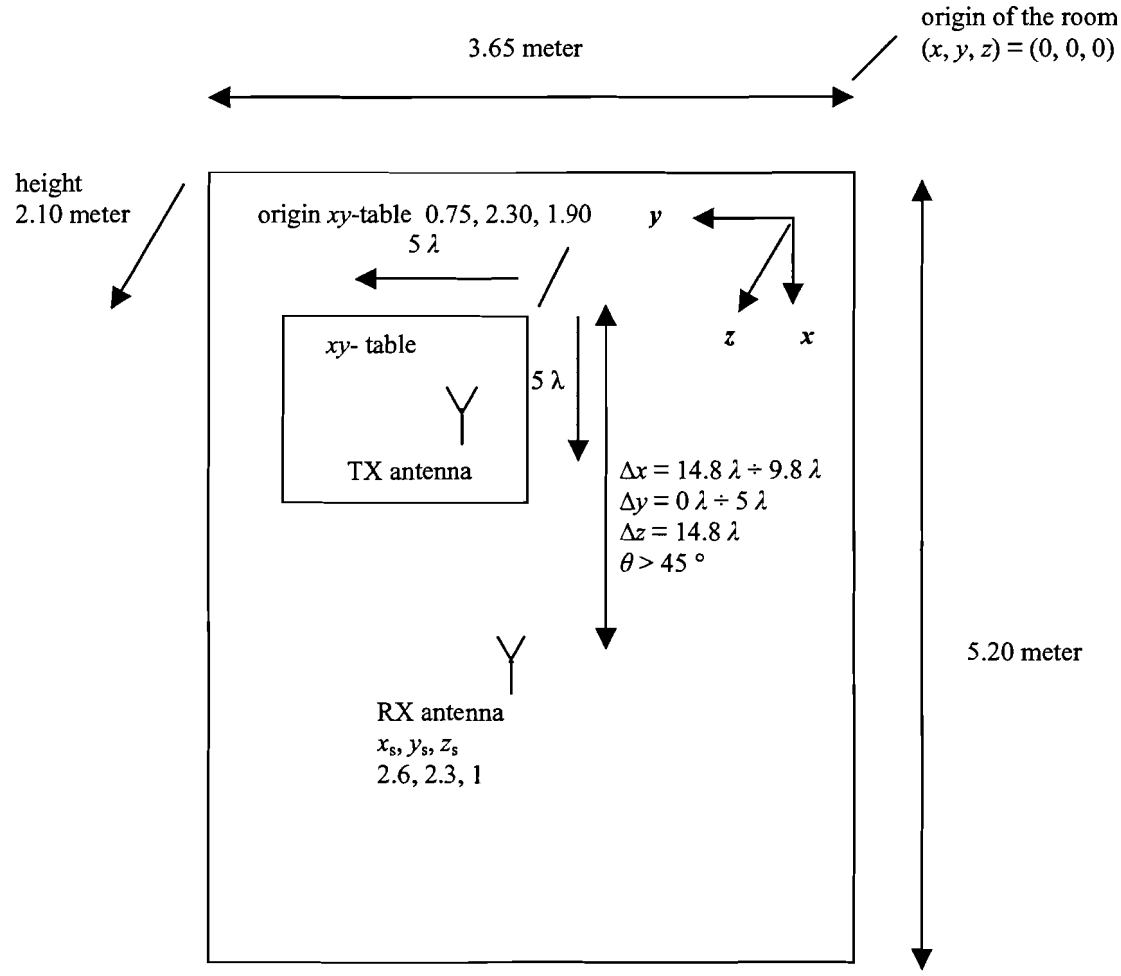

Figure 6.3: *Dimensions of the measurement room and position of the antennas.*

Before the measurements are performed the network analyser is calibrated at 201 frequencies at the end of the cables with a short, open, load and a through connection. After calibration a correction matrix is calculated. With this correction matrix the network analyser is (mathematical) perfectly 50 Ω at the end of the cables. In this way the reference planes for the S_{21} measurements are at the input terminals of both antennas.

For each frequency the power transfer $|S_{21}|^2$ between transmitter and receiver is measured. This can be represented as:

$$\frac{P_{received}}{P_{transmitted}} = |S_{21}|^2 = |S_{12}|^2 . \tag{6.1}$$

where $P_{received}$ is the received power, $P_{transmitted}$ is the transmitted power, $S_{21} = \{ S_{21}(f_1, x_1, y_1), \cdots, S_{21}(f_k, x_l, y_m)\}$, f_i is the frequency and where it is assumed that the propagation is reciprocal, i.e., $|S_{21}| = |S_{12}|$. In free-space, equation (6.1) would become the well-known radio equation, namely

$$\frac{P_{received}}{P_{transmitted}} = (1-|S_{11}|^2)(1-|S_{22}|^2)\, G_t(\theta_t,\phi_t)\, G_r(\theta_r,\phi_r)\, \eta_{rad}\, \eta_{pol} \left(\frac{\lambda}{4\pi r}\right)^2 , \tag{6.2}$$

where $|S_{11}|$ and $|S_{22}|$ are reflection coefficients of the antennas, G_t and G_r are the antenna gain of the transmit and receive antenna, respectively, η_{rad} is the antenna efficiency and η_{pol} is the polarisation efficiency. For free-space propagation the attenuation is $(4\pi r/\lambda)^2$, which corresponds to $40+20\log r$ dB at 2.4 GHz. The modulus of the reflection coefficient of the antennas, $|S_{11}|$ and $|S_{22}|$, is about 0.01 at 2.4 GHz, so S_{11} and S_{22} can be neglected in Eq. (6.2).
When *S*-parameters are measured it becomes possible to derive radio channel propagation parameters like: amplitude and phase distribution, delay spread, spatial correlation, frequency correlation and polarisation correlation.

6.2 Field strength measurement results

For all positions the propagation parameter S_{21} is put into a matrix M:

$$M(x,y,f_1) = \begin{bmatrix} S_{21}(x_1,y_1,f_1) & \cdots & S_{21}(x_1,y_{51},f_1) \\ \cdot & \cdot & \cdot \\ S_{21}(x_{51},y_1,f_1) & \cdots & S_{21}(x_{51},y_{51},f_1) \end{bmatrix}, \tag{6.3}$$

where there are 51 positions in the x-direction and 51 positions in the y-direction. The measurements are carried out at 201 frequencies, and M becomes an element of a matrix N,

$$N(f) = [M(f_1), \cdots, M(f_{201})]. \tag{6.4}$$

This matrix N can then be used to make a plot of the phase and amplitude distribution of the measured complex S_{21} coefficients.

The measurement parameters are:

- x-direction 5 λ resolution 1/10 λ, y-direction 5 λ resolution 1/10 λ,
- 2601 points (51x51) at each frequency,
- vertical transmit polarisation and vertical receive polarisation (z to z),
- vertical transmit polarisation and horizontal receive polarisation (z to x, z to y),
- transmit antenna and receive antenna are $\lambda/4$ monopoles,
- measurement of S_{21} at 201 frequency points,
  start frequency 2.34 GHz, stop frequency 2.54 GHz and frequency step 1 MHz.

The expected variation in the field has a period of 5/10 λ, so a step size of 1/10 λ is a good start. With the measurement set-up shown in figure 6.3, we have Line Of Sight (LOS) propagation. However, the monopole antennas are at a different height and have a reduced antenna gain in the line of sight direction, so the direct waves are not dominant. We start with the most important measurement results, the phase distribution and the amplitude distribution of the propagation. The

power transfer at the xy-table, $|S_{21}|^2$, without reflections at the cable antenna interface, is depicted in figure 6.4.

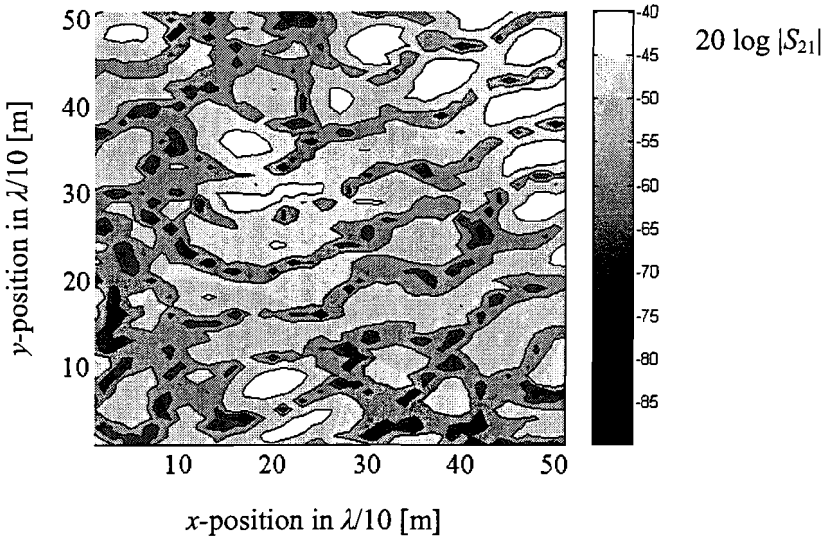

Figure 6.4: *Contour plot of the measured power transfer* 20 log $|S_{21}|$ *at the centre frequency 2.44 GHz.*

The fades, positions with a low power transfer, are spread more or less uniformly over the measured xy-domain. The distance over which the power is correlated is the average radius of an area with the same colour. From figure 6.4 we can observe that the dark area has a radius of about 5 units or half a wavelength.
In figure 6.5 a histogram of the phase of S_{21} is depicted. Due to the bin size of the histogram the data is smoothed. It appears that the phase is concentrated at two values separated by 180° with a little spread. The measured phase distribution as shown in figure 6.5 is very similar to the expected phase distribution in a perfectly conducting room, that is in phase and 180° out of phase with zero spread. The calibration of the network analyser, depicted in figure 6.1, is performed at the end of the measurement cables and not at the antennas. This can be the reason that there is an overall shift of about –60° in the phase distribution. A LOS propagation measurement, where the direct waves are dominant, gives a more uniform phase spread (see appendix A). In this case, the set-up of figure 6.3, the ratio between direct waves and scattered waves is small.

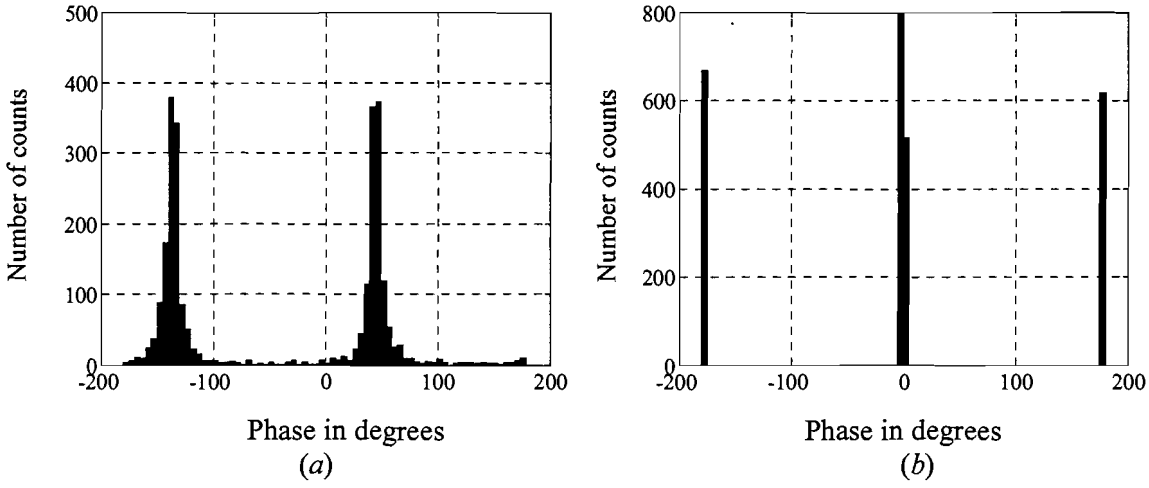

Figure 6.5: *Measured phase distribution (a) at centre frequency and (b) phase distribution of the perfect conducting cavity.*

In figure 6.6 a histogram is shown of the real part of S_{21} and the imaginary part of S_{21}. Both are Gaussian distributed with zero mean and a standard deviation of 0.005.

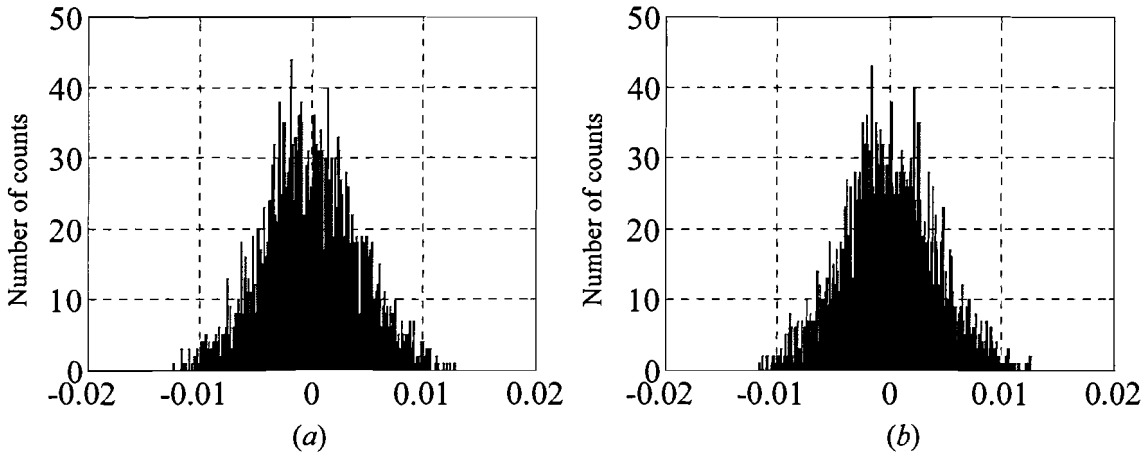

Figure 6.6: *Distribution of the (a) real and (b) imaginary part of the measured S_{21} at the centre frequency.*

The envelope of two orthogonal (independent), and Gaussian distributed signals with zero mean and equal variance is Rayleigh distributed (see appendix A). Figure 6.7 shows the histogram of the amplitude of S_{21}. From this histogram and the fitting we observe that we have a Rayleigh-type of fading.

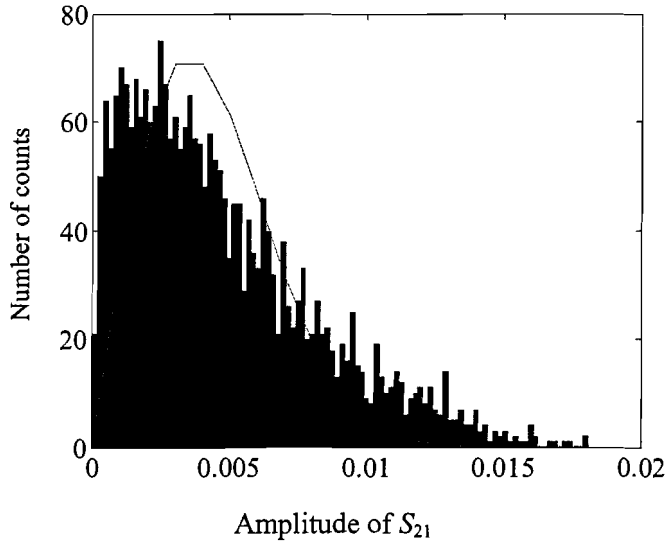

Figure 6.7: *Distribution of the measured amplitude of S_{21} and a Rayleigh fit at the centre frequency.*

The red trace in figure 6.7 is the best fit, $f(x) = \frac{x}{0.0035^2} \exp(-(x/0.0035)^2/2)/2.4$. This function is the Rayleigh distribution fit with a variance of 0.0035. The relation between the histogram (number of points) and the pdf is given by:

$$\Pr\{x < |S_{21}| \le x + \Delta x\} = \frac{\#\text{number of points in the interval (x, x + } \Delta x]}{\#\text{total number of points}} \approx f\,\Delta x\,. \qquad (6.5)$$

In general a histogram is not normalised, i.e., the number of points times the bin size Δx is not equal to one. To scale the distributions to the same magnitude we have to divide the pdf by a factor of 2.4. The power distribution, depicted in figure 6.8, seems to be an exponential distribution, which is in agreement with Rayleigh fading (see Appendix A).

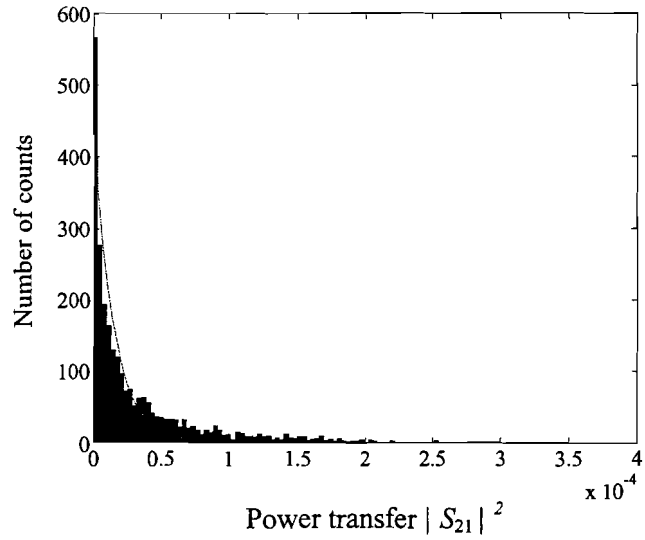

Figure 6.8: *Distribution of the measured* | S_{21} | ^{2} *and a Rayleigh fit at the centre frequency.*

In figure 6.9 the power transfer 20 log $|S_{21}|$ is shown along the measurement trace of figure 6.2. The propagation has deep fades, a fade of 30 dB is quite common.

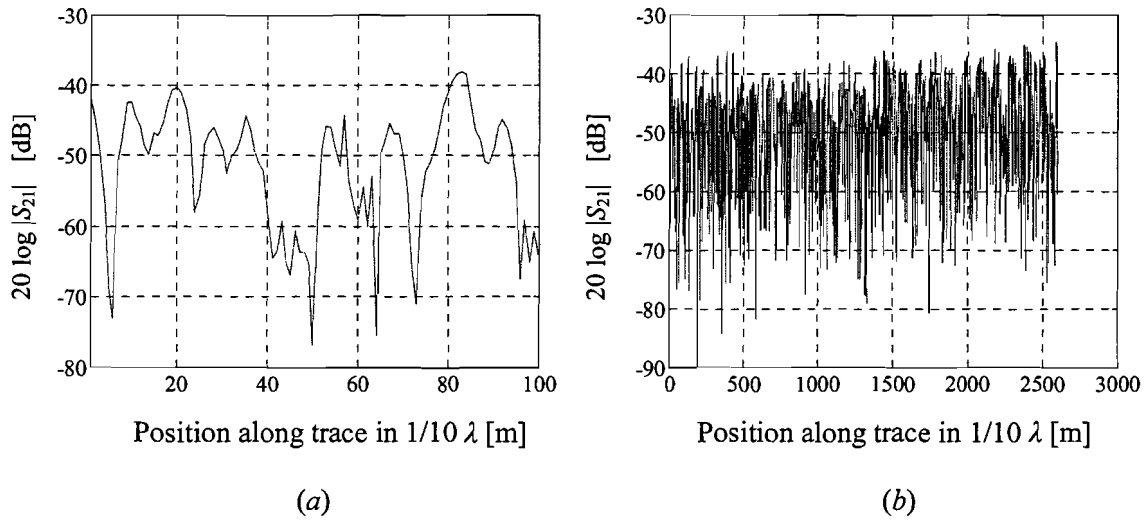

Figure 6.9: *Measured power transfer 20 log* $|S_{21}|$ *at the xy-table (a) 1 = (x = 0, y = 0) up to position 100 and (b) up to position 2601 = (x = 5 λ, y = 5 λ) at the centre frequency.*

The frequency dependence of the power transfer is also very important for wireless communication. The spectrum of a modulated signal becomes distorted if the power transfer spectrum is not flat. Figure 6.10 shows the measured frequency dependence of the received power. From figure 6.10 we can observe that not only in the spatial domain but also in the frequency domain fades of 30 dB occur. When the radio performs a frequency hopping sequence the SNR will become very small for some frequencies. The frequency hopping sequence is pseudo random so the radio will still be able to maintain a radio link with less bandwidth. However, synchronic data packets like voice data can get lost, and this is the cause of clicks in an audio link. So it is not a good strategy for Bluetooth to use only frequency hopping or frequency diversity to avoid fades. Frequency hopping in combination with, e.g., space diversity will decrease the chance of a fade dramatically. Bluetooth has an instantaneous bandwidth of only 1 MHz so the performance will drop in a fade of a few MHz. When we look at WLAN the bandwidth is about 20 MHz. Due to redundancy in the frequency domain the performance of WLAN is less sensitive to fades of a few MHz in the frequency domain.

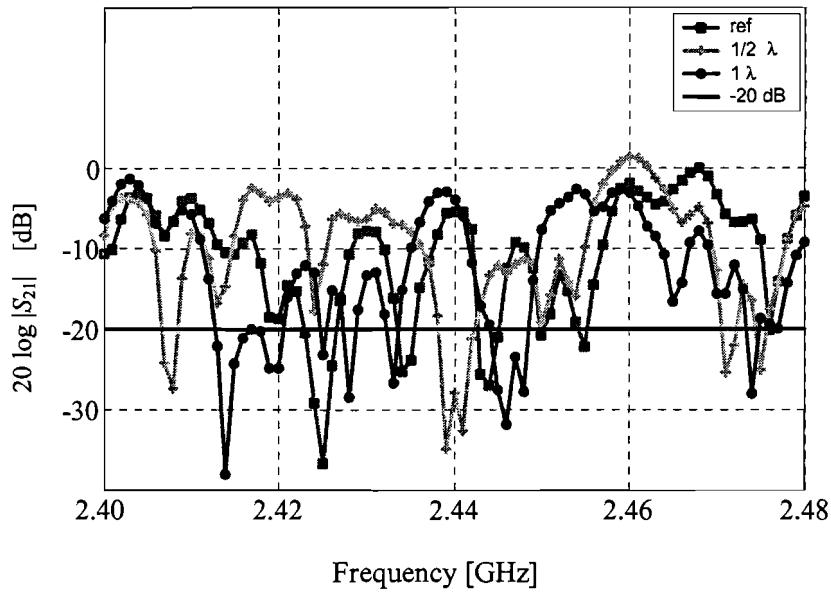

Figure 6.10: *Normalised measured power transfer as function of the frequency with the position of the receive antenna as parameter.*

The frequency coherence bandwidth is a measure for the width over which the channel can be considered flat, i.e., the maximum distance in frequency where the signals are still strongly correlated (the correlation is at least 0.5) [Jakes, 1974]. From the frequency dependence of the power transfer as shown in figure 6.10 we can estimate that the frequency coherence bandwidth is about 4 MHz or 4 % of the Bluetooth bandwidth for hopping (80 MHz). We can approximate the coherence bandwidth using S_{21}:

$$\hat{C}(\Omega)=\frac{\int_{\omega 1}^{\omega 2} H(\omega)H^{*}(\omega+\Omega)\,d\omega}{\int_{\omega 1}^{\omega 2} H(\omega)H^{*}(\omega)\,d\omega} \approx \frac{\sum_{\omega 1}^{\omega 2} S_{21}(\omega_1+n\Delta\omega)\,S_{21}^{*}(\omega_1+n\Delta\omega+\Omega)\,\Delta\omega}{\sum_{\omega 1}^{\omega 2} S_{21}(\omega_1+n\Delta\omega)\,S_{21}^{*}(\omega_1+n\Delta\omega)\,\Delta\omega} \tag{6.6}$$

where $\hat{C}(\Omega)$ is the coherence function evaluated in the band $\omega_1<\omega<\omega_2$, Ω is the frequency difference and $H(\omega)$ is the transfer function. The coherence function as shown in figure 6.11 is calculated using the measured data and Eq. (6.6). The step size $\Delta\omega$ used for the midpoint integration is 1 MHz. Each trace in figure 6.11 represents the coherence function at a certain *xy*-position in the measurement plane.

In order to determine the delay spread we need to analyse the response of the propagation in the time domain. For the spread in frequency (coherence bandwidth) of a signal and its spread in time the following inequality or uncertainty relation holds, $\Delta t\,\Delta\omega \geq 1$ [Nicholls, 2004]. So we can expect a time spread of at least 39 ns at a frequency spread of 8 MHz (coherence bandwidth is 4 MHz). The transformation from the frequency domain to the time domain is done using a DIFFT (discrete inverse fast Fourier transform) algorithm. The measured frequency response is only valid within the bandwidth of the antennas. Therefore a window in the frequency domain has to be used. Furthermore, a window has to be used to decrease inaccuracy's caused by discontinuities at the start and stop frequency. The inverse discrete fast Fourier transformation is defined by [www.matworks.com]:

$$\tilde{h}(i)=\frac{1}{N}\sum_{k=1}^{N} H(k)\exp\left[(j2\pi i/N)\,(i-1)\,(k-1)\right] \tag{6.7}$$

where $\tilde{h}(i)$ is the approximate time-response and $H(k)$ is the response in the frequency domain. The Gaussian filter that is used in the DIFFT, has the following transfer function [Leyten, 2001]:

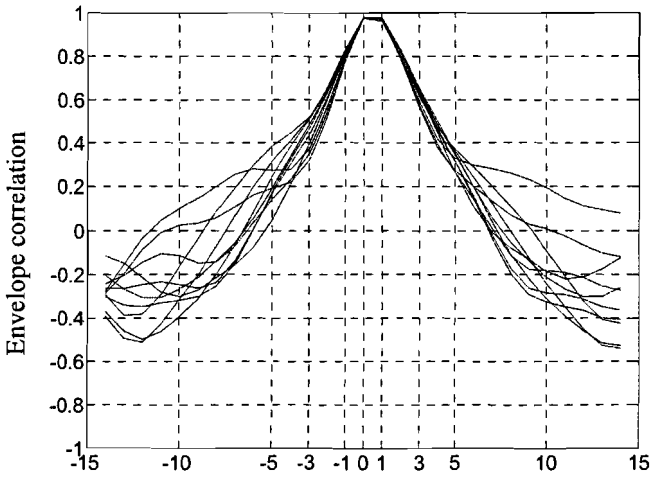

Figure 6.11: *Frequency correlation of the measured propagation shows a coherence bandwidth of 3 MHz at a coherence ρ = 0.5.*

$$G(f) = \frac{-j\sqrt{\pi}}{a}\exp\left[-\{(2\pi f - 2\pi f_0)/2a\}^2\right]\exp\left[-j\,(\tau + t_{filter}/2)\right], \tag{6.8}$$

where a = 0.8886 B, B is the bandwidth of the signal, t_{filter} is the filter response time, τ is the propagation delay. The frequency response with the Gaussian filter becomes $H(k,\vec{r}) = \sum_{k=1}^{N} H(k)G(k)$. The time response of the Gaussian window with a_3 = 0.8886 B is convoluted with the time response of the signal. Therefore, a Gaussian window with a_3 = 0.8886 B will give distortions in the time response like spurious responses (leakage) up to –42 dB [[Leijten, 2001]. The inverse discrete fast Fourier transform evaluated over a part of the frequency domain is not the impulse response but the time domain response. Furthermore, the time response may be complex. In [Leijten, 2001] the power delay profile is defined with:

$$\tilde{P}(i\Delta t,\vec{r}) = \left|\tilde{h}(i\Delta t,\vec{r})\right|^2 \tag{6.9}$$

where $\tilde{P}(i\Delta t,\vec{r})$ is the power at $t = i\Delta t$ and Δt is the time step. The bandwidth of the Gaussian filter for this measurement is 200 MHz (± 100 MHz). The time domain response is shown in figure 6.12. The time response can start at $t < 0$. A delay $\tau + t_{filter}/2$ is used to take into account the time the waves take to travel from transmitter to receiver $\tau = c_0\,\Delta r$, and to compensate for the negative Gaussian filter delay $-t_{filter}/2$. To get a reasonable resolution in the time domain the frequency sweep should be large. The relation between the frequency step size frequency and time step size is, $\Delta t = 1/(N\Delta f) = 1/(200*1E6)$, so the time resolution is about 5 ns. The data in the frequency domain is sampled at an interval of 1 MHz. The Nyquist condition gives $t_{max} < 1/(2 \times \Delta f) = 500$ nS, where t_{max} is the maximum time. Figure 6.12 shows the calculated time domain response from the measurement data using equation (6.6). Delay spread can cause serious problems like inter-symbol interference. It is related to the dimensions of the room. The propagation speed of the electromagnetic waves is 0.3 m/ns. When we take into account only two reflections the delay spread is about 40 nS in a room with a length of 5 meter. The first generation Bluetooth has a bit rate of 1 Mbit/s and a bit time 1 μs. For this version of Bluetooth, delay spread does not influence

the BER, the amplitude of reflections from the previous bit are not noticeable at the sampling moment. The rms delay spread is calculated using Eq. (6.10) [Leijten, 2001]:

$$\tau = \sqrt{\frac{\int_0^\infty \left[t - \int_0^\infty tP(t)\,dt \Big/ \int_0^\infty P(t)\,dt \right]^2 P(t)dt}{\int_0^\infty P(t)\,dt}} \tag{6.10}$$

where due to the DIFFT the upper bound of the integral is $\frac{1}{2\Delta f} = 500\,ns$ and not ∞.

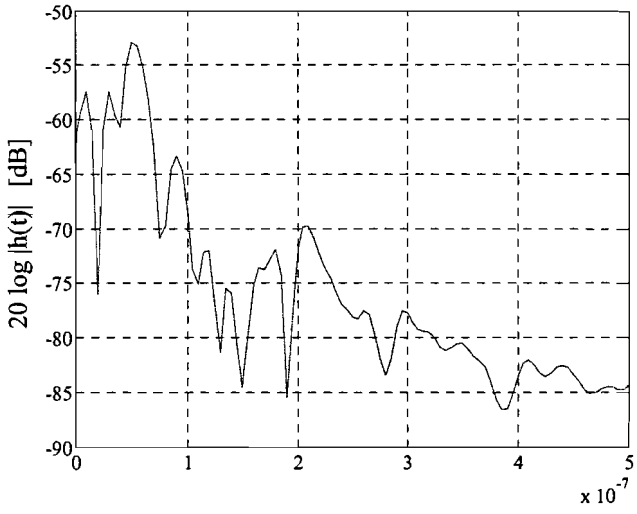

Figure 6.12: *Time domain response.*

An important parameter for diversity is the separation between the two antennas. A criterion for a good separation when switching between two antennas is the correlation of the envelope of the signals. Theoretically, the best correlation coefficient would be –1, but in practice this cannot be achieved and a correlation of less than 0.2 is acceptable [Lee, 1998]. In a Rayleigh-fading environment the predicted envelope correlation is (see Appendix B),

$$\rho_{env}(d) = [J_0(k_0 d)]^2 . \tag{6.11}$$

where d is the distance between the receive antennas and k_0 is the wave number in free-space.

The matrix M of Eq. (6.3) can be used to calculate the correlation between the S_{21} parameters. Correlation of complex signals is needed for a complex combining technique; the relation between complex correlation and envelope correlation is given by (see Appendix B):

$$\begin{aligned} \rho_{XY}(X,Y) &= \frac{\sigma_{XY}(X^*,Y)}{\sqrt{\sigma_{XX}(X,X)}\sqrt{\sigma_{YY}(Y,Y)}} \\ &= \frac{\left\langle (X^* - \langle X^* \rangle)(Y - \langle Y \rangle) \right\rangle}{\sqrt{\left\langle (X^* - \langle X^* \rangle)(X - \langle X \rangle) \right\rangle}\sqrt{\left\langle (Y^* - \langle Y^* \rangle)(Y - \langle Y \rangle) \right\rangle}}, \end{aligned} \tag{6.12}$$

where ρ is the correlation and σ is the covariance. The correlation between the amplitudes of two columns is the inner product of columns normalised by their length when the mean of the columns is zero. The calculated correlation between columns in the matrix M is the correlation between the received signals if the received antennas are separated in the y-direction. With zero mean Eq. (6.12) reduces to an inner product,

$$\rho(X_1,Y_1)=\frac{\left(X_1^*,Y_1\right)}{\|X_1\|\|Y_1\|}. \tag{6.13}$$

We can correlate column 1 (points with $y = y_1$ on the xy-table) with column 2 of the matrix M, and column 1 with column 3 etc. A way of presenting this is to calculate the covariance matrix. This gives the correlation between the columns, e.g., element (2,4) represents the correlation between the measurements at $y = 2$ and $y = 4$. The magnitudes of the elements in the covariance matrix are displayed in the contour plot shown in figure 6.13a. The diagonal represents the correlation of a column with itself, so the correlation is one.

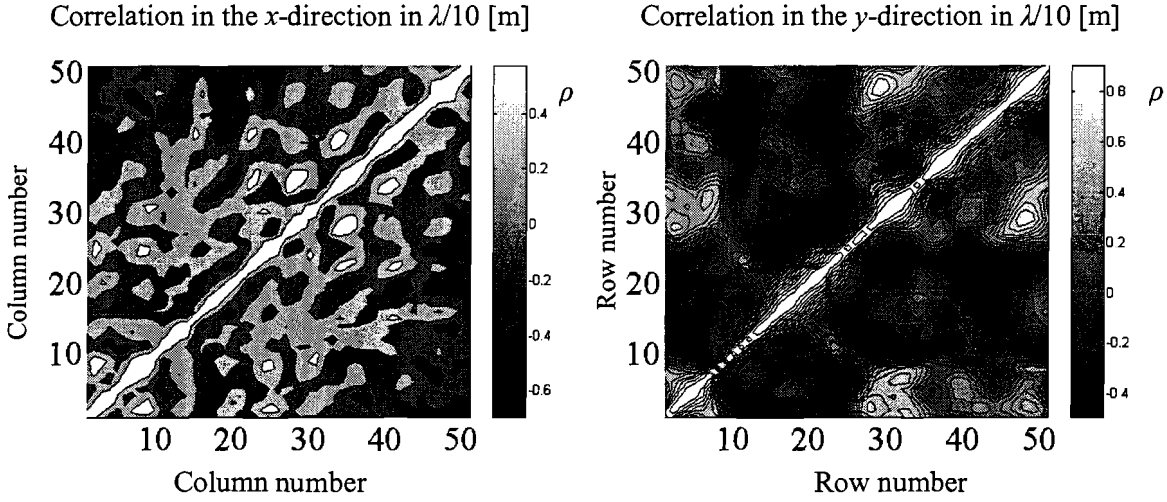

Figure 6.13: *Correlation contour plot of the measured envelope* $|S_{21}|$ *at the centre frequency.*

From figure 6.13 we can observe that the envelope is correlated over a longer distance in the y-direction. The average correlation of the envelope as a function of the distance between the antennas in the x-direction can also be calculated and is shown in figure 6.14. From figure 6.14 we can observe that the envelope correlation has its first zero at an antenna separation of half a wavelength. Antenna diversity requires de-correlated received signals, so the antennas should be separated at least half a wavelength.

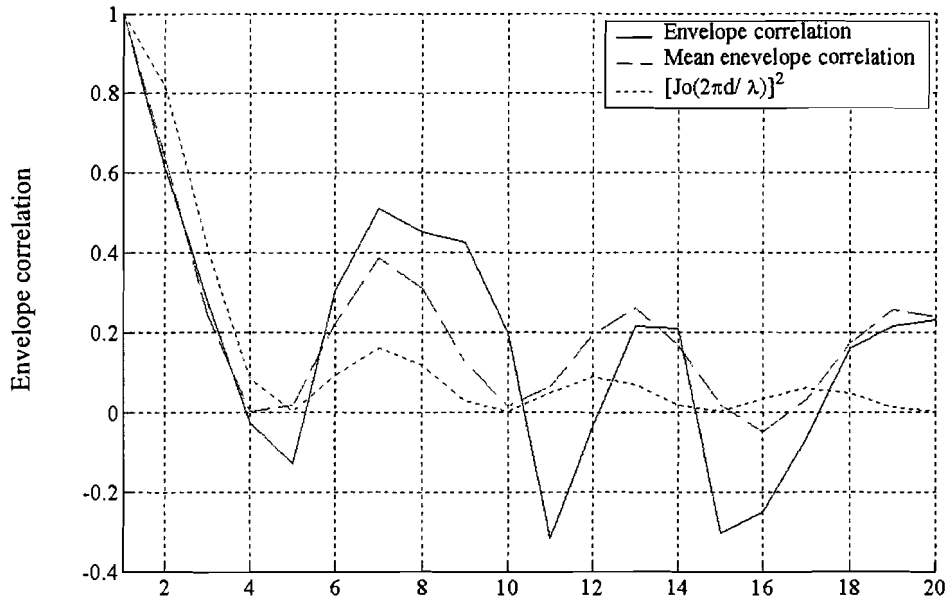

Figure 6.14: *Measured envelope correlation as function of the separation in the x- direction.*

Next to correlation in the spatial domain also correlation of the envelope in the frequency domain is calculated. The points with coordinates (x_1, y_1) to (x_1, y_{20}) of the matrix M, have been measured at 201 frequencies. In figure 6.15 the envelope correlation of two points, in the Bluetooth band at 80 frequencies, is shown.

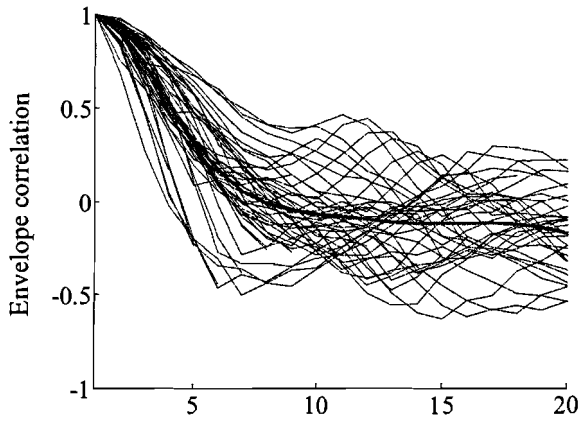

Figure 6.15: *Measured envelope correlation in the y-direction, calculated at 80 frequencies, the mean correlation is the red trace.*

The correlation in figure 6.15 is the normalised inner product at two fixed y-positions performed over 80 frequencies. From figure 6.15 we can observe that at a separation of half a wavelength the signals are de-correlated using a 0.2 threshold when the correlation is performed over the complete Bluetooth band.

We will now use the measured data to predict the improvement of using antenna diversity. If we have two receive antennas separated at $\lambda/2$ we get a difference in received power. This difference is an instantaneous diversity gain. When we have fades in the measured data with a power drop of 20 dB below the mean power we can calculate the instantaneous diversity gain for those points, as depicted in figure 6.16.

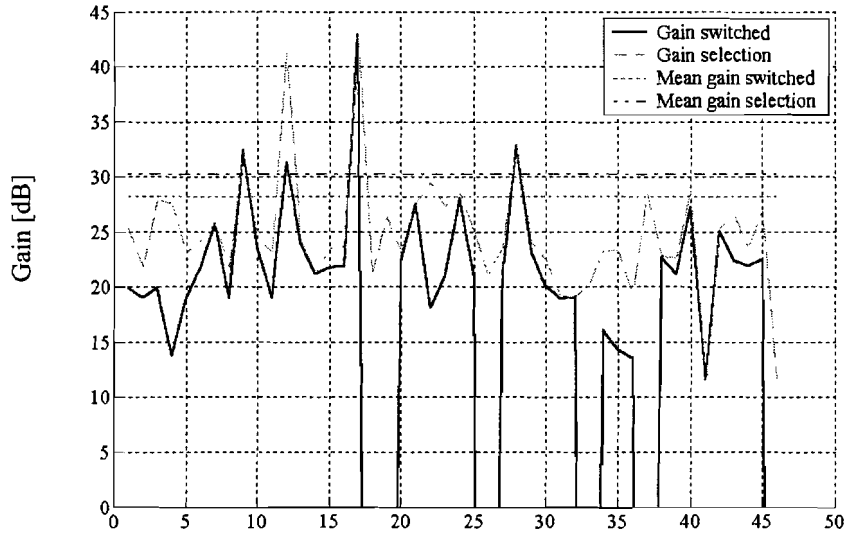

Points on the *xy*-table with a power level 20 dB below the mean power level.

Figure 6.16: *Measured space diversity gain in fades with antenna separation in the x-direction.*

From figure 6.16 we can observe that the instantaneous diversity gain at deep fades is about 25 dB. In figure 6.9 we observe that fades are about 30 dB and that the fades last only one measurement point. So if the two antennas are de-correlated we expect an instantaneous diversity gain of about 30 dB in a deep fade.

The outage is defined as the probability that the SNR γ is smaller than a reference value γ_{ref}. The outage can also be expressed in terms of the measured data using the matrix of equation (6.3),

$$\text{outage} = \frac{\#\text{cells with } \gamma < \gamma_{\text{ref}}}{\#\text{measurement cells}} \tag{6.14}$$

where # represents the cardinality of a set. One has to be careful with counting the total number of cells where S_{21} is measured. If the outage is calculated at one frequency, the total number of cells is then 2601 (2601 positions on the *xy*-table). It is also possible to calculate the outage for both the frequency and spatial domain and the total number of cells is in this case 81 x 2601 = 210681 (2601 positions on the *xy*-table measured at 81 frequencies, start frequency is 2400 MHz and the stop frequency is 2480 MHz). It is important to consider the complete measurement space, the spatial domain and the frequency domain, if we investigate diversity for Bluetooth. Only a statistical statement over the complete domain gives a realistic estimate of the improvement of the quality of service using a diversity system. First the average power, over frequency and space, is calculated. The threshold for activated switching combining is 1 % of the average power level.
In figure 6.17 the outage at the centre frequency is shown. When we measure the horizontal distance at an outage level of 1 % we see that the difference in the normalised power is about 10 dB. So the effect of applying diversity is the same as increasing the transmitter power with 10 dB. This increase of the received power is the diversity gain. From figure 6.17 we can observe that the diversity gain increases when the outage decreases. In practice this means that a radio link without diversity and a only a few fades (less than 1 % of the room), will become a radio link without fades (less than 0.01 % of the room)

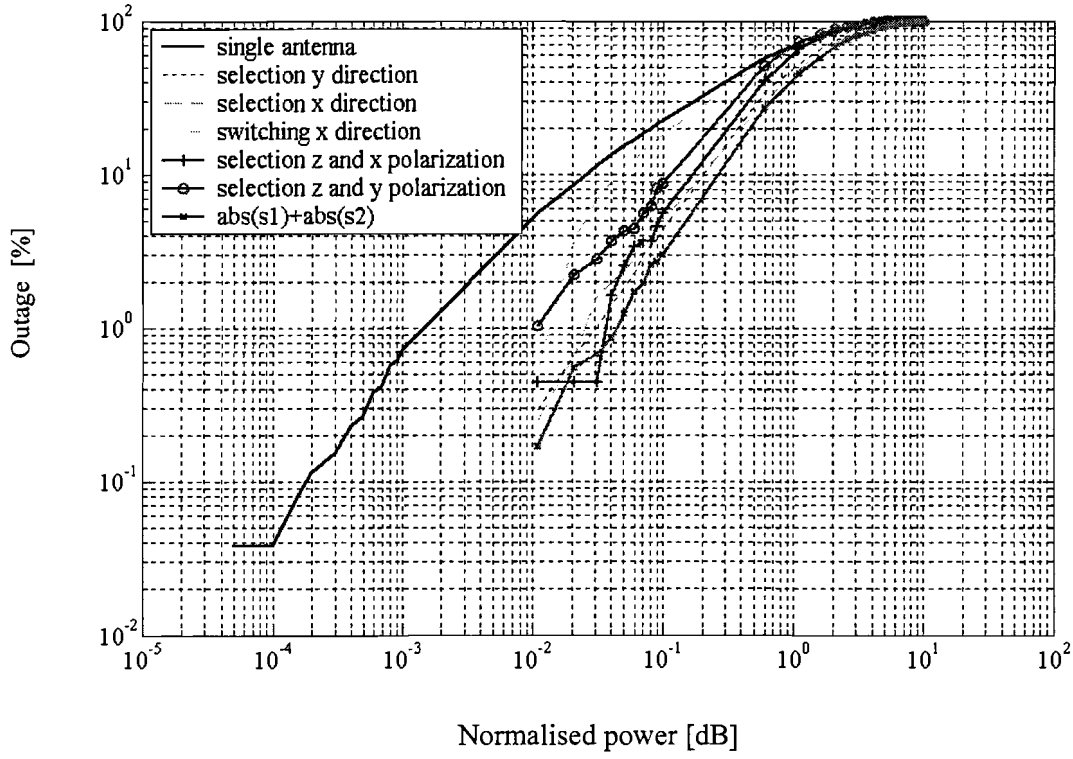

Figure 6.17: *Outage of measured data at the centre frequency 2.44 GHz.*

The outage of the measured propagation and the outage for Rayleigh-fading are shown in figure 6.18.

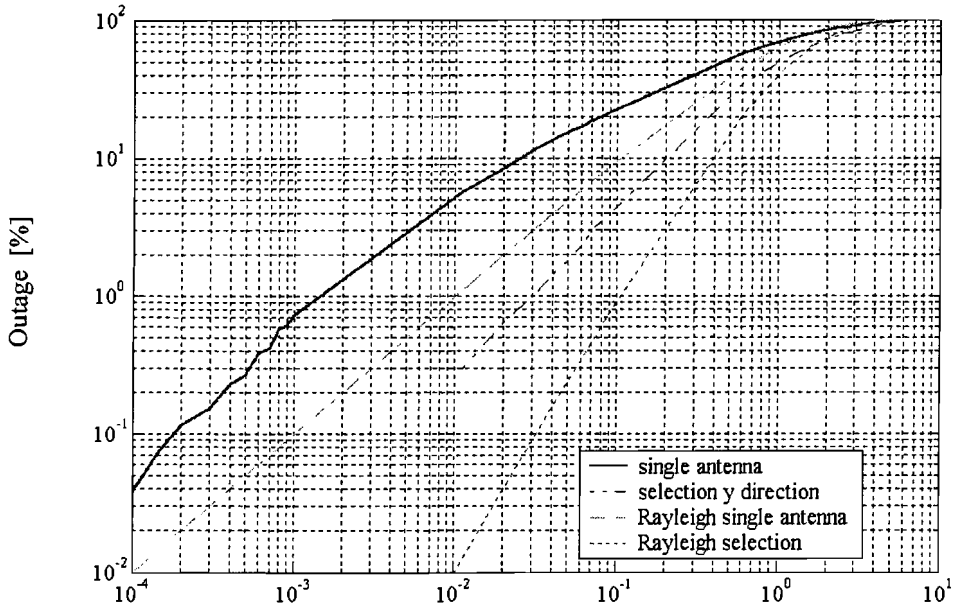

Figure 6.18: *Outage of measured data and Rayleigh distributed data at the centre frequency 2.44 GHz.*

The outage of the measured data at a certain normalised power level is higher. This means that the measured data has more fades than the calculated Rayleigh fading. From figure 6.18 we can observe that the diversity gain of the measured data and the calculated Rayleigh fading is the same.

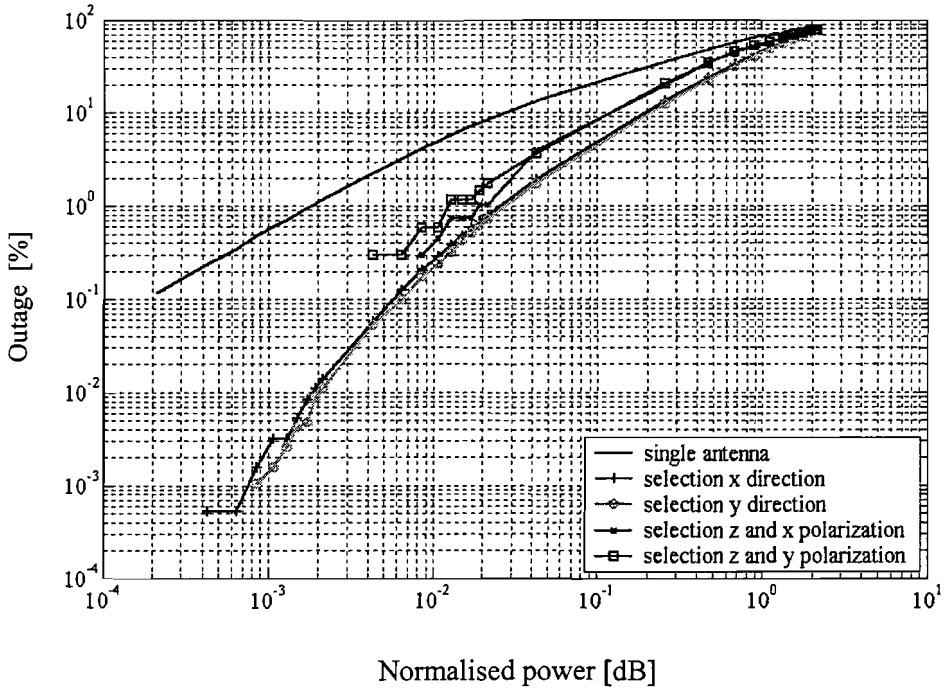

Figure 6.19: *Outage of measured data calculated over space and frequency.*

The outage calculated over the xy-coordinates and the Bluetooth frequencies is shown in figure 6.19. Due to the large number of measurements the plot becomes much smoother. Furthermore, we can observe that the outage plot is similar to the plot of at the centre frequency (figure 6.17).

The separation between the receive antennas is $\lambda/2$ for space diversity in the x-direction and space diversity in the y-direction.

The measurements of the power transfer from z-polarised waves to x, y and z-polarised waves, respectively, are used to calculate the outage for each polarisation. The measurements were not performed at the same time. This makes it difficult to compare the measurements because the propagation properties of the room and the measurement equipment change a little in time. There is no separation between the receive antennas for polarisation diversity. However, the receive antenna was rotated 90° to change the polarisation, so there also is a change in position of about $\lambda/10$. These errors in the position of the antennas will probably have a minor effect on the measurement results, the received powers are still strongly correlated at a distance of $\lambda/10$. Two received powers are used, one from the vertical polarisation (co-polarisation) and one from the horizontal polarisation (cross-polarisation). For the horizontal polarisation we take an x-directed antenna or a y-directed antenna.

The measurement results for the receive antennas at the different polarisations are summarised in table 6.1. It appears from the measured data that most of the propagation parameters are roughly the same at all the polarisations. The power in the cross-polarisation is about 6 dB below the power in the co-polarisation. So the diversity gain will be smaller when we use polarisation diversity instead of space diversity. However, polarisation diversity will improve quality of the radio link by decreasing the number of fades. The correlation in space is the same for all the polarisations. So space diversity will be effective for all polarisations if the receive antennas are separated at least $\lambda/2$.

table 6.1: *Overview of the measurement results.*

Polarisation transmit → receive	Max $\|S_{21}\|$	Phase distribution	Rms delay spread	De-correlation distance at the receiver	De-correlation distance in frequency
$z \rightarrow z$	0.01	Peaks −140°, 60°	40 ns	$\lambda/2$	$\lambda/2$
$z \rightarrow x$	0.007	Peaks −140°, 60°	50 ns	$\lambda/2$	$\lambda/2$
$z \rightarrow y$	0.005	Peaks −140°, 60°	60 ns	$\lambda/2$	$\lambda/2$

There is a difference in the delay spread between the z-, x- and y-polarisation. The reason could be the dimensions of the room and the reflection coefficients of the walls and objects in the room.

6.3 Comparison between simulated and measured field strength data

In chapter 3 we discussed several propagation models. The measured field strength data and the simulated data can be compared using the hybrid model to calculate the simulated field strength. The phase distribution as shown in figure 6.20 is used to tune the hybrid model. With tuning we mean adding a uniform phase distribution (free-space model) until the distributions are the same.

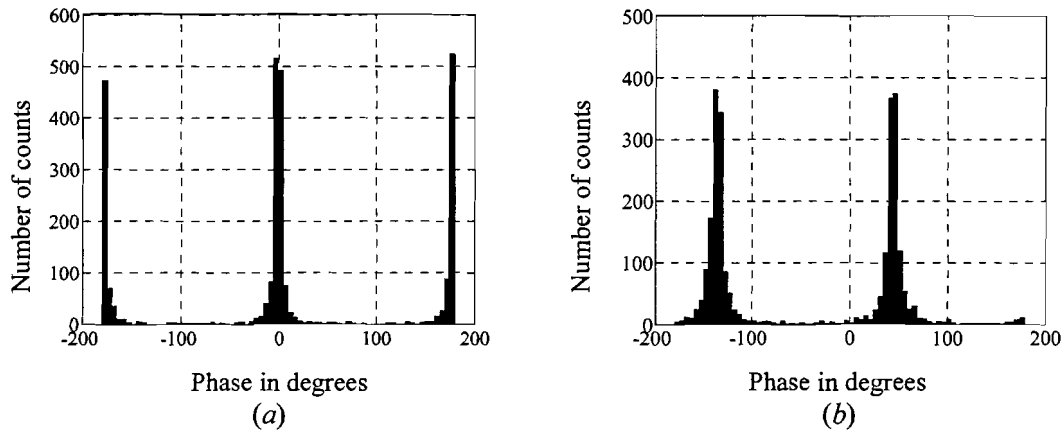

Figure 6.20: *Phase distribution (a) simulated hybrid model and (b) measured phase distribution.*

The histogram of the phase for free-space propagation (used in the hybrid model) is depicted in figure 6.21. If we use more points and a larger area on the xy-table the distribution will become uniform.

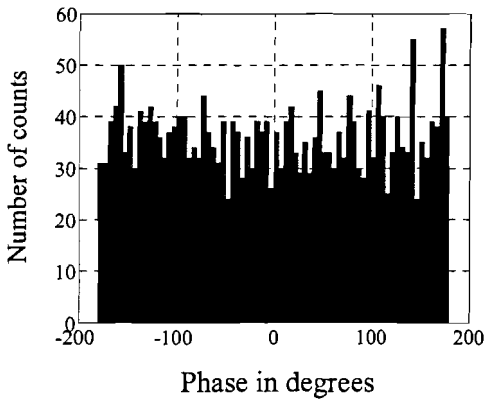

Figure 6.21: *Phase distribution of simulated free space propagation in the measurement plane.*

The simulated and measured amplitude distributions are shown in figure 6.22.

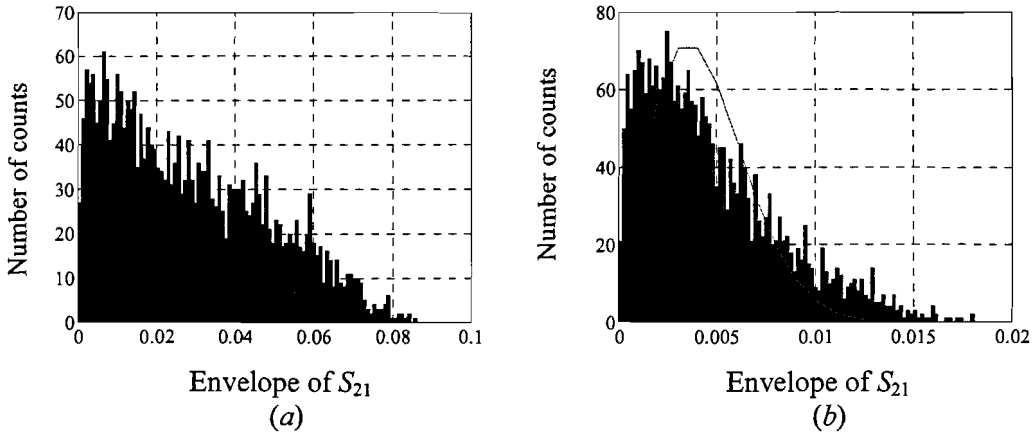

Figure 6.22: *Envelope distribution (a) simulated hybrid model and (b) measured data with Rayleigh fit.*

The frequency dependence of the power transfer at four points on the *xy*-table is shown in figure 6.23. There clearly is a difference between the simulation and the measured data. The coherence bandwidth is considerably smaller in the simulation. Other points on the *xy*-table have a similar frequency dependence. The resonant behaviour of the cavity model is the cause of the spikes in figure 6.23 a.

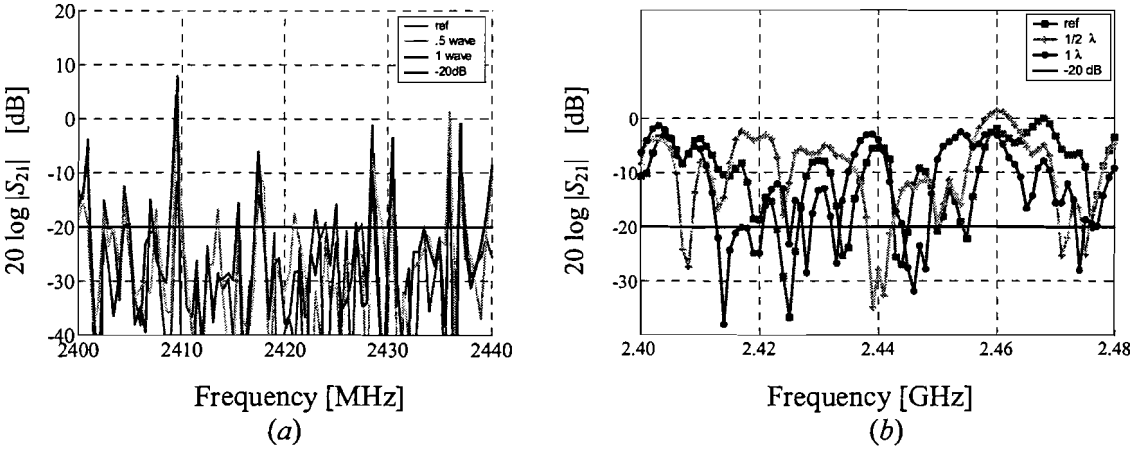

Figure 6.23: *Frequency dependence (a) simulated hybrid model for a small antenna and (b) measured data.*

The power transfer on the *xy*-table is shown in figure 6.24, where a contour plot is used to display the magnitude of the received power. Although the statistical data looks the same, the actual field patterns are quite different. For a more exact simulation detailed properties of the walls and the objects in the room should be taken into account.

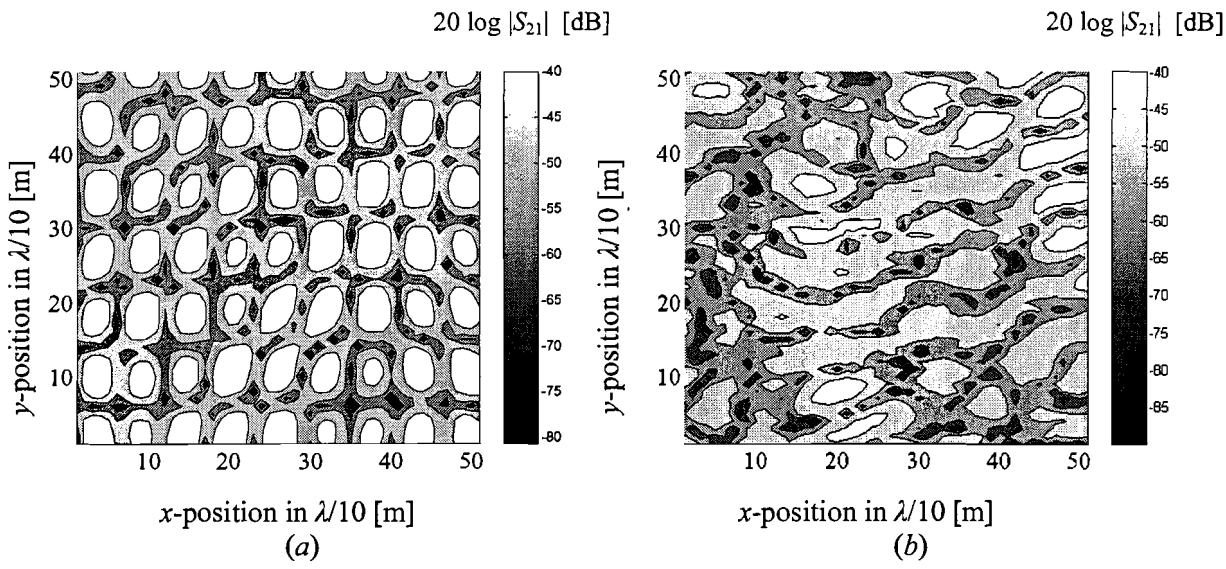

Figure 6.24: *Power distribution (a) simulated hybrid model and (b) measured data at the centre frequency.*

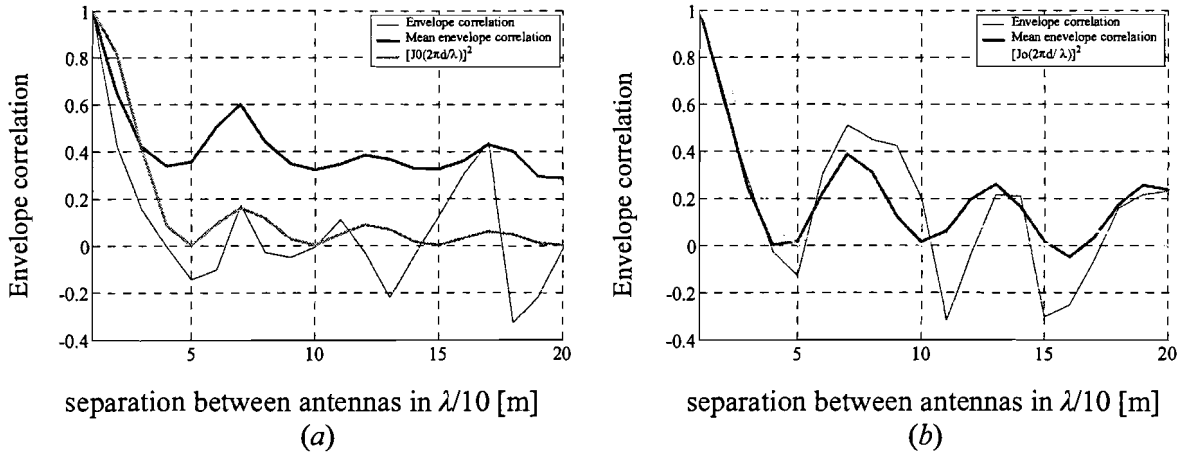

Figure 6.25: *Envelope correlation (a) simulated hybrid model and (b) measured data at the centre frequency.*

In figure 6.25 the envelope correlation as function of the antenna separation shows a similar trend for the simulation and the measurement. The outage following from the hybrid model is depicted in figure 6.26. The diversity gain at an outage of 1 % is 11 dB if we use space diversity. The outage plot of the measured data is shown in figure 6.27. The diversity gain at an outage of 1 % is also 11 dB if we use space diversity.

The predicted diversity gain is too high in the cavity model with perfect conducting walls. The superposition of the free space model and the cavity model decreases the fades and leads to a lower diversity gain. The hybrid model gives a reasonable fit in the propagation parameters: phase distribution, space correlation and outage. There is a quite large difference between the simulation and the measured data for the coherence bandwidth and time domain response.

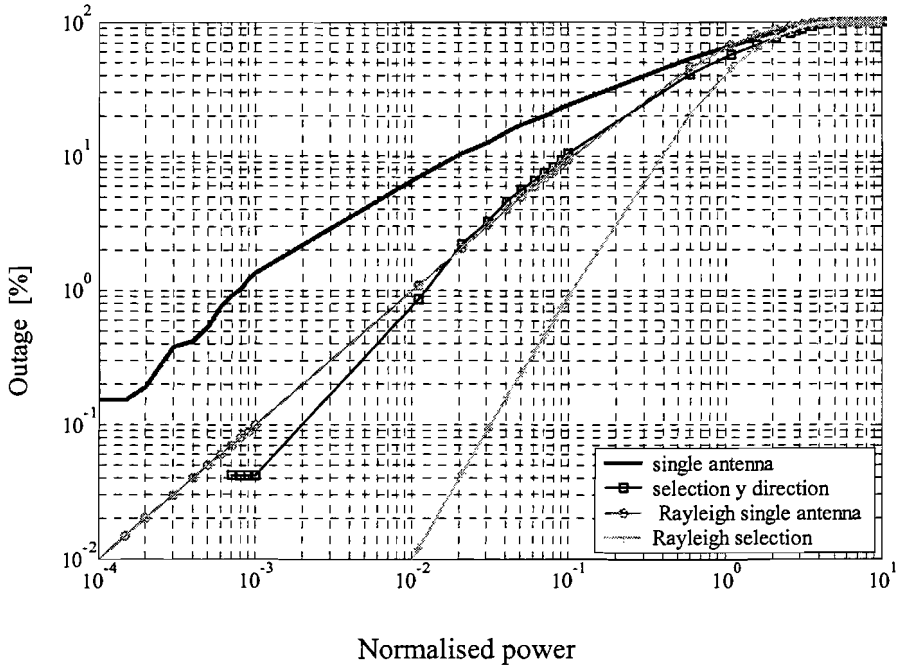

Figure 6.26: *Outage of the simulation with the hybrid model.*

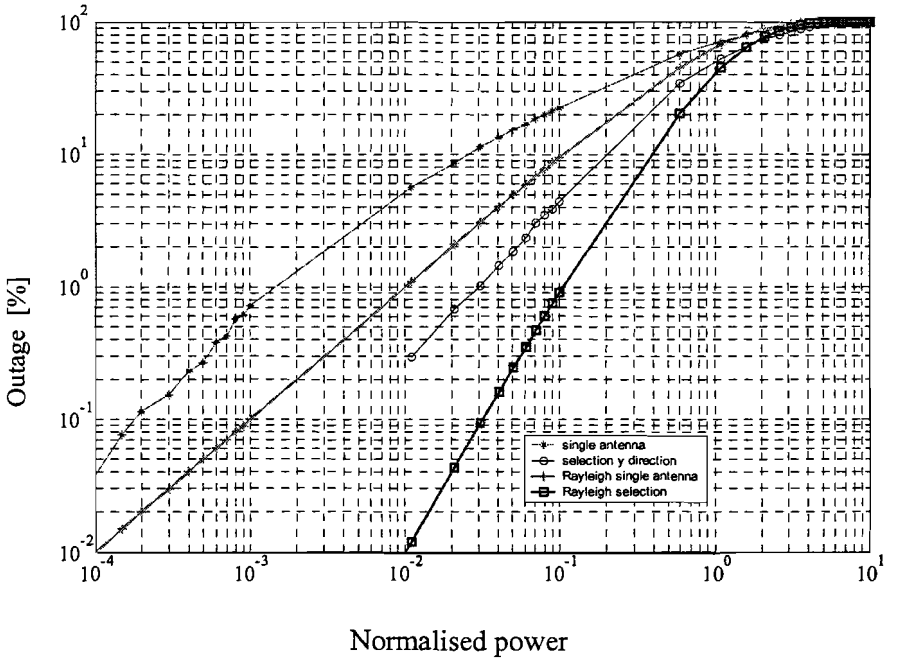

Figure 6.27: *Outage of the measured data.*

6.4 BER measurement set-up with Bluetooth demonstrator module

The BER (Bit-Error-Rate) measurement was done in the same room as the field strength measurement using the *xy*-table. A photograph is shown in figure 6.28. The Bluetooth module with embedded diversity switch from chapter 5 was used in the diversity tests.

Figure 6.28: *XY-table with SMIQ and pc. The Bluetooth demonstrator module is on the table on the right side.*

The measurement set-up consists out of the vector signal generator SMIQ and the Bluetooth module. The SMIQ transmits a GFSK-modulated carrier at a centre frequency of 2.44 GHz. The data generated in the SMIQ is a pseudo random sequence. The module is programmed to receive continuously at a frequency of 2.44 GHz. The connection of the SMIQ and the Bluetooth module, called EUT, is depicted in figure 6.29.
The BER is measured at each position with coordinates (x, y, z), where z is kept constant. First the BER is measured using the embedded slot antenna of the Bluetooth module. Then the BER is measured with the external monopole antenna that is connected to the other input of the Bluetooth module. The receiving antennas were put at a fixed position and the transmit antenna was mounted on the *xy*-table. The demodulated data, with an adjustable delay for sampling, is cross-correlated and then compared with the transmitted data. We used 1,000,000 data bits and 10,000 error bits as stop criteria to calculate the BER. This gives a resolution of 0.00001 % up to a BER of 1 %. The measurement was performed at several transmitter power levels, different *xy*-grids and two positions of the receiving module.

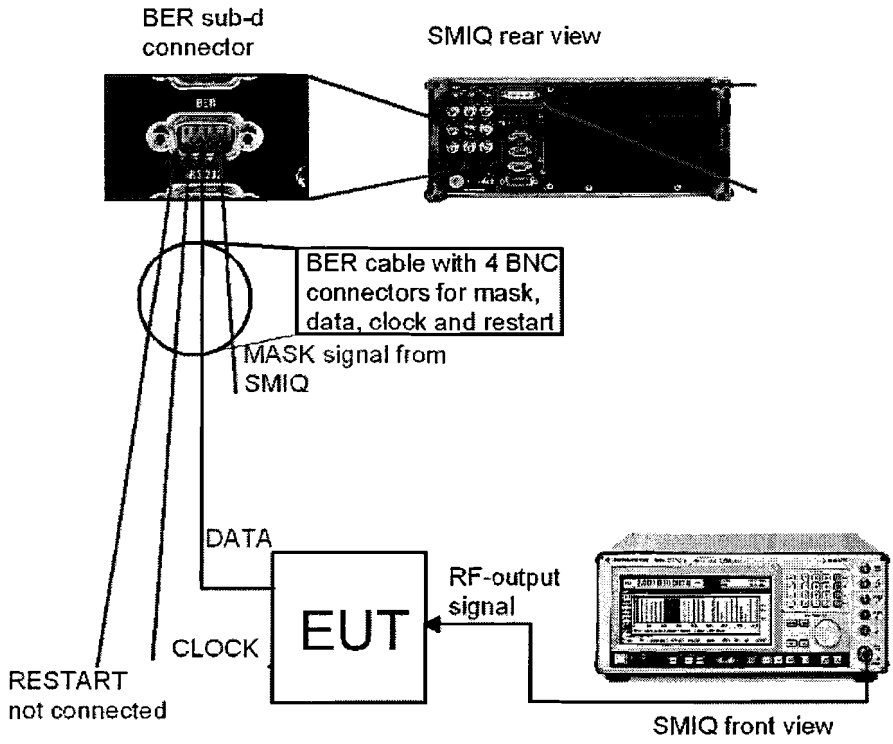

Figure 6.29: *Measurement set-up for BER measurement.*

6.5 BER measurement results

6.5.1 BER measurement with a Bluetooth module without antenna switch

To get a reliable BER measurement we start the BER measurement with a standard Bluetooth demo board. The Bluetooth module without switch and with a monopole antenna has an excellent sensitivity. Furthermore, we do not need to switch between the receive antennas, so the measurement will be faster. The Bluetooth module with embedded antenna switch is a prototype and does not have antenna matching, so we can expect a decreased sensitivity.
The measurement was done using several power levels and *xy*-grids. For a useful result we need a BER between 0.0001 % and 10 %. For Bluetooth a BER of 0.1 % is an acceptable bit error rate [Bray et al, 2001]. The BER on the xy-table is depicted in figure 6.30. In figure 6.30 the minimum displayed BER is 1E-6, this gives a better resolution of the picture. In reality the BER is zero at a few measurement points on the *xy*-table. The distance over which signals are correlated is about the radius of an area with equal level (color) in a contour plot. The distance where the fades are correlated as shown in figure 6.30 is about $\lambda/2$. The coverage of this measurement is the area with a BER < 0.1 % divided by the total area, about 75 %. The relation between the BER measurement and the powertransfer measurement is, $\mathrm{BER}_\gamma(\vec{r}) = \frac{1}{2}\exp(-\gamma(\vec{r})/2)$, where γ is the signal-to-noise ratio. To increase the resolution of the plot we display the logarithm of the BER, $\log_{10}\mathrm{BER}_\gamma(\vec{r}) = (-\gamma(\vec{r})/4)/\ln 10$, which results in a scaled plot of the signal-to-noise ratio.

We can observe from figure 6.31 that we have a coverage, Pr {BER < 0.1 %}, of about 75 %. The diversity in figure 6.32 is simulated using the measurement data. An algorithm selects the signal with the lowest BER (highest SNR) from the measured BER and the measured BER at a distance of ½ λ. This selection combining procedure is the same as the selection based on signal strength. From figure 6.32 we can observe that there is coverage, Pr {BER < 0.1 %}, of 70 % or an outage, Pr {BER > 0.1 %}, of 30 %. With the simulated diversity we have coverage of 90 % or an outage of 10 %, so the outage is decreased by a factor of 3.

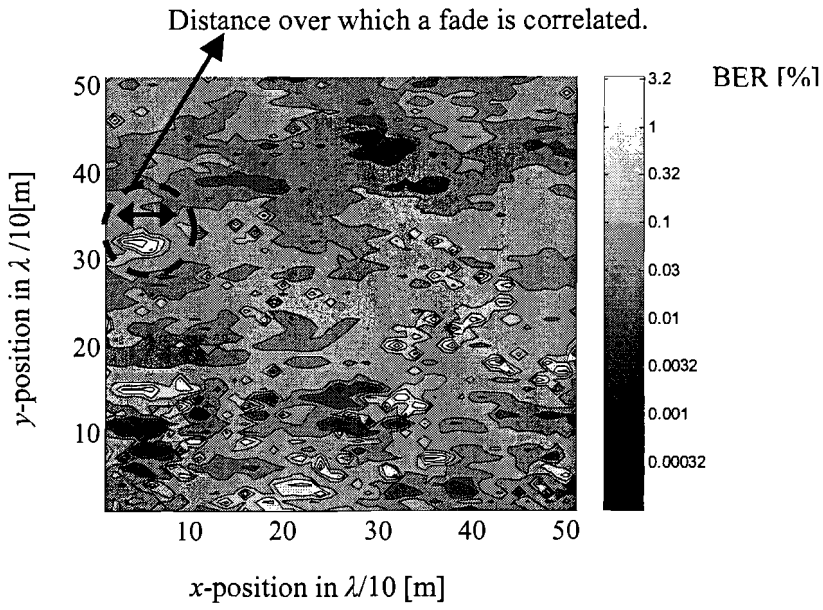

Figure 6.30: *Measured BER on the xy-table in logarithmic scale, log_{10} BER, using the monopole antenna ($P_{transmitter}$ = -25 dBm at the centre frequency).*

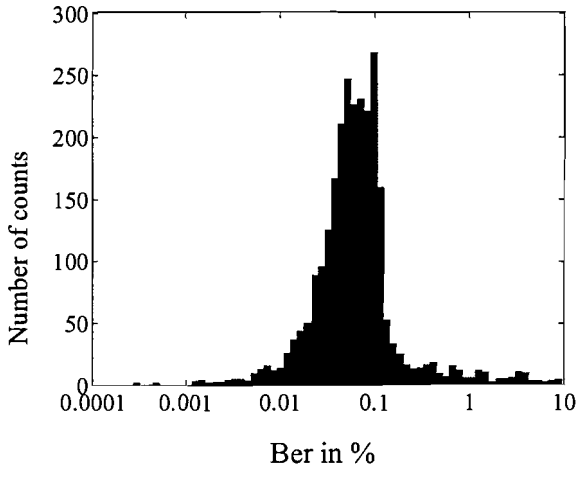

Figure 6.31: *Histogram of the measured BER, log_{10} BER ($P_{transmitter}$ = -25 dBm, centre frequency).*

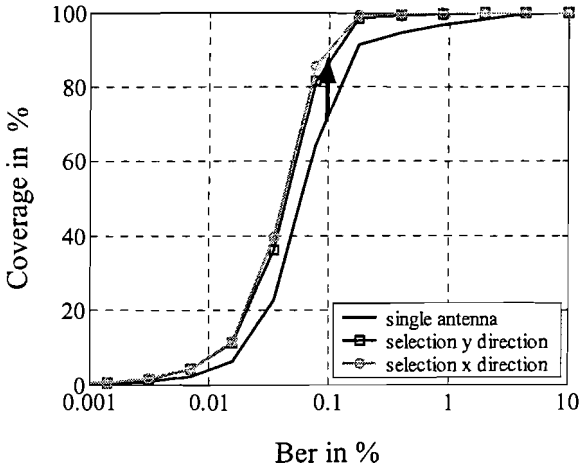

Figure 6.32: *Cdf of measured BER with a single antenna and simulated diversity ($P_{transmitter}$ = -25 dBm at the centre frequency).*

To calculate the diversity gain it is useful to plot the coverage, Pr {BER < 0.1 %}, as a function of the transmitter power. In figure 6.33a the coverage is shown. The outage is shown in figure 6.33b. If we subtract the two transmitter power levels (shown by the arrow) at the same outage we get the diversity gain. The measurement was done on only 4 power levels at a different time. Furthermore, at high transmitter power levels the number of points with a BER > 0.1 % becomes very small. This explains why the curves are less smooth as expected and probably have large measurement errors.

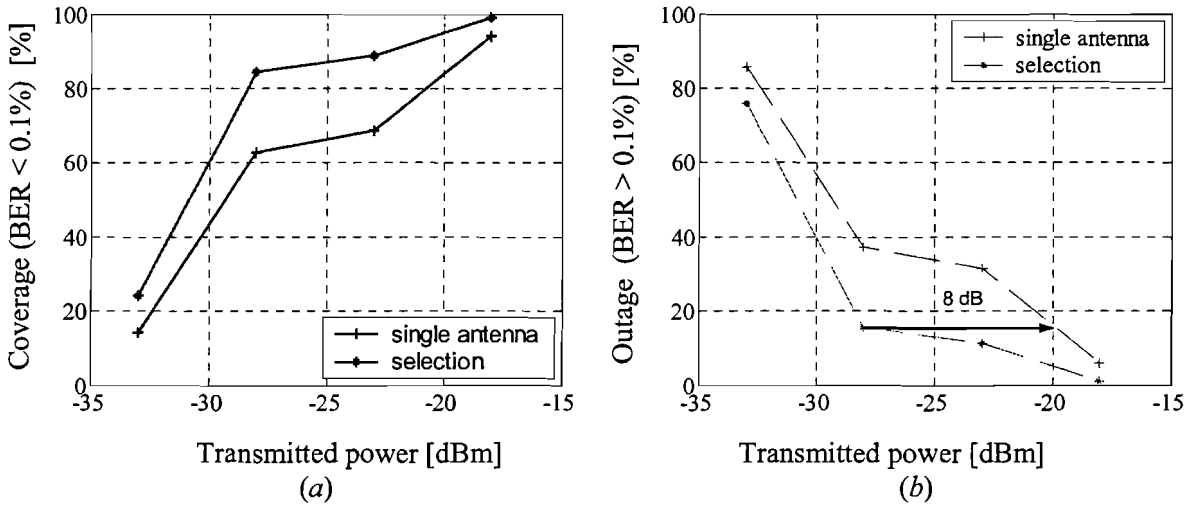

Figure 6.33: *Measured coverage (a) (BER < 0.1 %) and (b) measured outage (BER > 0.1 %) with single antenna and with selection diversity at the centre frequency.*

From figure 6.33 we can observe that at an outage of 15 % the diversity gain, the difference in transmitted power, is 8 dB.

6.5.2 BER measurement with a Bluetooth module with embedded antenna switch

The Bluetooth module mounted on a pcb and the external antenna are shown in figure 6.34. The measured BER of the Bluetooth module with embedded antenna switch and slot antenna is shown in figure 6.35. The switch seams to work well, both BER measurements show almost the same average BER in figure 6.36, so the switch with antennas is symmetrical. Although the slot antenna is not matched to the transmitter, and the critical connection from the transmitter to the resonance point along the slot is based on a simple measurement, the slot antenna seems to work well. As was expected from the analysis of antennas in a multi-path environment, we can observe that the distribution of the BER is quite different. The orientation of the antennas, different radiation patterns and sensitivity to different polarisations and the distribution of the incident field is causing the different distributions of the BER on the *xy*-table.

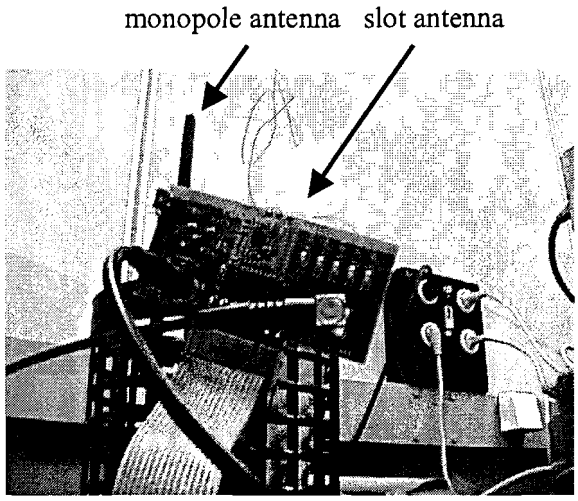

Figure 6.34: *Orientation of the antennas during a measurement.*

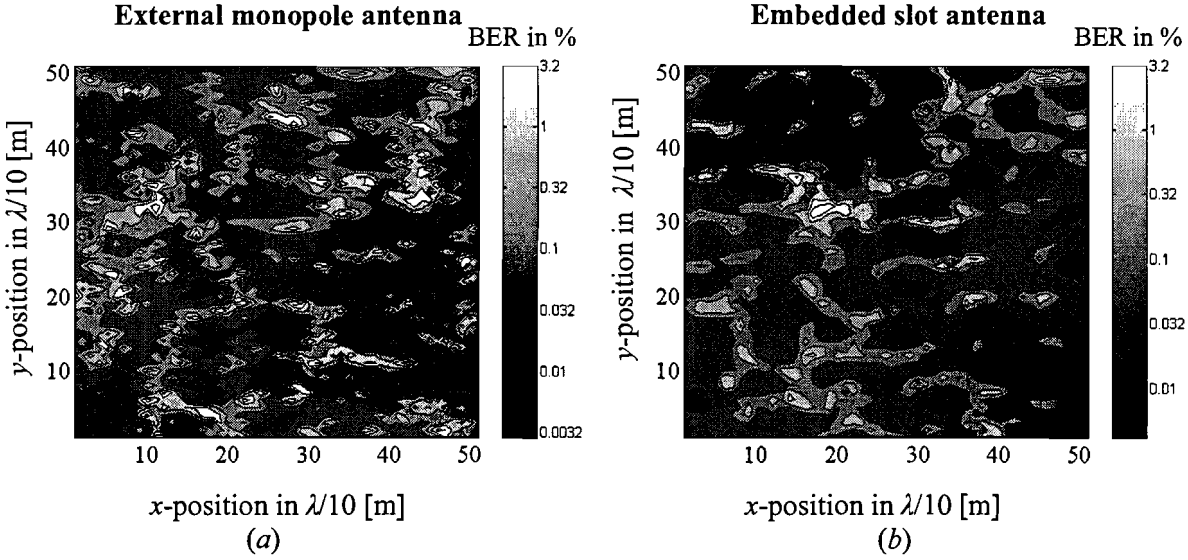

Figure 6.35: *Measured spatial distribution of the BER using a log scale, (a) the external monopole antenna and (b) the embedded slot antenna.*

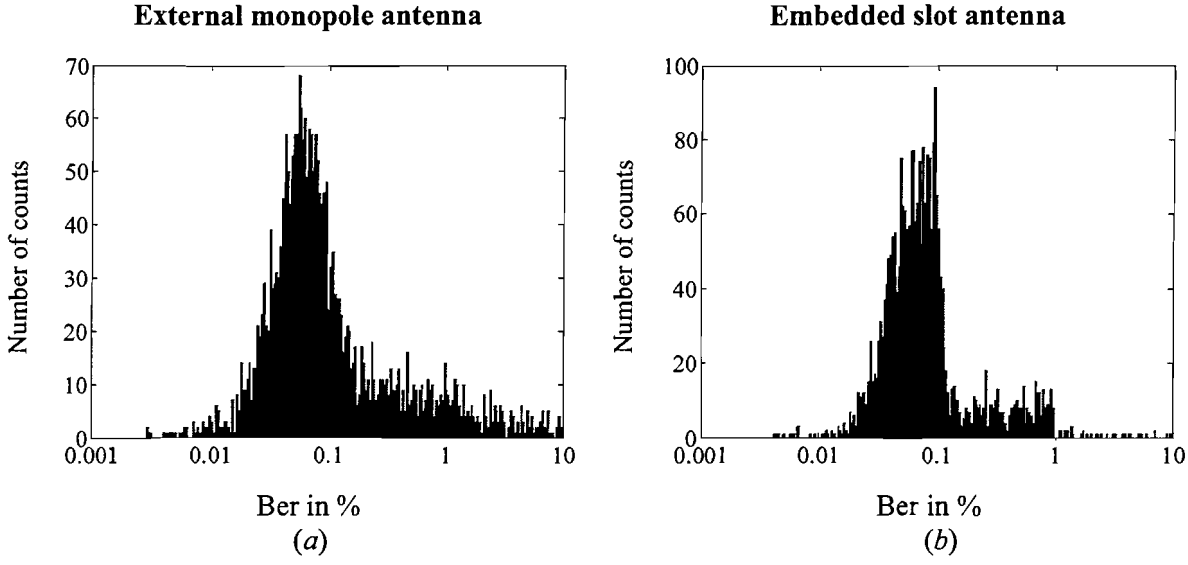

Figure 6.36: *Measured distribution of BER using(a) the external monopole antenna and (b) the embedded slot antenna.*

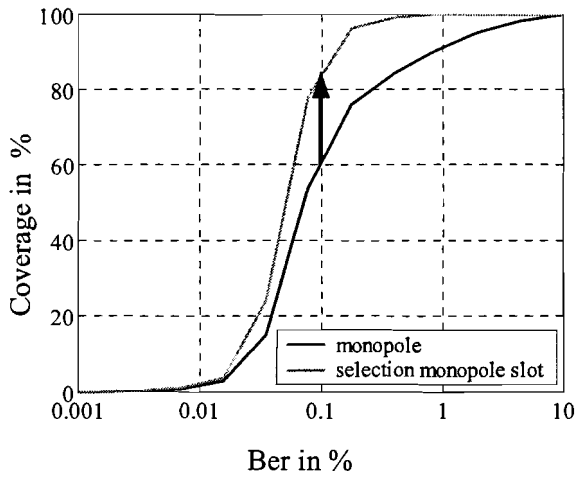

Figure 6.37: *Measured cdf of the BER for a single antenna, selection between slot and monopole antenna.*

From figure 6.36 we can observe that the single antenna receiver has a coverage, Pr {BER < 0.1 %}, of 60 % and an outage, Pr {BER > 0.1 %}, of 40 %. With diversity we have coverage of 85 % and an outage of 15 %. This means that the outage is decreased by a factor of 2.7. At a coverage of 70 % without diversity, the coverage with diversity is 90 % with diversity, and again the outage is decreased by a factor of 3.

6.6 Comparison between simulation and measurement

6.6.1 Calculation of the BER of a Bluetooth receiver

The relation between BER and the EM-field can be calculated with bit errors due to the signal-to-noise ratio and bit errors due to the delay spread. A delay spread in the order of the bit time, 1 μs for Bluetooth, will give inter-symbol interference [Leijten, 2001]. The BER can be expressed with two components,

$$\mathrm{BER}(\vec{r}) = \mathrm{BER}_{SNR}(\vec{r}) + \mathrm{BER}_{\tau}(\vec{r}) \tag{6.15}$$

where the first term is the BER caused by the signal-to-noise ratio and the second term is the BER caused by the delay spread. For GFSK modulation the BER caused by the SNR is given by [Leijten, 2001]

$$\mathrm{BER}_{SNR}(\vec{r}) = \frac{1}{2}\exp\left(-\frac{P_r(\vec{r})}{2P_{noise}}\right) \tag{6.16}$$

where P_r is the received power and P_{noise} is the noise power. The BER caused by inter-symbol interference for a DECT system is given by [Leijten, 2001]

$$\mathrm{BER}_{\tau}(\vec{r}) = \frac{1}{2}\left(\frac{\tau_{\delta}(\vec{r})}{T_{b,30}}\right)^2 \tag{6.17}$$

where $T_{b,30}$ is the bit time at a signal level of –30 dB, and the normalised spread, the delay spread divided by the bit time, is between 0.01 and 0.3. For a good SNR the interference part becomes dominant. When the transmitter power was increased the BER went to zero. The measurement resolution is 1 error bit / 1 million data bits = 1E-6. Even for several measurements the BER stayed

zero so the last term is much smaller than 1E-6. According to Eq (6.17) the BER at a delay spread of 40 ns and a bit time of 1 μs is 8E-4, so this equation cannot be used for Bluetooth. For Bluetooth in an indoor environment we can neglect the second term in Eq (6.15) if the BER is above 1E-6.

The BER of a random binary signal is given by:

$$\begin{aligned} p_e &= \Pr\{1\}\Pr\{0|x=1\}+\Pr\{0\}\Pr\{1|x=0\} \\ &= \frac{1}{2}\Pr\{0|x=1\}+\frac{1}{2}\Pr\{1|x=0\} = \Pr\{1|x=0\} \end{aligned} \tag{6.18}$$

where x is the bit value, p_e is the probability of a bit error, Pr {1} is the probability that a '1' symbol occurs which is ½ for random data. The BER can be derived using the assumption that we have a signal plus added Gaussian noise. We calculate the probability of error for non-coherent detection of frequency-shift-keyed signals. The demodulator has two detectors, one for the maximum frequency with output voltage v_u and one for the minimum frequency with output voltage v_l. The output of the demodulator is v_u-v_l. There is a bit error if the detector voltage of the maximum frequency is larger than the detector voltage of the minimum frequency if the minimum frequency is received [Couch, 1997]

$$p_e = \Pr\{v_u > v_l | f_1\}, \tag{6.19}$$

where f_1 is the minimum frequency. If there is only Gaussian noise the detector voltage is Rayleigh distributed [Couch, 1997]:

$$f(v_u|f_1)=\begin{cases}\frac{v_u}{N}\exp\left(-\frac{v_u^2}{2N}\right) & v_u \geq 0, \\ 0 & v_u < 0,\end{cases} \tag{6.20}$$

where N is the average noise power. When the signal is dominant we get a Rayleigh-Rice distribution when we take the modulus using a detector [Couch, 1997]:

$$f(v_l|f_1)=\begin{cases}\frac{v_l}{N}\exp\left(-\frac{v_l^2+A^2}{2N}\right)I_0\left(\frac{v_l A}{N}\right) & v_l \geq 0, \\ 0 & v_l < 0.\end{cases} \tag{6.21}$$

where A is the amplitude of the received signal, v_l is the output of the detector with added Gaussian noise and I_0 is the modified Besselfunction of the first kind order zero. Using Eq (6.20) and Eq (6.21) this can be expressed as:

$$\begin{aligned} p_e &= \iint\limits_{v_u>v_l} f(v_u, v_l \mid f_1)dv_u dv_l = \int\limits_0^\infty\int\limits_{v_l}^\infty f(v_u \mid f_1)f(v_l \mid f_1)\, dv_u dv_l, \\ &= \int\limits_0^\infty \frac{v_l}{N}\exp\left(-\frac{{v_l}^2+S}{2N}\right)I_0\left(\frac{v_l\sqrt{S}}{N}\right)\int\limits_{v_l}^\infty \frac{v_u}{N}\exp\left(-\frac{{v_u}^2}{2N}\right)dv_u\, dv_l. \end{aligned} \tag{6.22}$$

And finally the probability of an error is

$$p_e = \exp\left(-\frac{S}{2N}\right)\int\limits_0^\infty \frac{v_l}{N}\exp\left(-\frac{{v_l}^2}{N}\right)I_0\left(\frac{v_l\sqrt{S}}{N}\right)dv_l = \frac{1}{2}\exp\left(-\frac{S}{2N}\right). \tag{6.23}$$

6.6.2 Calculation of the BER for Rayleigh fading

We are able to calculate the distribution of the bit error rate if we know the distribution of the signal-to-noise ratio and vice versa, i.e., the relation between the bit error rate and the signal-to-noise ratio is bijective. Furthermore, we will be able to calculate the diversity gain using bit error rates. For Bluetooth the relation between the SNR and the BER is,

$$BER = \frac{1}{2}\exp(-\gamma/2), \quad \gamma = -2\ln(2BER). \tag{6.25}$$

where $0 \le \gamma < \infty$ and $0 \le \text{BER} \le ½$. The pdf of the BER can be expressed in the pdf of the SNR γ,

$$f_{BER}(BER) = f_{\gamma}(-2\ln(2BER))\left|\frac{d-2\ln(2BER)}{d\,BER}\right|. \tag{6.26}$$

For Rayleigh fading and one receive antenna we get

$$\begin{aligned} f_{BER}(BER) &= -\frac{1}{\gamma_0}\exp\left(\frac{2\ln(2BER)}{\gamma_0}\right)\frac{2}{BER} = -\frac{1}{\gamma_0}(2BER)^{2/\gamma_0}\,\frac{2}{BER}, \\ &= -\frac{2^{1+2/\gamma_0}}{\gamma_0}BER^{2/\gamma_0-1}, \end{aligned} \tag{6.27}$$

where $f(\gamma) = \frac{1}{\gamma_0}\exp\left(-\frac{\gamma}{\gamma_0}\right)$, and the average SNR can be expressed in the average BER, $\gamma_0 = 1/\langle BER\rangle - 2$. The cdf of the BER is

$$F(BER_{ref}) = \int_0^{BER_{ref}} f_{BER}(BER)\,dBER. \tag{6.28}$$

Using Eq. 6.24 or the relation between the SNR and the BER we can derive the cdf of the BER using the pdf of the SNR,

$$F_{\text{BER}}(BER_{ref}) = \Pr\{BER < BER_{ref}\} = \Pr\{\gamma > -2\ln 2\,BER_{ref}\}. \tag{6.29}$$

And the cdf of the BER is

$$\begin{aligned} F_{\text{BER}}(BER_{ref}) &= \int_{-2\ln 2\,BER_{ref}}^{\infty} f(\gamma)\,d\gamma = \int_{-2\ln 2\,BER_{ref}}^{\infty} \frac{1}{\gamma_0}\exp(-\gamma/\gamma_0)\,d\gamma \\ &= 2^{2/\gamma_0}BER_{ref}^{2/\gamma_0} = (2BER_{ref})^{\frac{2\langle BER\rangle}{1-2\langle BER\rangle}}. \end{aligned} \tag{6.30}$$

We can calculate the effect of diversity using the BER instead of the SNR. For Raleigh fading with two antennas and selection the pdf of the SNR is,

$$f_n = \frac{N}{\gamma_0}\exp(-\gamma/\gamma_0)[1-\exp(-\gamma/\gamma_0)]^{N-1}. \tag{6.31}$$

Substituting the BER in Eq. (6.31) using Eq. 6.25 gives

$$
\begin{aligned}
f_{BER}(BER) &= -\frac{2}{\gamma_0}\exp\left(\frac{2\ln(2BER)}{\gamma_0}\right)\left[1-\exp\left(\frac{2\ln(2BER)}{\gamma_0}\right)\right]\frac{2}{BER} \\
&= \left[-\frac{4}{\gamma_0}(2BER)^{2/\gamma_0}+\frac{4}{\gamma_0}(2BER)^{4/\gamma_0}\right]/BER \\
&= -\frac{2^{2+2/\gamma_0}}{\gamma_0}BER^{2/\gamma_0-1}+\frac{2^{2+4/\gamma_0}}{\gamma_0}BER^{4/\gamma_0-1}.
\end{aligned}
\tag{6.32}
$$

For the cdf of the BER we can use the cdf of the SNR:

$$
\begin{aligned}
F_{\mathrm{BER}}(BER_{ref}) &= \Pr\{\gamma_1 > \gamma_{ref} \text{ or } \gamma_2 > \gamma_{ref} \text{ or} \cdots \gamma_n > \gamma_{ref}\} \\
&= 1-\Pr\{\gamma_1 < \gamma_{ref} \text{ and } \gamma_2 < \gamma_{ref} \text{ and} \cdots \gamma_n < \gamma_{ref}\} \\
&= 1-\left(1-\exp(-\gamma_{ref}/\gamma_0)\right)^N
\end{aligned}
\tag{6.33}
$$

The cdf of the BER for N antennas is then:

$$
F_{\mathrm{BER}}(BER_{ref}) = 1-(1-(2BER_{ref})^{2/\gamma_0})^N \tag{6.34}
$$

For two antennas, $N = 2$, this becomes

$$
\begin{aligned}
F_{\mathrm{BER}}(BER_{ref}) &= 2\,(2BER_{ref})^{2/\gamma_{div}}-(2BER_{ref})^{4/\gamma_{div}}, \\
&= 2^{1+2/\gamma_{div}}BER_{ref}^{2/\gamma_{div}}-2^{4/\gamma_{div}}BER_{ref}^{4/\gamma_{div}}.
\end{aligned}
\tag{6.35}
$$

where γ_{div} is the average SNR using diversity. The cdf of the BER with and without diversity is presented in figure 6.38.

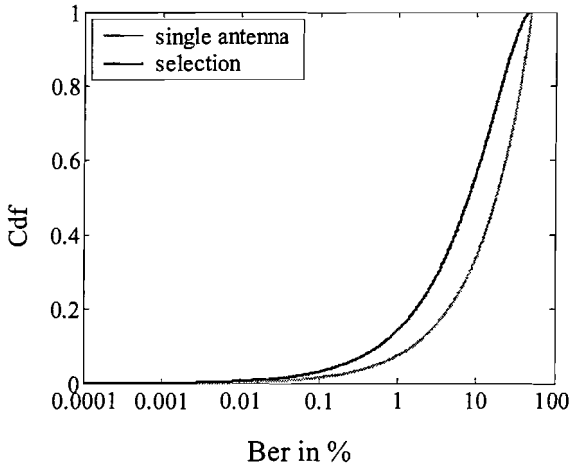

Figure 6.38: *Cdf of the BER using one antenna and two antennas with selection.*

For Raleigh fading with two antennas and selection the diversity gain can be derived using the cdf's of the BER's at the same outage x or coverage 1-x,

$$
2^{2/\gamma_{\mathrm{single}}}BER_{ref}^{2/\gamma_{\mathrm{single}}} = 2^{1+2/\gamma_{div}}BER_{ref}^{2/\gamma_{div}}-2^{4/\gamma_{div}}BER_{ref}^{4/\gamma_{div}} = 1-x, \tag{6.36}
$$

where γ_{single} is the average SNR for a single receive antenna. We can de-couple the two average SNR's,

$$\begin{cases} 2^{2/\gamma_{\text{sin gle}}}\,\mathrm{BER}_{\text{ref}}^{\,2/\gamma_{\text{sin gle}}} = 1-\mathrm{x}, \\ 2^{1+2/\gamma_{div}}\,\mathrm{BER}_{\text{ref}}^{\,2/\gamma_{div}} - 2^{4/\gamma_{div}}\,\mathrm{BER}_{\text{ref}}^{\,4/\gamma_{div}} = 1-\mathrm{x}. \end{cases} \tag{6.37}$$

The SNR's become,

$$\begin{cases} \gamma_{\text{single}} = 2\dfrac{\ln(2BER_{ref})}{\ln(1-x)}, \\ \gamma_{\text{div}} = 2\dfrac{\ln(2BER_{ref})}{\ln(1-\sqrt{x})}. \end{cases} \tag{6.38}$$

where γ_{div} is the root of a second-order polynomial of $2^{2/\gamma_{\text{div}}}\,\mathrm{BER}_{\text{ref}}^{\,2/\gamma_{\text{div}}}$:

$$\begin{aligned} &-2^{4/\gamma_{div}}\,\mathrm{BER}_{\text{ref}}^{\,4/\gamma_{div}} + 2^{1+2/\gamma_{div}}\,\mathrm{BER}_{\text{ref}}^{\,2/\gamma_{div}} - 1 + x = 0, \\ &2^{2/\gamma_{div}}\,\mathrm{BER}_{\text{ref}}^{\,2/\gamma_{div}} = \frac{-2 \pm \sqrt{4+4(x-1)}}{-2} = 1 \pm \sqrt{x}, \\ &F(BER) = 2^{2/\gamma_{\text{sin gle}}}\,\mathrm{BER}_{\text{ref}}^{\,2/\gamma_{\text{sin gle}}} \le 1, \\ &2^{2/\gamma_{div}}\,\mathrm{BER}_{\text{ref}}^{\,2/\gamma_{div}} = 1-\sqrt{x}. \end{aligned} \tag{6.39}$$

The diversity gain is the ratio of the mean SNR's. Note that the mean SNR is related to the radiated power.

$$G_{diversity} = \frac{\gamma_{\text{single}}}{\gamma_{\text{div}}} = \frac{\ln(1-\sqrt{x})}{\ln(1-x)}. \tag{6.40}$$

To give an example we calculate the diversity gain at an outage of 1 %:

$$G_{diversity} = \frac{\gamma_{\text{single}}}{\gamma_{\text{div}}} = \frac{\ln(1+\sqrt{0.01})}{\ln(1-0.01)} = 10.48 = 10.2\ \text{dB}. \tag{6.41}$$

We see that the diversity gain derived using signal-to-noise ratios and the diversity gain derived using bit error rates are the same. This is as expected, the relation between SNR and BER is bijective so the cdf's are the same, and from the cdf we derive the diversity gain. The SNR at a $\mathrm{BER}_{\text{ref}}$ of 0.1 % and an outage of 1 % is,

$$\begin{aligned} &\gamma_{\text{single}} = 2\frac{\ln(2BER_{ref})}{\ln 0.99} = 1236.7 = 30.9\ \text{dB}, \\ &\gamma_{\text{div}} = 30.9 - 10.2 = 20.7\ \text{dB}. \end{aligned} \tag{6.42}$$

The average BER with one receive antenna is:

$$\langle BER \rangle_1 = \frac{1}{2+\gamma_1} = 8.07\text{E}-4 = 0.081\,\%. \tag{6.43}$$

and with selection and two receive antennas the average BER is:

$$\langle BER \rangle_2 = \frac{1}{2+3\gamma_1/2+\gamma_1^2/4} = 2.60\text{E}-6 = 0.00026\,\%. \tag{6.44}$$

6.6.3 Calculation of the BER for Rayleigh-Rice fading

In case of Rayleigh-Rice fading, a LOS radio link, we get:

$$F_{BER}(\mathrm{BER}_{\mathrm{ref}}) = \Pr\{BER < BER_{ref}\} = \Pr\{\gamma > \gamma_{ref}\}$$
$$= \int_{-2\ln 2\,ref}^{\infty} \frac{1+K}{\gamma_0}\exp\left[-K-\frac{\gamma}{\gamma_0}(1+K)\right] J_0\left[2\sqrt{\frac{\gamma}{\gamma_0}(K^2+K)}\right] d\gamma \qquad (6.45)$$

From the measured BER, as shown in figure 6.31, we can calculate the amplitude distribution with the mapping from the BER to the amplitude. The result of the mapping from the measured BER with the diversity switch to the amplitude is the amplitude distribution as shown in figure 6.39.

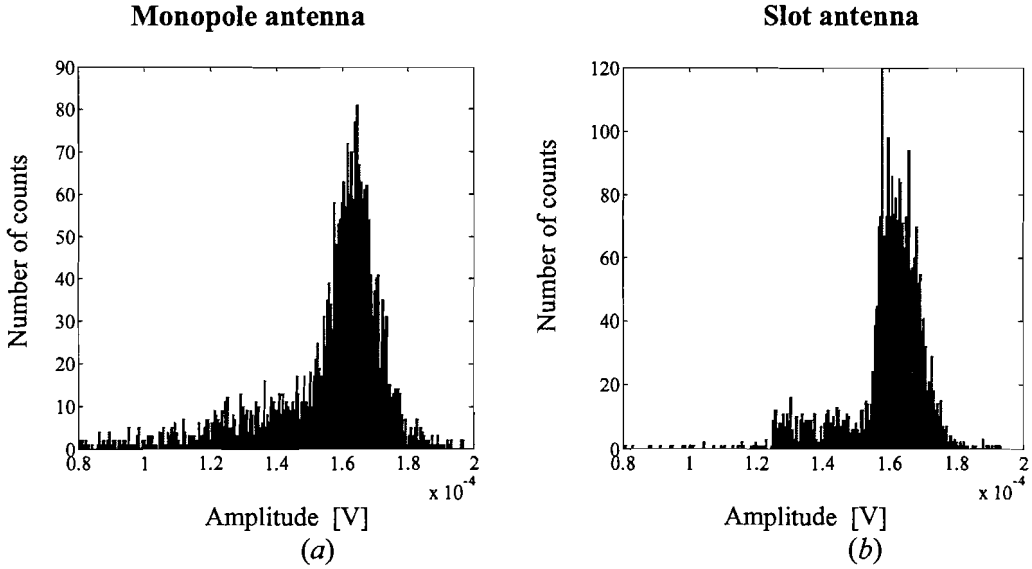

Figure 6.39: *Amplitude distribution calculated from the measured BER (a) using the external monopole antenna and (b) using the embedded slot antenna.*

It appears that the measurement has a LOS behaviour due to the set-up of the antennas. Using the amplitude distribution we get can calculate the K-factor, $K = \frac{\text{power direct waves}}{\text{power scattered waves}}$, and the K = 2.6 or 4 dB. For $K >> 1$ we can rewrite Eq. (6.31) using a asymptotic expansion for large x [Sampei, 1997], $I_0(x) \approx \frac{\exp(x)}{\sqrt{2\pi x}}$, we get for the pdf of the amplitude a:

$$f(r) = \frac{1}{\sqrt{2\pi\sigma}}\exp\left[-\frac{(a-A_{dir})^2}{2\sigma}\right], \qquad (6.46)$$

where A_{dir} is the amplitude from the direct waves at the receiver. When we use the mapping from BER to amplitude, $\gamma = \frac{a^2/(2\,Z_0)}{P_{noise}} = \frac{a^2/100}{P_{noise}} = -2\ln(2BER)$, we get for the amplitude a:

$$a = 10\sqrt{P_{noise}\,2\ln(2BER)} = \sqrt{10^{-8.4}\,10^{-3}\,2\ln(2BER)}, \qquad (6.47)$$

where P_{noise}, the noise level of the receiver, is taken –84 dBm. We can try to fit the amplitude distribution using Eq. (6.47) with the Rayleigh-Rice distribution using Eq. (6.46). There is a good match between the distribution of the amplitude using the Rayleigh-Rice model depicted in figure

6.40b, and the measured amplitude distribution of a Bluetooth module without diversity, as depicted in figure 6.40a.

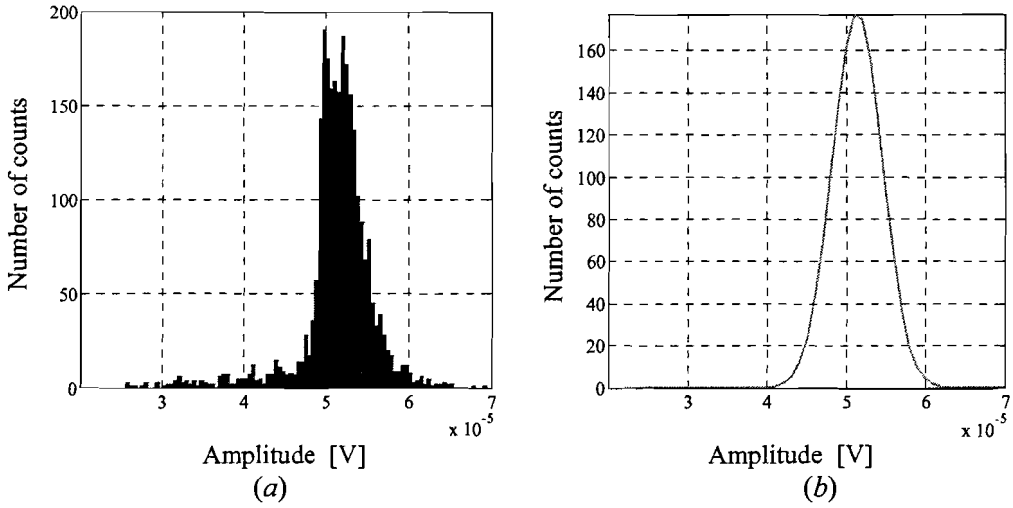

Figure 6.40: *Calculated amplitude distribution using (a) BER measurement data of a module without switch with an monopole antenna and (b) Rayleigh-Rice model fit of the amplitude distribution.*

7 Conclusions and recommendations

7.1 Conclusions

A Bluetooth antenna diversity demonstrator was built to perform a diversity measurement. Selection between the embedded slot antenna and the external monopole antenna improves the quality of the radio link. The BER measurement with the demonstrator shows that the measured BER of the antennas is de-correlated. For the measurement shown in chapter 6 the fades (BER> 0.1 %) disappear if antenna diversity is used.

Analytical propagation models like the cavity model are a good starting point to investigate indoor propagation. In practice, we need a statistical model to take into account reflections, absorbing and shadowing objects in a room.
For a non-line-of-sight measurement the propagation in the room shows two dominant phases, just like the cavity model predicts. A combination of the free-space model and the cavity model was used to fit the measured data.

The radio channel can be characterized using the measurement set-up at Philips Research. With the use of monopole antennas the propagation in the Bluetooth band was measured. Several propagation parameters can be derived from the measurement results. We can investigate the time response of the radio channel. However, the transformation from the frequency domain, using the measurements, to the time domain is difficult due to the limited bandwidth of the measurement. The coherence bandwidth is derived from the measured data without a transformation to the time domain. The quality improvement of the radio link after implementation of antenna diversity can be calculated using the measured data.

To understand the performance of a receive antenna in an indoor environment we need the incident field distribution and the radiation pattern of the antenna. The measurements with a slot antenna and a monopole antenna show that the influence of the radiation pattern and orientation of the antenna on the received power is large. A statistical analysis suggests that if an antenna is in a reflective environment the chance of a fade decreases if the radiation pattern is omnidirectional and the antenna is sensitive to several polarisations. If diversity is implemented using two antennas, the two antennas should have either a different: radiation pattern, orientation or position, in order to get independent received powers.

If the BER is small, it changes very slowly as function of the received power and the BER measurement is insensitive to propagation changes. For Bluetooth it was observed from the measurements that the BER depends only on the signal to noise ratio and not on the delay spread.

For synchronous data transfer, e.g., an audio link, frequency hopping is not robust enough. The indoor radio channel has a coherence bandwidth of only a few MHz in the Bluetooth band. So the chance of hopping in a fade is considerable. Therefore, selective frequency hopping or frequency hopping in combination with antenna diversity will dramatically decrease the chance of a fade. Another option to decrease the chance of a fade is to control the frequency hopping sequence. This will be implemented in the new Bluetooth protocol (V1.2).

If two receive antennas are used and the received signals are independent, the chance of a fade decreases quadraticly. The predicted probability of a fade at all outage levels is, ($Pr\{SNR<X\} = Pr\{SNR_1<X\}*Pr\{SNR_2<X\}$). From the measurements we can observe that the combination of a monopole and a slot antenna gives independent received powers. For space diversity and non-line-of sight propagation, the predicted fade probability and the measured fade probability are the same. If polarisation diversity is used the measured fade probability is higher. For example, the measured fade probability decrease for space diversity is 10 dB and the measured fade probability decrease

for polarisation diversity is 8 dB. The measured diversity gain for non-line-of sight propagation is about 10 dB at an outage of 1 %. The predicted diversity gain for Rayleigh-fading is also 10 dB at an outage of 1 %.

The simple adaptive combiner presented in [Dolmans, 1997], using the signal and the signal shifted 180° in phase, will perform as an equal gain combiner if the signals at the two antennas differ 180° in phase. This phase difference was measured in a NLOS measurement.

7.2 Recommendations

Although field strength measurements are useful to examine the radio channel, they should be translated to bit error rates (BER) for a digital communication system. Therefore, it is better to measure the BER directly to avoid problems with the translation from the field strength to the bit error rate. The measurements of the field strength and the BER measurements can be done simultaneously if some extra equipment is connected to the measurement set-up. In this way it becomes possible to measure the relation between bit error rate and the radio channel characteristics like power transfer, delay spread and coherence bandwidth.

The approximation of the time domain response can be improved if the frequency step size is reduced and the bandwidth of the antennas is increased.

It would be interesting to perform the field measurement with different antenna types. Measurements with different antennas should result in a different distribution of the magnitude and power of the received signal. Furthermore, the optimum antenna pattern for a receive and transmit antenna in a typical indoor environment can be investigated.
The propagation measurements should be performed in a range from NLOS to a strong LOS character. Using the measurement set-up it should be possible to measure the main effective gain of an antenna.

An interesting option for diversity is the use of field diversity. A magnetic loop antenna and a slot antenna could be embedded in a module. The design of the two antennas requires a numerical simulation due to the coupling between the antennas.

References

Bektas, F.
Investigation of antenna diversity techniques for Bluetooth communication.
Ph.D. Thesis, Technischen Universität Wien, February 2003.

Bray, J and Sturman, C.F.
Bluetooth:connect without cables.
Upper Saddle River, Prentice–Hall, 2001.

Collin, R.E.
Field theory of guided waves.
IEEE Press, Piscataway NJ, 1991.

Couch, L.W.
Digital and analog communication systems.
Upper Saddle River, Prentice–Hall, 1997.

Dehling, H.G. and Kalma, J.N.
Kansrekening het zekere van het onzekere.
Utrecht, Epsilon, 1995.

Dijk, N.
Some initial considerations on the application of mode-stired chambers for EMC testing.
Technical Note 2001/239, Philips Research, 2001.

Dolmans, W.M.C.
Effect of indoor Fading on the performance of an adaptive antenna system.
Ph.D. Thesis, Eindhoven University of Technology, October 1997.

Dolmans, W.M.C.
Diversity systems for mobile communication in a large room.
EUT Report 96-E-297, Eindhoven University of Technology, 1996.

Glazunov, A.A.
Theoretical analysis of mean effective gain of mobile terminal antennas in Ricean channels.
IEEE 56th Vehicular Technology Conference, Vol. 3, September 2002, pp. 1796-1800.

Gradshteyn, I.S. and Ryzhik, I.M.
Table of integrals, series , and products.
London, Acadamic Press, 1994.

Grauw, A. and Uddink, M.
Integration of the antenna function with the radio module for Bluetooth systems.
Feasibility report Bluetooth antenna integration, June 2001.

Green, B.M. and Jensen, M.A.
Diversity performance of dual-antenna handsets near operator tissue.
IEEE Transactions on Antennas and Propagation, Vol. 48, No.7, July 2000, pp. 1017-1024.

Griffel, D.H.
Applied functional analysis.
New York, Dover, 2002.

Haartsen, J.C. and Mattisson, S.
Bluetooth-a new low-power radio interface providing short-range connectivity.
IEEE Proceedings of the IEEE, Vol. 88, No.10, October 2000, pp. 1651-1661.

Haartsen, J.C. and Zürbes, S.
Frequency hop selection in the Bluetooth radio system.
IEEE 7th Int. Symp. on Spread-Spectrum Tech. & Appl., Prague, September 2002, pp. 83-87.

Harrington, R.F.
Field computation by moment methods.
IEEE Press, Piscataway NJ, 1993.

Helstrom, C.W.
Probability and stochastic processes for engineers.
Upper Saddle River, Prentice–Hall, 1991.

Herben, M.H.A.J.
Antennes en propagatie.
Lecture notes, Eindhoven University of Technology, 2000.

Hill, D.A.
Linear dipole response in a reverberation chamber.
IEEE Transactions on Elecromagnetic Compatability, Vol. 41, November 1999, pp. 365-368.

Jackson, J, D.
Classical electrodynamics.
New York, Wiley, 1963.

Jakes, W.R.
Microwave mobile communications.
New York, Wiley, 1974.

Kalliola, K.;Sulonen, K.;Laitinen, H.;Kivekäs, O.;Krogerus, J.;Vainikainen, P.
Angular power distribution and mean effective gain of mobile antenna in different propagation environments.
IEEE Transactions on Vehicle Technology, Vol. 51, No. 5, September 2002, pp. 823-838.

Kraus, J.D.
Electromagnetics.
New York, McGraw Hill, 1992.

Lee, W.C.Y.
Mobile communications engineering.
New York, McGraw Hill, 1982.

Leijten, L.
Design of antenna-diversity transceivers for wireless consumer products.
Ph. D. Thesis, Eindhoven University of Technology, September 2001.

Mattheijssen, P.
Antenna pattern diversity for GSM handhelds.
Technical note 2000/263, Philips Research, 2000.

Mattheijssen, P.;Herben, M.;Dolmans, G.;Leyten, L.
Antenna pattern diversity versus space diversity for use at handhelds.
IEEE Transactions on Vehicle Technology, Vol. 53, No. 4, July 2004, pp. 1035-1042.

Nicholls, J.
Lecture notes PH 2130 Mathematical methods.
Royal Holloway University of London.

Nørklit, O.;Teal, P.D.;Vaughan, R.G.
Measurement and evaluation of multi-antenna handsets in indoor communication.
IEEE Transactions on Antennas and Propagation, Vol. 49, No. 3, March 2001, pp. 1017-1024.

Philips Semiconductors.
2.45 GHz T/R, RF switch for e.g. Bluetooth application using PIN diodes.
Application note AN10173-01.

Pozar, D.M.
Microwave engineering.
Chichester, Wiley, 1998.

Sampei, S.
Applications of digital wireless technologies to global wireless communications.
Upper Saddle River, Prentice–Hall, 1997.

Saunders, S.R.
Antennas and propagation for wireless communication systems.
Chichester, Wiley, 1999.

Smolders, A.B.
Microstrip phased-array antennas:a finite array approach.
Ph. D. Thesis, Eindhoven University of Technology, October 1994.

Smolders, A.B.
Elektromagnetische antennes.
Lecture notes, Eindhoven University of Technology, Februari 2000.

Strauss, W.A.
Partial differential equations an introduction.
Chichester, Wiley, 1992.

Taga, T.
Analysis for mean effective gain of mobile antennas in land mobile radio environments.
IEEE Transactions on Vehicle Technology, Vol. 39, May 1990, pp. 117-131.

Vaughan, R.G.
Polarisation diversity in mobile communications.
IEEE Transactions on Vehicle Technology, Vol. 39, August 1990, pp. 177-186.

Vaughan, R. and Andersen, J.B.
Channels, propagation and antennas for mobile communications.
London, The Institution of Electrical Engineers, 2003.

Internet:

www.bluetooth.com

www.ericson.com

www.matworks.com

Bluetooth Radio Module with Embedded Antenna Diversity

J.J. Breur*, A.B. Smolders*, W.M.C. Dolmans**, H.J. Visser***

Abstract—**A complete Bluetooth radio SiP (System-in-Package) is presented that includes antenna diversity requiring only one external antenna. The module measures only 140 mm^2 and has an on-board diversity switch and an embedded antenna. Measured Bit-Error-Rate with and without diversity are presented for a typical indoor environment. It is shown that by using antenna diversity a diversity gain of approx. 9 dB can be obtained for an indoor Bluetooth connection.**

I. Introduction

BLUETOOTH is currently being introduced into several market segments, like mobile phones, headsets, PC's etc. Bluetooth operates in the ISM-band between 2.4 GHz and 2.48 GHz and uses 80 channels, with a channel spacing of 1 MHz. Bluetooth was orginally specified in such a way that the complete system, i.e. radio and baseband, could be integrated into a single CMOS integrated circuit. This resulted in a quite poor specification for the sensitivity (-70 dBm) and output power (0 dBm, Class II) [1], [2]. In practice, it now becomes clear that systems that just meet this relaxed specification show a quite poor quality especially with indoor voice/audio applications. Therefore, the newest generation of Bluetooth BiCMOS radios show a much improved performance, with a sensitivity better than -80 dBm and output power up to +4 dBm or higher.

Another way to improve the so-called "quality-of-service" in a Bluetooth connection is the use of antenna diversity. This technique has already been succesfully used in systems like DECT and WLAN. Originally one thought that the Bluetooth standard, which incorporates frequency hopping, was robust enough to cope with indoor fading. However, in this paper it will be shown by means of measurements supported by a theoretical model that a significant improvement in the quality of a Bluetooth connection can be estabished in an indoor environment. Based on these results a demonstrator radio with embedded diversity was developed.

II. Effect of antenna diversity in a Bluetooth connection

The indoor environment behaves like a cavity with dielectric walls. A theoretical model of an indoor environment was developed to predict the diversity gain that can be expected from a Bluetooth radio. The model is based on the work previously done at Philips Research and reported in [3],[4]. In this approach, a rigorous modal expansion of the unknown electromagnetic fields is used in a room where the devices operate. The theoretical model is verified with measurements that were performed on a special diversity test bench that is available at Philips Research [3]. From these simulations with a cavity model, it came out that the power of the receiving antenna has a Rayleigh-type of distribution. Figure 1 shows the measured and simulated outage when

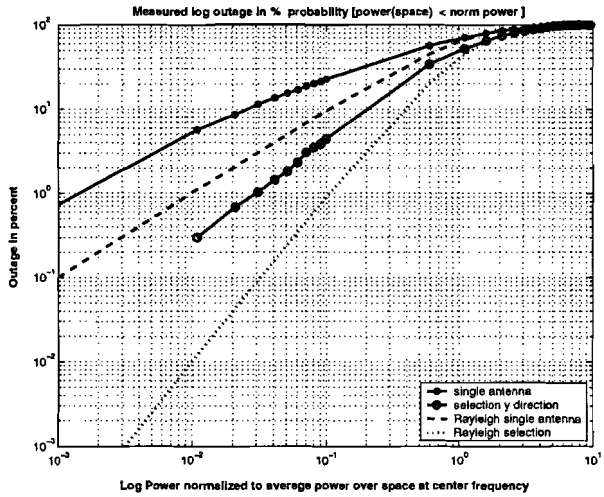

Fig. 1. *Measured and simulated outage for a Bluetooth radio module with and without space diversity, frequency is 2.45 GHz, antennas are separated by* $\frac{\lambda}{2}$

a combination of space diversity and selection combining is used. The simulation is based on a Rayleigh distribution. The measurements were done with monopole antennas. The outage is here defined as the probability that the normalized Signal-to-Noise Ratio (SNR) values are lower than a certain level μ [4], [5]. Note that diversity is only applied in receive mode with two antennas that are separated by $\frac{\lambda}{2}$. Measurements and calculations show that a distance of $\frac{\lambda}{2}$ is sufficient to decorrelate the signals for space diversity. From Figure 1 it can be seen that the diversity gain at an outage level of 1% is approximately 9 dB. Moreover, deep fades of 30 dB or more are avoided with antenna diversity.

III. Bluetooth radio demonstrator with embedded antenna diversity

A demonstrator Bluetooth radio module (System-in-Package) was developed to show the improvement that can be obtained with a complete Bluetooth system by using antenna diversity. Figure 2 shows the schematic of this radio. It consists of a low-IF BiCMOS transceiver, TX and RX baluns, a diversity switch and an antenna filter for out-of-band blocking. The module also contains a very small-size embedded slot antenna that is optimised over the Bluetooth

* These authors are with Philips Semiconductors, BL RF Modules, Nijmegen, The Netherlands, E-mail: Bart.Smolders@philips.com

** This author is with Philips Research, Eindhoven, The Netherlands, E-mail: Guido.Dolmans@philips.com

*** This author is with the Eindhoven University of Technology, Eindhoven, The Netherlands E-mail: H.J.Visser@tue.nl

frequency band. The other antenna that is used in the diversity scheme is external and will typically be an inverted-F antenna. The total size of the module is approx. $140mm^2$. The radio is build on a LTCC ceramic substrate in which several passive RF functions are integrated.

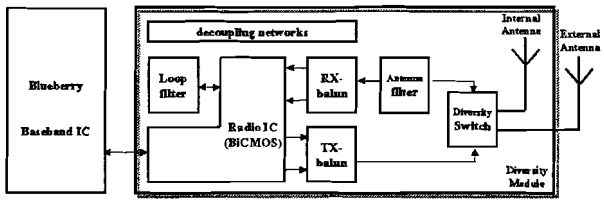

Fig. 2. *Schematic of the Bluetooth radio module with antenna diversity*

The diversity switch is shown in figure 3 and is build up with three low-cost PIN diodes, giving excellent isolation and low insertion loss. In receive mode both the internal as well as the external antenna can be selected by means of the two control signals that are controlled via the baseband processor. In transmit mode only the external antenna is used. The insertion loss and isolation of the switch is shown in figure 4 and is lower than 0.7 dB and 21 dB, respectively.

Figure 5 shows the complete module. The selection of

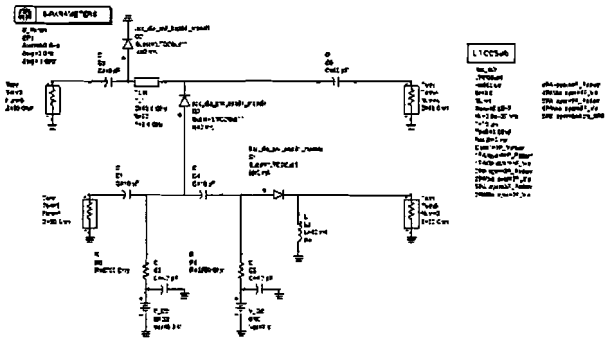

Fig. 3. *Detailed schematic diversity switch*

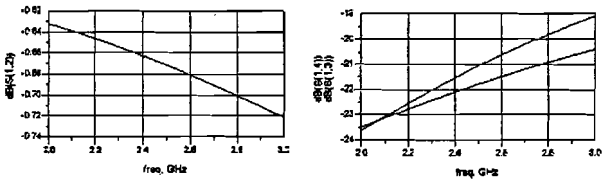

Fig. 4. *Insertion loss and isolation of the diversity switch*

the "best" antenna is done by the baseband processor and is based on RSSI (Receiver Signal Strength Indicator) information. Diversity switching from the baseband can be done with two methods: 1) using the received RSSI information at the beginning of each slot (preamble), or 2) the selection of an optimal antenna can be put into a look-up table, where for each frequency an optimal antenna is allocated. The first scenario is difficult to use in practice, since the pre-amble consists of 4 bits only. This is due to the fact that the Bluetooth V1.1 protocol was not written to support diversity. The second method can be used succesfully if the look-up table is continuously updated with new information.

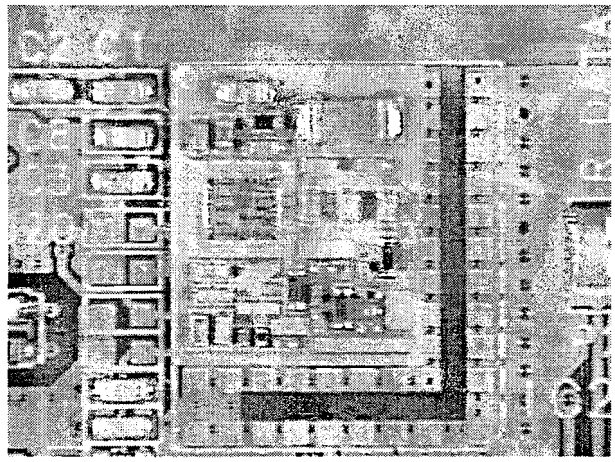

Fig. 5. *Bluetooth radio module with antenna diversity functionality*

IV. Diversity tests with the diversity module

Extensive tests were performed on the diversity module with integrated antenna. The Bluetooth module is placed in a diversity test bench that simulates a typical indoor environment with deep fades as low as -30 dB. The diversity module was set in receive mode at a static location and the transmit antenna (monopole) was moved over an area of 62.5x62.5 cm^2 with a stepsize of $1.25cm = 0.1\lambda$. The external antenna of the Bluetooth module was also a monopole antenna. The efficiency of the internal antenna is almost equal to the efficiency of the external antenna that was used. The separation between the internal and external antenna is approx. $\frac{\lambda}{2}$. Since the polarisation characteristics and the radiation pattern of the internal antenna is different from the external antenna, we will have a mixture of space, polarisation and radiation pattern diversity.

As a first step, the BER (Bit-Error-Rate) was measured with the internal antenna selected at each position of the transmit antenna. Secondly, this test was repeated with the external antenna selected. The BER was measured with a SMIQ BER tester over 1,000.000 data bits. Since the module contains a complete transceiver, we need to use the BER as a measure to indicate the performance of the diversity module. The power level of the transmitting antenna was set in such a way that that the average BER was close to 0.1%. Note that the sensitivity of the module is -83 dBm. Figure 6 shows an example of the measured raw data, where the spatial distribution of $log_{10}(BER)$ is shown when the internal antenna is selected. The correlation in BER can be seen by looking at the average radius of a area with the same colour, which is close to the theoretically expected value of $\frac{1}{2}\lambda$.

Figure 7 shows the measured outage for various power levels of the transmitting antenna for BER > 0.1%. Figure 7 shows the measured coverage ($P_r(BER < x\%)$) versus BER at a single power level for which the average BER was close to 0.1%. From this figure we can conclude that selection diversity improves the BER significantly in an indoor environment. The relation between BER and the Signal-to-Noise ($\frac{S}{N}$) ratio at the input of the Continuous-Phase (CP) FSK non-coherent demodulator is given by [4]:

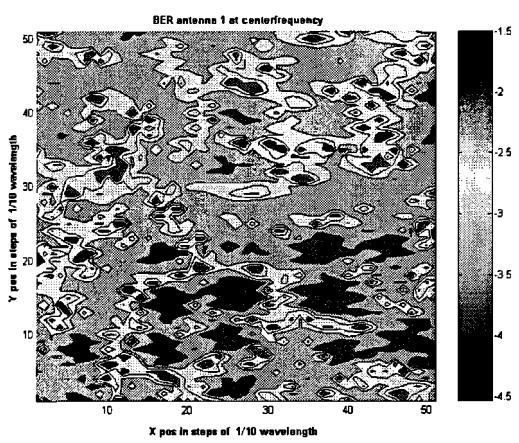

Fig. 6. *Measured spatial distribution of* $log_{10}(BER)$ *using the internal slot antenna at 2.44 GHz*

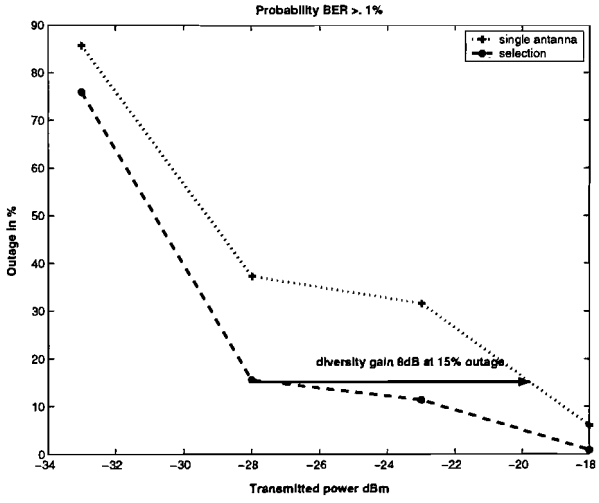

Fig. 7. *Measured outage versus power of transmitting antenna at 2.44 GHz for BER* $> 0.1\%$ *of the Bluetooth module with and without antenna diversity*

$$BER = \frac{1}{2} exp[-\frac{S}{2N}] \quad (1)$$

In equation 1 the BER due to delay-spread is ignored. The measured improvement with diversity in figure 7 corresponds quite well with the measured and predicted outage of figure 1. For example, in figure 7 we can observe that diversity requires 8 dB less input power for an outage level of 15%. The same improvement can be seen in figure 1.

V. Conclusions

Measurements supported by calculations show that a significant improvement in the reliability of a Bluetooth connection can be obtained by using antenna diversity. A simple switching scheme was implemented in a complete Bluetooth radio module with embedded antenna, using LTCC technology. An improvement of 8dB was measured with the demonstrator module.

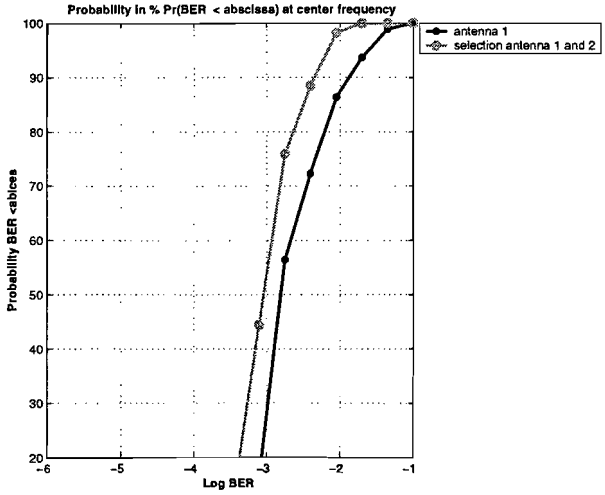

Fig. 8. *Measured coverage versus BER at 2.44 GHz of the Bluetooth module with and without antenna diversity*

References

[1] Specification of the Bluetooth system V1.1 (On-line), Available: http:/www.bluetooth.com.

[2] J. C. Haartsen and S. Mattisson, "A new low-power radio interface providing short-range connectivity," *Proceedings of the IEEE*, Vol.47, pp. 1651-1661, October 2000.

[3] W.M.C. Dolmans, "Effect of indoor fading on the performance of an adaptive antenna system," *Ph.D. Thesis*, Eindhoven University of Technology, October 1997.

[4] L. Leyten, "Design of antenna-diversity transceivers for wireless consumer products," , *Ph.D. Thesis*, Eindhoven University of Technology, September 2001.

[5] B. Green and M. Jensen, "Diversity performance of dual-antenna handsets near operator tissue," *IEEE Transactions Antennas and Propagation*, Vol.48, pp. 1017-1024, July 2000.

Appendix A: Rayleigh-Rice distribution

The Rayleigh-Rice distribution describes the 2-dimensional EM-wave propagation. The propagation consists out of line-of-sight (direct waves) and a non-line-of-sight (reflected waves). The reflected waves are independent in magnitude, phase and polarisation. Only one spatial component of the field is considered. This component has two orthogonal parts, an in phase signal i and a quadrature signal q. The variables i and q are independent. I and q are Gaussian distributed with expected values m_i and m_q and equal variances σ^2. We seek the probability density function of the envelope [Helstrom, 1991],

$$\begin{aligned} &i = i_{reflected} + i_{direct}, \quad q = q_{reflected} + q_{direct}, \quad z = i + jq, \quad |z| = a = \sqrt{i^2 + q^2}, \\ &\Pr\{a < a \le a + da\} = f_a(a)\,da. \end{aligned} \tag{A.1}$$

Where for z, i and q an $\exp(j\omega t)$ time dependence is assumed and suppressed. The probability in (A.1) is the measure of the annulus A of radius a and width da in the iq-plane as shown in figure A.1.

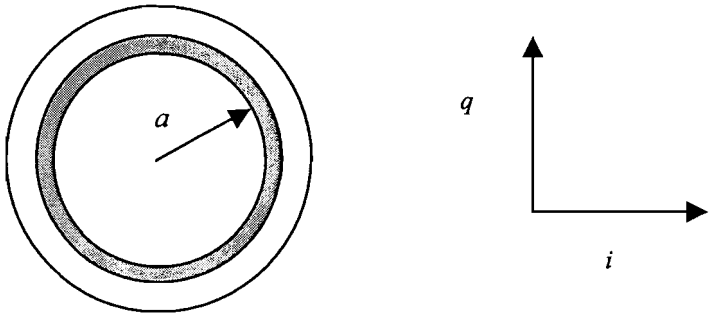

(*a*) (*b*)

Figure A.1: *Annulus is the grey area in (a) and (b) the iq-plane.*

The probability sought is then the integral of the product of two Gaussian distributions,

$$\begin{aligned} &\Pr\{a < a \le a + da\} = \Pr\{(i,q) \mid a^2 < i^2 + q^2 \le (a + da)^2\} = \Pr\{i\}\,\Pr\{q\} \mid a^2 < i^2 + q^2 \le (a + da)^2, \\ &f_a(a)\,da = \iint_A \frac{1}{2\pi\sigma^2} \exp\left[-\frac{(i - m_i)^2 + (q - m_q)^2}{2\sigma^2}\right] di\,dq. \end{aligned} \tag{A.2}$$

We evaluate the integral by converting the integrand to polar coordinates,

$$m = m_i + jm_q, \quad i = r\cos\theta_1, \quad q = r\sin\theta_1, \quad di\,dq = r\,dr\,d\theta_1.$$

We can express the probability as function of the phase and amplitude of the signal,

$$f_{a\theta}(a,\theta)\,da\,d\theta = \frac{1}{2\pi\sigma^2} \int_a^{a+da} \int_\theta^{\theta+d\theta} \exp\left[-\frac{r^2 - 2r\,(m_i\cos\theta_1 + m_q\sin\theta_1) + m_i^2 + m_q^2}{2\sigma^2}\right] r\,dr\,d\theta_1. \tag{A.3}$$

Let us put: $m_i = m\cos\alpha, \quad m_q = m\sin\alpha, \quad m_i\cos\theta_1 + m_q\sin\theta_1 = m\cos(\theta_1 - \alpha).$

Because dr is infinitesimal we can replace r by a

$$f_a(a) = \frac{1}{2\pi\sigma^2}\, a \exp(-(a^2+m^2)/2\sigma^2) \int_0^{2\pi} \exp(ma\cos(\theta_1-\alpha)/\sigma^2)\, d\theta_1 . \tag{A.4}$$

As the integrand is periodic in θ_1, the result will be independent of α and we find that

$$\begin{aligned} f_a(a) &= \frac{a}{\sigma^2}\exp\left(-\frac{a^2+m^2}{2\sigma^2}\right) I_0\left(\frac{ma}{\sigma^2}\right) U(a), \quad \text{with} \\ I_0(a) &= \frac{1}{2\pi}\int_0^{2\pi} \exp(a\cos\theta_1)\, d\theta_1 . \end{aligned} \tag{A.5}$$

Where I_0 is the modified zeroth order Bessel function of the first kind. Equation (A.5) is called the Rayleigh-Rice distribution. The pdf of the phase is calculated with $f_\theta(\theta) = \int_0^\infty f_{a\theta}(a,\theta)\, da$ and we obtain [Sampei, 1997]:

$$f_\theta(\theta) = \frac{1}{2\pi}\exp\left(-\frac{m^2}{2\sigma^2}\right) + \frac{m\cos\theta}{2\sqrt{2\pi\sigma^2}}\left\{1+\operatorname{erf}\left(\frac{m\cos\theta}{\sqrt{2\sigma^2}}\right)\right\}\exp\left(-\frac{m^2}{2\sigma^2}\right), \tag{A.6}$$

where erf is the error function. When the mean of i and q is zero we get the Rayleigh distribution with

$$f_\theta(\theta) = \frac{1}{2\pi} \text{ and } f_{a\theta}(a,\theta) = f_a(a)\, f_\theta(\theta) . \tag{A.7}$$

The statistical properties of the Rayleigh distribution are:

- mean amplitude $\quad \langle a \rangle = \int_0^\infty a\, f(a)\, da = \sqrt{\pi/2}\ \sigma \approx 1.25\sigma ,$
- mean power $\quad \langle a^2 \rangle = \int_0^\infty a^2 f(a)\, da = 2\sigma^2 ,$
- variance in amplitude $\quad \sigma_a^2 = \langle a^2 \rangle - \langle a \rangle^2 = (1-\pi/4)\, 2\sigma^2 \approx 0.43\ \sigma^2 .$

What could be the physical interpretation of this distribution ? When we have multi-path fading the field at every point in space is a summation of waves. If $m > \sigma$ there is a dominant line-of-sight path, and for $m = 0$, we have none line of sight. For a room we can define for every point $\vec{E}_1 = |\vec{E}_1| e^{j\xi_1}$ as the wave arriving at the angle φ_1 with phase ξ_1. To calculate the electric field strength we can add the waves. If we add the z-components we get

$$\vec{E}(x,y) = \sum_{k=1}^{n} \vec{E}_k(x,y), \quad E_z = E_{1z} + E_{2z} + \ldots + E_{nz} = \Re\{E_z\} + j\Im\{E_z\}, \tag{A.8}$$

where $\Re$ means the real part and $\Im$ means the imaginary part. In Eq. (A.7) the arriving angle probability is $1/2\pi$, physically this means that waves arrive with equal probability from all directions. The real and complex components, i and q, are the result of the arrival angle probabilities and path length differences. The central limit states that when every term is equally

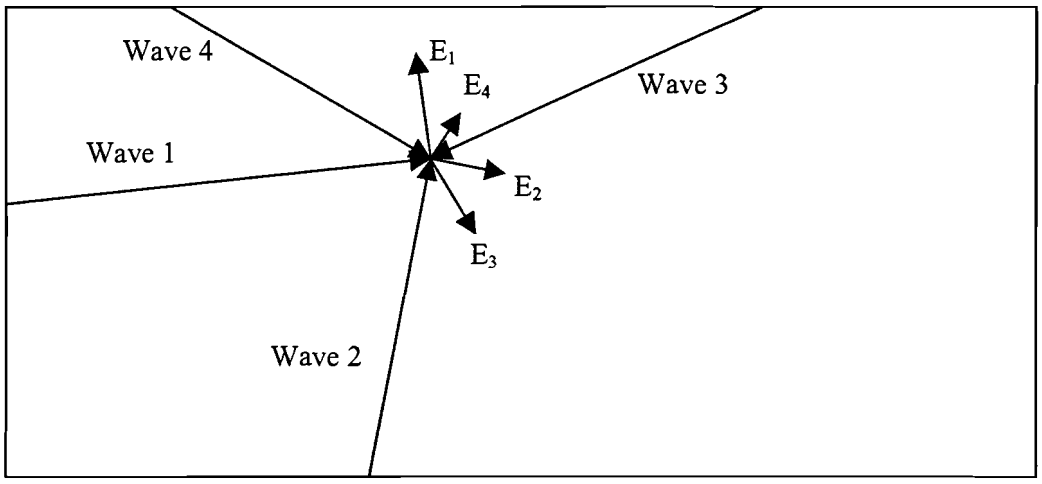

Figure A.2: *Reflected waves are added in the xy-plane using a 2-dimensional model.*

distributed the sum approaches a normal distribution. There is a stronger version of the theorem that states that the sum of different distributions approaches a normal distribution [S.R.Saunders]. The summation is physical realised with an antenna. The NLOS measurements showed that the distribution of E_x, E_y and E_z have a Gaussian shape with zero mean. When one term is dominant, a line-of-sight situation, we get the Rayleigh-Rice distribution. In equation (A.5) we assume that the arriving angle probability is not $1/2\pi$ when $m \neq 0$, this means that the waves arrive mainly from one angle or the antenna is directional.

In a rectangular cavity the arriving angle and phase distribution of propagating waves could be uniform for a two-dimensional summation. In a lossless cavity there exist only two phases because we have standing waves caused by propagating waves. The lossless cavity also has escavent modes with also two temporal phases. So we end up with something like a Rayleigh distributed amplitude and a discrete temporal phase distribution. The E-vector in figure A.1 has a x and y-component and they are independent and Gaussian distributed. The mean is zero and for an antenna sensitive to the x and y-component of the electric field vector we get four degrees of freedom, so instead of integrating the annulus in R^2, we have to integrate a region in R^4. The amplitude of the received signal a is: $a^2 = E^2 = |E_x|^2 + |E_y|^2 = \Re^2 E_x + \Im^2 E_x + \Re^2 E_y + \Im^2 E_y$. The pdf of the amplitude is defined in analogy with Eq. (A.2)

$$f_a(a)\,da = \oint_{\Omega \subset R^4} \frac{1}{4\pi^2\sigma^4} \exp\left[-\frac{\Re^2 E_x + \Im^2 E_x + \Re^2 E_y + \Im^2 E_y}{2\sigma^2}\right] d\Omega = \oint_{\Omega} g(a)\,d\Omega . \qquad \text{(A.9)}$$

We can extend this model to three dimensions with an antenna sensitive to all the polarisation. There are six degrees of freedom and the integration is on a hypersphere in R^6. The hypersphere S^n is the derivative of the hypervolume so

$$V^n(a) = \frac{\pi^{\frac{n}{2}}}{\Gamma(n/2+1)} a^n, \quad S^n(a) = \frac{dV^n(a)}{da} = \frac{\pi^{\frac{n}{2}}}{\Gamma(n/2+1)} n a^{n-1}, \qquad \text{(A.10)}$$

where a is the radius of a sphere. For six degrees of freedom, $n = 6$, we obtain

$$f_a(a)da = \iint_{\Omega} g(a) dS_n da = g(a) S^n da, \quad f_a^n(a) = \frac{2^{1-n/2} a^{n-1} e^{-a^2/2\sigma^2}}{\sigma^n \Gamma(n/2)},$$
$$f_a^6(a) = \frac{a^5 e^{-a^2/2\sigma^2}}{8\sigma^6}. \qquad \text{(A.11)}$$

Indoors with isotropic antennas sensitive to all polarisations we have to consider all field components. The distributions stay the same, we add Gaussian signals with zero mean and equal variances, but the degree of freedom changes from 2 to 6. So we now use 6 signals to calculate the amplitude. In practice we will have less degrees of freedom so between 2 and 6. The Rayleigh distribution is the χ- distribution with two degrees of freedom. If the antenna pattern is uniform and two-dimensional the antenna gain is $G(\varphi,\theta)=2\,\delta(\theta-\theta_0)$ and for a uniform three-dimensional antenna the gain is $G(\varphi,\theta)=1$. For the power distribution we get the χ^2 distribution, this is just a monotonous transformation of the variate x and with the Jacobian we get $p=a^2,\quad a=\sqrt{p},\quad f_a(r)=f_a(a)\dfrac{1}{2a}$. For zero means we get the central distribution $f_p^n(p)=\dfrac{p^{n/2-1}e^{-p/2\sigma^2}}{(2\sigma^2)^{\frac{n}{2}}\Gamma(n/2)}$. For two and six degrees of freedom this becomes

$$f_p^2(p)=\frac{e^{-p/2\sigma^2}}{2\sigma^2},\quad f_p^6(x)=\frac{p^2e^{-p/2\sigma^2}}{16\sigma^6},\quad \langle p\rangle=n\sigma^2. \tag{A.12}$$

The non-central χ- distribution can be used with LOS transmission [Vaughan et al, 2003]. With the sum of the squared means $p_\mu=\sum_{n=1}^{N}m_n^2$ the pdf is

$$f_p^n(p)=\frac{1}{2\sigma^2}(p/p_\mu)^{(n-2)/4}\exp(-(p+p_\mu)/2\sigma^2)\,I_{(n/2-1)}(\sqrt{p\,p_\mu}/\sigma^2)\,U(p). \tag{A.13}$$

For even n the cdf of the power is $F_p(p)=\Pr\{p\le p\}=1-Q_m\left(\sqrt{p_\mu}/\sigma,\sqrt{p}/\sigma\right)$ with $m=n/2$, where $Q_m(a, b)$ is the generalised Marcum Q function and the probability that the sum of powers of m Rician signals with envelope $\sqrt{p_\mu}/\sigma$ is greater than $\sqrt{p}/\sigma$. To get a feeling for the statistics and to recognise measurement data we make some statistical simulations using a random generator set to Gaussian, zero mean, standard deviation one for i and q and 10,000 samples.

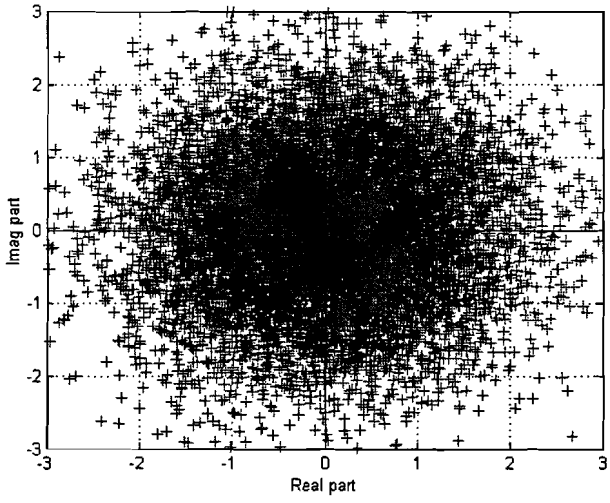

Figure A.3: *The real part and the imaginary part of the signal are independent and Gaussian distributed.*

With two Gaussian distributions we obtain the Rayleigh distribution as depicted in figure A.3. This is the distribution in a highly reflective environment and a non-line of sight transmission. The amplitude and phase distributions are shown in figure A.4.

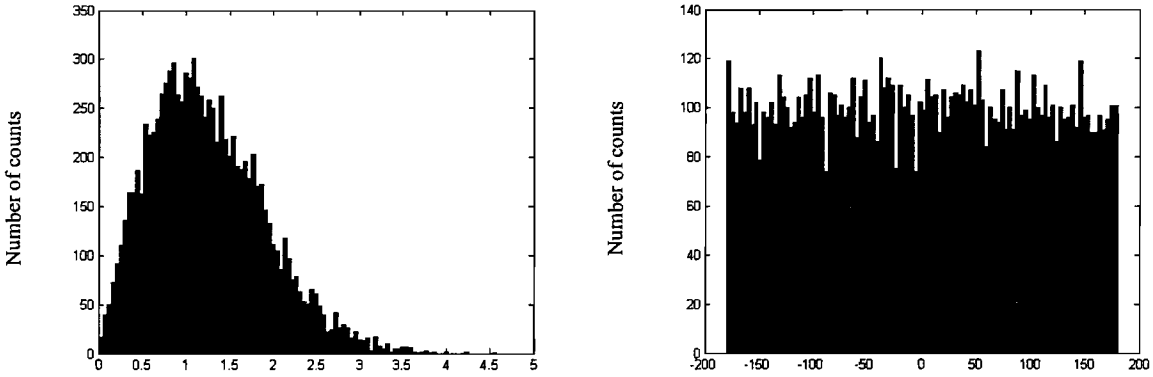

(*a*) (*b*)

Figure A.4: *The histogram of (a) the amplitude distribution and (b) phase distribution.*

The distribution becomes a Rayleigh-Rice distribution if the mean of the signal amplitude is larger than zero. The signal and the amplitude distribution is shown in figure A.5.

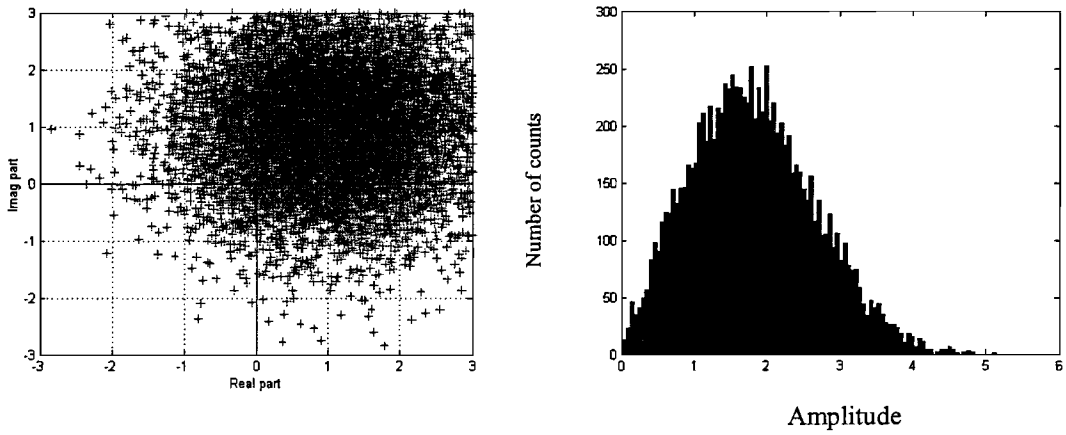

(*a*) (*b*)

Figure A.5: *This is the distribution with m = 1 + j and α = 45° for (a) the signal and (b) the amplitude distribution.*

So there is there is line of sight transmission and the dominant signal is 1.41 angle 45°. The phase distribution for line-of-sight propagation is depicted in figure A.6.

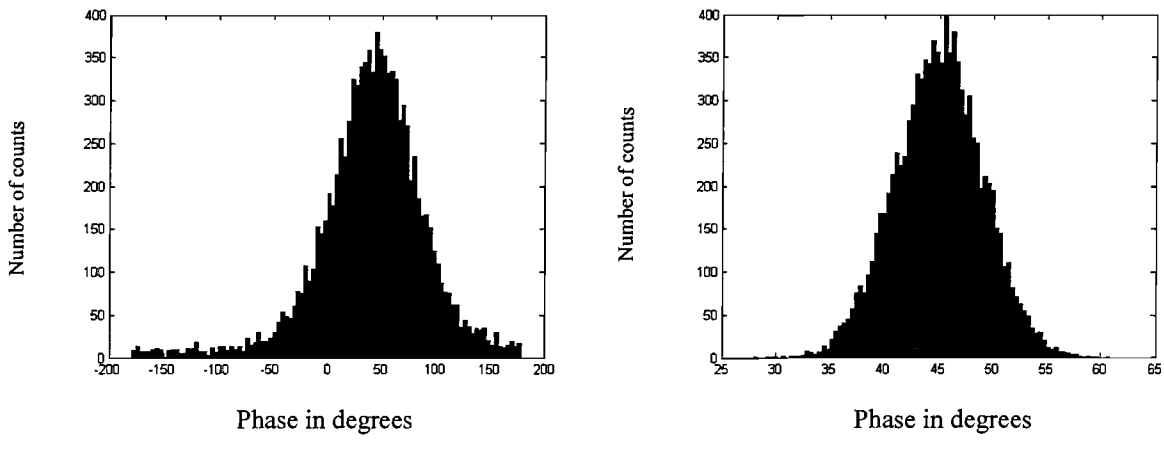

(*a*) (*b*)

Figure A.6: *Phase distribution with (a) m = 1 + j and (b) m = 10 + 10 j and α = 45°.*

The strong version of the central limit theorem can also be shown with random generators.

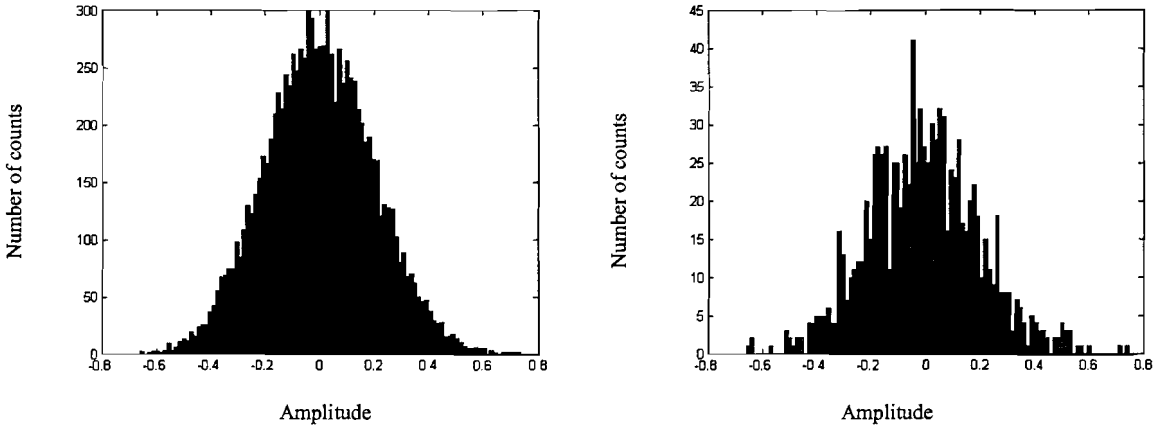

(*a*) (*b*)

Figure A.7: *Amplitude distribution after (a) 10,000 samples and (b) 1000 samples.*

The distribution depicted in figure A.7 is the sum of 5 normal distributions, 5 modified Rayleigh distributions and 5 uniform distributions. All distributions have a similar mean and variance, so there is no dominant distribution. Each distribution has 10,000 samples so the sum has also 10,000 samples. With 1000 samples we obtain figure A.7b, with a lower number the distribution becomes very noisy. So, in a highly reflective environment we can expect a large number of reflections and the signal distribution becomes a Gaussian distribution. We can rewrite the distribution using the propagation parameter K. K is a measure of the power ratio between direct waves and scattered waves. When $K = 0$ we have Rayleigh fading and when $K >> 1$ there is LOS so Rayleigh-Rice fading. The parameter K is defined by

$$K = \frac{\sum_{n=1}^{N} m_n^2}{N\sigma^2} = \frac{m_i^2 + m_q^2}{2\sigma^2}, \tag{A.14a}$$

and the amplitude distribution is

$$f_a^2(a) = \frac{a}{\sigma^2} \exp\left(-K - \frac{a^2}{2\sigma^2}\right) I_0\left(\frac{a\sqrt{K}}{\sigma^2}\right) U(a). \tag{A.14b}$$

The phase distribution is

$$f_\theta^2(\theta, K) = \frac{1}{2\pi} \exp(-K)\left(1 + \sqrt{\pi K}\cos\theta \exp(K\cos^2\theta)\left[1 + \mathrm{erf}(\sqrt{K}\cos\theta)\right]\right), \tag{A.15}$$

where erf is the error function. For $K \to 0$ we get a uniform distributed phase, and when $K \to \infty$ we get a discrete phase distribution. The power is the sum of the direct power and scattered power $\langle p \rangle = m^2/2 + 2\sigma^2 = 2\sigma^2(1+K)$. Cumulatively we get [Vaughan et al ,2003]

$$F_p(p) = 1 - Q_1(m/\sigma, K/\sigma). \tag{A.16}$$

Appendix B: Space diversity

The space correlation of the complex amplitude can be estimated with a simple two-dimensional model as depicted in figure B.1a. The scattering factors, s, have a Gaussian distribution with zero mean and equal angular probability, i.e., we have Rayleigh fading. The phase difference between the waves incident on the antennas is then $\Phi = k_0 d \sin\varphi$, where the geometry is depicted in figure B.1b. The fields at the two isotropic antennas resulting from this scattering are

$$\alpha_1 = \sum_{i=1}^{Ns} s_{1i} \text{ and } \alpha_2 = \sum_{i=1}^{Ns} s_{2i} \exp(j\phi_i) = \sum_{i=1}^{Ns} s_{1i} \exp(j\phi_i). \tag{B.1}$$

where i is the i^{th} scatterer of Ns scatterers and ϕ_i is the phase difference between the waves. Furthermore, we assume that the reflection coefficient s is the same for both antennas. The complex correlation between the two signals is defined by

$$\rho_{12} = \frac{\left\langle (\alpha_1 - m_1)(\alpha_2 - m_2)^* \right\rangle}{\sigma_1 \sigma_2}, \tag{B.2}$$

where m_1 and m_2 are the means of α_1 and α_2, respectively. Note that the correlation can be complex. When we substitute Eq. (B.1) in Eq. (B.2) we get Eq. (B.3). If the scatterers are de-correlated, i.e., $\left\langle s_{1n} s_{2m}^* \right\rangle = 0$ if $n \neq m$ and $s_{1i} = s_{2i}$ we obtain

$$\begin{aligned} \rho_{12} &= \frac{\left\langle \sum_{i=1}^{Ns} s_{1i} \sum_{i=1}^{Ns} s_{2i}^* \exp(j\phi_i)^* \right\rangle}{\sigma_1 \sigma_2} = \frac{\left\langle \sum_{i=1}^{Ns} s_{1i} s_{2i}^* \exp(-j\phi_i) \right\rangle}{\sigma_1 \sigma_2}, \\ &= \frac{\left\langle \sum_{i=1}^{Ns} |s_i|^2 \exp(-j\phi_i) \right\rangle}{\sigma^2}. \end{aligned} \tag{B.3}$$

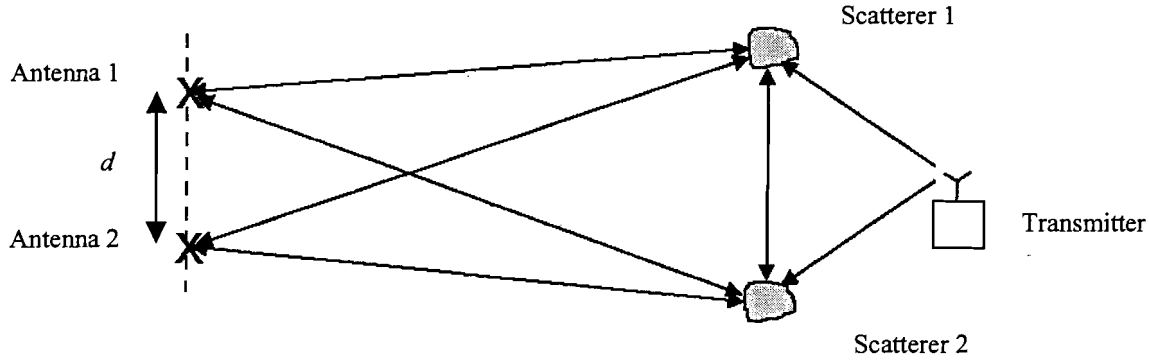

(*a*)

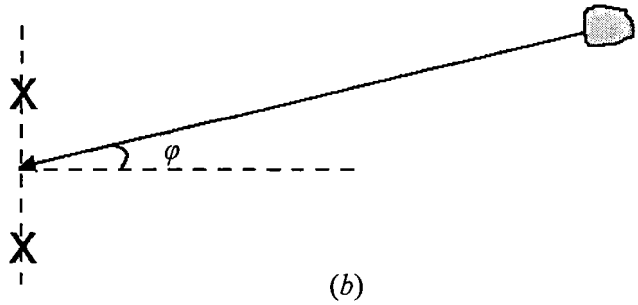

(*b*)

Figure B.1: *Two-dimensional scatter model (a) and (b) geometry for calculation.*

Equation B.3 can be rewritten for a continuous model,

$$\rho_{12} = \left\langle \sum_{i=1}^{Ns} \exp(jkd\sin\varphi_i) \right\rangle \quad \rightarrow \quad \rho_{12}(d) = \int_0^{2\pi} f(\varphi)\exp(jkd\sin\varphi)d\varphi \,. \tag{B.4}$$

When the arriving angle distribution and radiation pattern of the receive antenna are uniform, $f(\varphi) = 1/2\pi$, the following expression is obtained:

$$\rho_{12}(d) = J_0(2\pi\, d/\lambda)\,, \tag{B.5}$$

where J_0 is the Bessel function of the first kind order zero. In a three-dimensional model with a uniform incident field, we get for the envelope correlation of the total electric field [Hill, 1999]:

$$\rho_{env}(d) = \sin kd/kd = 1 - \frac{1}{6}(kd)^2 + O(k^4 d^4)\,. \tag{B.6}$$

If only the z-component of the field is considered the envelope correlation of the electric field is [Hill, 1999]:

$$\rho_{env}(\Delta z) = \frac{3}{(k_0\Delta z)^2}\left[\frac{\sin(k_0\Delta z)}{k_0\Delta z} - \cos(k_0\Delta z)\right] = 1 - \frac{1}{10}(k_0\Delta z)^2 + O(k_0^4\Delta z^4)\,. \tag{B.7}$$

Equation B.4 is a transformation similar to the Fourier transformation, depending on the phase distribution we get a correlation distribution. For Rayleigh fading we get a first zero of the correlation at only 0.38 λ. When we take into account the reflections in a three-dimensional model and we have isotropic antennas the first zero of the envelope correlation occurs at $\lambda/2$ [Vaughan et al, 2003]. When we have little angular spread in the scatterers the signals stay longer correlated in space. This is comparable with the Fourier transformation where a uniform frequency distribution gives a very narrow time distribution and vice versa. The envelope correlation is difficult to calculate. Auto-correlation of the envelope can be expressed in series expansion of a hypergeometric function of the magnitude of the complex correlation [Jakes, 1974]

$$R_{env}(d) = \frac{\pi}{2}\sigma^2\left[1 + \frac{1}{4}|\rho|^2(d) + \frac{1}{64}|\rho|^4(d) + \cdots\right], \tag{B.8a}$$

where $\rho_{power} = |\rho|^2(d)$ is the power correlation [Vaughan et al, 2003].. The envelope correlation is

$$\rho_{env}(d) = \frac{R_{rr}(d) - \langle r\rangle^2}{R_{rr}(0) - \langle r\rangle^2} \approx \frac{\frac{\pi}{2}\sigma^2[1 + \frac{1}{4}|\rho|^2(d)] - \frac{\pi}{2}\sigma^2}{\frac{5\pi}{8}\sigma^2 - \frac{\pi}{2}\sigma^2} = |\rho|^2(d)\,, \tag{B 8b}$$

where R is the auto-correlation. Another possible approach is the use of the identity

$$\rho_{power} = \rho_{ii}^2 + \rho_{iq}^2\,, \tag{B.9}$$

where the real part i and the imaginary part q are de-correlated. As one would expect $\rho_{env} \approx \rho_{power}$, with a relative error smaller than 10 % [Vaughan et al, 2003]. Using Eq. (B8a) we observe that the maximum error is about 4/64 = 6 %.
Space correlation and time correlation are linked through the propagation speed c_0,

$$\rho(d) = J_0(2\pi d/\lambda) = J_0\left(\frac{2\pi c\tau}{c/f}\right) = J_0(2\pi f\tau)\,. \tag{B.10}$$

We can try a more physical approach. With a path length difference of $\lambda/4$ the complex signals are orthogonal. When we use a model with scatterers like figure B.1b, with the sources on the circle having a uniform phase distribution. The difference in path length is $d\sin\theta$. When we estimate the optimum d we first calculate the average path difference. The assumption is that this should be $\lambda/4$,

$$\frac{1}{\pi/2}\int_0^{\pi/2} d\sin\xi\, d\xi = \frac{\lambda}{4}, \quad d \approx 0.39\lambda\,. \tag{B.11}$$

This estimate is close to the solution of Eq. (B.5), 0.38λ.
Equation (B.4) gives a transformation from arriving angle spread to correlation distance. When we consider a plane wave incident at $\varphi = 0$ and $\theta = \pi/2$, the arriving angle distribution is $\delta(\varphi)$ and we find $\rho(d) = 1$. This is precisely what we expected, a plane wave has a uniform amplitude and phase distribution along the antennas and the received signals at the antenna terminals are fully depended. For a reflective environment with a different phase spread we can calculate the space diversity with Eq. (B.4) and (B.7). A realistic arriving angle spread is given by [Saunders, 1999],

$$f(\varphi) = \begin{cases} \dfrac{\pi}{4|\varphi_m|}\cos\dfrac{\pi\varphi}{2\varphi_m} & |\varphi| \le |\varphi_m| \le \dfrac{\pi}{2}, \\ 0 \quad \text{elsewhere}, \end{cases} \tag{B.12}$$

where φ_m is maximum arriving angle. Numerical integration of (B.4), for several arriving angle distributions, results in the power correlation. From figure B.2 we can observe that there is hardly any power correlation after an antenna spacing of $\lambda/2$ when waves arrive at angle spread of at least 120°.

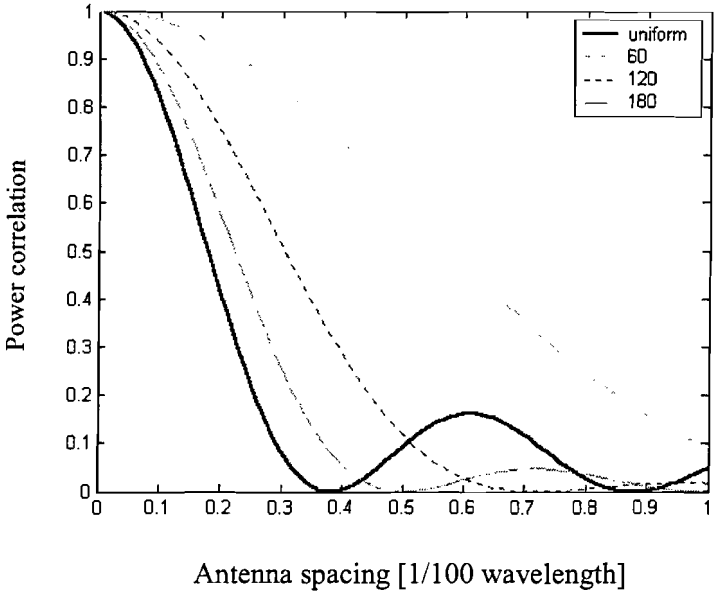

Figure B.2: *Envelope correlation as function of the antenna spacing and angle of arrival spread.*

Appendix C: EM field in a cavity

The following derivation is based on the thesis of [Dolmans, 1997]. It is convenient to use a point source to calculate the EM-field in a cavity, as shown in figure C.1. The solution of this excitation is the Green's dyad multiplied by the source intensity. What is a dyad? A scalar is a tensor with rank zero, a vector is a tensor with rank one and a dyad is a tensor with rank two. The dyad can be expressed as follows

$$\overline{\overline{G}} = G_{xx}\vec{e}_x\vec{e}_x + G_{xy}\vec{e}_x\vec{e}_y + G_{xz}\vec{e}_x\vec{e}_z + G_{yx}\vec{e}_y\vec{e}_x + \cdots + G_{zz}\vec{e}_z\vec{e}_z . \tag{C.1}$$

For the one-dimensional case the Green's function is the solution of the equation $LG(x,x_s) = \delta(x-x_s)$, where L is for example a linear second order differential operator, $L = a\frac{d^2}{dx^2} + b\frac{d}{dx} + c$, and G the Green's function. When this operator L is self adjoint, i.e., $(\phi, L\psi) = (L\phi, \psi)$, all its eigenvalues are real and its eigenfunctions form an orthogonal set under an innerproduct ( ) [Griffel, 2002]. Note the equivalence with a matrix equation $LG = \delta$, if the delta function can be expressed in the eigenfunctions, the Green's function becomes the inverse operator, $L^{-1}LG = \delta \quad G = L^{-1}\delta$. We can calculate the Green's function for the magnetic vector potential $\vec{A}$ because $\nabla \cdot \vec{H} = 0$. The magnetic field strength is

$$\vec{H}(\vec{r}) = \frac{1}{\mu}\nabla \times \vec{A}(\vec{r}) . \tag{C.2}$$

The vector potential and Green's function are related with

$$\vec{A}(\vec{r}) = \iiint_{V_0} \overline{\overline{G}}_A(\vec{r},\vec{r}_0)\, \vec{J}(\vec{r}_0)\, dV_0 , \tag{C.3}$$

where the Green's function is the response to a point source

$$\vec{J} = I_0\delta(\vec{r}-\vec{r}_s)\frac{\vec{r}_j}{|\vec{r}_j|} \quad [Am^{-2}], \tag{C.4}$$

where $\vec{r}_j$ is the direction of the current. And $\overline{\overline{G}}_A$ written in matrix form

$$\overline{\overline{G}}_A = \begin{bmatrix} G_{Axx} & G_{Axy} & G_{Axz} \\ G_{Ayx} & G_{Ayy} & G_{Ayz} \\ G_{Azx} & G_{Azy} & G_{Azz} \end{bmatrix} . \tag{C.5a}$$

According to [Dolmans, 1997] this can be reduced to

$$\overline{\overline{G}}_A = \begin{bmatrix} G_{Axx} & G_{Axy} & G_{Axz} \\ 0 & G_{Ayy} & 0 \\ 0 & 0 & G_{Azz} \end{bmatrix} . \tag{C.5b}$$

When only a x-directed point source is present Eq. (C.2) reduces to

$$\vec{A}(\vec{r}) = I_0 G_{Axx}(\vec{r},\vec{r}_s)\vec{e}_x = A_x\vec{e}_x . \tag{C.6}$$

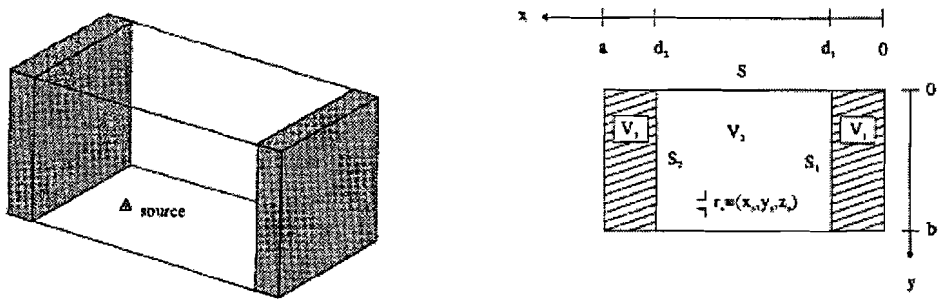

(*a*) (*b*)

Figure C.1: *Room with (a) soure and (b) coordinate system.*

The thesis of W.M.C. Dolmans assumes a dielectric inside volume V_1 and V_3. In the perfect conducting room $V_1 = 0$, $V_3 = 0$ and δV is a perfect conductor. We seek a solution that may be a distribution. This allows us to use generalised derivatives. The distribution generated by a function f is, $(f,\phi) = \int_{-\infty}^{\infty} f(x)\phi(x)dx$, where ϕ is a test function and for our problem the function f has a bounded support. The boundary conditions for G_{Axx} can be derived using the boundary conditions for the electric field

$$\vec{n}(\vec{r})\times\vec{E}(\vec{r}) = 0\,. \tag{C.7}$$

With Eq.(C.6) $\vec{H}(\vec{r}) = \frac{1}{\mu}\begin{bmatrix} \partial_y A_z - \partial_z A_y \\ \partial_z A_x - \partial_x A_z \\ \partial_x A_y - \partial_y A_x \end{bmatrix}$ becomes $\vec{H}(\vec{r}) = \frac{1}{\mu}\begin{bmatrix} 0 \\ \partial_z A_x \\ -\partial_y A_x \end{bmatrix}$ and

$$\vec{E}(\vec{r}) = -\frac{j\omega}{k_0^2}\begin{bmatrix} (k^2+\partial_x^2)A_x \\ \partial_x\partial_y A_x \\ \partial_x\partial_z A_x \end{bmatrix} \text{ or } \vec{E}(\vec{r}) = -\frac{j\omega}{k_0^2}\begin{bmatrix} -(\partial_y^2+\partial_z^2)A_x \\ \partial_x\partial_y A_x \\ \partial_x\partial_z A_x \end{bmatrix} \tag{C.8}$$

When $y = 0$, $\vec{e}_x$ and $\vec{e}_z$ span $(x, 0, z)$, so with (C.8) we get E_x, $E_z = 0$, when J_y, $J_z = 0$,

$$(k_0^2+\partial_x^2)\,A_x = 0, \quad \partial_z\partial_x A_x(x,0,z) = 0, \quad \forall_{x,y,z} \in \{[0,a],0,[0,c]\}. \tag{C.9}$$

When we look for solutions with separated variables we get

$$A_x = X(x)Y(y)Z(z), \quad \partial_z\partial_x A_x = X'YZ',$$

$$\left.\begin{aligned} X'YZ' &= 0 \\ k_0^2 XYZ + X''YZ &= 0 \end{aligned}\right\} \Rightarrow \left.\begin{aligned} X' = 0 = X'' \text{ or } Y = 0 \text{ or } Z = 0 \\ \Downarrow \qquad\qquad \Downarrow \qquad \Downarrow \\ XYZ = 0 \qquad XYZ = 0 \quad XYZ = 0 \end{aligned}\right\} \Rightarrow A_x = 0\,. \tag{C.10}$$

When $y = b$ the conditions are the same so

$$G_{Axx}(x, 0, z) = 0 \text{ and } G_{Axx}(x, b, z) = 0. \tag{C.11}$$

When $z = 0$, $\vec{e}_x$ and $\vec{e}_y$ span $(x, y, 0)$ so E_x, $E_y = 0$, with J_y, $J_z = 0$. We get two equations

$$(k_0^2 + \partial_x^2) A_x = 0, \quad \partial_x \partial_y A_x = 0, \quad \forall_{x,y,z} \in \{[0,a],[0,b],0\},$$

$$\left.\begin{array}{l} X'Y'Z = 0 \\ k_0^2 XYZ + X''YZ = 0 \end{array}\right\} \Rightarrow \left.\begin{array}{ccc} X' = 0 = X'' \text{ or } Y = 0 = Y' \text{ or } Z = 0 & & \\ \Downarrow & \Downarrow & \Downarrow \\ XYZ = 0 & XYZ = 0 & XYZ = 0 \end{array}\right\} \Rightarrow A_x = 0. \tag{C.12}$$

When $z = c$, the conditions are the same so

$$G_{Axx}(x, y, 0) = 0 \text{ and } G_{Axx}(x, y, c) = 0. \tag{C.13}$$

When $x = 0$, $\vec{e}_y$ and $\vec{e}_z$ span $(0, y, z)$ so E_y, $E_z = 0$, with J_y, $J_z = 0$ and

$$\partial_y \partial_x A_x = 0, \quad \partial_z \partial_x A_x = 0, \quad \partial_y^2 \partial_x A_x = 0, \quad \partial_z^2 \partial_x A_x = 0, \quad \partial_x \partial_y \rightarrow \partial_y \partial_x,$$

$$\left.\begin{array}{l} X'Y'Z = 0 \\ X'YZ' = 0 \end{array}\right\} \Rightarrow \left.\begin{array}{ccc} X' = 0 \text{ or } & Y = 0 = Y' \text{ or } & Z = 0 = Z' \\ \Downarrow & \Downarrow & \Downarrow \\ X'YZ = 0 & XYZ = 0 = X'YZ & XYZ = 0 = X'YZ \end{array}\right\} \Rightarrow \partial_x A_x = 0. \tag{C.14}$$

The conditions are the same at $x = a$,

$$\frac{\partial}{\partial x} G_{Axx}(x, y, z)\Big|_{x=0,a} = 0. \tag{C.15}$$

The net electric field in the wall is zero, a surface charge can compensate the incident electric field. Although there is a current induced on the walls there is no power flow through the wall

$$\vec{S}(\vec{r}) \cdot -\vec{n}(\vec{r}) = 0, \quad \vec{r} \in \text{wall}. \tag{C.16}$$

The vector Helmholtz equation [Smolders, 2000] is reduced to a scalar Helmholtz equation

$$\nabla^2 A_x(\vec{r}) + k_0^2 A_x(\vec{r}) = -\mu_0 J_x(\vec{r}), \quad \vec{r} \in V. \tag{C.17}$$

Substituting Eq. (C.4) into Eq. (C.3) gives

$$\nabla^2 G_{Axx}(\vec{r}, \vec{r}_s) + k_0^2 G_{Axx}(\vec{r}, \vec{r}_s) = -\mu_0 \delta(\vec{r} - \vec{r}_s), \quad \vec{r} \in V. \tag{C.18}$$

The solution of the differential equation is the sum of the null space (homogenous solution) and the particular solution. The homogenous solution has the form

$$\frac{\partial^2}{\partial x^2} G_{Axx}(\vec{r}, \vec{r}_s) + \frac{\partial^2}{\partial y^2} G_{Axx}(\vec{r}, \vec{r}_s) + \frac{\partial^2}{\partial z^2} G_{Axx}(\vec{r}, \vec{r}_s) + k_0^2 G_{Axx}(\vec{r}, \vec{r}_s) = 0. \tag{C.19}$$

With the general solution for the modes m, n and i (Bernoulli method)

$$G_{Axxmni} = \left(A_m \sin(k_{xm}x) + B_m \cos(k_{xm}x)\right)\left(C_n \sin(k_{yn}y) + D_n \cos(k_{yn}y)\right)\left(E_i \sin(k_{zi}z) + F_i \cos(k_{zi}z)\right)$$

$$k_{xm}^2 + k_{yn}^2 + k_{zi}^2 = k_0^2$$

or $$G_{Axx} = \sum_{m=1}^{\infty}\sum_{n=1}^{\infty}\sum_{i=1}^{\infty} G_{Axxmni} \,. \tag{C.20}$$

It is possible to write this triple series as a double series due to the conditions in y and z boundaries (Fourier transform to y and z). Using the boundary conditions simplifies the equation,

$$G_{Axx} = \sum_{m=1}^{\infty}\sum_{n=1}^{\infty} \sin(k_{ym}y)\sin(k_{zn}z)F_{mn}(x) \text{ with } k_{ym} = \frac{m\pi}{b} \text{ and } k_{zn} = \frac{n\pi}{c}. \tag{C.21}$$

The delta function can be written as a Fourier series

$$\delta(y - y_s) = \sum_{m=1}^{\infty} A_m \sin(k_{ym}y), \quad \delta(z - z_s) = \sum_{n=1}^{\infty} B_n \sin(k_{zn}z) \quad (y,z) \in V \,. \tag{C.22}$$

The coefficients A_m and B_n are found by solving the following orthogonality relationships:

$$\begin{aligned} \int_0^b \sin\left(\frac{n\pi}{b}y\right)\delta(y - y_s)\,dy &= \sum_{m=1}^{\infty} A_m \int_0^b \sin\left(\frac{m\pi}{b}y\right)\sin\left(\frac{n\pi}{b}y\right)dy \,, \\ \int_0^c \sin\left(\frac{m\pi}{c}z\right)\delta(z - z_s)\,dz &= \sum_{m=1}^{\infty} B_n \int_0^c \sin\left(\frac{m\pi}{c}z\right)\sin\left(\frac{n\pi}{c}z\right)dz \,. \end{aligned} \tag{C.23}$$

The integrals on the right are zero fore $m \neq n$, for $m = n$ we obtain

$$A_m = \frac{2}{b}\sin(k_{ym}y_s), \qquad B_n = \frac{2}{c}\sin(k_{zn}z_s) \text{ with } k_{ym} = \frac{m\pi}{b} \text{ and } k_{zn} = \frac{n\pi}{c}. \tag{C.24}$$

The source can then be expressed as

$$\delta(\vec{r} - \vec{r}_s) = \frac{4}{bc}\sum_{m=1}^{\infty}\sum_{n=1}^{\infty} \sin(k_{ym}y)\,\sin(k_{ym}y_s)\,\sin(k_{zn}z)\,\sin(k_{zn}z_s)\,\delta(x - x_s) \,. \tag{C.25}$$

Substitution of (C.21) and (C.25) in equation (C.18) results in

$$\begin{aligned} &\frac{\partial^2}{\partial x^2}\sum_{m=1}^{\infty}\sum_{n=1}^{\infty} \sin(k_y y)\,\sin(k_z z)\,F_{mn}(x) + k_x^2 \sum_{m=1}^{\infty}\sum_{n=1}^{\infty} \sin(k_y y)\,\sin(k_z z)\,F_{mn}(x), \\ &= \frac{4}{bc}\sum_{m=1}^{\infty}\sum_{n=1}^{\infty} \sin(k_{ym}y)\,\sin(k_{ym}y_s)\,\sin(k_{zn}z)\,\sin(k_{zn}z_s)\,\delta(x - x_s), \end{aligned} \tag{C.26}$$

where F_{mn} is a linear combination of a homogenous part and a particular part. This can be simplified to

$$\begin{aligned} &\frac{d^2}{dx^2}F_{mn}(x) + k_x^2 F_{mn}(x) = -\frac{4\mu}{bc}\sin(k_{yn}y_s)\,\sin(k_{zn}z_s)\,\delta(x - x_s) \\ &k_x = \sqrt{k_0^2 - k_{ym}^2 - k_{zn}^2} \end{aligned} \tag{C.27}$$

The solution is divided in two parts due to discontinuity in the derivative at x_s

$$F_{mn}(x)=\begin{cases}F^1_{mn}(x) & 0<x\le x_s\\ F^2_{mn}(x) & x_s<x<a\end{cases} \tag{C.28}$$

Applying (C.28) and the boundary condition (C.10) for the vector potential we arrive at

$$\begin{aligned}F^1_{mn}(x)&=A^1_{mn}\cos(k_x x)+B^1_{mn}\sin(k_x x)\\ F^2_{mn}(x)&=A^2_{mn}\cos(k_x(x-a))+B^2_{mn}\sin(k_x(x-a))\end{aligned} \tag{C.29}$$

If $F_{mn}(x)$ is a solution of (C.27), $F_{mn}(x)$ has to be continuous at $x = x_s$. The derivative has a discontinuity at $x = x_s$. When Eq. (C.29) is substituted in Eq. (C.27) we obtain,

$$-\frac{d}{dx}F^2_{mn}(x_s+\varepsilon)+\frac{d}{dx}F^1_{mn}(x_s-\varepsilon)=-\frac{4\mu}{bc}\sin(k_{yn}y_s)\sin(k_{zn}z_s)$$

At this point six boundary conditions are available for solving the four unknowns in (C.29). First the boundary condition at $x = 0$ and $x = a$, Eq.(C.10) will be used

$$\frac{d}{dx}F^1_{mn}(x=0)=0 \quad \text{gives} \quad B^1_{mn}=0,\ \frac{d}{dx}F^2_{mn}(x=a)=0 \quad \text{gives} \quad B^2_{mn}=0 \tag{C.31}$$

To obtain the relationship between A^1_{mn} and A^2_{mn}, we need the boundary condition at $x = x_s$

$$\begin{aligned}&F^1_{mn}(x_s)=F^2_{mn}(x_s),\quad A^1_{mn}\cos(k_x x_s)=A^2_{mn}\cos(k_x(x_s-a)),\\ &A^1_{mn}=A^2_{mn}\frac{\cos(k_x(x_s-a))}{\cos(k_x x_s)}.\end{aligned} \tag{C.32}$$

The boundary condition of the derivative at $x = x_s$ results in the second relationship between A^1_{mn} and A^2_{mn},

$$\begin{aligned}&\frac{d}{dx}A^2_{mn}\cos(k_x(x_s+\varepsilon-a))=\frac{d}{dx}A^1_{mn}\cos(k_x(x_s-\varepsilon))+\frac{4\mu}{bc}\sin(k_{ym}y_s)\sin(k_{zn}z_s)\\ &-A^2_{mn}\,k_x\sin(k_x(x_s-a))=-A^1_{mn}k_x\sin(k_x x_s)+\frac{4\mu}{bc}\sin(k_{ym}y_s)\sin(k_{zn}z_s)\quad \varepsilon\to 0\end{aligned} \tag{C.33}$$

Elimination of A^1_{mn} from Eq.(C.32) and (C.33) gives

$$A^2_{mn}=-\frac{4\mu}{bc}\frac{\sin(k_{ym}y_s)\sin(k_{zn}z_s)\cos(k_x x_s)}{-k_x\cos(k_x x_s)\sin(k_x(x_s-a))-k_x\sin(k_x x_s)\cos(k_x(x_s-a))} \tag{C.34}$$

$$A^1_{mn}=-\frac{4\mu}{bc}\frac{\sin(k_{ym}y_s)\sin(k_{zn}z_s)\cos(k_x(x_s-a))}{-k_x\cos(k_x x_s)\sin(k_x(x_s-a))-k_x\sin(k_x x_s)\cos(k_x(x_s-a))} \tag{C.35}$$

Both coefficients (A^1_{mn}, A^2_{mn}) are given by equations (C.34) and (C.35). The component G_{Axx} of the Green's dyad can now be calculated:

Interval 1: $0 \le x \le x_s$

$$G_{Axx} = -\frac{4\mu_0}{bc}\sum_{m=1}^{\infty}\sum_{n=1}^{\infty} \sin\frac{m\pi y}{b}\sin\frac{m\pi y_s}{b}\sin\frac{n\pi z}{c}\sin\frac{n\pi z_s}{c}\frac{\cos k_x(x_s-a)\cos(k_x x)}{k_x \sin(k_x a)}. \quad \text{(C.36)}$$

The electric Green's function is related to the magnetic Green function,

$$\left.\begin{aligned} \vec{E}(\vec{r}) &= -j\omega \iiint_{V_s} \overline{\overline{G}}_E(\vec{r},\vec{r}_s)\,\vec{J}\,dV_s \\ \vec{E}(\vec{r}) &= -j\omega[\vec{A}(\vec{r}) + \frac{1}{k_0^2}\nabla\nabla\cdot\vec{A}(\vec{r})] \\ \vec{A}(\vec{r}) &= \iiint_{V_s} \overline{\overline{G}}_A(\vec{r},\vec{r}_s)\,\vec{J}(\vec{r}_s)\,dV_s \end{aligned}\right\} \Rightarrow \overline{\overline{G}}_E(\vec{r},\vec{r}_s) = \overline{\overline{G}}_A(\vec{r},\vec{r}_s) + \frac{1}{k_0^2}\nabla\nabla\cdot\overline{\overline{G}}_A(\vec{r},\vec{r}_s). \quad \text{(C.37)}$$

The function G_{Exx} is obtained by

$$\begin{aligned} &G_{Exx} = G_{Axx} + \frac{1}{k_0^2}\frac{\partial^2}{\partial x^2}G_{Axx}, \\ &G_{Ayx}, G_{Azx} = 0. \end{aligned} \quad \text{(C.38)}$$

From (C.30) it is clear that the derivative of $F_{mn}(x)$ has a discontinuity at $x = x_s$. Therefore, the second derivative must contain a delta distribution,

$$\frac{d}{dx}F_{mn}(x) = \frac{d}{dx}\{F^1_{mn}(x)\}[1-U(x_s-x)] + \frac{d}{dx}\{F^1_{mn}(x)\}[1-U(x_s-x)], \quad \text{(C.39)}$$

where

$$U(x) = \begin{cases} 1 & \text{for} \quad x > 0, \\ 0 & \text{for} \quad x < 0. \end{cases} \quad \text{(C.40)}$$

The second derivative is given by

$$\begin{aligned} &\frac{d^2}{dx^2}F_{mn}(x) = \frac{d^2}{dx^2}F^1_{mn}(x)[1-U(x_s-x)] + \frac{d^2}{dx^2}F^2_{mn}(x)[1-U(x_s-x)] \\ &-\frac{4\mu}{bc}\sin(k_{yn}y_s)\sin(k_{zn}z_s)\,\delta(x-x_s). \end{aligned} \quad \text{(C.41)}$$

The function G_{Exx} is now written as

$$G_{Exx} = G_{Axx} + \frac{1}{k_0^2}\sum_{m=1}^{\infty}\sum_{n=1}^{\infty}\sin(k_y y)E_n\sin(k_z z)\left[\frac{d^2}{dx^2}F_{mn}(x) - \frac{4\mu}{bc}\sin(k_{yn}y_s)\sin(k_{zn}z_s)\,\delta(x-x_s)\right]. \quad \text{(C.42)}$$

With (C.20) we get

$$G_{Exx} = G_{Axx} + \frac{1}{k_0^2}\sum_{m=1}^{\infty}\sum_{n=1}^{\infty}\left[\sin(k_y y)E_n\sin(k_z z)\frac{d^2}{dx^2}F_{mn}(x)\right] - \frac{\mu}{k_0^2}\delta(\vec{r}-\vec{r}_s) \quad \text{(C.43)}$$

and we arrive at the final expression

Interval 1: $0 \le x \le x_s$,

$$G_{Exx} = \frac{4\mu_0}{bc}\sum_{m=1}^{\infty}\sum_{n=1}^{\infty}\left[(1-k_x^2)\sin\frac{m\pi y}{b}\sin\frac{m\pi y_s}{b}\sin\frac{n\pi z}{c}\sin\frac{n\pi z_s}{c}\frac{\cos k_x(x_s-a)\cos(k_x x)}{k_x \sin(k_x a)}\right] - \frac{\mu}{k_0^2}\delta(\vec{r}-\vec{r}_s)\,. \tag{C.44}$$

Appendix D: Polarisation expansion of a λ/2 dipole

The final results of this derivation were given in the paper of [Taga, 1990]. In this appendix the antenna gain for different polarisation of the incident waves is calculated. To obtain an expansion of the gain in the polarisation we consider a dipole inclined at an angle α with the z-axis in the xz-plane as shown in figure D.1.

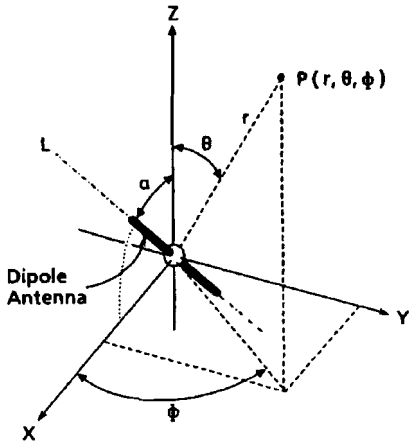

Figure D.1: *Coordinate system.*

The polar coordinates are:

$$\begin{aligned} x &= r\sin\theta\cos\varphi, & & x_\alpha = r\sin\theta_\alpha\cos\varphi_\alpha, \\ y &= r\sin\theta\sin\varphi, & \xrightarrow{\text{rotate }\alpha} & y_\alpha = r\sin\theta_\alpha\sin\varphi_\alpha, \\ z &= r\cos\theta, & & z_\alpha = r\cos\theta_\alpha. \end{aligned} \tag{D.1}$$

where r and y are invariant for the rotation. We change the basis and define the standard basis $(\vec{e}_x,\vec{e}_y,\vec{e}_z)$ β, and the basis α is with respect to the dipole coordinate system. The rotation angle α is always positive. The standard basis and the dipole basis are linked with a rotation over α, $R(\alpha)$. And the transformation is $R(\alpha)(\vec{e}_{x\alpha},\vec{e}_{y\alpha},\vec{e}_{z\alpha}) \rightarrow (\vec{e}_x,\vec{e}_y,\vec{e}_z)$. The associated transformation matrix ${}_\beta S_\alpha$ from the dipole basis to the standard basis is

$$\begin{bmatrix} \cos\alpha & 0 & -\sin\alpha \\ 0 & 1 & 0 \\ \sin\alpha & 0 & \cos\alpha \end{bmatrix} \begin{bmatrix} \vec{e}_{x\alpha} \\ \vec{e}_{y\alpha} \\ \vec{e}_{z\alpha} \end{bmatrix} = \begin{bmatrix} \vec{e}_x \\ \vec{e}_y \\ \vec{e}_z \end{bmatrix}, \quad \begin{aligned} \vec{e}_x &= \cos\alpha\vec{e}_{x\alpha} + \sin\alpha\vec{e}_{z\alpha}, \\ \vec{e}_y &= \vec{e}_{y\alpha}, \\ \vec{e}_z &= -\sin\alpha\vec{e}_{x\alpha} + \cos\alpha\vec{e}_{z\alpha}. \end{aligned} \tag{D.2}$$

The relation between dipole coordinates and the standard coordinates is

$$\begin{bmatrix} \cos\alpha & 0 & -\sin\alpha \\ 0 & 1 & 0 \\ \sin\alpha & 0 & \cos\alpha \end{bmatrix} \begin{bmatrix} r\sin\theta_\alpha\cos\varphi_\alpha \\ r\sin\theta_\alpha\sin\varphi_\alpha \\ r\cos\theta_\alpha \end{bmatrix} = \begin{bmatrix} x \\ y \\ z \end{bmatrix} = \begin{bmatrix} r\sin\theta\cos\varphi \\ r\sin\theta\sin\varphi \\ r\cos\theta \end{bmatrix},$$

$$\begin{bmatrix} \cos\alpha\sin\theta_\alpha\cos\varphi_\alpha - \sin\alpha\cos\theta_\alpha \\ \sin\theta_\alpha\sin\varphi_\alpha \\ \sin\alpha\sin\theta_\alpha\cos\varphi_\alpha + \cos\alpha\cos\theta_\alpha \end{bmatrix} = \begin{bmatrix} \sin\theta\cos\varphi \\ \sin\theta\sin\varphi \\ \cos\theta \end{bmatrix}. \tag{D.3}$$

For a dipole the antenna gain for θ-polarised waves is [Smolders, 2000]

$$G = G_\theta = 1.641 \frac{\cos^2((\pi/2)\cos\theta)}{\sin^2\theta}, \quad G_\varphi = 0. \tag{D.4a}$$

In the dipole coordinate system with Eq. (D.8c) we get for θ_α-polarised waves

$$G_{\theta\alpha} = 1.641 \frac{\cos^2((\pi/2)\xi)}{1-\xi^2}. \tag{D.4b}$$

We consider how the inclined antenna reacts for θ and φ-polarised waves. The angle of arrival is already in Eq. (D.4b), we only have to take an inner product of polarisation vectors to take into account the coordinate change. The unit vector in the θ-direction is

$$\vec{e}_\theta = \frac{\partial P/\partial\theta}{|\partial P/\partial\theta|} = \frac{\partial}{\partial\theta}\{r\sin\theta\cos\varphi\vec{e}_x + r\sin\theta\sin\varphi\vec{e}_y + r\cos\theta\vec{e}_z\} \Big/ |\partial P/\partial\theta|, \tag{D.5a}$$

$$\begin{aligned}\vec{e}_\theta &= \cos\theta\cos\varphi\vec{e}_x + \cos\theta\sin\varphi\vec{e}_y - \sin\theta\vec{e}_z, \\ &= \frac{xz}{\rho r}\vec{e}_x + \frac{yz}{\rho r}\vec{e}_y - \frac{\rho}{r}\vec{e}_z, \quad \text{with} \quad \rho = r\sin\theta.\end{aligned} \tag{D.5b}$$

where P is a point with coordinates (x, y, z). For the unit vector in the φ-direction we obtain

$$\vec{e}_\varphi = \frac{\partial P/\partial\varphi}{|\partial P/\partial\varphi|} = -\sin\varphi\vec{e}_x + \cos\varphi\vec{e}_y = -\frac{x}{\rho}\vec{e}_x + \frac{y}{\rho}\vec{e}_y. \tag{D.5c}$$

A dipole emits only θ_α-polarised waves in the far field. So we only have to calculate the projection of the incident field on this field component,

$$\vec{e}_\theta \cdot \vec{e}_{\theta_\alpha} = \left(\frac{xz}{\rho r}\vec{e}_x + \frac{yz}{\rho r}\vec{e}_y - \frac{\rho}{r}\vec{e}_z\right) \cdot \left(\frac{x_\alpha z_\alpha}{\rho_\alpha r}\vec{e}_{x_\alpha} + \frac{yz_\alpha}{\rho_\alpha r}\vec{e}_{y_\alpha} - \frac{\rho_\alpha}{r}\vec{e}_{z_\alpha}\right), \tag{D.6}$$

We also have the φ-component

$$\vec{e}_\varphi \cdot \vec{e}_{\theta_\alpha} = \left(-\frac{y}{\rho}\vec{e}_x + \frac{x}{\rho}\vec{e}_y\right) \cdot \left(\frac{x_\alpha z_\alpha}{\rho_\alpha r}\vec{e}_{x\alpha} + \frac{yz_\alpha}{\rho_\alpha r}\vec{e}_{y_\alpha} - \frac{\rho_\alpha}{r}\vec{e}_{z_\alpha}\right). \tag{D.7}$$

The transformation from the standard basis to the dipole basis is the transpose of the rotation, ${}_\alpha S_\beta^T = {}_\beta S_\alpha$, with a positive α (when we defined a negative α this is still true).

$$\begin{bmatrix} \cos\alpha & 0 & \sin\alpha \\ 0 & 1 & 0 \\ -\sin\alpha & 0 & \cos\alpha \end{bmatrix} \begin{bmatrix} r\sin\theta\cos\varphi \\ r\sin\theta\sin\varphi \\ r\cos\theta \end{bmatrix} = \begin{bmatrix} r\sin\theta_\alpha\cos\varphi_\alpha \\ r\sin\theta_\alpha\sin\varphi_\alpha \\ r\cos\theta_\alpha \end{bmatrix}, \tag{D.8a}$$

$$\begin{aligned}&\vec{e}_{x_\alpha} = \cos\alpha\,\vec{e}_x - \sin\alpha\,\vec{e}_z, \quad \vec{e}_{y_\alpha} = \vec{e}_y, \quad \vec{e}_{z_\alpha} = \sin\alpha\,\vec{e}_x + \cos\alpha\,\vec{e}_z, \\ &x_\alpha = x\cos\alpha - z\sin\alpha, \quad y_\alpha = y, \quad z_\alpha = z\cos\alpha + x\sin\alpha,\end{aligned} \tag{D.8b}$$

$$\cos\theta_\alpha = \sin\alpha\sin\theta\cos\varphi + \cos\alpha\cos\theta = \xi. \tag{D.8c}$$

To calculate the antenna gain for φ-polarised waves we substitute Eq. (D.8b) in Eq. (D.7),

$$\vec{e}_\varphi \cdot \vec{e}_{\theta_\alpha} = \left(-\frac{y}{\rho}\vec{e}_x + \frac{x}{\rho}\vec{e}_y \right) \cdot \left(\frac{x_\alpha z_\alpha}{\rho_\alpha r}(\cos\alpha\,\vec{e}_x - \sin\alpha\,\vec{e}_z) + \frac{y_\alpha z_\alpha}{\rho_\alpha r}\vec{e}_y - \frac{\rho_\alpha}{r}(\sin\alpha\,\vec{e}_x + \cos\alpha\,\vec{e}_z) \right). \tag{D.9}$$

We can simplify this by rewriting the z_α-component

$$\begin{aligned}\vec{e}_{\theta_\alpha} &= \left(\frac{(x\cos\alpha - z\sin\alpha)(z\cos\alpha + x\sin\alpha)}{\rho_\alpha r}\cos\alpha - \sin\theta_\alpha \sin\alpha \right)\vec{e}_x + \frac{y(z\cos\alpha + x\sin\alpha)}{\rho_\alpha r}\vec{e}_y \\ &= \left[\frac{x^2\cos\alpha\sin\alpha + zx(\cos^2\alpha - \sin^2\alpha) - z^2\sin\alpha\cos\alpha}{r^2\sin\theta_\alpha}\cos\alpha - \sin\theta_\alpha\sin\alpha \right]\vec{e}_x \\ &\quad + \frac{yz\cos\alpha + xy\sin\alpha}{r^2\sin\theta_\alpha}\vec{e}_y.\end{aligned} \tag{D.10}$$

And the inner product is

$$\begin{aligned}\vec{e}_\varphi \cdot \vec{e}_{\theta_\alpha} &= -\frac{x^2\cos\alpha\sin\alpha + zx\cos^2\alpha - zx\sin^2\alpha - z^2\sin\alpha\cos\alpha}{r^2\sin\theta_\alpha}\cos\alpha\sin\varphi \\ &\quad + \sin\varphi\sin\theta_\alpha\sin\alpha + \frac{yz\cos\alpha + xy\sin\alpha}{r^2\sin\theta_\alpha}\cos\varphi,\end{aligned} \tag{D.11}$$

$$\begin{aligned}&= -\frac{\sin^2\theta\cos^2\varphi\cos\alpha\sin\alpha + \cos\theta\sin\theta\cos\varphi\cos^2\alpha - \cos\theta\sin\theta\cos\varphi\sin^2\alpha - \cos^2\theta\sin\alpha\cos\alpha}{\sin\theta_\alpha} \\ &\quad \times\cos\alpha\sin\varphi + \frac{\sin\varphi(1-\xi^2)\sin\alpha}{\sin\theta_\alpha} + \frac{\sin\theta\sin\varphi\cos\theta\cos\alpha + \sin^2\theta\cos\varphi\sin\varphi\sin\alpha}{\sin\theta_\alpha}\cos\varphi.\end{aligned}$$

Finally, the result in the standard basis is found as

$$G_\varphi = 1.641\sin^2\varphi\sin^2\alpha\frac{\cos^2((\pi/2)\xi)}{(1-\xi^2)^2}. \tag{D.12}$$

Equation (D.12) has a removable singularity and some special results are

$$G_\varphi(\alpha = 0) = 0, \quad G_\varphi(\alpha = 90°, \varphi = \theta_\alpha) = 1.641\sin^2\varphi\frac{\cos^2((\pi/2)\cos\theta_\alpha)}{\sin^4\theta_\alpha}.$$

The derivation of G_θ proceeds in a similar way with the inner product in Eq. (D.6). The result is [Taga, 1990]

$$G_\theta = 1.641\,(\cos\theta\cos\varphi\sin\alpha - \sin\theta\cos\alpha)^2\,\frac{\cos^2((\pi/2)\xi)}{(1-\xi^2)^2}. \tag{D.13}$$

For $\alpha = 0°$ we have a vertical dipole and it appears that horizontal dipole, $\alpha = 90°$, has a antenna gain for θ-polarised waves of

$$G_\theta = 1.641\cos^2\theta\cos^2\varphi\frac{\cos^2((\pi/2)\xi)}{(1-\xi^2)^2}. \tag{D.14}$$

Appendix E: Combination of space, polarisation and antenna pattern diversity

The auto-correlation of the stochastic variable S as function of the parameter d is defined as [Lee, 1997]:

$$R_s = \left\langle S^*(y)\, S(y+d) \right\rangle. \tag{E.1}$$

where S^* is the complex conjugate of S. For several parameters this becomes for example:

$$R_s = \left\langle S^*(x,y,z,\varphi,p)\, S(x,y+d,z,\varphi+\alpha,p+pat) \right\rangle, \tag{E.2}$$

where x, y and z are the spatial coordinates, d is the separation in the y-direction, α is the polarisation angle difference p is the antenna pattern constant, e.g. Gaussian shape, and *pat* is the antenna pattern difference parameter, e.g., rotation angle around the axis of a directional antenna. With radiation pattern diversity we mean; changing magnitude of the antenna gain without changing the co- or cross-polarisation sensitivity. Antenna pattern correlation is based on the normalised innerproduct of radiation patterns [Mattheijssen, 2000]. The auto-correlation of the antenna patterns can be expressed with a parameter if the radiation pattern of the two antennas are described with a parametric equation, e.g., is the antenna gain for antenna 1 is $G_\theta(\theta,\varphi) = 4\pi\,\delta(\theta-\theta_1)\delta(\varphi-\varphi_1)$, $G_\varphi = 0$, and the antenna gain for antenna 2 is $G_\theta(\theta,\varphi) = 4\pi\,\delta(\theta-\theta_1)\delta(\varphi-\varphi_1)$, $G_\varphi = 0$. For this extremely directional antenna pattern, the patterns are de-correlated almost everywhere and the pattern correlation is $\rho(\Delta\theta,\Delta\varphi) = \int_\Omega \delta(\theta_1-\theta_2)\delta(\varphi_1-\varphi_2)\, d\Omega$. If the antennas have the same radiation pattern except for a rotation around the antenna axis the correlation becomes $\rho(\Delta\varphi) = \int_\Omega \delta(\varphi_1-\varphi_2)\, d\Omega$. If R_S does not depend on x and z, Eq (E.2) simplifies to

$$R_s(d,\alpha,pat) = \left\langle S^*(y,\varphi,p)\, S(y+d,\varphi+\alpha,p+pat) \right\rangle. \tag{E.3}$$

The auto-correlation for a continuous variable S is:

$$R_s = \iiint_{V\cup\Omega} S^*(y,\varphi,p)\, S(y+d,\varphi+\alpha,p+pat)\, dy\, d\varphi\, d\Omega. \tag{E.4}$$

where V the domain containing y and φ, $\Omega = 4\pi$, the solid angle domain. The auto-correlation coefficient of the stochastic variable S as function of the parameter d is defined as [Lee, 1997]:

$$\rho_s(d) = \frac{R_s(d) - \langle s \rangle^2}{R_s(0) - \langle s \rangle^2}. \tag{E.5}$$

When the stochastic variable S is a function of three parameters this becomes:

$$\rho_s(d,\alpha,pat) = \frac{R_s(d,\alpha,pat) - \langle s \rangle^2}{R_s(0,0,0) - \langle s \rangle^2}. \tag{E.6}$$

When the mean of S is zero Eq. (E.6) reduces to:

$$\rho_s(d,\alpha,pat)=\frac{R_s(d,\alpha,pat)}{R_s(0,0,0)}. \tag{E.7}$$

Indoors there is no correlation between spatial position, polarisation and radiation pattern. If spatial, polarisation and pattern diversity are independent the variable S can be written as a product of a factor depending on space, a factor depending on polarisation and a factor depending on the radiation pattern,

$$S(y,\varphi,p)=U(y)V(\varphi)W(p). \tag{E.8}$$

The auto-correlation can be rewritten using Eq.(E.8),

$$R_s(d,\alpha,pat)=\iiint_{V\cup\Omega}U^*(y)V^*(\varphi)W^*(p)U(y+d)V(\varphi+\alpha)W(p+pat)\,dy\,d\varphi\,d\Omega. \tag{E.9}$$

The auto correlation in one variable then becomes

$$R_s(d,0,0)=\int U^*(y)\,U(y+d)\,dy\iint V^*(\varphi)\,W^*(p)\,V(\varphi)\,W(p)\,d\varphi\,d\Omega, \tag{E.10}$$

for spatial auto-correlation. For polarisation auto-correlation we get

$$R_s(0,\alpha,0)=\int V^*(\varphi)\,V(\varphi+\alpha)\,d\varphi\iint U^*(y)\,U(y)\,W^*(p)\,W(p)\,dy\,d\Omega. \tag{E.11}$$

The auto-correlation of the antenna pattern can be expressed with

$$R_s(0,0,pat)=\int W^*(p)W(p+pat)d\Omega\iint U^*(y)U(y)V^*(\varphi)V(\varphi)dy\,d\varphi. \tag{E.12}$$

For the total correlation, using all degrees of freedom we get

$$R_s(d,\alpha,pat)=R_s(d,0,0)R_s(0,\alpha,0)R_s(0,0,pat)/[R_s(0,0,0)]^2, \tag{E.13}$$

and the correlation becomes,

$$\rho_s(d,\alpha,pat)=\frac{R_s(d,\alpha,pat)}{R_s(0,0,0)}=\frac{R_s(d,0,0)R_s(0,\alpha,0)R_s(0,0,pat)}{R_s(0,0,0)^3}. \tag{E.14}$$

Finally we arrive at

$$\rho(d,\alpha,pat)=\rho(d)\rho(\alpha)\rho(pat). \tag{E.15}$$

We can conclude that it is plausible that the correlation can be factorised. If we want to decreases the power correlation between two receive antennas we can use a combination of space, polarisation and radiation pattern diversity to obtain uncorrelated received powers.

Acknowledgments

This Msc. thesis could not have been completed without the moral support and valuable contributions of various people. I would like to express my gratitude to the following people working at Philips Research, dr. ir. Guido Dolmans for the discussions that I had with him and for helping me with the measurements and ir. Bertrand Vandewiele for modifying the measurement program.

I would like to thank my supervisor at Philips Semiconductors dr. ir. Bart Smolders for reviewing this report, his support, advice and discussions. Furthermore, I would like to thank Martijn Uddink for helping me with the slot antenna, the people at the pilot line for the assembly of the module and Rob Boesten for his support.

Within the Electromagnetics Group of the Eindhoven University of Technology (TU/e) I would like to thank ir. Huib Visser for helping me to improve my technical writing skills. I would like to thank prof. dr. Anton Tijhuis for reviewing this report.

I am indebted to the management of Philips Semiconductors for financing my partime study.
Finally I would like to thank my family for their moral support.